MARCIN GRABOWICZ

Biogenesis of *Shigella flexneri* IcsA Protein

Biogenesis of *Shigella flexneri* IcsA Protein

MARCIN GRABOWICZ, B.SC. (HONS.)

Submitted for the degree of
Doctor of Philosophy

Discipline of Microbiology and Immunology
School of Molecular and Biomedical Science
The University of Adelaide

March, 2010

Declaration

This work contains no material which has been accepted for the award of any other degree or diploma in any university or other tertiary institution to Marcin Grabowicz and, to the best of my knowledge and belief, contains no material previously published or written by another person, except where due reference has been made in the text.

I give consent to this copy of my thesis, when deposited in the University Library, being made available for loan and photocopying, subject to the provisions of the Copyright Act 1968.

I also give permission for the digital version of my thesis to be made available on the web, via the University's digital research repository, the Library catalogue, the Australasian Digital Theses Program (ADTP) and also through web search engines, unless permission has been granted by the University to restrict access for a period of time.

Adelaide, Australia, March, 2010

Marcin Grabowicz

Abstract

The IcsA autotransporter is a vital virulence factor for *Shigella flexneri*, a human-specific causative agent of bacillary dysentery that accounts for over a million global deaths annually. Ingested Shigellae invade and spread throughout the colonic epithelium. IcsA confers motility to intracellular bacteria by engaging host actin regulatory proteins to polymerise filaments of actin in a processes termed actin-based motility. This IcsA-dependent motility potentiates the intercellular spreading.

IcsA is displayed at one pole of the bacterium, thereby providing a functional focus for actin polymerisation that generated propulsive force. This work investigated the biogenesis of IcsA, seeking to identify factors that direct the cytoplasmic deliver of the nascent protein towards the pole. A refined polar targeting region, $IcsA_{532-570}$ has been identified. Additionally, insertion mutant, i532 and i563, within the recognised targeting sequence $IcsA_{506-620}$ that have been identified that are defective, though not entirely deficient, in polar targeting. GFP+ fusions to these mutated targeting sequences revealed rapid motion of fluorescent foci throughout the cytoplasm, a process that likely precedes polar targeting in the wild-type. The delivery of the polarly targeted $IcsA_{506-620}$ region was shown to occur contemporaneously with segregating origins of chromosomal replication (*oriC*) and likely shares a common cell cycle cue.

The diffusive properties of exported IcsA in outer-membrane have also been investigated, addressing whether the protein diffuses in the outer membrane or is masked by LPS. To directly observe the behaviour of IcsA soon after it appears at the cell surface, a strategy exploiting metabolic biotinylation was developed and used to rapidly and specifically label nascent IcsA in the outer membrane. In further investigation of the IcsA-LPS interplay, the profile of polar LPS was shown to be uniform in comparison to the lateral cell body in *S. flexneri*. Reciprocal co-purification presented biochemical evidence that confirmed IcsA-IcsA interactions in the outer-membrane, supporting functional oligomerisation of IcsA in the outer-membrane.

Acknowledgments

Foremost, I thankfully acknowledge the support and guidance of Associate Professor Renato Morona. I feel most fortunate to have worked and learned under his mentorship: these past years have been an instructive beginning to life in science.

Throughout these studies I have been fortunate to work among people who generously shared their knowledge, ideas, and experiences; I especially thank Dr Uwe Ströher, Dr Leanne Purins and Dr Tony Focareta. I am grateful to friends—in and out of the laboratory—who helped me remain sane at the worst of times and who were always on hand for drink and laugh: James Aslanidis, James Byrne, Dr Rikki Graham, Arend Grosse, Dr Sylvia Herold, Dr Kim LeMessurier, Khang Nguyen, Tom Murphy, Dr Adam Potter, and Dr Alistair Standish. Thank you all for showing me that all problems can be solved at the Exeter Hotel.

I thank Luisa Van Den Bosch for her technical assistance throughout this work and I am grateful to researchers who have generously provided materials that collectively improved this work: Professor David Sherratt, Professor; Tony Pugsley; Professor Bill Dowhan; and Professor Elliott Crooke.

I thank my parents, Ewa and Paweł, for their long-standing love, encouragement and sacrifice; I will always be grateful to you both. I also thank my parents-in-law, Beverley and Trevor, for their advice and support.

On the whole, I look back at amazingly happy memories during these PhD studies. Overwhelmingly, these memories include my wife, Dr Kerrie May. Without her help, nurturing advice and loving care, I would be unable to write this work. She has read this thesis more often than is imaginable; yet has always been full of enthusiasm, ideas and empathy. Looking excitedly towards our future—filled with learning, astounding experiences, inherent anxieties, and surprising joys—I can see nothing more contenting than simply growing old, always with her.

Contents

Abbreviations

ABM	actin-based motility
ADP	adenosine diphosphate
ATP	adenosine triphosphate
ATPase	adenosine triphosphatase
cDNA	complementary DNA
CFU	colony-forming units
Da	Dalton
DNA	deoxyribonucleic acid
DNase	deoxyribonuclease
dsDNA	double-stranded DNA
ECFP	enchanced cyan fluorescent protein
EYFP	enhanced yellow fluorescent protein
GFP	green fluorescent protein
GTP	guanosine triphosphate
GTPase	guanosine triphosphatase
HRP	horse radish peroxidase
kb	kilobase
mRNA	messenger RNA
nt	nucleotide
Oag	O-antigen

PCR	polymerase chain reaction
PFU	plaque-forming units
RNA	ribonucleic acid
RNase	ribonuclease
rRNA	ribosomal RNA
Tris	tris(hydroxymethyl)aminomethane
U	units

Part I

INTRODUCTION AND METHODS

1

Introduction

1.1 Introduction

Historically, knowledge gleamed from bacterial experiments enlightened exploration of the eukaryotic world. However, the small cell size of bacteria later meant that subcellular architecture, cell division and DNA segregation were recognised with far greater detail in eukaryotes, and remained virtually unknown in prokaryotes. With recent developments, including an array of fluorescent proteins, improvements in microscopy techniques, and advances in computational image analysis, the fundamental cellular workings of bacteria are now being unravelled and framed into a more complete appreciation of the cell cycle.

Explorations of prokaryotic cell biology are being pursued amid a context of a declining potency in the antibacterial arsenal, and are hoped to inform the design of future clinical options. *Shigella*, a Gram-negative bacterium, has proven to be among the most well adapted of human pathogens. Despite many decades of concerted effort expended on understanding—in molecular detail—the pivotal events occurring at the host-pathogen interface, the promise of globally effective control of *Shigella* infection has remained elusive (Levine *et al.*, 2007). Alarmingly, the incidence of *Shigella* resistance to a range of antibacterials is prevalent and rising (Fullá *et al.*, 2005).

This chapter reviews *Shigella* pathogenesis and the role of the IcsA autotransporter, a key protagonist in the invasive stage of infection that enables dissemination of bacteria throughout an infected intestinal epithelium. An incompletely understood ability of IcsA to be localised at one bacterial pole is also reviewed, in light of discoveries in bacterial cell biology.

1.2 *Shigella*

Shigella spp. are globally the most prominent bacterial causative agent of human-specific dysentery, a bloody mucoid diarrhoea. Worldwide estimates of 165 million incidences of shigellosis, resulting in 1.1 million predominately paediatric deaths, underscore the heavy burden imposed by the bacterium on global human health (Kotloff *et al.*, 1999). The genus is comprised of four members—*Shigella flexneri*, *Shigella boydii*, *Shigella sonnei* and *Shigella dysenteriae*—each further catalogued according to variations in the chemical composition of the O-antigen (Oag) component of their lipopolysaccharide (LPS) (Simmons, 1993). The bulk of *Shigella* deaths are attributed to thirteen different serotypes of the *S. flexneri* species (Jennison and Verma, 2004; Levine *et al.*, 2007). *S. flexneri* serotype 2a is the predominant pathogenic serotype common to both the developing and developed worlds, has been the mainstay for basic research, and is the focus of the work contained herein (Jennison and Verma, 2004; Niyogi, 2005).

The genome of *S. flexneri* serotype 2a strain 2457T has been completely sequenced (Wei *et al.*, 2003). Comparative genomic analysis revealed *Shigella* to be essentially a member of the species *Escherichia coli*. Indeed, on comparison of housekeeping genes, the divergence between *E. coli* K-12 and *S. flexneri* 2457T is less pronounced than the divergence between K-12 and *E. coli* O157:H7 (Lan and Reeves, 2002). The convergent evolution of *Shigella* spp. was marked by loss of catabolic genes, acquisition of pathogenicity islands, and the introduction of a range of Oag genes (Rajakumar *et al.*, 1997; Maurelli *et al.*, 1998; Moss *et al.*, 1999; Coimbra *et al.*, 1999; Al-Hasani *et al.*, 2000). The carriage of a large (140 megadaltons), now sequenced, virulence plasmid (pINV) is essential for virulence (Hale, 1991). Genes provided by pINV permit invasion and colonisation of the host intestinal epithelium, as prerequisite to pathological disease.

1.2.1 *Pathogenesis*

Shigella transmission relies on the faecal-oral route. Genetic resistance to stomach acid allows for an extremely low infectious dose—ingestion of 100 organisms is sufficient to establish symptomatic disease in humans (Waterman and Small, 1996; DuPont *et al.*, 1989). On ingestion, the action of two *S. flexneri* 2a enterotoxins

(*Shigella* Enterotoxins 1 and 2; ShET1 and ShET2) in the jejunum can lead to watery diarrhoea with loss of solutes (Fasano *et al.*, 1995; Nataro *et al.*, 1995; Fasano *et al.*, 1997). Shigellae then pass to the colon, and enter the invasive phase of pathogenesis, triggering highly inflammatory responses that: damage epithelial integrity and surrounding tissue; release blood; and induce dysentery.

On reaching the colon, Shigellae are unable to cross the epithelium from the apical side (Mounier *et al.*, 1992). Instead, the bacteria trigger uptake into membraneous epithelial cells (M cells) and exploit the antigen sampling role of these cells to achieve transcytosis (**Figure 1.1**) (Sansonetti and Phalipon, 1996; Sansonetti *et al.*, 1999; Sansonetti and Phalipon, 1999). Shigellae are then released into underlying lymphoid follicles, where they are taken up by resident macrophage. Infected macrophage are killed by Shigellae in a poorly defined mechanism that has previously been described as pyroptosis—an inflammatory form of apoptosis (Zychlinsky *et al.*, 1992; Chen *et al.*, 1996; Zychlinsky *et al.*, 1996). However, more recent studies in human-derived macrophage report induction of necrotic cell death by necrosis/oncosis. The emerging picture suggests that apoptosis may be triggered indirectly in a virulence-independent manner, while internalised Shigellae directly induce necrosis, oncosis, or both during human macrophage infection (Fernandez-Prada *et al.*, 1997; Nonaka *et al.*, 2003). Death of the infected macrophage allows for bacterial escape in the submucosal tissue (**Figure 1.1**). Released *S. flexneri* gain access to the prone basolateral epithelial surface. Epithelial invasion relies on direct injection of proteins—including IpaA, IpaB, IpaC, IpgB1, IpgD and VirA—into the cell cytoplasm by the pINV-encoded Type III secretion system (TTSS) Mxi/Spa. These effectors act locally to reorganise the host cell actin and microtubulin cytoskeletal networks; to dissociate the actin cytoskeleton from the plasma membrane; and to disrupt adhesion between cellular actin and the extracellular matrix (Schroeder and Hilbi, 2008). Consequently, the host cell membrane becomes ruffled into a micropinocytic pocket that ultimately engulfs and internalises the bacterium (**Figure 1.1**). *S. flexneri* are internalised in a vacuole that is destroyed by the combined actions of TTSS effectors IpaB, IpaC, and IpaD, releasing bacteria freely into the cell cytoplasm (High *et al.*, 1992; Bârzu *et al.*, 1997; Harrington *et al.*, 2006).

Within the cytoplasm, *S. flexneri* freely multiply and initiate motility through directed polymerisation of host actin (**Figure 1.1**). This process, termed actin-

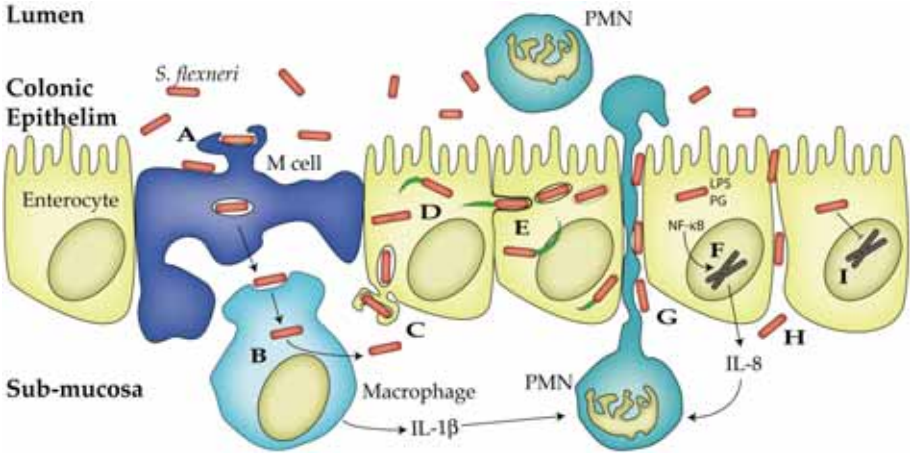

Figure 1.1: ***S. flexneri* pathogenesis**. (**A**) Ingested *S. flexneri* reach the colon and exploit M cell antigen sampling to traverse the epithelial barrier. (**B**) Bacteria are transcytosed to underlying lymphoid follicles and phagocytosed by resident macrophage. Shigellae induce inflammatory cell death of macrophages and are released into the sub-mucosa. (**C**) Bacteria invade the apical surface of the epithelium by triggering endocytosis into epithelial enterocytes. (**D**) Internalised bacteria escape the endocytic vacuole, replicate and undergo IcsA-dependent actin-based motility throughout the cytosol. (**E**) Motile *S. flexneri* form protrusions that are taken up by adjacent enterocytes. Vacuolar escape allows bacteria to resume a new cycle of replication, motility and intercellular spreading. (**F**) Internalised bacterial components, such as LPS and peptidoglycan, promote release of pro-inflammatory IL-8. The strong inflammation induced by *S. flexneri* in the sub-mucosa, attract polymorphonuclear (PMN) cells and promote PMN migration across the epithelium. (**G**) Migrating PMNs open an additional pathway for bacterial entry into the sub-mucosa. (**H**) Additionally, *S. flexneri* interferes with tight junctions for paracellular entry into the sub-mucosa. (**I**) *S. flexneri* also dampen inflammatory signalling through epigenetic control of enterocyte gene expression.

based motility (ABM), relies on the function of the IcsA (VirG) protein in engaging actin regulatory proteins and polymerising host soluble G-actin to filamentous F-actin, propelling bacteria throughout the cytosol with distinct trailing "comet tails" of polymerised actin (Lett *et al.*, 1989; Bernardini *et al.*, 1989). ABM propels bacteria throughout the cytoplasm and against the host plasma membrane, forming bacteria-containing protrusions that extend into adjacent enterocytes (**Figure 1.1**) (Goldberg, 2001). These protrusions are endocytosed and internalised in a double membrane vacuole (Kadurugamuwa *et al.*, 1991; Prévost *et al.*, 1992). Escape from this vacuole requires TTSS substrates IpaB, IpaC and IpaD (Schuch *et al.*, 1999; Rathman *et al.*, 2000a). *S. flexneri* are then free to initiate a new cycle of cytoplasmic

replication, intracellular motility and intercellular spreading (**Figure 1.1**). This process of intercellular spreading and dissemination of Shigellae throughout the colonic epithelium are key features of shigellosis. IcsA-dependent ABM is a prerequisite for such intercellular spread (Sansonetti *et al.*, 1994). Presumably, spreading is advantageous in broadening the infection focus in an environment protected from extracellular components of the immune system.

While the intracellular life-style of Shigellae minimises exposure to immune defences, the bacteria are also potent activators of inflammation. Cell death induced in infected macrophage elicits strong pro-inflammatory responses, releasing interleukin-1β (IL-1β) and IL-18 (**Figure 1.1**) (Zychlinsky *et al.*, 1994; Sansonetti *et al.*, 2000). Invasion of the epithelium also results in host signalling via pro-inflammatory bacterial components such (as lipopolysaccharide [LPS] and peptidoglycan), through nuclear factor-κB (NF-κB), promoting production and release of the chemokine IL-8 (Philpott *et al.*, 2000; Girardin *et al.*, 2003; Jung *et al.*, 1995; Sansonetti *et al.*, 1999). In turn, IL-8 recruits polymorphonuclear (PMN) cells to the site of infection (Singer and Sansonetti, 2004). Infiltration of PMN cells disrupts the integrity of the epithelium and opens a paracellular pathway for *Shigella* access to the basolateral surface (**Figure 1.1**) (Perdomo *et al.*, 1994). *Shigella* can also directly weaken tight junctions of the disrupted epithelium (Sakaguchi *et al.*, 2002), unlocking an additional avenue to the submucosa for further invasion of enterocytes (**Figure 1.1**). In this way, Shigellae are adept at exploiting inflammatory responses to the advantage of infection. Indeed, throughout pathogenesis, Shigellae retain the ability to modulate—positively and negatively—host immune responses. Remarkably, these abilities even extend to exerting epigenetic control over host gene expression by chromatin remodelling, to dampen pro-inflammatory signalling (**Figure 1.1**) (Zurawski *et al.*, 2009).

IcsA-dependent ABM is central to *S. flexneri* virulence in supporting motility, and in turn, allowing lateral spreading of infection throughout the epithelial layer. Bacterial spreading amplifies strong inflammatory host responses and leads to tissue destruction—hallmarks of *Shigella* pathology. Mutants deficient in ABM are highly attenuated in humans and all models of shigellosis (Makino *et al.*, 1986; Lett *et al.*, 1989; Kotloff *et al.*, 1996, 2002). Indeed, deletion of *icsA* is a prerequisite attenuating mutation of vaccine strains currently under development and in clinical trials (Levine *et al.*, 2007).

1.3 The IcsA autotransporter

Intracellular motility of *Shigella* was an early discovery from microscopic examination of bacteria within *in vitro* maintained epithelial monolayers. While the mechanisms that lead to bacterial motion were completely unknown, it was already apparent that motility exhibited asymmetry, with propulsion occurring at one bacterial pole (Ogawa *et al.*, 1968). The genetic basis for this motility was discovered during transposon mutagenesis of the virulence plasmid. Tn*5* insertions within an *Sal*I-*Eco*RI fragment of the virulence plasmid, termed *virG*, abolished the phenotype (Makino *et al.*, 1986). DNA sequencing helped later identify the 1,102 amino acid protein responsible, termed VirG by Lett *et al.* (1989). Concomitantly, Bernardini *et al.* (1989) also identified the protein (naming it IcsA, as the first identified protein involved in **i**nter**c**ellular **s**pread) and were the first to describe the underlying phenomenon driving motility, reporting IcsA-dependent accumulation of host F-actin at one bacterial pole of motile Shigellae.

ABM of *S. flexneri* has been studied using a range of model systems, including microscopy of infected tissue culture monolayers, *in vitro Xenopus* cell extracts, and protein reconstitution systems (Goldberg and Theriot, 1995; Egile *et al.*, 1999; Loisel *et al.*, 1999). Intercellular spreading ability of *S. flexneri* relies on efficient ABM and has likewise been investigated by microscopy of infected tissue culture monolayers, as well as (i) *in vitro* plaque formation assays, measuring destruction of adjacent cells following *S. flexneri* invasion of cell culture monolayers (Oaks *et al.*, 1985); and (ii) Sereny assays, detecting development of keratoconjunctivitis following *Shigella* infection of either guinea pig or mouse eye (Murayama *et al.*, 1986). Because spreading requires IcsA-dependent ABM, models of intercellular spreading are indirectly informative of the efficiency of IcsA function. In all these models, the requirement for IcsA expression is absolute; mutants lacking IcsA are non-motile and deficient for intercellular spreading (Goldberg and Theriot, 1995). Indeed, heterologous expression of IcsA in closely related *E. coli* K-12 confers the ability to polymerise actin and undergo ABM *in vitro* (Goldberg and Theriot, 1995; Kocks *et al.*, 1995).

1.3.1 *Activation of N-WASP in actin-based motility*

The requirement for host cell neural Wiskott-Aldrich Syndrome protein (N-WASP) in IcsA-dependent ABM of *Shigella* has been well established. *In vitro* depletion of N-WASP from cell extracts reduces F-actin tail formation, which can be restored when extracts are subsequently supplemented with purified N-WASP (Suzuki *et al.*, 1998). Likewise, in N-WASP-deficient cell lines, Shigellae retain ability for invasion and intracellular replication while, F-actin tail formation and intercellular spread are completely abrogated, but can be restored by expression of N-WASP in *trans* (Snapper *et al.*, 2001).

The activity of N-WASP is regulated primarily through auto-inhibition by an inherent intramolecular association of two domains (Kim *et al.*, 2000). Auto-inhibition seems to be stabilised by the WASP interacting protein (WIP) for the majority of cellular N-WASP (Ho *et al.*, 2001, 2004). WIP is also seen to be recruited to Shigellae inside cells (Moreau *et al.*, 2000). Activation of N-WASP by other proteins releases this interaction and exposes the binding site for the Arp2/3 complex of proteins that—when bound to N-WASP—support efficient polymerisation of soluble, globular actin monomers (G-actin) into insoluble filamentous actin (F-actin) (Kim *et al.*, 2000). N-WASP can, during the course of physiological processes, be activated by a range of host proteins: Cdc42 and phosphatidylinositol 4,5-bisphospate (PIP2) which can act synergistically; Nck; Grb2; and WISH (Miki and Takenawa, 2003). In addition, phosphorylation by Abl tyrosine kinase can enhance N-WASP activation (Miki and Takenawa, 2003).

The ability of IcsA to directly activate N-WASP remains incompletely understood, but IcsA, N-WASP and Arp2/3 form a complex that is capable of actin polymerisation *in vitro* (**Figure 1.2**) (Suzuki *et al.*, 1998; Egile *et al.*, 1999; Moreau *et al.*, 2000; Suzuki *et al.*, 2002). Other host factors such as profilin, Grb2, Toca-1 and Abl are required for efficient actin polymerisation, motility and *Shigella* intercellular spreading (Stevens *et al.*, 2006). Vinculin is the only other actin-regulatory protein proposed to directly interact with IcsA. However, the involvement of vinculin in ABM and intercellular spreading remains poorly defined and ligands of vinculin (such as VASP) do not seem to be involved in *S. flexneri* ABM (Ally *et al.*, 2004). Even the nature of the IcsA-vinculin interaction remains to be firmly established at molecular level (Suzuki *et al.*, 1998).

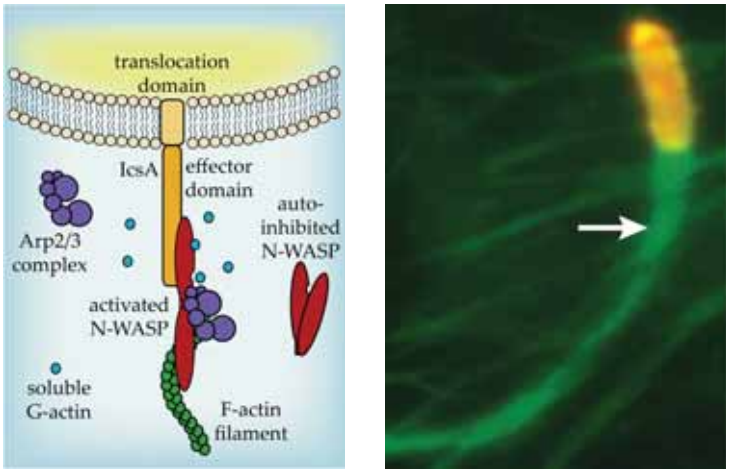

(a) (b)

Figure 1.2: **IcsA-dependent actin-based motility inside epithelial cells**. (**a**) The surface exposed effector domain of IcsA activates host cell N-WASP from its auto-inhibited state, exposing the host Arp2/3 complex binding site within N-WASP. The ternary complex polymerises globular G-actin to filamentous F-actin. While this ternary complex is sufficient to direct actin polymerisation *in vitro*, inside cells N-WASP auto-inhibition is additionally maintained by bound WIP protein (not shown). (**b**) Actin polymerisation produces motile force that propels *S. flexneri* (**orange**) throughout the cytosol with distinctive trailing "comet tail" (**arrow**) of actin filaments (**green**).

1.3.2 *A target of Autophagy*

IcsA has also been shown to interact with IcsB and Atg5 inside host cells. IcsB was initially identified as a mediator of vacuolar lysis following protrusion uptake during cell-to-cell spread, with mutants being trapped in the vacuole and consequently deficient in intercellular spread (Allaoui *et al.*, 1992). However, this mutation induced polar effects—notably among the *ipa* genes, now known to be required for vacuolar escape (Rathman *et al.*, 2000b). Whether a non-polar mutation of *icsB* leads to a spreading deficiency phenotype remains debated (Rathman *et al.*, 2000b; Ogawa *et al.*, 2003). More recently, IcsB secretion (via TTSS) has been detected within the host cell cytosol (Ogawa *et al.*, 2005). Exported IcsB was found to competitively bind IcsA from the host autophagy protein Atg5 (Ogawa *et al.*, 2005). In this way, the IcsA-IcsB interaction prevented Atg5 labelling of intracellular *S. flexneri* via IcsA and demarcating the bacterium for autophagic degradation, a novel avoidance mechanism of host defences.

1.4 IcsA structure and functional domains

IcsA is a member of the autotransporter family of proteins that collectively comprise the largest family of Gram-negative extracellular proteins (Pallen *et al.*, 2003). IcsA export from the cell proceeds via the Type Vb section pathway, a sub-group of autotransporter Type V secretion (Henderson *et al.*, 2004). Autotransporter proteins are prototypically divided into three domains: an N-terminal signal sequence directs secretion of the protein from the cytoplasm through the Sec translocon ($IcsA_{1-52}$); an internal effector domain (α-domain) determines the function of the mature protein ($IcsA_{53-758}$); and a C-terminal translocation domain (β-domain) anchors the protein into the outer membrane ($IcsA_{759-1102}$) (**Figure 1.3**) (Suzuki *et al.*, 1995; Henderson *et al.*, 2004). In outer membrane exported autotransporters, the effector domain is surface-exposed—where it can interact with ligands—and is anchored at the C-terminal to the outer membrane embedded translocation domain. Proteolytic cleavage and release of the effector domain from the cell is also a common strategy employed by autotransporters (Henderson *et al.*, 2004).

1.4.1 *The extended IcsA signal sequence*

The IcsA protein, along with a small subset of autotransporters, contains a 52 amino acid atypical extended signal sequence. Typical signal peptides consist of an N-terminal positively charged region (N region), an internal hydrophobic region (H region) and a C-terminal signal peptidase cleavage site (C region) and span 18-24 amino acids (Desvaux *et al.*, 2006). Atypical signal sequence extensions are phylogenetically restricted to autotransporters (Desvaux *et al.*, 2006). The extension is N-terminal and features both a second charged region (N1), and second hydrophobic region (H2), that are followed by the traditional signal sequence arrangement (N2, H2, C). The contribution of these signal peptide variants to protein biogenesis is still debated, and it may include targeting proteins to cotranslational export in a signal recognition particle (SRP)-dependent pathway (Peterson *et al.*, 2003; Sijbrandi *et al.*, 2003; Chevalier *et al.*, 2004). However, Brandon *et al.* (2003) have reported that translocation of IcsA is SRP-independent, and later work has implicated involvement of the DnaK chaperone (Janakiraman

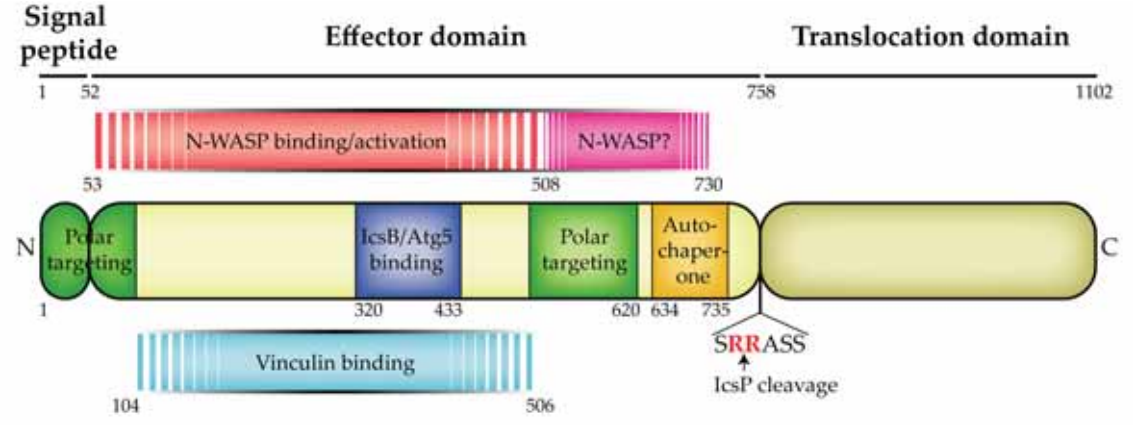

Figure 1.3: **IcsA functional domains**. IcsA comprises three major domains: an extended signal sequence ($IcsA_{1-52}$); an effector domain ($IcsA_{53-758}$); and a translocation domain ($IcsA_{759-1102}$). An N-WASP binding region ($IcsA_{103-433}$) has been reported, but a larger region ($IcsA_{53-508}$) is required for actin polymerisation. A vinculin binding region has been broadly placed within $IcsA_{104-506}$. Autophagy protein Atg5 and IcsB compete for binding to $IcsA_{320-433}$. Two regions are reported to direct polar targeting ($IcsA_{1-104}$ and $IcsA_{506-620}$). The IcsP protease cleaves IcsA between amino acids 758 and 759. May and Morona (2008) recently identified an autochaperone region ($IcsA_{634-735}$) and possibly an additional region ($IcsA_{508-730}$) capable of recruiting and activating N-WASP. Amino acid numbering is based on the VirG sequence from Lett *et al.* (1989).

et al., 2009). It seems more likely that extended signal peptides regulate the rate of protein export, thereby preventing improper folding in the periplasm (Chevalier *et al.*, 2004; Szabady *et al.*, 2005; Peterson *et al.*, 2006).

1.4.2 *The effector domain*

As with all autotransporters, the IcsA effector domain matures to a functional conformation once exported across the outer membrane (Henderson *et al.*, 2004). The effector domain is responsible for IcsA biological activity in ABM. The crystal structures of two effector domains (*Bortedella pertussis* P.96 Pertactin and *E. coli* Haemoglobin protease) adopt a right-handed parallel β-helical conformation (Emsley *et al.*, 1996; Otto *et al.*, 2005). Despite the divergent sequences—reflecting divergent functions—of effector domains across the autotransporter spectrum, modelling has predicted the conformation is overwhelmingly common among autotransporters (Bradley *et al.*, 2001; Junker *et al.*, 2006). Indeed, modelling using

the Robetta server set of modelling protocols (Kim *et al.*, 2004), predicts this structural arrangement for the IcsA effector domain (**Figure 1.4**) (May, 2007).

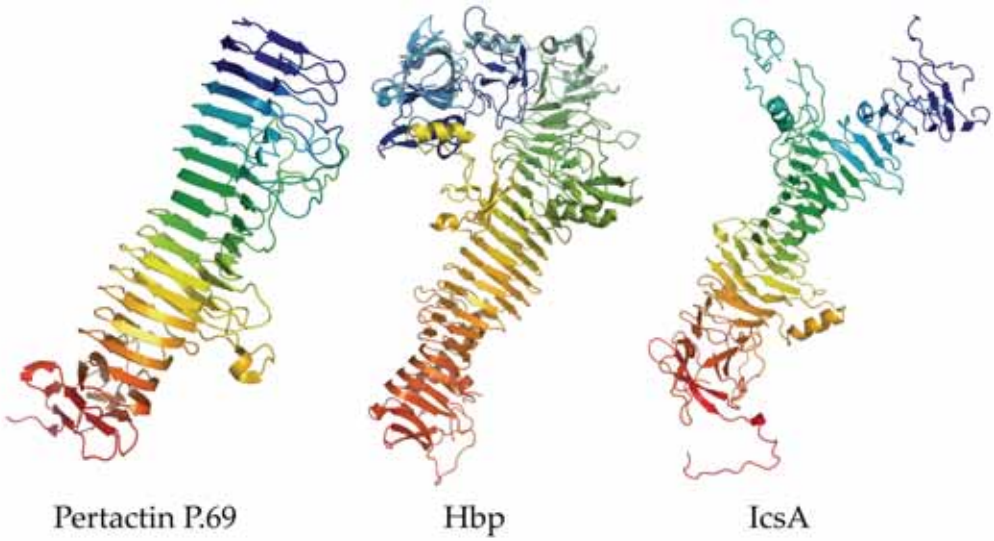

Figure 1.4: **Effector domain crystal structures of P.69 Pertactin and Hbp Haemoglobin protease and Robetta predicted IcsA effector domain structure**. Autotransporter effector domains form right-handed parallel β-helices, presumably as a backbone for variant functional domains. Topologically, N-terminals (**blue**) are furthest from the cell, and the effector domain is anchored into the outer membrane embedded translocation domain at the C-terminus (**red**). PDB identification for P.69 Pertactin structure is 1DAB (Emsley *et al.*, 1996); 1WXR for the Hbp structure (Otto *et al.*, 2005); structure prediction for IcsA was described by May (2007).

1.4.3 *N-WASP and vinculin binding regions*

The domain within IcsA that mediates the activation of N-WASP is incompletely defined. The region $IcsA_{103-433}$ is capable of binding N-WASP in pull-down assay (Suzuki *et al.*, 1998, 2002). However, *in vitro* studies suggest that a larger region ($IcsA_{53-508}$) is required for actin polymerisation (Suzuki *et al.*, 1996; Suzuki and Sasakawa, 2001). Indeed, deletion of $IcsA_{509-729}$ does not abrogate *S. flexneri* recruitment of N-WASP inside cultured cells (Suzuki *et al.*, 1998). This mutant also resulted in defective formation of F-actin tails, presumably due to loss of the polar targeting region $IcsA_{506-620}$ and the ensuing non-polar surface distribution (Suzuki *et al.*, 1996). However, May and Morona (2008) identified linker insertion

mutants within the polar targeting region that likewise lose unipolar distribution, but remained capable of F-actin tail formation, suggesting sequences within the $IcsA_{506-729}$ deletion could be involved in ABM. That same study demonstrated as much, when $IcsA_{\Delta 103-507}$ was seen to recruit N-WASP in *S. flexneri* LPS mutants that presumably improved the accessibility of the truncated IcsA protein. Additionally, vinculin has been proposed to interact with the $IcsA_{53-508}$ region.

1.4.4 *IcsP cleavage site*

Cleavage of autotransporters from the bacterial surface is a common occurrence—many even have auto-proteolytic activity (Henderson *et al.*, 2004). That IcsA was released from the *Shigella* surface was suggested following detection of IcsA throughout the F-actin tails trailing motile bacteria and *in vitro* secretion into supernatant (Goldberg *et al.*, 1993). A later study demonstrated that detection within tails was likely due to antiserum cross-reactivity (d'Hauteville *et al.*, 1996). Nonetheless, it is now well established that IcsA is cleaved by the pINV-encoded IcsP (SopA) outer membrane serine protease, an ortholog of the *E. coli* major outer membrane protease OmpT that is absent in *Shigella* (Lan and Reeves, 2002). IcsA is specifically cleaved between R758 and R759, releasing a 95 kDa fragment corresponding to the mature, functional effector domain (Fukuda *et al.*, 1995; d'Hauteville *et al.*, 1996; Egile *et al.*, 1997; Shere *et al.*, 1997; Steinhauer *et al.*, 1999). The relevance, if any, of the released IcsA product to pathogenesis remains unclear.

IcsP cleaves IcsA from the *Shigella* surface at low efficiency, leaving the majority of exported IcsA anchored to the outer membrane (Shere *et al.*, 1997; Steinhauer *et al.*, 1999). *E. coli* OmpT is likewise able to cleave IcsA, but at sufficiently high efficiency as to make IcsA undetectable on the cell surface (Goldberg *et al.*, 1993; Nakata *et al.*, 1993). Consequently, while functional IcsA can be expressed in *ompT*$^{-}$ K-12 strains to confer ABM, this cannot be achieved by expression in wild-type *E. coli* K-12 (Nakata *et al.*, 1993).

The loss of IcsP predictably results in an increase of detectable surface IcsA. As a consequence, the surface distribution of IcsA is altered from being unipolar to being circumferential with some polar reinforcement (Egile *et al.*, 1997; Shere *et al.*, 1997). However, there is disagreement on the effect of this altered IcsA localisation

on ABM and subsequent intercellular spread. While Egile *et al.* (1997) reported shorter protrusions and smaller plaques, Shere *et al.* (1997) recorded increased speed and frequency of motility, with wild-type-equivalent plaque formation. The use of different *Shigella* serotypes in these studies has confounded consensus; neither strain- nor serotype-specific differences can be excluded. Recently, a direct comparison of defined Δ*icsP* mutations in both strains investigated to-date, has found wild-type equivalent plaque formation consistently between the strains and supports the results of Shere *et al.* (1997) (communicated E. Tran, University of Adelaide).

Another approach to scrutinising the IcsA-IcsP relationship has been the use of non-cleavable IcsA variants $IcsA_{R758D}$, and $IcsA_{R758D+R759D}$. Expression of these proteins in substitution of $IcsA_{WT}$ also increases the amount of detectable IcsA and results in non-polar surface distribution. Fukuda *et al.* (1995) reported this increase in IcsA actually improved virulence. Their mutant retained wild-type-equivalent F-actin tail formation and plaque formation, while being more virulent than the wild-type parent in Sereny assays (Fukuda *et al.*, 1995). Contrary to this, d'Hauteville and Sansonetti (1992) observed altered accumulation of polymerised F-actin, which was not polar and often perpendicular to the long axis of the bacterium. This phenotype might be expected to reduce the efficiency of ABM and intercellular spread, but analysis of neither was reported.

IcsA proteolysis by IcsP reinforces unipolar surface distribution of the protein, but IcsP is not involved in the establishment of the polar gradient, which occurs prior to cytoplasmic translocation in *S.flexneri* and bacteria that lack IcsP (Section 1.8). Recent evidence by Wagner *et al.* (2009) suggests that IcsP acts to maintain quality control in the periplasm of proteins including IcsA destined for export.

1.4.5 *IcsB and Atg5 binding region*

As described in Section 1.3.2, IcsB and Atg5 compete for IcsA binding. Both IcsB and Atg5 could be pulled down using the same truncated effector domain constructs, ultimately refined to the region $IcsA_{320-433}$ (Ogawa *et al.*, 2005). Additionally, Shigellae expressing IcsA lacking the region 319-507 ($IcsA_{\Delta 319-507}$), did not label with GFP-LC3 autophagosome marker inside cells (Ogawa *et al.*, 2005).

1.4.6 *Phosphorylation region*

A phosphorylation consensus sequence (SRRASS; $IcsA_{756-762}$) had been identified and *in vitro* data suggested IcsA could be the target of host cyclic-dependent protein kinases (d'Hauteville and Sansonetti, 1992). Phosphorylation was touted to be a host strategy for reducing IcsA activity. In support of this notion, a R759D substitution variant of IcsA could not be phosphorylated *in vitro*, and expression of the protein by *S. flexneri* presented a phenotype marked by increased actin-based motility and improved intercellular spreading (d'Hauteville and Sansonetti, 1992). Subsequent identification of this region as the processing site for the IcsP protease, suggests the described phenotype could have arisen due to increased expression of IcsA owing to a lack of cleavage from the bacterial surface (Fukuda *et al.*, 1995; d'Hauteville *et al.*, 1996). Notably, failure to detect phosphorylated IcsA inside host cell supports this revised notion (d'Hauteville and Sansonetti, 1992; Frischknecht *et al.*, 1999).

1.4.7 *Polarity determining regions*

Two regions of the effector domain ($IcsA_{1-104}$ and $IcsA_{506-620}$) have been reported to be independently capable of delivering the nascent protein to the polar region of the cytoplasm for export, and subsequently dictate the polar surface distribution of IcsA (Charles *et al.*, 2001). Polar targeting provides an IcsA-concentrated focus for actin polymerisation that propels the bacterium (Sandlin *et al.*, 1995; Robbins *et al.*, 2001a). The mechanism of polar targeting is a focus of the work contained herein and a detailed review is presented in Section 1.8.

1.4.8 *Autochaperone regions*

A region of autotransporter effector domains, designated the autochaperone region, is thought to assist in protein export from the periplasm. Mutations in these regions detrimentally affect the folding of effector domains, leaving them susceptible to protease digestion (Ohnishi *et al.*, 1994; Dutta *et al.*, 2003; Oliver *et al.*, 2003b; Berthiaume *et al.*, 2007). An autochaperone region had been putatively identified as $IcsA_{634-735}$ by homology with the autochaperone region

described for the *B. pertussis* autotransporter BrkA (Oliver *et al.*, 2003b). Support for the presence of an IcsA autochaperone region comes from the phenotypes of IcsA insertion mutants between amino acids 633 and 716 that exhibit surface misfolding and reduced protein expression (May and Morona, 2008).

1.4.9 *The translocation domain*

As with conventional autotransporters, the IcsA translocation domain is assembled as a β-barrel comprised of 12 β-strands (Suzuki *et al.*, 1995; Oomen *et al.*, 2004; Barnard *et al.*, 2007). A subclass of autotransporters assemble as a homotrimeric complex, with each protein providing four β-strands to a β-barrel that is comparable to conventional autotransporters (Robert *et al.*, 2006). The translocation domain serves to anchor the effector domain into the outer membrane of the cell, and is essential for the translocation of the effector domain from the periplasm (Henderson *et al.*, 2004). The C-terminal residues are critical in directing export of the protein (Robert *et al.*, 2006). The export, assembly and structure of translocation domains—and their contribution to effector domain export—are further described in Section 1.5.3.

1.5 IcsA synthesis and export

1.5.1 *Cytoplasmic translocation*

In *S. flexneri*, optimal IcsA expression is appropriately coupled to environmental stimuli that occur once the bacterium has reached the colon. Expression is promoted by the VirF transcriptional factor, a thermally-regulated master inducer of pINV genes (Adler *et al.*, 1989; Dorman and Porter, 1998). Optimal induction occurs at 37°C in the presence of mild osmotic stress and physiological pH (Dorman and Porter, 1998). Additionally, a newly discovered antisense RNA, RnaG, that is expressed from the complementary strand of *icsA* acts to repress gene expression (Giangrossi *et al.*, 2010). Data cited by Giangrossi *et al.* (2010) suggest VirF may antagonise RnaG inhibition by directly stimulating expression from the *icsA* promoter, while also repressing expression from the RnaG promoter.

IcsA is exported unfolded from the cytoplasm. Delivery of IcsA to the export apparatus does not require the signal recognition particle (SRP) pathway, but rather could rely on the DnaK chaperone which prevents premature protein folding in the cytoplasm (Brandon *et al.*, 2003; Janakiraman *et al.*, 2009). While DnaK is capable of involvement in protein export, the SecB-dependent pathway is the major route of outer membrane protein translocation from the cytoplasm and is presumed to be involved in autotransporter export (Wild *et al.*, 1992; Henderson *et al.*, 2004). It is presently unknown whether SecB contributes to—or indeed predominates—IcsA chaperoning. Translated IcsA is exported through the SecYEG translocon when one is available (Brandon *et al.*, 2003). The signal sequence is lost during the translocation of IcsA into the periplasm.

1.5.2 *Periplasmic transit*

IcsA is only present transiently in the periplasm; the translocation domain seems to be rapidly inserted into the outer membrane while secretion of the effector domain across the outer membrane may be the rate-limiting step of export (Brandon and Goldberg, 2001). While in the periplasm, IcsA is in a protease-resistant, partially folded conformation and may form a single intramolecular disulfide bond (Brandon and Goldberg, 2001). This soluble intermediate is maintained by periplasmic chaperones DegP, Skp and SurA (Purdy *et al.*, 2002, 2007; Sklar *et al.*, 2007b; Wagner *et al.*, 2009). These chaperones are critical to IcsA export. In a *degP* mutant, the IcsA effector domain is liable to misfolding, despite the correct folding and membrane insertion of the translocation domain (Purdy *et al.*, 2002, 2007). Such misfolded IcsA, when presented at the *Shigella* surface, results in less efficient intercellular spreading (Purdy *et al.*, 2002, 2007). The action of these periplasmic chaperones is therefore thought to maintain the effector domain in a state competent for translocation across the outer membrane (Wagner *et al.*, 2009). Additionally, the intra-molecular autochaperone region of autotransporters seems to improve export from the periplasm, though is not essential (Oliver *et al.*, 2003a,b; Velarde and Nataro, 2004).

1.5.3 *Crossing the outer membrane*

Autotransporter export results in the formation of a membrane-embedded translocation domain β-barrel, and surface exposure of a folded and functional effector domain. This secretion method was unique among the Gram-negative generalised secretion pathways, since export across the outer membrane was thought to be entirely independent of other accessory proteins—hence a form of autotransportation (Pohlner *et al.*, 1987). However, recent discoveries in the biogenesis of the outer membrane seem to have debunked this notion. The *E. coli* BamA outer membrane protein—in concert with an associated complex of lipoproteins—is essential for the membrane insertion of β-barrel proteins (Voulhoux *et al.*, 2003; Voulhoux and Tommassen, 2004; Wu *et al.*, 2006; Sklar *et al.*, 2007a). Indeed, the absolute requirement of BamA for IcsA assembly into the outer membrane has been directly demonstrated by Jain and Goldberg (2007).

While it is now clear that BamA is essential for membrane insertion of the translocation domain β-barrel, the mechanism by which the effector domain of autotransporters is exported has long been controversial, with four mechanisms proposed (**Figure 1.5**) (Henderson *et al.*, 2004). Two of these—the threading and hairpin models—involve passage of the effector domain through a pore formed by the β-barrel of the membrane-inserted translocation domain.

In the threading model, the effector domain is threaded through the pore from the N-terminus (**Figure 1.5**) (Oomen *et al.*, 2004). However, the N-terminus does not possess targeting sequences which could direct this mechanism and exogenous peptide fusions to translocation domains are export competent (Suzuki *et al.*, 1995; Maurer *et al.*, 1999; Skillman *et al.*, 2005; Szabady *et al.*, 2005). In the other model, a hairpin structure is proposed to form inside the β-barrel, with the effector domain then sliding through from the C-terminus (**Figure 1.5**) (Pohlner *et al.*, 1987; Jose *et al.*, 1995). Supporting both these models, a small polypeptide of the region immediately N-terminal to the translocation domain of the *Neisseria meningitidis* NalP and *E. coli* EspP autotransporters is seen as an α-helical region within the β-barrels of the respective crystal structures (**Figure 1.6**) (Oomen *et al.*, 2004; Barnard *et al.*, 2007). However, modelling suggests that these narrow β-barrels cannot accommodate the passage of folded polypeptides (Khalid and Sansom, 2006). Despite this, autotransporter (including IcsA) folding

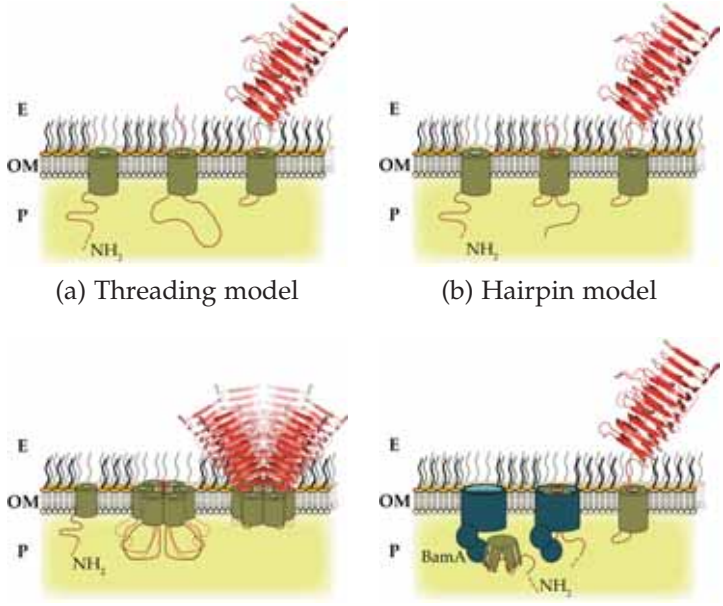

(a) Threading model (b) Hairpin model

(c) Oligomer model (d) BamA model

Figure 1.5: **Effector domain export across the outer membrane**. (**a**) The hairpin model proposes that the unfolded effector domain in the periplasm (P) passes from the N-terminus through the β-barrel formed by the outer membrane (OM) embedded translocation domain and is folded into an active conformation at the cell surface (E). (**b**) The hairpin model proposes the linker region between the effector and translocation domains inserts into the β-barrel and the protein is pulled from from the C-terminus. (**c**) The oligomer model proposes that oligomerisation of translocation domains of some autotransporters can assemble a larger pore through which even partially folded effector domains can pass. (**d**) The BamA model proposes that a proto-barrel is formed in the periplasm, and BamA simultaneously translocates both the effector and translocation domains.

in the periplasm has been reported, and folded proteins are competent for periplasmic secretion by fusion to translocation domains (Brandon and Goldberg, 2001; Skillman *et al.*, 2005).

A third model has arisen from the identification of homo-oligomerisation of the translocation domain of the conventional autotransporter IgA1 protease of *Neisseria meningitidis* (Veiga *et al.*, 2002). In this model, effector domain export is proposed to proceed through the larger central pore formed by oligomerised translocation domains (**Figure 1.5**). To-date, this oligomeric structure has only been observed for IgA1 protease and not in other autotransporters (Veiga *et al.*,

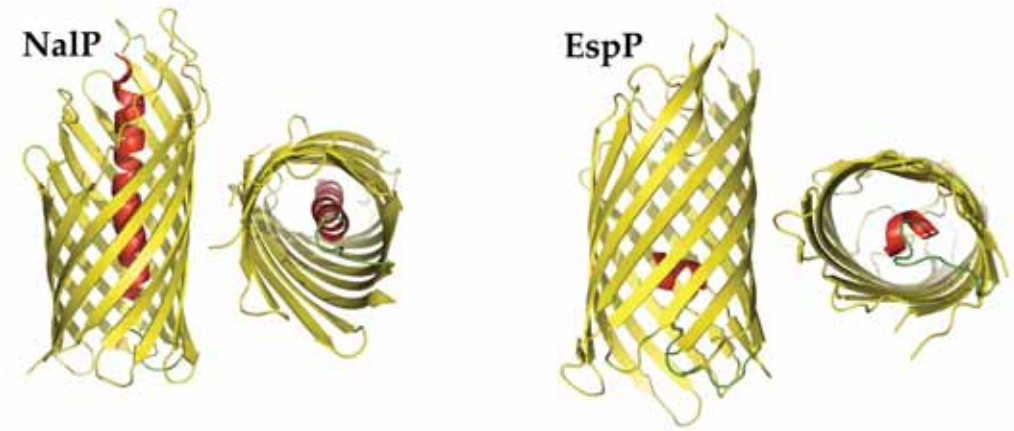

Figure 1.6: **Crystal structures of NalP and EspP β-barrels**. A small α-helical peptide (**red**) N-terminal from the translocation domain is present within the assembled translocation domain β-barrels (**yellow**) of the NalP and EspP autotransporters, and is linked by a short linker region (**green**). PDB identification for NalP structure is 1UYO (Oomen *et al.*, 2004); and 2QOM for the EspP structure (Barnard *et al.*, 2007).

2002; Oomen *et al.*, 2004; Müller *et al.*, 2005; Skillman *et al.*, 2005). Consequently, oligomerisation may only be applicable to a select subset of autotransporters.

A more recent investigation has presented strong evidence favouring a fourth model, where effector domain export is largely exogenous and assisted by BamA (**Figure 1.5**) (Ieva *et al.*, 2008; Ieva and Bernstein, 2009). At-least in the case of EspP, folding into a pre-assembly proto-barrel conformation occurs in the periplasm. At the same time, a region of the effector domain inserts into the proto-barrel (reflecting the crystallographic evidence). The Bam complex then simultaneously exports the effector domain while inserting the translocation domain into the outer membrane. During this export, the N-terminal end of the effector domain is chaperoned in the periplasm in a translocation-competent state. In this model, the essentiality of the translocation domain is maintained by its role in targeting the export of the protein through BamA. Indeed, the final C-terminal residues of the translocation domain were reported to constitute species-specific targeting signals for *E. coli* BamA and its *N. meningitidis* homologue, Omp85 (Robert *et al.*, 2006).

1.6 The interplay between lipopolysaccharide and IcsA

Once exported and embedded into the outer membrane, the exposed effector domain of IcsA is able to engage its substrates. However, the surrounding LPS context of the outer membrane is influential in not only the ability of IcsA to interact with its cognate host cell interactors, but also in the spatial distribution of IcsA at the *Shigella* surface.

1.6.1 *Lipopolysaccharide*

Lipopolysaccharide (LPS) is the major constituent of outer face of the outer membrane. The structure of LPS can be broadly defined by three key components—lipid A, core sugars, and O-antigen—that are synthesised independently but assembled prior to translocation across the outer membrane (**Figure 1.7**) (Nikaido, 2003). The lipid A component anchors the molecule within the outer membrane and is critical for maintaining the integrity of the outer membrane barrier function in Gram-negative bacteria (Ruiz *et al.*, 2009). However, lipid A-deficient mutants of *N. meningitidis* and *E. coli* K-12 have been reported (Steeghs *et al.*, 1998; Meredith *et al.*, 2006). The core sugar region is assembled on lipid A. O-antigen (Oag), a polysaccharide polymer of variable length, is attached to the core. The length of the Oag chain is determined by the polysaccharide co-polymerase family of proteins, with each member imparting a characteristic modal value for the number of Oag repeats displayed at the surface (Morona *et al.*, 2009). In *S. flexneri 2a*, the chromosome encoded Wzz_{SF} regulates the polymerisation of short (S) type (12-17 repeat units); while a plasmid-borne Wzz_{pHS-2} mediates the polymerisation of very long (VL) type (>90 repeat units) (Morona *et al.*, 1995; Hong and Payne, 1997).

1.6.2 *The IcsA-LPS relationship*

In terms of virulence, *S. flexneri* require LPS for resistance against innate immune responses. Mutation of the non-essential genes within the Oag biosynthetic pathway (*galU*, *wecA*, *wzy*, *rfb*, *rmlD*) yield truncated LPS molecules lacking the Oag chain termed 'rough LPS'; wild-type LPS retains the Oag chain and is termed

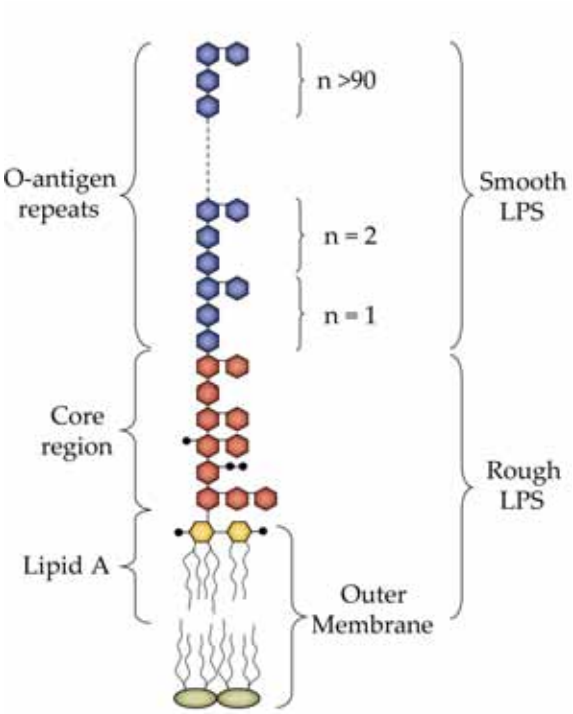

Figure 1.7: **Structure of lipopolysaccharide (LPS)**. LPS consists of three components. The lipid A component forms the outer leaflet of the outer membrane and is critical for cell viability in *E. coli* and *S. flexneri*. The core region is ligated to lipid A and links a polysaccharide of polymerised O-antigens (Oag). The number of Oag repeats is variable among LPS molecules, but is regulated in *S. flexneri* 2a by two Wzz polysaccharide co-polymerases, each imparting a modal length to the Oag polysaccharide component.

'smooth LPS'). Such mutations have demonstrated the additional requirement of smooth LPS for the normal function of IcsA-dependent ABM and intercellular spread (Okada *et al.*, 1991; Sandlin *et al.*, 1995, 1996; Hong and Payne, 1997; Van Den Bosch and Morona, 2003). Clear interpretation of this dependence on the LPS context for IcsA function is complicated by essentiality of LPS for cell viability and pleiotropy affecting the distribution of IcsA.

While surface expression of IcsA at the *Shigella* (and *E. coli*) surface is confined to one pole in smooth strains, unipolarity is lost in rough mutants and IcsA can be detected over the entire bacterial surface with a polar cap (Van Den Bosch *et al.*, 1997; Robbins *et al.*, 2001a). Two hypotheses have been put forward explaining this loss of polarity. The first of these, proposes that rough mutations alter the biophysical properties of the outer membrane in lowering the barrier to diffusion.

Increased diffusion is suggested to permit polar IcsA migration to non-polar sites on the cell surface (Rottem and Leive, 1977; Yeh and Jacobs, 1992; Robbins *et al.*, 2001a). The alternative view contends that loss of Oag allows for observation of IcsA at non-polar sites that is otherwise undetectable (by both antibodies and IcsA substrates) due to masking by steric hindrance of Oag polymers in smooth strains (Morona *et al.*, 2003; Morona and Van Den Bosch, 2003a). That both diffusion and greater surface exposure are cooperatively at play in causing loss of IcsA polarity remains plausible, and both are reviewed herein. Moreover, while loss of unipolarity is generally cited as the cause of the impaired ABM phenotype, over-expression of IcsA in a smooth strain, to attain a rough mutant-equivalent circumferential localisation, does not seem to compromise the wild-type ABM phenotype (Morona and Van Den Bosch, 2003b). This finding may hint at a more fundamental role for LPS in the function of IcsA, though to-date no such direct functional interaction has been demonstrated.

The nature of the outer membrane environment likely contributes significantly to the virulence of bacteria. In *Shigella*, a *vacJ* mutant remained competent for invasion and intracellular replication, but was defective in vacuolar escape during the process of intercellular spread (Suzuki *et al.*, 1994). VacJ (now named MlaA) has recently been shown to be an outer membrane lipoprotein involved in preventing accumulation of phospholipids in the outer leaflet of the outer membrane (Malinverni and Silhavy, 2009). Insertion of phospholipids leads to increased outer membrane permeability that could either directly account for the reported defective virulence, or indirectly affect the function of other virulence factors (Malinverni and Silhavy, 2009).

IcsA diffusion in the outer membrane

Early studies suggested that the Oag chain length of LPS molecules is a key determinant of outer membrane fluidity, such that fluidity increases with shortening Oag polymer (Rottem and Leive, 1977; Yeh and Jacobs, 1992). Consequently, the circumferential localisation of IcsA on the surface of rough LPS expressing bacteria could arise from increased membrane fluidity permitting greater diffusion away from the polar site of export. Indeed, indirect immunofluorescence detecting surface IcsA can be fitted to an exponential decay function in bacteria expressing smooth LPS, and the function is significantly shallower in the absence

of Oag, possibly suggesting lateral diffusion away from the pole (Robbins *et al.*, 2001a).

Outer membrane diffusion is supported by a study of LamB λ phage receptor in *E. coli*. Single particle tracking revealed a helical spiral distribution pattern and distinct populations of membrane-embedded LamB: a rapidly moving, fluid population; and a slower, essentially immobile population (Gibbs *et al.*, 2004). However, subpopulations of LamB attach non-covalently to the underlying cell wall peptidoglycan, which itself is constantly being re-modelled along a helical track. Whether these observations of diffusion hold true for proteins—such as autotransporters—that are integrated solely into the outer membrane remains unknown. Moreover, while LamB motion was observed along the cell lateral body, whether the outer membrane surface at the poles is comparably fluid is also unknown. A broader investigation into the behaviour of all surface proteins in *E. coli* has suggested the presence of stable and immobile islands of protein and LPS at the pole, amid more fluid regions along the lateral body (Ghosh and Young, 2005).

IcsA masking by LPS

An alternate view of IcsA behaviour in the outer membrane, purports that IcsA is exported preferentially at the pole, but that export can also occur along the lateral body of the bacterium. In this model, the masking nature of LPS reduces the ability to detect the low concentration lateral IcsA, and by the same token, ability of ligands to interact with this same IcsA population. Effectively, LPS masking is suggested to sharpen the polar gradient generated in the cytoplasm (Morona *et al.*, 2003). Indeed, Morona and Van Den Bosch (2003a) showed that when *S. flexneri* expressing smooth LPS and unipolar IcsA distribution were chemically fixed and the Oag component of LPS enzymatically removed (to reveal the underlying constituents of the outer membrane), subsequent IcsA localisation was revealed to be circumferential and comparable to that observed for rough mutants. Moreover, in *S. flexneri* expressing IcsA solely from an arabinose-inducible promoter, the induction of protein expression in smooth *S. flexneri* resulted in wild-type equivalent unipolar distribution of nascent IcsA as observed by indirect immunoflourescence of chemically fixed cells. However, hydrolysing the LPS Oag of these fixed bacteria, revealed existing lateral populations of nascent IcsA

and a circumferential distribution equivalent to that observed in rough mutants (Morona and Van Den Bosch, 2003a). These data support a hypothesis that IcsA export is directed to the poles, but also occurs at the lateral regions, and that masking by LPS sharpens the unipolar gradient.

1.7 Bacterial cell biology and the cell cycle

Bacterial cell division is an energetically expensive process that demands accurate and faithful replication and division of genetic material and cellular proteins. Belying early models of a simple cell cycle, a range of cytoskeletal components and structures that permit bacteria to accomplish division with fidelity and accuracy has been brought to light. Together, these systems coordinate the temporal sequence of cell division, the spatial distribution of replicated genetic content between mother and daughter cell, and the placement of the septum. The ability of bacteria to target proteins (such as IcsA) to the pole has been an intriguing instance of subcellular organisation in cells that not long ago were considered simple bags of enzymes and nucleic acids.

Many of the components of the bacterial cytoskeleton have been seen to adopt complex and dynamic spatial distributions. Since these proteins regulated the cell at the fundamental levels of cell architecture, cell cycle and cellular division, they were optimistically seen as likely contributors to the mysterious mechanism that provided cues for subcellular positioning of other proteins, such as the polar delivery of IcsA. Consequently, the quest to elucidate the process of polar targeting proceeded almost in parallel with studies of the prokaryotic cytoskeleton, and the contribution of many cytoskeletal proteins has been directly scrutinised.

1.7.1 *Staying in shape: MreB, the actin homologue*

The cell shape of *E. coli* is determined by the rigid cell wall composed of cross-linked peptidoglycan (Lutkenhaus, 2007). Mutagenesis of the *mre* locus transformed rod shaped *E. coli* into spherical cells, some with associated sensitivity to cell wall inhibitors (Wachi *et al.*, 1987). MreB was identified as the cytoskeletal protein that governed cell shape and ultimately proved to be a prokaryotic structural homologue of eukaryotic actin (van den Ent *et al.*, 2001). Indeed, gene

homologues of *mreB* have been phylogenetically correlated with non-spherical bacteria (Jones *et al.*, 2001). MreB can bind either ATP or GTP to polymerise into two parallel stranded filaments (Esue *et al.*, 2005, 2006). Filaments of MreB have been seen as helical structures at the cytoplasmic membrane extending along the length of the cell (Kruse *et al.*, 2003). MreB is widely thought to be essential to *E. coli*; depletion of MreB, or its chemical inhibition, leads to large irregularly rounded cells that are not viable (Iwai *et al.*, 2002; Gitai *et al.*, 2005; Nilsen *et al.*, 2005).

MreB interacts with MreC (a dimeric bitopic inner membrane protein), that in-turn interacts with MreD (an inner membrane protein) (Kruse *et al.*, 2005; van den Ent *et al.*, 2006). In the periplasm, MreC recruits cell wall synthesising penicillin binding proteins (PBPs) (Divakaruni *et al.*, 2005, 2007; van den Ent *et al.*, 2006). Additionally, MreC seems to form helices that alternate with MreB (Dye *et al.*, 2005). It has been proposed that MreB helices interact with MreCD inner-membrane helices, and the MreBCD proteins thereby exert spatial and temporal control over cell wall synthesis and, consequently, cell shape (Kruse *et al.*, 2005; Gerdes, 2009). Indeed, a fluorescent derivative of cell wall inhibitor vancomycin was helically incorporated into *E. coli* cell wall (Varma *et al.*, 2007). However, a recent result suggests that MreB is not alone in controlling helical deposition of cell wall, and have implicated the helically distributed FtsZ prokaryotic tubulin homologue (Varma *et al.*, 2007, 2008).

MreB has additionally been implicated in segregation of replicated chromosomes and polar protein targeting (Madabhushi and Marians, 2009; Karczmarek *et al.*, 2007; Kruse *et al.*, 2003, 2006; Nilsen *et al.*, 2004). Consequently, it was suggested that MreB filaments within helices may define the topology of the longitudinal axis of *E. coli*. However, single molecule tracking experiments in *C. crescentus* revealed MreB is polymerised into short filaments that undergo actin-like treadingmilling, and that lack any uniform orientation or polarity (Kim *et al.*, 2006). Moreover, while loss of MreB filaments leads to an irregular spherical-like shape morphology, designated intracellular polar and septal sites can still be identified (Nilsen *et al.*, 2004). Therefore, it seems unlikely that global cellular positional cues—including polar targeting—are derived directly from MreB filaments, but this remains to be conclusively determined.

1.7.2 *The FtsZ tubulin homologue*

Cellular division in prokaryotes is driven principally by the action of the FtsZ protein, a structural homologue of eukaryotic tubulin (Löwe and Amos, 1998). The *ftsZ* gene is broadly conserved among bacteria, archea, chloroplasts and some mitochondria (Lutkenhaus, 2007). FtsZ protofilaments assemble into the Z ring: a ring structure at the cytoplasmic face of the inner-membrane (**Figure 1.8**). This Z ring demarcates the site of cell division, recruits a host of accessory proteins that assist in septation, and drives cytokinesis (Lutkenhaus, 2007).

FtsZ is polymerised into highly dynamic protofilaments in a GTP-dependent assembly (de Boer *et al.*, 1992; RayChaudhuri and Park, 1992). FtsZ polymerisation is polarised and protofilaments are extended in a head-to-tail fashion (Mukherjee and Lutkenhaus, 1994). GTP hydrolysis by FtsZ is rapid and contributes to the frequent turnover of subunits—with an approximate half-life of 10 seconds— in

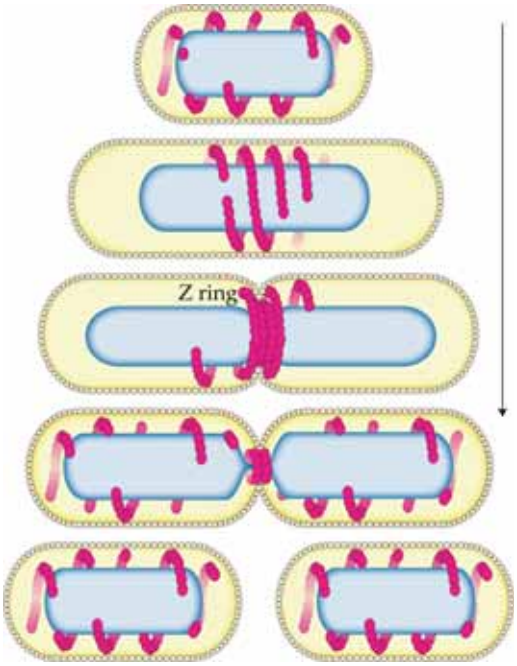

Figure 1.8: **FtsZ helices and Z ring**. FtsZ (**pink**) polymerisation leads to filaments of highly dynamic helices at the cytoplasmic membrane. Lateral interactions between FtsZ protofilaments likely contribute to assembly of the Z ring and the ring is tethered to the membrane by ZipA and FtsA. Z ring formation is spatially restricted by the Min system to the mid-cell and temporally regulated by nucleoid occlusion to preventing Z ring closure over segregating chromosomes (**blue**).

FtsZ protofilaments (Stricker *et al.*, 2002; Chen and Erickson, 2005). Consequently, only short FtsZ protofilaments are possible, and the Z ring consists of a network of such protofilaments (Lutkenhaus, 2007). Lateral interactions between protofilaments had been reported and have recently been validated *in vivo*—in *Bacillus subtilis*—as critical in the assembly and function of the Z ring (Erickson and Stoffler, 1996; Erickson *et al.*, 1996; Löwe and Amos, 1999; Monahan *et al.*, 2009).

In vivo, FtsZ protofilaments undergo a transition from helical distribution that spans length of the cell, to a condensation at the mid-cell and finally formation of the Z ring (Thanedar and Margolin, 2004; Peters *et al.*, 2007). Lateral association of protofilaments is critical to this transition, and presumably aids in stabilising the Z ring structure (Monahan *et al.*, 2009). The cell cycle cue for this FtsZ transition has remained elusive.

The Z ring requires the function of ZipA and FtsA proteins that tether the ring to the inner-membrane (Hale and de Boer, 1997, 1999; Liu *et al.*, 1999; Hale *et al.*, 2000; Pichoff and Lutkenhaus, 2005). In turn, these proteins sequentially recruit accessory proteins (Hale and de Boer, 1999; Pichoff and Lutkenhaus, 2002). Consequently, the assembled Z ring acts as a molecular scaffold for the recruitment and assembly of accessory proteins involved in septation and chromosome segregation. During cytokinesis, the Z ring constricts, exerting an inward force on the cytoplasmic membrane and the Z ring remains at the leading edge of the septum, driving septal invagination (Bi and Lutkenhaus, 1991; Addinall and Lutkenhaus, 1996; Osawa *et al.*, 2008). The mechanism of Z ring constriction remains poorly defined, and no motor proteins analogous to eukaryotic dynein or kinesin have yet been found in prokaryotes. Indeed, it is becoming apparent that lateral biophysical interactions of FtsZ protofilaments within the Z ring are sufficient to produce directional contractile force (Dajkovic *et al.*, 2008; Osawa *et al.*, 2008; Lan *et al.*, 2009; Osawa *et al.*, 2009).

1.7.3 *Placing the Z ring: the oscillating Min system*

Spatial regulation of the division plane—the site of Z ring formation and constriction—in *E. coli*, and many other bacteria, is determined by the dynamic action of the Min system (Lutkenhaus, 2007). The system comprises three proteins encoded by the *minCDE* locus. The production of small anucleate minicells that arise from

the poles of mother cells is the hallmark of the *min* mutant phenotype (Adler *et al.*, 1967; Teather *et al.*, 1974). When such misplaced division occurs, it also results in mother cells that have increased average length than wild-type *E. coli* cells. This correlation indicated that the poles—like the mid-cell—are valid division sites that are inhibited in wild-type cells. Mechanistic insight into this inhibition emerged following observations that FtsZ overexpression yielded minicells in otherwise wild-type *E. coli*, and suggested these bacteria overcame Min-mediated suppression present at the poles (Ward and Lutkenhaus, 1985). This inhibition of FtsZ polymerisation is achieved by a highly dynamic series of interactions between MinC, MinD and MinE that rapidly oscillate from pole to pole (Raskin and de Boer, 1999).

The underlying foundation to this oscillation is the interaction between MinD, the inner membrane and MinE (Lutkenhaus, 2007). MinD is an ATPase that binds to the inner membrane via a C-terminal amphipathic helical region that inserts asymmetrically into anionic phospholipids (Szeto *et al.*, 2002; Mileykovskaya *et al.*, 2003; Zhou and Lutkenhaus, 2003). Membrane insertion of MinD is reversible, requires ATP and favours homodimerisation (Hu *et al.*, 2002; Szeto *et al.*, 2003). MinC is the effector of Z ring inhibition and is recruited to the membrane by MinD, which increases the inhibitory activity (de Boer *et al.*, 1992). MinC does not inhibit FtsZ GTPase activity and presumably prevents lateral interactions between protofilaments, destabilising Z ring formation (Hu *et al.*, 1999; Lutkenhaus, 2007; Lan *et al.*, 2008). MinE is an inhibitor of the MinCD complex. MinE displaces MinC from membrane bound MinD and then activates its ATPase activity, thereby releasing MinD from the membrane (Hu and Lutkenhaus, 2001).

In a convincing and elegant model of Min oscillation that mirrors experimental observations, Huang *et al.* (2003) propose the oscillation of this system is accomplished by slow nucleotide exchange of MinD-ADP to MinD-ATP (**Figure 1.9**). In this oscillation, MinC—although the effector of system—is a passenger molecule (Raskin and de Boer, 1999). As MinCD forms a polar zone at a denoted old pole, MinE is recruited and displaces MinC. MinE then stimulates membrane detachment of MinD-ATP, and release of the ADP form. MinD-ADP undergoes a slow nucleotide exchange for ATP and the cytoplasmic pool of MinD-ATP in the vicinity of the old pole is drained by cooperative binding by dimerisation into the membrane that already contains bound MinD. This allows an increase in cy-

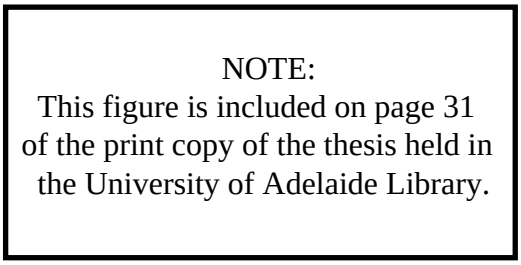

Figure 1.9: **Oscillation of the Min system**. Oscillation of the Z ring inhibitory Min system about the long bacterial axis of *E. coli* is accomplished by the nature of the MinE interaction with MinD, and MinC is a passenger in the system. MinD-ATP binds to the inner membrane, recruiting MinC. MinCD act to prevent localised FtsZ assembly into a cytokinetic Z ring. A ring of MinE displaces MinC, binding MinD and activating its ATPase activity, that displaces MinD from the membrane. MinD-ADP undergoes a slow nucleotide exchange and this leads to a depletion of MinD-ATP at the first pole, since cytoplasmic MinD-ATP binds cooperatively to the present membrane bound MinD. At the opposite pole, the cytoplasmic concentration of MinD-ATP increases and membrane binding begins, again recruiting MinC and establishing a new zone of Z ring inhibition. The MinE ring then begins to displace the leading edge of this new MinCD zone. Figure adapted from Lutkenhaus (2007).

toplasmic MinD-ATP concentration at the opposing pole, as nucleotide exchange proceeds. MinD-ATP then binds the membrane at the pole and forms a new polar zone of MinCD. As MinE completes displacement of MinD at the old pole, it is recruited as a ring to the leading edge of the new MinCD polar zone, and the process resumes. Oscillation of the MinCD inhibitor of Z ring formation about the polar regions has a periodicity of approximately 40 seconds. The time-averaged minimum concentration of Z ring inhibitor MinCD occurs at the mid-cell. Thus, in this dynamic way, the Min system is capable of placing the division place at the mid-cell position.

However, the Min system is not alone in ensuring accurate Z ring formation. In cells that are made anucleate through interference in chromosome segregation, the Z ring is placed with less accuracy than in nucleated cells, indicating the involvement of additional factors (Sun and Margolin, 1998). Moreover, the Z ring continues to form at the mid-cell, between nucleoids, in *min* mutants (Yu and

Margolin, 1999). The latter observation lead to the nucleoid occlusion hypothesis that suggests active prevention of septation over the nucleoids (Woldringh *et al.*, 1991). The *E. coli* SlmA protein is involved in nucleoid occlusion (Bernhardt and de Boer, 2005). SlmA prevents Z ring assembly and is distributed asymmetrically over the nucleoid and predominantly at the replicated regions of segregating chromosomes (Bernhardt and de Boer, 2005). It seems that as the nucleoids are segregated away towards opposing poles, SlmA is removed from the mid-cell, permitting Z ring formation and septation in the nucleoid-free region.

1.7.4 *Chromosome replication*

The earliest models of bacterial DNA partitioning proposed that chromosomes were attached to the cytoplasmic membrane and were separated passively during cell elongation prior to cell division. Such models belied the evolutionary adaptiveness afforded to organisms with generation times measured in minutes, and the picture emerging from the laboratory suggests the requirement for faithful inheritance of genetic material has lead prokaryotes to develop dynamic and tightly regulated mechanisms for chromosome replication and segregation.

The *E. coli* chromosome is highly condensed and occupies a specific region within the cytoplasm, termed the nucleoid (Thanbichler and Shapiro, 2006a). Choreographed DNA segregation is particularly important for *E. coli*, since the bacterium is optimally capable of multiple generations before the completion of a single round of DNA replication (Cooper and Helmstetter, 1968). Multifork replications present as many as eight origins of chromosome replication within a single cell that must be resolved into progeny cells by appropriate coupling to cellular division and septation (Lutkenhaus, 2007).

Chromosome dynamics and segregation

Chromosome replication is initiated by the DnaA protein at the *oriC* locus, the chromosomal origin. DnaA activity is regulated to ensure synchrony and timeliness of replication in the cell cycle (Kaguni, 2006). Soon after being replicated at the mid-cell, sister *oriC* loci move rapidly towards opposing poles and are positioned at the respective quarter cell positions, such that *oriC* is located at the mid-cell of progeny cells (**Figure 1.10**) (Webb *et al.*, 1998; Lau *et al.*, 2003;

Reyes-Lamothe *et al.*, 2008). This motion outpaces cell elongation, disproving early models of passive DNA segregation (Webb *et al.*, 1998; Viollier *et al.*, 2004). Chromosomal loci proximal to *oriC* are also seen to sequentially migrate in opposing directions once replicated (**Figure 1.10**) (Lau *et al.*, 2003; Viollier *et al.*, 2004). During this segregations, the left-right architecture of the chromosome is maintained (**Figure 1.10**) (Wang *et al.*, 2006). The underlying mechanism driving *oriC* separation, and the subsequent movement of the bulk of the replicated chromosomal DNA is presently poorly understood.

Current proposals contend that forces of DNA replication, transcription, or transertion (the coupling of co-transcriptional translation and cytoplasmic translocation that could transiently link chromosomal loci to the inner membrane) could be sufficient to drive *oriC* motion and chromosome segregation (Dworkin and Losick, 2002; Kruse *et al.*, 2006; Woldringh and Nanninga, 2006). In support of these notions, RNA polymerase has been reported to be required for *oriC* and DNA segregation and its inhibition rapidly stops segregation in *E. coli* and *B. subtilis* (Dworkin and Losick, 2002; Kruse *et al.*, 2006). Despite this, others contend that rifampicin inhibition of RNA polymerase does not cause defective segregation (communicated in Reyes-Lamothe *et al.*, 2008). The implication of RNA polymerase involvement in segregation remains to be fully resolved.

The discovery of *migS*, a centromere-like sequence near *oriC* that may mediate the pole-ward migration of the replicated *oriC*, has not aided identifying the segregation mechanism, and *migS* is not ultimately required for bulk DNA segregation (Yamaichi and Niki, 2004). Gitai *et al.* (2005) reported that, in *C. crescentus*, MreB was required for the initial bidirectional polar movement of replicated origins, but was not required for chromosome segregation thereafter. Similar implication of MreB involvement was reported in *E. coli* by Kruse *et al.* (2006). These findings suggest that movement of replicated *ori*s may be distinct from the movement of bulk chromosomal DNA. However, a direct role for MreB in segregation remains to be conclusively demonstrated, and has been challenged (Karczmarek *et al.*, 2007). Moreover, polar positional markers seem to be retained despite MreB chemical inhibition in *E. coli* (Nilsen *et al.*, 2005).

An elegant solution to the observed segregation patterns may ultimately be derived from the biophysical properties of the compacted nucleoid (Jun and Mulder, 2006). Upon replication, sister *oriC* regions would be strongly self-avoiding

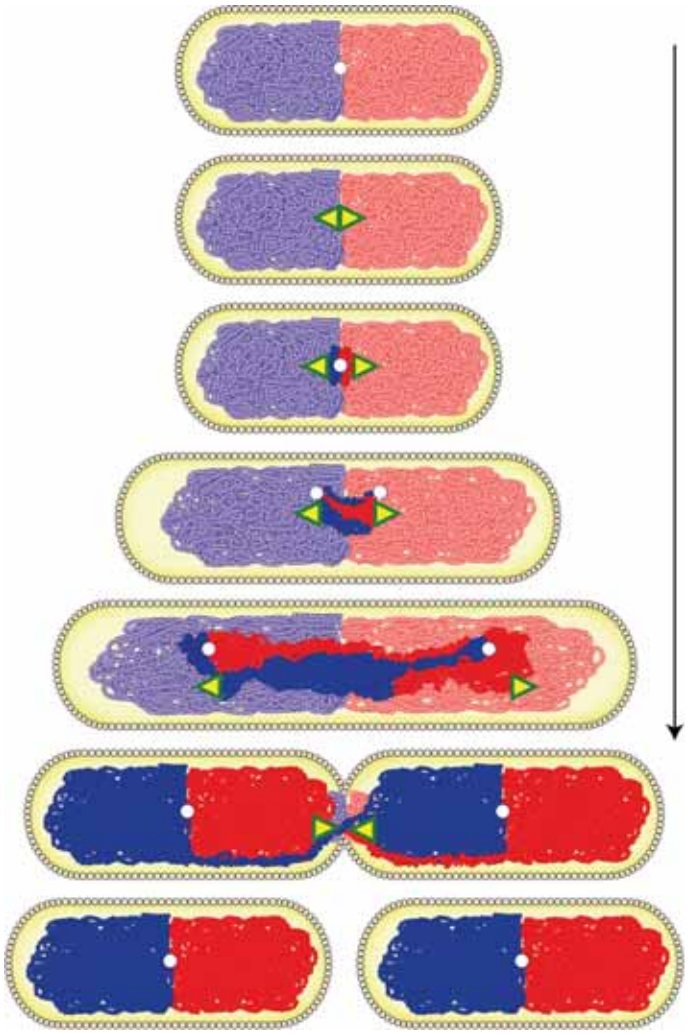

Figure 1.10: **Dynamics of replicated chromosomes in *E. coli*.** Chromosome replication is triggered by DnaA at *oriC* (**white**). Bidirectional replication is triggered, and DNA replication complexes (**yellow triangles**) proceed along the left (**pale blue**) and right (**pale red**) arm of the chromosome. Soon after being replicated, sister *oriC* loci migrate towards opposing poles. Loci proximal to *oriC* follow sequentially once replicated so that the replicated left arm (**dark blue**) and the replicated right arm (**dark red**) adopt left-right orientation. Unreplicated DNA remains in the nucleoid. MukBEF retains *oriC* at the quarter cell positions that correspond to the mid-cell of progeny cells. As replication approaches the chromosome *ter* region at mid-cell, FtsK and XerCD resolve recombination events, dimers and catenanes, permitting final translocation of chromosomes into daughter cells and cytokinesis to conclude. Figure adapted from Reyes-Lamothe *et al.* (2008).

when confined to the small volume of the cytoplasm. This repulsive force could spontaneously produce the experimentally observed segregation (Jun and Mulder, 2006). As bidirectional replication proceeds, distal loci would likewise be repelled. A recent report that DnaA forms helices along the inner-membrane may provide an additional mechanism, since DnaA is specific for *oriC* and is the earliest recruit in replication (Boeneman *et al.*, 2009).

The complex of MukBEF proteins binds to the *oriC* region and is involved in maintaining the organisation of the chromosome during segregation (Danilova *et al.*, 2007). MukBEF additionally facilitates retention of *oriC* positioning at the quarter cells position as chromosome replication continues prior to cell division (**Figure 1.10**) (Danilova *et al.*, 2007). In *mukBEF* mutants, *oriC* is placed polarly, at the periphery of the nucleoid (Danilova *et al.*, 2007).

As replication forks proceed to the mid-cell located *ter* region of termination sequences, the actions of FtsK (a component of the cytokinetic ring) and XerCD at the mid-cell allow for resolution of sister nucleoids and couple the final translocation of chromosomes into daughter cells with the closing of the septum (**Figure 1.10**) (Bigot *et al.*, 2005, 2007).

1.8 IcsA polar targeting

The discovery that IcsA is displayed at one pole of *S. flexneri*, rationalised the earliest observations of polar actin polymerisation and motility (Goldberg *et al.*, 1993, 1994). Specifically, IcsA is displayed at the "old pole"—the pole not derived from the previous septum (Goldberg *et al.*, 1993). Polar protein targeting is now recognised across a spectrum of bacterial species and is applied to a range of proteins, including a number of autotransporters (Janakiraman and Goldberg, 2004b; Jain *et al.*, 2006). Understanding the mechanism generating polar spatial organisation of proteins in bacteria became an important goal amid the burgeoning field of bacterial cell biology. Because the regions of IcsA involved in polar targeting had been defined (see below), IcsA became a key model for probing polar targeting mechanisms.

Heterologous expression of IcsA in *E. coli ompT* strains preserved the polar surface distribution of the protein, and excluded involvement of *S. flexneri* pINV gene products in delivering IcsA to the pole. Later, Charles *et al.* (2001) identified

two regions of the IcsA protein that independently imparted the polar positioning information. When either $IcsA_{1-104}$ or $IcsA_{506-620}$ were fused to GFP, fluorescence was restricted to foci at the polar regions of *E. coli* or *S. flexneri* (Charles *et al.*, 2001). Fusions with other regions of IcsA resulted in diffuse fluorescence throughout the cell. This important study demonstrated that polar targeting was achieved in the cytoplasm and prior to translocation, since the $IcsA_{506-620}$-GFP fusion does not possess export sequences, and since GFP fusions exported through the SecYEG translocon do not fluoresce outside the cytoplasm (Thomas *et al.*, 2001). A later study demonstrated that the Sec translocon likely does not impart positioning informations since it appears to be evenly distributed throughout the inner-membrane of *E. coli* (Brandon *et al.*, 2003).

1.8.1 *Multiple pathways for polar targeting*

Earlier work presumed the existence of a common and broadly conserved mechanism of polar targeting. Indeed, it was demonstrated the polarly localised EpsM, a component of the type II secretion machinery in *Vibrio cholera*, was co-localised to polar regions that corresponded to $IcsA_{506-620}$ localisation in *E. coli* and shape defective mutant derivatives (Scott *et al.*, 2001; Nilsen *et al.*, 2004). Likewise, the *B. subtilis* cell division protein DivIVA is also capable of polar distribution in *E. coli*, and even in the fission yeast *Schizosaccharomyces pombe* (Edwards *et al.*, 2000). More recently, *Lactococcus lactis* LI.LtrB mobile group II intron reverse transcriptase LtrA was identified as targeted to both poles when a GFP fusion was expressed in *E. coli* (Zhao and Lambowitz, 2005). Indeed, LtrA was reported to outcompete $IcsA_{506-620}$-GFP for polarity, raising hope of a common polar targeting mechanism in *E. coli* (Zhao and Lambowitz, 2005). However, a subsequent study by the same group concluded that cytoplasmic concentration of polyphosphate was the determinant of LtrA polar localisation (Zhao *et al.*, 2008). High concentrations of polyphosphate displaced LtrA from the poles, probably by direct binding to the basic protein (Zhao *et al.*, 2008). In contrast, the slightly acidic (pI = 7.1) $IcsA_{506-620}$ polar targeting region was unaffected by polyphosphate concentration, and a GFP fusion remained unipolar (Zhao *et al.*, 2008). While spatial regulation of LtrA by polyphosphate represents an elegant mechanism, polar targeting of IcsA clearly proceeds along an independent pathway.

1.8.2 *Scrutinising the role of the bacterial cytoskeleton*

Contemporaneously, the progress being made in understanding newly discovered elements of the bacterial cytoskeleton was being applied to addressing polar targeting. The tubulin homologue FtsZ that forms the cytokinetic ring (Section 1.7.2) does not seem to be involved in establishing $IcsA_{506-620}$ polar targeting. Indeed, the process of septation does not seem to provide polar positioning cues. Inhibition of cell wall building PBP3/FtsI with the antibiotic aztreonam prevents closing of the septum and results in filamented *E. coli* cells (Janakiraman and Goldberg, 2004a). In these cells, $IcsA_{506-620}$ fused to GFP remains polarly positioned and also appears as foci at regular intervals along the length of the filament. These foci correspond to nuceloid-free regions that are potential division sites inhibited by the antibiotic. Indeed, Z rings localise to sites adjacent to these foci (Janakiraman and Goldberg, 2004a). Inhibition of FtsZ function also filamentous cells, and a comparable phenotype is seen when $IcsA_{506-620}$-GFP is visualised in a *ftsZ84* temperature-sensitive strain (Janakiraman and Goldberg, 2004a).

Because it places the division site, the Min system (Section 1.7.3) could have established the regularly spaced intervals marked as future poles that have been seen in filamented *E. coli*. However, in a Δ*minCDE* mutant, $IcsA_{506-620}$ remained at intervals throughout the cell (Janakiraman and Goldberg, 2004a). Clearly, positional cues remained in these filaments, suggesting Min is not required for polar targeting. Moreover, despite the presence of $IcsA_{506-620}$-GFP in nucleoid-free regions, the process of nucleoid occlusion did not perturb polar localisation (Janakiraman and Goldberg, 2004a).

As introduced in Section 1.7.1, chemical inhibition of MreB filaments with the specific inhibitor A22 results in altered cell shape morphology. In these cells, $IcsA_{506-620}$-GFP forms distinct foci that co-localise with those formed by fluorescent fusions with EpsM (another polarly targeted protein) (Nilsen *et al.*, 2005). Consequently, it was believed that polar spatial cues were preserved in *mreB*-deficient cells despite loss of shape. This view seems confirmed by heterologous expression of the novel actin homologue—MamK from magnetotactic *Magnetospirillum* spp.—that forms a long filament spanning the length of rod-shaped *E. coli* from pole-to-pole. In MreB-deficient, spherical cells, the MamK filaments

remain orientated towards ectopic poles that are marked by fluorescently tagged $IcsA_{506-620}$ (Pradel *et al.*, 2006).

To-date, no polar landmark protein that could guide polar targeting has been discovered in *E. coli*, despite their existence in *B. subtilis* and *C. crescentus* (Edwards and Errington, 1997; Huitema *et al.*, 2006; Lam *et al.*, 2006). How polar patterning of the long axis is imposed in *E. coli* is yet to be resolved. Despite this, insight into this process has come from mutants lacking low molecular weight PBPs (LMW PBPs) (de Pedro *et al.*, 1997; Pedro *et al.*, 2003; Nelson and Young, 2000, 2001; Nilsen *et al.*, 2004). While these are non-essential for *E. coli* viability, their loss results in deformed, bent, and kinked shape morphologies. The tips of these branched cell protrusions likely correspond biochemically to poles, since $IcsA_{506-620}$-GFP and EpsM-GFP are both attracted to these sites, in addition to recognisable poles (Nilsen *et al.*, 2004). While it is unclear how these ectopic poles arise, it has been suggested that loss of LMW PBPs introduces an imbalance in either FtsZ substrates or dependent reactions, thereby triggering misplaced synthesis of septal cell wall that would normally establish a new pole (Young, 2003). In support of cell wall involvement in landmarking the pole, findings by Pradel *et al.* (2007) suggest the polar demarcation that attracts targeting of $IcsA_{506-620}$ is imposed—at least in part—by periplasmic factors.

Studies of the involvement of the prokaryotic cytoskeleton, while valuable and informative in excluding components, have so far yielded few clues as to the mechanism of polar protein positioning.

1.8.3 *Other factors implicated in IcsA polar localisation*

The *S. flexneri phoN2* encoded apyrase (ATP-diphosphohydrolase) carried on pINV has been implicated in intercellular spreading, and a *phoN2* mutation was reported to result in loss of IcsA unipolarity (Santapaola *et al.*, 2006). Apyrase is a periplasmic enzyme that is capable of depleting host ATP following invasion, a metabolic hallmark of *Shigella* infection (Santapaola *et al.*, 2006). It remains unclear how apyrase might act in the polar targeting process, particularly since the enzyme's dNTP hydrolysing activity of apyrase was not required for the observed IcsA polarity and no direct interaction could be detected (Santapaola *et al.*, 2006).

1.8.4 *Genetic and proteomic approaches to polar targeting*

A recent proteomic screen by Janakiraman *et al.* (2009) for cytoplasmic *E. coli* proteins that form FtsZ-independent polar foci when fused to GFP, identified DnaK as being polarly targeted. DnaK co-localised with $IcsA_{506–620}$, and was required for polar placement of $IcsA_{506–620}$ (Janakiraman *et al.*, 2009). Since DnaK is a chaperone with many targets, it remains to be seen if DnaK acts directly to establish polarity or if its depletion in that study interferes with the folding (or export) of as yet unidentified components of the polar targeting mechanism.

To-date, it has been difficult to isolate mutations that perturb IcsA polar targeting. One such recent attempt visually screened more than 7,000 *E. coli* mutants and identified only *mreB*, mutation of which resulted in cell shape defects but preserved sites of polar positioning (Nilsen *et al.*, 2005). This difficulty could itself be informative, potentially being a consequence of the essentiality of the polar targeting mechanism (or components) to cell viability. The lack of an effective screening procedure has hampered genetic means to address polar targeting, but the continued advances in computational image analysis hold the promise of exciting prospects.

1.9 Aims of this work

The work presented herein sought to investigate the biogenesis and behaviour of IcsA, as a key virulence determinant of *S. flexneri*. Among the key aims of this work was to identify components and determine the mechanism that generates cytoplasmic polar targeting of IcsA. Additionally, this work sought to further investigate the relationship between IcsA and LPS at the bacterial surface, and to characterise the properties of the protein in the outer membrane. A method that allows specific and rapid labelling of nascent exported IcsA was sought to directly assess the properties of IcsA in the outer membrane. The state of IcsA in the outer membrane was also investigated, with the goal of verifying if IcsA is capable of oligomerisation.

2

Materials and Methods

2.1 Chemicals and reagents

Unless otherwise stated, chemicals and reagents were sourced from the following suppliers: Ajax (Analytical grade), Amresco, BDH Chemicals (AnalaR grade), Difco, Gibco BRL, New England Biolabs, Roche and Sigma-Aldrich.

2.1.1 *Antibodies and antisera*

Affinity purified rabbit polyclonal anti-IcsA antisera was made by Luisa Van Den Bosch from our laboratory as described by Van Den Bosch *et al.* (1997). The anti-IcsA antibody was used at 1:500-1:4000 for Western immunoblotting and 1:50-1:100 for immunofluorescence microscopy. The mouse anti-FLAG M2 (F3165; Sigma-Aldrich) and rabbit anti-FLAG antibody (F7425; Sigma-Aldrich) was used at 1:1000-1:2000 for Western immunoblotting. Mouse antibodies against the His_6 epitope (70796-3; Novagen) were used for Western immunoblotting at dilutions of 1:700-1:2000.

2.2 Bacterial strains and plasmids

A listing of *Escherichia coli* and *Shigella flexneri* host strains described in the results of this work is presented in Appendix A. Cloning vectors and plasmids used in these studies are listed in Appendix B. A complete list of strains constructed during the work is presented in Appendix G.

2.3 Bacterial growth media

2.3.1 *Liquid growth media*

All *E. coli* and *S. flexneri* strains were grown at 37°C or, for temperature sensitive strains, at 30°C and 42°C (as appropriate) in Luria Bertani (LB) broth (LB, 10 g/L tryptone [BD Bioscience], 5 g/L yeast extract [BD], 5 g/L NaCl) with the appropriate antibiotics unless stated otherwise. Additionally, the following liquid media were used for cultivation of bacteria: Tryptic soy broth (TSB, 30 g/L TSB [BD]); and SOC (20 g/L tryptone [BD], 5 g/L yeast extract, 20 mM glucose, 8.6 mM NaCl, 2.5 mM KCl, 20 mM $MgSO_4$). For high protein yield, Terrific broth (24 g/L yeast extract, 12 g/L tryptone, 0.4 [v/v] glycerol, 0.017 mM KH_2PO_4, 72 mM K_2HPO_4) was used. All were prepared in distilled water and sterilised by autoclaving.

2.3.2 *Solid growth media*

Solid growth media used were: Luria Bertani agar (15 g/L Bacto-agar [BD] in LB); Tryptic soy agar (TSA, 15 g/L Bacto-agar in TSB); R-TOP soft agar (10 g/L tryptone, 8 g/L NaCl, 1 g/L yeast extract, 8 g/L agar, autoclaved and supplemented with 2 mM $CaCl_2$, 0.1% [w/v] glucose); R-agar plates (R-TOP agar with 12 g/L of agar).

In order to confirm virulence-plasmid expression in *Shigella*, strains were grown on TSA supplemented with 0.01% (v/v) Congo Red solution and incubated at 37°C, a permissive temperature for virulence-plasmid expression of dye binding proteins. Virulence-plasmid positive colonies appeared red, while virulence-plasmid negative colonies appeared white. When blue/white colony screening was required, plates were supplemented with 40 μg/ml 5-bromo-4-chloro-3-indolyl-β-D-galactoside (X-Gal; Progen) and 0.5 mM isopropyl-β-D-thiogalacto-pyranoside (IPTG; Biovectra). Blue/white selection allowed identification of recombinant plasmids in suitable *E. coli* via disruption of the LacZα peptide in cloning plasmids such as pGEMT-Easy (Promega) and pBBR1MCS2 (Kovach *et al.*, 1995).

For the selection of tetracycline sensitivity (Tc^S) from Tn*10* carrying bacteria, the adaption of Bochner's media (Bochner *et al.*, 1980) described by Maloy and Nunn (1981) was used. Since the selection of trimethoprim resistance (Tp^R) is impeded by the presence of thymidine in LB medium, Mueller-Hinton (MH; Difco) broth and agar were used.

2.3.3 *Antibiotics and Congo Red solution*

When selection was required, antibiotics were added to broths and solid media at the following concentrations: ampicillin (Ap), 100 μg/ml; chloramphenicol(Cm); gentamicin (Gm) 50 μg/ml; kanamycin sulphate (Km), 50 μg/ml; tetracycline (Tc) 50 μg/ml, trimethoprim (Tp) 10 μg/ml. Antibiotics were also used for cell assays: 30 μg/ml cephalexin, 150 μg/ml rifampicin, 40 g/ml anhydrotetracycline (AhTc). Stocks of Congo Red solutions were made with 1% (w/v) Congo Red (Sigma) in Milli Q water (MQ, 18.2MΩcm^{-1}; Millipore).

2.4 Maintenance of bacterial strains

2.4.1 *General*

Bacterial strains were maintained in a suspension of 30% (v/v) glycerol and 1% (w/v) peptone (Difco) in glass vials (Wheaton) for long-term storage at -70°C. Cultivation from glycerol stocks was achieved by streaking a loop-full of the frozen suspension onto LB agar plates or TSA plates supplemented with Congo Red, with appropriate antibiotics.

2.5 Nucleic acid methods

2.5.1 *Isolation of bacterial DNA*

Chromosomal DNA was isolated using the Wizard Genomic DNA purification kit (Promega), in accordance with the manufacturer's instructions. Plasmid DNA was isolated using the QIAprep spin miniprep kit (Qiagen), in accordance with the manufacturer's instructions.

2.6 Analysis of DNA

2.6.1 *DNA quantitation*

DNA concentration was determined by the measurement of absorption at 260 nm with the assumption that an optical density of 1.0 is equal to 50 μg/ml of double stranded DNA. Purity of DNA was assessed using the ratio of A_{260nm} to A_{280nm}. Purified DNA with a ratio of approximately 2.0 was considered sufficient for further manipulation.

2.6.2 *Restriction endonuclease digestion of DNA*

Restriction digests of plasmid DNA and PCR amplicons for either analytical purposes or in preparation for *in vitro* cloning (Section 2.9.4) were performed with 1-2 μg of DNA with the appropriate enzyme(s) (2 U of each) in the commercial buffers provided by New England Biolabs (NEB; Buffers 1-4) as per the manufacturer's instructions. Restriction enzyme digests intended for gel extraction (Section 2.8.1), were performed on a larger scale with 4-8 μg of DNA in an 80 μl reaction volume. Wherever possible, restriction enzymes were heat inactivated according to the manufacturer's instructions, prior to further manipulation.

2.6.3 *Agarose gel electrophoresis*

DNA samples for electrophoresis were added to one-tenth volume of tracking dye (1 mg/ml bromophenol blue, 20% [v/v] glycerol, 0.1 mg/ml RNase; boiled for 30 min) and loaded onto 1-2% (w/v) agarose gels in 1 x TBE buffer (67 mM Tris, 22 mM boric acid, 1 mM EDTA). The DNA samples were electrophoresed at 80-120 V for 45-60 min in 1 x TBE. Gels were stained for 5 min in distilled water containing 2 μg/ml ethidium bromide and de-stained in distilled water for 15-30 min. Alternatively, gels were stained in 3× GelRed (Biotium) DNA bands were visualised using an UV trans-illuminator and photographed using either a Mitsubishi video imaging system (Tracktel) or GelDoc XR system (Biorad).

2.6.4 *Calculation of DNA fragment length*

The sizes of DNA fragments were determined according to their relative mobilities along an agarose gel relative to the DNA fragments of *Eco*RI digested bacteriophage SPP1 or *Hpa*II digested pUC19 DNA standards. The SPP1 sizes (kb) were 8.51, 7.35, 6.11, 4.84, 3.59, 2.81, 1.95, 1.86, 1.51 1.39, 1.16, 0.98, 0.72, 0.48, 0.36 and 0.09. SPP1-*Eco*RI digested molecular weight standards were prepared as described by Ratcliff *et al.* (1979). The pUC19 sizes (bp) were 501, 489, 404, 331, 242, 190, 147, 111, 110, 67, and 34. pUC19-*Hpa*II digested molecular weight standards were purchased from Geneworks.

2.6.5 *DNA sequencing*

DNA sequencing was performed on extracted plasmid DNA (Section 2.5.1), using the ABI Prism Dye Terminator Cycle Sequencing Ready Reaction Kit TM. Reactions totalled 12 µl and consisted of 100 ng of template, 50 pmoles of primer, 4 µl of BIG DYE reaction mix (Version 3.1). The sequencing reaction consisted of 25 cycles (95°C for 30 sec, 50°C for 15 sec, 60°C for 4 min) followed by a hold at 4°C in an Eppendorf Mastercycler. The 12 µl reaction mix was adjusted to a volume of 20 µl by the addition of 8 µl of MQ. Then the reaction mix was purified to using a Sodium acetate/ethanol precipitation method. 20 µl samples were added to 80 µl of a precipitation solution (3.0 µl of 3M sodium acetate, 62.5 µl of 95% [v/v] ethanol, 14.5 µl MQ) and incubated for 1 h at RT. The DNA was pelleted by centrifugation (13,200×*g*, 20 min, 4°C) and washed in 250 µl of 70% (v/v) ethanol and centrifuged for 5 min as before. The supernatant was discarded and the pellet dried for 1 h at RT. Sequencing reactions were analysed at the Australian Genomic Research Facility (AGRF), Gehrmann laboratories, University of Queensland and AGRF, Plant Genomics Centre, University of Adelaide.

2.7 DNA amplification

2.7.1 *Synthesis of oligodeoxynucleotides*

Oligodeoxynucleotides (primers) used in this study were purchased from Geneworks (Adelaide). Oligonucleotides used for epitope assembly are presented in Appendix D; oligos used for sequencing are listed in Appendix E; and oligos used for cloning are presented in Appendix F. Primers were supplied in lyophilised form and resuspended in MQ water at a concentration of 100 pmoles/µl and stored at -20°C. Working stocks of primers were made by further diluting in MQ water to 50 pmoles/µl.

2.7.2 *Polymerase chain reaction (PCR)*

PCR from either vector or genomic template was performed in a 20 µl reaction volume containing PCR buffer (NEB), 1-2 U of Taq DNA polymerase (NEB), 20 pmoles of each primer, at least 100 ng DNA template, 200 µM of dNTPs (Sigma). PCR reactions were performed in an Eppendorf Mastercycler and subjected to 20 amplification cycles with conditions adjusted according to the specific DNA being amplified. A standard cycle involved denaturation of the template at 95°C for 30 sec, annealing of primers to the DNA was at a temperature 1°C below the primer melting temperature (T_m), estimated from the calculation T_m= 2°C (A+T) + 4°C (G+C) followed by extension at 72°C. The extension time was calculated according to a replication rate of 1 kb of DNA per minute. Similarily, PCR products intended for cloning were amplified with Phusion high-fidelity DNA polymerase (Finnzymes), though a standard PCR cycle involved denaturation at 98°C for 30 s, and extension at 72°C at a replication rate of 15 s per 1 kb.

2.8 DNA purification

2.8.1 *DNA gel extraction*

80 µl restriction enzyme digested DNA samples were added to 8 µl of tracking dye (Section 2.6.3) and were electrophoresed in 1% (w/v) low melting point

agarose (Progen) in TBE. 80 µl was used for gel extraction and loaded into a central well; 4 µl samples were loaded into flanking wells. The flanking lanes were cut from the rest of the gel and stained with ethidium bromide or GelRed. The position of the desired DNA fragment was visualized by UV trans-illumination and marked with a scalpel. These marked flanking lanes were aligned with the unstained central lanes enabling excision of the desired DNA fragment. DNA was extracted from the gel slice and purified using a QIAquick Gel Extraction Kit (Qiagen) following the manufacturer's protocol for fragments between 500 bp and 4 kb. Purified DNA was resuspended in 20 µl of MQ water and stored at 4°C.

2.8.2 *Purification of PCR products*

PCR products were purified with a QIAquick PCR Purification Kit (Qiagen) as per the manufacturer's instructions. The DNA was eluted in 50 µl of MQ water and stored at 4°C and analysed by agarose gel electrophoresis (Section 2.6.3).

2.9 Manipulation of DNA

2.9.1 *Oligdeoxynucleotide Annealing for insertions*

Oligonucleotides encoding epitopes or restriction enzyme sites (Appendix D) were annealed in preparation for insertion into plasmid vectors according to the method of Enninga *et al.* (2005). 1 µl (corresponding to 1 nmole) of each oligodeoxynucleotide was added to 48 µl of annealing buffer (100 mM potassium acetate, 30 mM Hepes pH 7.4, 2 mM magnesium acetate in MQ). Annealing reactions were incubated in a Perkin Elmer Thermal Cycler at 95°C for 4 min, then 70°C for 10 min. The thermal cycler was then switched off and allowed to equilibrate to RT. The annealing reaction was then cooled to 4°C in the Perkin Elmer Thermal Cycler by incubation at 15°C for 5 min, 10°C for 5 min and then 4°C for 5 min.

2.9.2 *Phosphorylation of Annealed Oligodeoxynucleotides*

Annealed oligos (Section 2.9.1) were phosphorylated in order to enable their ligation into Shrimp Alkaline Phosphatase (SAP; Roche) treated vectors (Section 2.9.3). 2 µl of annealed oligos were mixed with 10 U of T4 polynucleotide kinase (NEB) and 1× T4 polynucleotide kinase buffer (NEB) in a 10 µl reaction in MQ. Reactions were incubated at 37°C for 30 min, followed by deactivation of the enzyme at 70°C for 10 min. 2 µl of this reaction was subsequently used in a 10 µl ligation reaction (Section 2.9.4).

2.9.3 *Shrimp Alkaline Phosphatase (SAP) treatment*

SAP treatment was performed to prevent re-ligation of digested plasmid vectors (Section 2.6.2). 5 µl of digested plasmid was mixed with 1 U of SAP (Roche) and 1× of SAP buffer (Roche) in a 10 µl reaction in MQ. Reactions were incubated at 37°C for 20 min, followed by deactivation of the enzyme at 65°C for 15 min. 1 µl of SAP treated plasmid was used in a 10 µl ligation reaction (Section 2.9.4).

2.9.4 *Ligation of DNA fragments into cloning vectors*

PCR products and plasmids for ligation were first purified (Section 2.8.2 & Section 2.8.1), restriction enzyme digested (Section 2.6.2) and mixed in a molar ratio of 3:1 (insert:vector). The ligation reactions were typically performed in a total volume of 10 µl with 2 U of T4 DNA ligase (NEB) and 1× T4 DNA ligase buffer (NEB) and incubated at 16°C for up to 16 h. Ligation of PCR products into pGEMT-Easy was performed as instructed by the manufacturer (Promega). Ligation products were transformed directly into chemically competent *E. coli* (Section 2.10.1 & Section 2.10.2). Alternatively, DNA was desalted by drop dialysis and then electroporated into electrocompetent *E. coli* or *S. flexneri* (Section 2.10.3 & Section 2.10.4). Desalting was achieved by spotting DNA directly onto a 13 mm nitrocellulose disk (0.025 µm pore size; Millipore VSWP01300) floating in a petri dish filled with MQ. Passive dialysis was allowed for 15-20 min, and the DNA was carefully aspirated and mixed with electrocompetent cells prior to electroporation.

2.10 Transformation procedures

2.10.1 *Preparation of chemically competent E. coli*

A 10 ml overnight (16 h) culture of *E. coli* DH5α in LB broth was sub-cultured 1:20 into a fresh 10 ml broth and incubated with aeration for 2 h, followed by centrifugation (2,200×*g*, 5 min, 4°C). The bacterial pellet was resuspended in 10 ml ice-cold Solution α (30 mM KAc, 100 mM KCl, 10 mM $CaCl_2$, 50 mM $MnCl_2$, 15% [v/v] glycerol), incubated on ice for 20 min and then centrifuged (2,220×*g*, 5 min, 4°C). The pellet was then resuspended in 1 ml ice-cold Solution β (10 mM MOPS, 75 mM $CaCl_2$, 10 mM KCI, 15% [v/v] glycerol) and stored on ice (2 h). 100 µl aliquots were transferred to sterile 1.5 ml reaction tubes and stored at -70°C until required.

2.10.2 *Transformation of chemically competent E. coli*

Competent cells were thawed on ice before the addition of 1 µg of plasmid DNA. The mix was left on ice for 10 min before heat shock (37°C water-bath, 5 min) and further incubation on ice for 10 min. 900 µl LB was added and the mix was incubated at 37°C (or as appropriate for temperature-sensitive strains or constructs) for 30-90 min with aeration to allow expression of antibiotic resistance genes on the plasmid(s). 100 µl aliquots of ten-fold dilutions were plated on LB-agar plates containing the appropriate antibiotic selection, and incubated overnight. All transformation procedures were accompanied by appropriate positive and negative controls.

2.10.3 *Preparation of electrocompetent S. flexneri and E. coli*

A 10 ml overnight culture of *S. flexneri* or *E. coli* was sub-cultured 1:20 in LB broth and grown for 2 h before centrifugation (2,200×*g*, 10 min, 4°C). Bacterial pellets were washed twice by resuspension in 1 ml of ice-cold MQ and centrifuged as before. Then, bacteria were washed twice by resuspension in 1 ml of ice-cold 10% (v/v) glycerol and centrifuged as before. Washed pellets were resuspended in 100

µl of 10% (v/v) glycerol. 100 µl aliquots of the suspension were stored at -70°C until required.

2.10.4 *Electroporation of S. flexneri and E. coli*

A 100 µl aliquot of electrocompetent cells was thawed on ice and an electroporation cuvette (1 mm electrode gap; Bio-Rad) was chilled. The cells and 5-10 µl of plasmid preparation (Section 2.5.1) were electroporated (Bio-Rad Gene Pulser, 1.8 kV, 25 µ F, Pulse Controller 200 Ω) in the cold cuvette, with resultant time constants of 4.4-5.0 msec. The cells were added to 900 µl of LB in a 20 ml narrow-necked McCartney bottle and incubated with aeration for 30-90 min at either 37°C, or as appropriate for temperature sensitive strains. 100 µl of neat and 1:10 (diluted in LB) electroporated cultures were plated on LB-agar with appropriate antibiotics and incubated for 16-24 h at either 37°C or 30°C, as required.

2.10.5 *Conjugation*

Donor and recipient strains were grown overnight in 10 ml of LB with the appropriate antibiotics. Cultures were pelleted by centrifugation (2,200×*g*, 10 min, 4°C), the supernatant containing antibiotics was discarded and the bacterial pellets were resuspended in 10 ml of LB without antibiotics. 100 µl of the donor strain was mixed with 900 µl of the recipient strain and plated onto sterile 0.45 µm HA gridded membrane filters (Millipore) on LB plates. Following incubation overnight at 37°C (or as appropriate) filters were transferred to 10 ml of LB, vortexed to resuspend the bacteria, and diluted 1:1,000 and 1:10,000 in LB. 100 µl of each dilution was plated on LB-agar containing antibiotics specific for the plasmid and the recipient strain, and incubated 16 h at 37°C.

2.11 Construction of chromosomal mutations

2.11.1 *Allelic-exchange mutagenesis using the λ Red phage mutagenesis system*

Mutagenesis using the λ Red mutagenesis system was performed essentially as described by Datsenko and Wanner (2000). Briefly, pKD46 was electroporated

(Section 2.10.4 into the recipient strain. An Ap^R transformant was selected and, after growth of this strain at 30°C in 10 ml of LB in the presence of 0.2% (v/v) arabinose, the bacteria were made electrocompetent (Section 2.10.3) and the concentrated (up to 100× for *S. flexneri* strains). PCR products were purified according to Section 2.8.2 and resuspended in MQ, concentrating the DNA 10-fold in the process. 5 µl of this purified PCR product was mixed with 50 µl of electrocompetent bacteria.

After electroporation, bacteria were resuspended in SOC medium (Section 2.3.1) and incubated at 37°C for 1 h prior to selection on LB plates containing Km. The absence of the temperature sensitive plasmids pKD46 and PCR template plasmids was confirmed by plating on LB containing the appropriate antibiotics. Strains that retained one of the plasmids were subjected to growth at 42°C for 16 h to ensure plasmid loss.

The antibiotic resistance marker used in this method was flanked by FRT (FLP recognition target) sites, allowing FLP-mediated excision of the marker. Accordingly, the mutated strain was transformed with the temperature sensitive FLP expression plasmid (pCP20; Appendix B; Section 2.10.4). Ap^R transformants were selected and incubated overnight at 30°C in LB broth with aeration. Overnight cultures were incubated at 42°C 2 h (statically) and diluted to 10^{-3} and 10^{-4} in LB, and plated onto LB agar plus the appropriate antibiotics and incubated 16 h at 37°C. Colonies were selected on the basis of sensitivity to the antibiotic to which the antibiotic resistance marker previously conferred resistance.

2.11.2 *Transduction using P1vir phage*

Preparation of P1*vir* phage stocks was performed using a modification of the method described by Miller (1972). Transduction was performed as described by Bob Sauer's lab (http://openwetware.org/wiki/Sauer:P1vir_phage_transduction).

Preparation of P1vir Phage stocks

In order to prepare phage stocks, the P1*vir* phage propagation strain AB1157 (Appendix A) was grown overnight at 37°C with aeration in 10 ml of LB broth. The bacteria were pelleted by centrifugation (2,220×*g*, 5 min, RT) and resuspended in 1 ml of MC salts (0.1 M $MgSO_4$, 5 mM $CaCl_2$ in MQ). Bacteria were then

incubated at 37°C for 15 min with aeration. A P1*vir* phage stock was diluted to 10^{-2}, 10^{-4} and 10^{-6} in LB and 100 µl of neat and diluted phage stocks were incubated with 100 µl of bacteria and incubated at 37°C for 20 min with aeration. The mixture of bacteria and phage was added to 3 ml of pre-warmed (45°C) R-TOP agar (Section 2.3.2) and poured onto pre-warmed (42°C) R-agar plates (Section 2.3.2). Plates were incubated face up at 37°C for 7-9 h. Initially, phage stocks were prepared from an isolated plaque. In preparing working phage stocks, plates exhibiting >50% lysis were used to prepare stock. Overlays from these plates were scraped off using a tissue culture cell scraper and transferred to 2 ml of LB. 200 µl of chloroform was added and the broths incubated at 37°C for 30 min with aeration at to kill any bacteria. The broth was centrifuged (2,220×*g*, 10 min, 4°C) to pellet the agar, and the supernatant (containing the phage stock) was collected and stored at 4°C. The titre of the prepared phage stock was determined by following the above method and counting plaques at higher dilutions of phage.

High titre stocks were prepared using liquid cultures. Overnight donor strain was subcultured 1:100 into 2.5 ml LB broth supplemented with 5 mM $CaCl_2$ and 0.2% (w/v) glucose and grown to early log-phase. 100 µl of P1*vir* phage was added and the culture was incubated for a further 2-3 h until complete lysis was observed. A few drops of chloroform were added to kill bacteria and the broth was incubated at 37°C for 30 min with aeration at to kill any bacteria. The broth was centrifuged (2,220×*g*, 10 min, 4°C) to remove debris, and phage were stored at 4°C. The titre of the phage stock was determined as described above.

P1 Phage Transduction

Overnight cultures of the recipient strain grown in LB broth were centrifuged and resuspended in fresh LB supplemented with 100 mM $MgSO_4$ and 5 mM $CaCl_2$. 100 µl of diluted P1*vir* lysates were mixed with 100 µl of the recipient and incubated at 37°C for 30 min. 200 µl 1 M Na-citrate (pH 5.5) was added, followed by 1 ml of LB. Transductions were incubated at 37°C for 1-2 h and harvested by centrifugation. Bacteria were resuspended in 100 µl LB supplemented with 100 mM sodium-citrate (pH 5.5) and plated onto selective media. Transduction of temperature sensitive markers (e.g. *dnaA5*) was achieved by increasing the absorption time to 1 h and subsequent incubation to 3-4 h.

2.12 Protein techniques

2.12.1 *Preparation of whole-cell lysates*

Overnight (16 h) cultures of bacterial strains were sub-cultured 1:50 in LB (10 ml) with antibiotics and incubated with aeration for 2 h at 37°C. The bacterial cell concentration was calculated on the basis that an absorbance at 600nm (A_{600}) of 1.0 was equivalent to 5×10^8 cells/ml. The equivalent of 5×10^8 bacteria were pelleted by centrifugation (13,200×*g*, 6 min, 4°C) and resuspended in 100 µl of 2× Sample Buffer (0.125 M Tris-HCl, pH 6.8, 4% [w/v] SDS, 20% [v/v] glycerol, 10% [v/v] β-mercaptoethanol, 0.04% [w/v] Bromophenol blue).

2.12.2 *SDS-PAGE*

Samples for SDS-PAGE analysis were heated at 100°C for 5 min prior to loading, unless otherwise stated. The SDS-PAGE gel apparatus used were the either the Bio-Rad Mini-Protean System III or a Sigma vertical gel electrophoresis unit (gel dimensions: 16.5 cm width x 14.5 cm height). SDS-PAGE was performed by electrophoresing samples through 7.5%, 12%, 15% or 20% (w/v) acrylamide gels in PAGE running buffer (0.025 M Tris-HCl, 0.2 M glycine, 0.1% [w/v] SDS) at 200 V for 1-4 h as required. Proteins were visualised by either staining with Coomassie blue (Section 2.12.3 or by Western immunoblot analysis (Section 2.12.4). Benchmark™ pre-stained standard (Invitrogen; 190 kDa, 120 kDa, 85 kDa, 60 kDa, 50 kDa, 40 kDa, 25 kDa, 20 kDa, 15 kDa, 10 kDa); HiMark pre-stained standard (Invitrogen; 460 kDa, 268 kDa, 238 kDa, 171 kDa, 117 kDa, 71 kDa, 55 kDa, 41 kDa, 31 kDa); and protein Low molecular weight standards (Pharmacia; 95 kDa, 67 kDa, 43 kDa, 30 kDa, 20 kDa, 14.4 kDa) were included to allow estimation of protein molecular mass.

2.12.3 *Coomassie blue staining*

Proteins separated by SDS-PAGE (Section 2.12.2) were incubated in Coomassie blue staining solution (5% [v/v] perchloric acid, 0.09% [w/v] Coomassie blue G250 [Sigma]) overnight (16 h), then destained in 5% (v/v) acetic acid until the

background colour was removed. Alternatively, where sensitive detection was desired, the following colloidal Coommassie staining was used: SDS-PAGE gels were fixed in 10% (v/v) acetic acid and 40% (v/v) ethanol for 30 min. The fixer was decanted and gel was stained in 100-300 ml of colloidal stain (8% [w/v] ammonium sulphate, 0.8% [w/w] phosphoric acid, 0.08% [w/v] Coomassie Blue G-250, 20% [v/v] methanol). Gels were stained overnight, or as required up to 2 days. When stained sufficiently, staining solution was decanted and the gel rinsed with MQ to remove residual stain.

2.12.4 *Western transfer and detection*

Proteins separated by SDS-PAGE (Section 2.12.2) were transferred to a membrane (Protran nitrocellulose membrane BA85 [Schleicher and Schuell] or Nitrobind 0.45 micron pure nitrocellulose [GE Water and Process Technologies]) for 1-2 h at 200 mA in transfer buffer (3.06 g/L Tris, 0.2 M glycine, 5% [v/v] methanol). The membrane was then blocked for 1 h in TTBS (2.4 g/L Tris, 0.12 M NaCl, 0.05% [v/v] Tween 20 [Sigma]) with 5% (w/v) skim milk and then incubated with the desired primary antibody (Section 2.1.1) in the same buffer for up to 16 h. After three 10 min washes in TTBS the membrane was incubated with horseradish peroxidase (HRP)-conjugated goat anti-rabbit or a HRP-conjugated goat anti-mouse secondary antibodies (Biomediq DPC) for 2 h, washed three times in TTBS, then two times in TBS (2.4 g/L Tris, 120 mM NaCl). The membrane was incubated with Chemiluminescence Blotting Substrate (Roche) or CPS 3500 chemiluminescence substrate (Sigma) for 5 min. Chemiluminescence was detected by exposure of the membrane to X-ray film (AGFA). The film was developed using a Curix 60 automatic X-ray film processor (AGFA). Alternatively, chemiluminescence was visualised using a Kodak ImageStation 4000MM system. In each instance, exposure times were determined empirically.

2.12.5 *Purification of outer membrane protein oligomers*

Oligomers of the IcsA autotransporter were prepared essentially as described in Veiga *et al.* (2002). Briefly, a 3 L overnight culture grown in Terrific broth at 30°C was pelleted (11,400×*g*, 10 min, RT) and resuspended in 20 ml of TN

buffer (20 mM Tris-HCl pH 8.0, 10 mM NaCl) supplemented with 0.1 mg/ml DNase (Roche), 0.1 mg/ml RNase (Roche), 0.1 mM phenylmethanesulfonyl fluoride (PMSF). Bacteria were lysed by 4 passages in a French pressure cell (SLM instruments) operated at 12,000 psi. Unbroken cells were removed by pelleting (5,500×*g*, 10 min, 4°C).

Lysates were then centrifuged (100,000×*g*, 60 min, 4°C; 40,000 rpm, 80Ti rotor, Optima L-100 XP ultracentrifuge [Beckamn-Coulter]). The supernatant was discarded and the whole membrane-containing pellet washed in TN buffer, and then thoroughly resuspended in 20 ml TN buffer with 1.5% (v/v) Triton X-100 (Sigma; T8787) using a glass tissue homogeniser. The suspension was incubated on ice for 30 min, and then centrifuged (100,000×*g*, 60 min, 4°C; 40,000 rpm, 60Ti rotor, Optima L-100 XP ultracentrifuge [Beckamn-Coulter]). The supernatant was discarded and the outer membrane-containing pellet was rinsed in TN buffer, and resuspended in 2 ml TNZ buffer (TN buffer with 1% [w/v] Zwittergent 3-14 [Calbiochem]) using a clean glass tissue homogeniser. The suspension was incubated for 30 min on ice, and then centrifuged (100,000×*g*, 60 min, 4°C; 50,000 rpm; TLA100.4 rotor; OptimaTLX ultracentrifuge [Beckman]). The supernatant was collected and diluted 1:10 in TN buffer (to a final 0.1% [w/v] Zwittergent 3-14 concentration) and 5 ml was used for affinity purification with either 100 µl of streptavidin-Dynabeads (Invitrogen, 656.01) or 100 µl of FLAG M2 resin (Sigma, A2220).

Purification was performed at 4°C at all times and in the presence of 1 mM PMSF. The solubilised outer-membrane proteins were mixed with either streptavidin-Dynabeads or FLAG M2 resin in a 10 mL Falcon tube, and incubated for 4 h with gentle agitation on a rocking platform. Samples were then centrifuged at 2,200×*g* for 20 min at 4°C to pellet beads or resin. The supernatant was carefully removed and discarded. In the case of streptavidin-Dynabeads, pellet integrity was maintained by placing tubes in a magnetic rack when removing supernatant. 8 ml of TN buffer supplemented with 0.1% Zwittergent 3-14 and 1 mM PMSF was then applied to resuspend and wash resin or beads. Each wash step proceeded for 1.5 h at 4°C with gentle agitation as above, and was repeated 8 times. Prior to SDS-PAGE, purified proteins were eluted from both FLAG M2 resin streptavidin-Dynabeads by resuspending pelleted resin or beads in 50µl of 2× Sample buffer (Section 2.12.1) and incubating samples at 100°C for 10 min.

Samples were then pelleted at 16,000×*g* for 5 min, the supernatant carefully removed, and 5 µl of supernatant was resolved by SDS-PAGE. The pelleted resin and beads were discarded. In the case of streptavidin-Dynabeads, samples were placed in a magnetic tube rack after boiling to maintain pellet integrity when the supernatant was being removed.

2.12.6 *Indirect immunofluorescence of whole bacteria*

Overnight (16 h) cultures were sub-cultured 1:50 and grown to log-phase in LB broth (10 ml) at 37°C. Bacteria were pelleted by centrifugation (16,000×*g*, 1 min), and the supernatant discarded. Bacteria were fixed in formalin (3.7% [w/v] paraformaldehyde in 0.85% [w/v] saline) for 15 min at RT. Sterile coverslips were placed into 24-well trays (Falcon) and incubated with 10% (v/v) poly-L-lysine (Sigma) in PBS for 1 min. The poly-L-lysine was aspirated and formalin fixed bacteria were centrifuged (789×*g*, 5 min, 25°C) onto the coverslips. Bacteria were incubated for 2 h at room temperature with the desired primary antibody (Section 2.1.1) diluted 1:100 in PBS with 10% (v/v) foetal calf serum (FCS). Bacteria were washed three times in PBS and incubated for 1 h at 37°C with either Alexa 488-conjugated donkey anti-rabbit or Alex 488-conjugated donkey anti-mouse secondary antibodies (Molecular Probes); diluted 1:100 in PBS with 10% (v/v) FCS. The coverslips were mounted on glass microscope slides with mounting medium (Section 2.17.1) and analysed by immunofluorescence microscopy as described in Section 2.12.6.

2.13 Minicell purification

2.13.1 *Purification of minicells by sucrose gradients*

Minicells were purified according to the method of Achtman *et al.* (1979), described herein.

Preparation of sucrose gradients

Sucrose gradients were prepared by placing 32 ml of 20% (w/v) sucrose in buffered saline gelatin (BSG; 0.85% [w/v] NaCl, 0.03% [w/v] KH_2PO_4, 0.06%

[w/v] Na_2HPO_4, 100 μg/ml gelatin) into Ultra-ClearTM tubes (25 x 89 mm; Beckman), freezing at -20°C and allowing to thaw overnight at 4°C.

Purification of minicells

Overnight (16 h) cultures of minicell strains grown in LB broth were sub-cultured 1:25 in 250 ml of fresh LB broth with antibiotics and incubated with aeration overnight at 37°C to produce stationary phase cultures. Log-phase cultures of minicells strains were also prepared by sub-culturing overnight cultures 1:20 in 1 L of LB with antibiotics and incubated with aeration for 2 h at 37°C. Bacteria and minicells from both log-phase and stationary-phase cultures were pelleted by centrifugation (8,600×*g*, 20 min, 4°C; Beckman J2-M1) and resuspended in 10 ml of BSG (Section 2.13.1). Cells were pelleted again by centrifugation (20,400×*g*, 8 min, 4°C) and resuspended in 2 ml of BSG. Cells were layered onto sucrose gradients and centrifuged (5500 rpm, 30 min, 4°C, acceleration 1, deceleration 1, rotor Nr. 11133, Sigma 3K15). The minicell fraction in the middle of the tube was extracted using a syringe. A sample of the whole cell fraction at the bottom of the tube was also collected and diluted in 50 mM Tris pH7.5. The minicells were centrifuged (20,400×*g*, 8 min, 4°C), resuspended in 1 ml of BSG and purified once more on a sucrose gradient as described above. The minicells were then centrifuged (20,400×*g*, 8 min, 4°C) and resuspended in 2 ml of 50 mM Tris pH7.5. Cell concentrations were approximated on the basis that an A_{600} = 1.0 represents 5×10^8 whole cells and 2×10^9 minicells.

Proteins and LPS analysis of minicells

Purified minicells and whole cells were lysed by sonication in TN buffer (Section 2.12.5) with 0.1 mg/ml DNase, 0.1 mg/ml RNase, 0.1 mM phenylmethanesulfonyl fluoride (PMSF). Unbroken cells were removed by centrifugation (5,500×*g*, 25 min, 4°C) and the lysate was then centrifuged (100,000×*g*, 60 min, 4°C). The supernatant was aspirated and the pelleted whole membrane fraction was rinsed with TN buffer and then thoroughly resuspended in TN buffer with 1% SDS using a glass tissue homogeniser. Suspensions were incubated on ice for 1 h, then centrifuged (100,000×*g*, 60 min, 4°C) to remove insoluble and undissolved material. The supernatant was collected and protein content assessed using a BCA Protein Estimation assay, in accordance with manufacturer's instructions

(Pierce). Samples from minicells and whole cells were standardised to equivalent total membrane protein concentration and subsequently used for further protein (Section 2.12.4) and LPS analysis (Section 2.14.1 & Section 2.14.2).

2.14 Lipopolysaccharide techniques

2.14.1 *Preparation of LPS samples*

LPS samples were prepared according to the method of Hitchcock and Brown (1983). Overnight (16 h) cultures of bacterial strains grown in LB broth were sub-cultured 1:20 in fresh LB (10 ml) with antibiotics and incubated with aeration for 3-4 h at 37°C. The equivalent of 10^9 bacteria were pelleted by centrifugation (13,200×*g*, 6 min, 4°C) and resuspended in 50 µl of Lysing Buffer (0.66 M Tris pH 7.6., 2% [w/v] SDS, 10% [v/v] glycerol, 4% [v/v] β-mercaptoethanol, 0.1% [w/v] bromophenol blue). Samples were heated at 100°C for 5-10 min, and allowed to cool before the addition of 10 µl of 2.5 mg/ml Proteinase K (Invitrogen) in Lysing Buffer. Samples were treated with Proteinase K for 4-18 h at 56°C.

2.14.2 *Analysis of LPS by silver-stained SDS-PAGE*

The SDS-PAGE gel apparatus used for LPS gels were the either the Bio-Rad Mini-Protean System III or a Sigma vertical gel electrophoresis unit (gel dimensions: 16.5 cm width x 22 cm height). LPS samples prepared in Section 2.14.1 were heated at 100°C for 5 min prior to loading 5-10 µl on 15% SDS (w/v) polyacrylamide gels (Macpherson *et al.*, 1991). For mini-Protean gels (Biorad) samples were diluted 1:4 in Lysing Buffer (Section 2.14.1) and 5-10 µl of the diluted sample was used. Samples were electrophoresed at 15 mA for 14.5 h. Silver-staining was performed as described by Tsai and Frasch (1982). Briefly, the gel was fixed for 2 h in fixing solution (40% [v/v] ethanol, 5% [v/v] glacial acetic acid in MQ) with gentle agitation and then oxidised for 5 min in oxidising solution (40% [v/v] ethanol, 5% [v/v] glacial acetic acid, 0.7% [w/v] periodic acid in MQ). After 1 h of washing in MQ water (changed at 10 min intervals), the gel was stained for 10 min in staining solution (0.08% [w/v] NaOH, 1.33% [v/v] ammonium hydroxide, 0.66% [w/v] silver nitrate) and washed again as above. Developing was achieved with

developing solution (0.05 mg/ml citric acid, warmed to 56°C, with 500 µl of formaldehyde solution (UNIVAR; 37% [w/w] added just prior to developing) and stopped by the addition of stopping solution (4% [v/v] acetic acid).

2.15 Chemical cross-linking

2.15.1 *DSP cross-linking*

Overnight (16 h) cultures of bacterial strains grown in LB were sub-cultured 1:50 in fresh LB broth (10 ml) with antibiotics and incubated with aeration for 2 h at 37°C. The equivalent of 10^9 bacteria were pelleted by centrifugation (13,200×*g*, 6 min, RT) and washed once in 1 ml of buffer (120 mM NaCl, 20 mM Na_2PO_4/NaH_2PO_4 buffer pH 7.2) and resuspended in 1 ml of the same buffer. Dithio-bis(succinimidylpropionate) (DSP; Pierce) from a 50 mM stock in dimethyl sulphoxide (DMSO; Sigma) was added to each sample at a final concentration of 0.2 mM and samples were incubated for 30 min at 37°C, or 2 h at 4°C. Excess DSP was quenched with 20 mM Tris pH 7.5 and samples were then washed once again and resuspended in 100 µl of 1× Sample buffer (Section 2.12.1) without β-mercaptoethanol. Duplicates of each sample were prepared in 100 µl of 1× Sample Buffer (Section 2.12.1) with β-mercaptoethanol, as a control.

2.16 Tissue culture

2.16.1 *Maintenance of cell lines*

HeLa cells (Human, cervical, epithelial cells ATCC CCL-2) and CV-1 cells (African green monkey, kidney, fibroblast cells ATCC CCL-70) were maintained in Modified Eagle's medium (MEM, Gibco BRL) with 4 mM L-glutamine adjusted to contain 1.5 g/L sodium bicarbonate and 4.5 g/L glucose, 10% (v/v) FCS and 100 U/ml penicillin and 100 U/ml streptomycin. Cells were grown and maintained in a humidified atmosphere at 37°C, 5% CO_2.

2.16.2 *Plaque assays*

Plaque assays were performed with HeLa cells using a modification of the method described by Oaks *et al.* (1985). HeLa cells were seeded to 60 mm diameter, 6-well trays (Falcon) at 1×10^6 cells/ml in MEM, 10% (v/v) FCS with penicillin and streptomycin. Cells were grown to confluence overnight and washed twice with Dulbecco's PBS (D-PBS; 0.1% [w/v] $CaCl_2$, 0.1% [w/v] $MgCl_2$ in PBS) and once in Dulbecco's MEM (DMEM, Gibco BRL) prior to inoculation. Overnight (16 h) cultures of *S. flexneri* strains grown in LB broth were sub-cultured 1:50 in LB (10 ml) with antibiotics and incubated with aeration for 2 h at 37°C. Bacteria were diluted to 1:100 and 1:300 in DMEM, and 200 µl was added to each well. Trays were incubated at 37°C in a humidified CO_2 (5%) incubator and the trays were rocked gently every 15 min to ensure that the inoculum was spread evenly across the monolayer. At 90 min post-infection the inoculum was carefully aspirated and 4 ml of the first overlay (DMEM, 5% [v/v] FCS, 20 mug/ml of gentamicin, 0.5% [w/v] agarose [Seakem ME]) was added to each well. The second overlay (DMEM, 5% [v/v] FCS, 20 µg/ml of gentamicin, 0.5% [w/v] agarose, 0.1% [v/v] Neutral Red solution [Gibco BRL]) was added at either 24 h or 48 h post-infection and plaque formation observed 6-8 h later. Plaques were generally visible without staining at 48 h.

2.17 Microscopy & imaging

2.17.1 *Mounting medium*

Mowiol 4-88, for mounting medium was prepared by mixing 0.4 g of Mowiol 4-88 (Calbiochem), 1 g of glycerin and 1 ml of MQ. This was incubated for 2 h at 56°C, before adding 2 ml of 0.2 M Tris-HCl pH 8.5 and heating at 50°C for at least 10 min, or until dissolved. To remove remaining solids, this preparation was centrifuged at 5,000×*g* for 15 min, and the supernatant collected and stored at 4°C. A fresh stock of *p*-phenylenediamine (PPD; Sigma) was prepared each time at 25 mg/ml in ethanol. The stock was vortexed and centrifuged (13,200×*g*, 1 min, RT) to remove undissolved PPD. The PPD solution was added to Mowiol 4-88 at a ratio of 1:5 (PPD:Mowiol). This mounting medium was vortexed and

centrifuged (13,200×*g*, 1 min, RT) to remove any air bubbles. Coverslips were mounted (cell-side down) onto glass slides using 3-4 µl of mounting medium and sealing the edge of the coverslip with nail polish.

2.17.2 *Mounting for live bacterial imaging*

Imaging of live bacteria was performed either on solid or liquid media. In all instances, solutions and media used in live microscopy were filtered through a 0.2 µm nitrocellulose filter (16534, Minisart, Sartorius stedim). Solid media consisted of 1% agarose (SeaKem LE) pads dissolved by heating in appropriate liquid media (e.g. LB or M9 media). Thin pads were created by applying 70 µl of molten agarose solution directly onto a microscope slide and allowing the agarose to set and dry for 10 min at RT. Pads were made to be smaller than coverslips. 100 µl of mid-log phase bacteria were washed with 300 µl filtered LB broth and resuspended in 60 µl of filtered LB. 5 µl of this suspension was spotted onto agarose pads and allowed to adsorb. A coverslip was gently placed onto the agarose pad, its edges were sealed with VALAP, a 1:2:2 mixture of vaseline, lanolin, and paraffin.

Alternatively, when live imaging in an aqueous environment was required, 100 µl of mid-log phase bacteria was pelleted (13,200×*g*, 2 min, RT) and resuspended in 190 µl of filtered LB broth to which 2×10^7 Polybead Amino 1.00 µm Microspheres (0.5 µl of stock; 17010, Polysicence) were added. The suspension was pelleted again, the supernatant carefully removed and pellet of bacteria and microspheres resuspended in 60 µl of fresh filtered LB. 0.5 µl was then applied to a microscope slide and a coverslip gently placed on top. Sides were sealed with VALAP. Addition of 1 µm microspheres ensured a single focal plane for imaging.

2.17.3 *Microscopy*

Slides were examined with an Olympus IX-70 microscope with phase-contrast optics using a 100× oil immersion objective and on occasion using a 1.5× enlarger. The Omega optical filter set XF67-1 set was used with a filter wheel (Sutter) containing a narrow band excitation filter (X67, Pinkel Set [Omega]), and was

controlled by MetaMorph (Version 6.3r7, Molecular devices). Fluorescence and phase-contrast images were false colour merged using MetaMorph.

When timelapse imaging were required, bacteria were placed at the centre of glass microscope slides and imaged with an Olympus IX-70 microscope from a fixed stage(Olympus IX2-SP) and in a chamber heated to 37°C, or as appropriate.

2.17.4 *Automated image analysis*

Analysis of microscopy images was performed with MetaMorph software. Automated image analysis was developed with Dr. Neal Gliksman (Molecular Devices, USA). Briefly, a threshold selecting bacteria in a phase image was manually applied. Identified bacteria were automatically, assigned sequential labels and classified as valid (99 pixels $\leqslant$ total area $\leqslant$ 10,000 pixels), thereby excluding bacteria in contact with each other from analysis. The thresholded image was then binarized and a Euclidean distance map generated. Bacterial centroid and length were recorded. The corresponding fluorescence image was then manually thresholded for foci of fluorescence. Foci were taken to be peaks of fluorescence at least 150% above background cellular fluorescence. Identified foci were then used to create an object mask which was applied to the Euclidean distance map and distances measured. Automated analysis sequentially labelled foci, enumerated foci per valid bacterium, determined foci centroids, measured distance to furthest edge of bacterium, and measured distance between foci centroid and bacterial centroid.

2.17.5 *Flow cytometry*

Overnight (16 h) cultures were sub-cultured 1:50 and grown to log-phase in LB broth (10 ml) at 37°C. Bacteria were pelleted by centrifugation (16,000$\times g$, 1 min), and the supernatant discarded. Bacteria were fixed in formalin (3.7% [w/v] paraformaldehyde in 0.85% [w/v] saline) for 15 min at RT. 1×10^6 bacteria were taken, pelleted and resuspended in 50 µl mouse anti-FLAG M2 antibodies diluted 1:100 in filtered PBS. Labelling was performed for 3 h at RT. Bacteria were then washed 4$\times$ in 200 µl PBS, pelleted and resuspended in 100 µl of a 1:100 dilution of anti-mouse antibodies conjugated to AlexaFluor 488 (Molecular

probes) in PBS. Labelling was performed for 2 h at RT. Bacteria were then washed 4× in filtered PBS, and finally diluted 10-fold with filtered PBS. The fluorescence intensity of these labelled bacteria was then assessed using a FACSCanto flow cytometer (instrument settings: forward scatter [FSC]: height, 270 V; side scatter [SSC]: area, 390 V; FITC: area, 478 V; thresholds: FSC >200 AND SSC >200). In general, 50,000 events were captured at a rate of approximately 100-200 events per sec. BD FACSDiva software was used to analyse fluorescence intensities.

Part II

RESULTS

3

Polar targeting domains of IcsA

3.1 Introduction

The accumulation of polymerised F-actin at one end of *S. flexneri* was an early indirect observation of IcsA polar targeting that was later visualised at the bacterial surface (Ogawa *et al.*, 1968; Goldberg *et al.*, 1993). The regions of IcsA responsible for directing the protein towards the "old pole"—the pole not arising from the previous division—were more recently identified by GFP fusion experiments. Charles *et al.* (2001) reported that two different IcsA subregions could deliver fused GFP fluorescence to the pole within the *E. coli* and *S. flexneri* cytoplasm. These regions, $IcsA_{1-104}$ and $IcsA_{506-620}$, were therefore concluded to independently confer polar positioning to the full IcsA protein. Surprisingly, those authors also reported that the presence of the extended signal sequence ($IcsA_{1-52}$) actually improved polar targeting of the first region, despite the likely distribution of SecYEG translocon being helical along the length of *E. coli* (Brandon *et al.*, 2003; Shiomi *et al.*, 2006).

The aim of this chapter was to confirm the polar targeting regions of IcsA and to better define the domain responsible for this targeting.

3.2 GFP+ fusions

An initial verification of the polar targeting regions described by Charles *et al.* (2001) was undertaken by fusion of IcsA fragments to an improved green fluorescent protein, GFP+ (Scholz *et al.*, 2000). The *gfp+* gene was expressed from the broad host range vector pBBR1MCS2 (Kovach *et al.*, 1995) following sub-cloning of the gene from pWH1012*gfp+* (Scholz *et al.*, 2000). Briefly, an *Eco*RV—*Eco*RI fragment containing *gfp+* was cloned into the corresponding sites of pBBR1MCS2, downstream of a tetracycline-regulated promoter (P_{tet}) (**Figure 3.1**; gift of Rohan Russell, University of Adelaide).

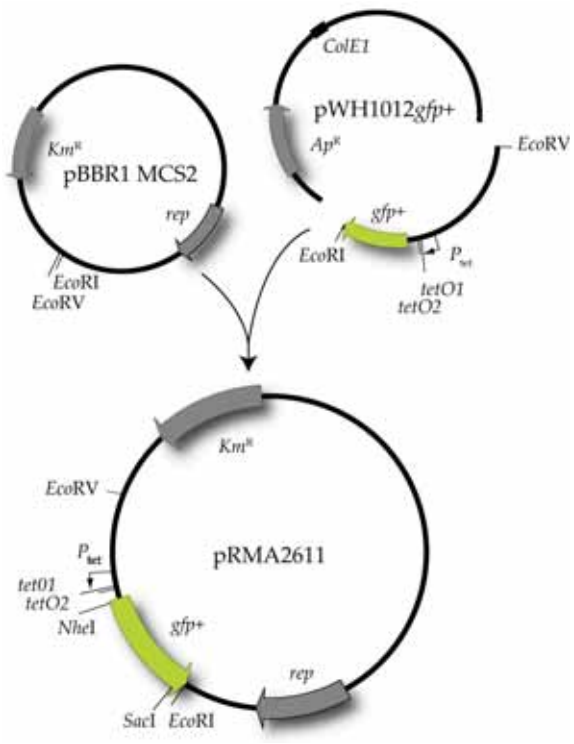

Figure 3.1: **Construction and composition of *gfp+* vector pRMA2611**. The *gfp+* bearing *Eco*RV—*Eco*RI fragment of pWH1012*gfp+* was subcloned into corresponding sites of pBBR1 MCS2. An upstream P_{tet} tetracycline promoter drove *gfp+* expression and two *tetO* operator sequences were immediately upstream of *gfp+*, allowing repression by TetR, when supplied in *trans*. Gene fusions were made by in-frame cloning at the *Nhe*I site; subcloning of GFP+ fusions was achieved by exploiting the 3′ *Sac*I site within *gfp+*.

Gene fusions were made by PCR amplification of *icsA* fragments from plasmid pIcsA (Appendix B) with oligonucleotides that introduced a 5′ *Nhe*I and a 3′ *Xba*I site, allowing in-frame cloning at the *Nhe*I site at nt 5 of *gfp+* in pRMA2611. Since an inherent *Xba*I site is present at *icsA* nt 304, regions spanning this site were amplified with a reverse oligonucleotide that incorporated an *Nhe*I site. A complete list of oligonucleotides used to create each of the GFP+ fusions described in this chapter is presented in Appendix C. Recombinant plasmids were transformed into DH5α and cloning confirmed by sequencing. Fusion proteins were expressed at a low level in *E. coli* TOP10F′ (Appendix A) that carries Tn*10* *tetR* on the F′ episome, thereby allowing for repression of *gfp+* fusions in the absence of tetracycline. Alternatively, where the observed fluorescence in that strain was weak, fusions were also expressed in *E. coli* DH5α. There was no

difference in the observed localisation for any fusion protein between DH5α and TOP10F' (not shown). For analysis of fusion protein localisation, strains were grown to mid-log phase in LB broth, washed in medium, placed on a 1% agar pad and visualised by microscopy, as described in Section 2.17.2. For each strain, a total of 200 bacteria from two independent experiments were chosen from phase contrast images, and the profile of fluorescence scored as having polar focus or having no focus (non-polar) (represented in **Figure 3.2**). Foci were defined as having peak fluorescence that was greater than 150% of background fluorescence. Bacterial cell shapes are outlined from corresponding phase contrast images. The polarity of generated fusions is summarised in **Figure 3.3**.

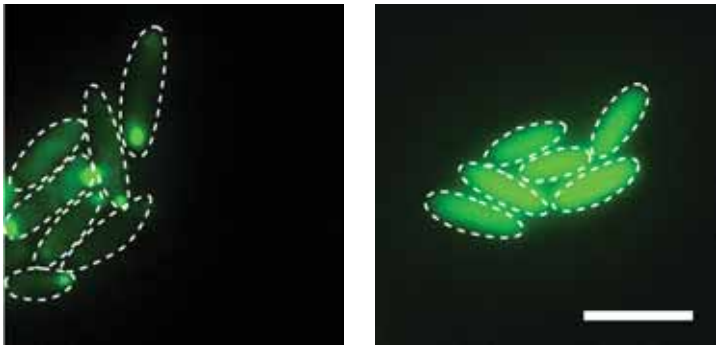

(a) (b)

Figure 3.2: **Representative images of GFP+ fusion protein polarity**. (**a**) Polar focus of fluorescence of IcsA$_{506-620}$-GFP+; and (**b**) non-polar diffuse cytoplasmic fluorescence of IcsA$_{105-505}$-GFP+. Bacterial cell shapes from corresponding phase contrast images are outlined. Scale bar represents 3 μm.

GFP+ fusion to the entire *icsA* gene (IcsA$_{1-1102}$-GFP+, strain MG54) or the sequence corresponding to the effector domain (IcsA$_{1-758}$-GFP+, strain MG44) displayed weak fluorescence, with approximately 20% of bacteria expressing polarly localised fluorescence (**Figure 3.3**). Consequently, polar targeting was preserved when the translocation domain (IcsA$_{759-1102}$) was excluded, demonstrating that this domain was not involved in targeting. Fusion of the amino terminal proximal polar targeting region (IcsA$_{1-104}$, strain MG342) described by Charles *et al.* (2001) was not polar (**Figure 3.3**). Removal of the signal sequence (IcsA$_{1-52}$) from this region had been reported to reduce, but not abolish, polar localisation of the remaining IcsA$_{53-104}$ peptide (Charles *et al.*, 2001). The presence of the signal sequence could have limited the amount of detectable cytoplasmic IcsA$_{1-104}$-

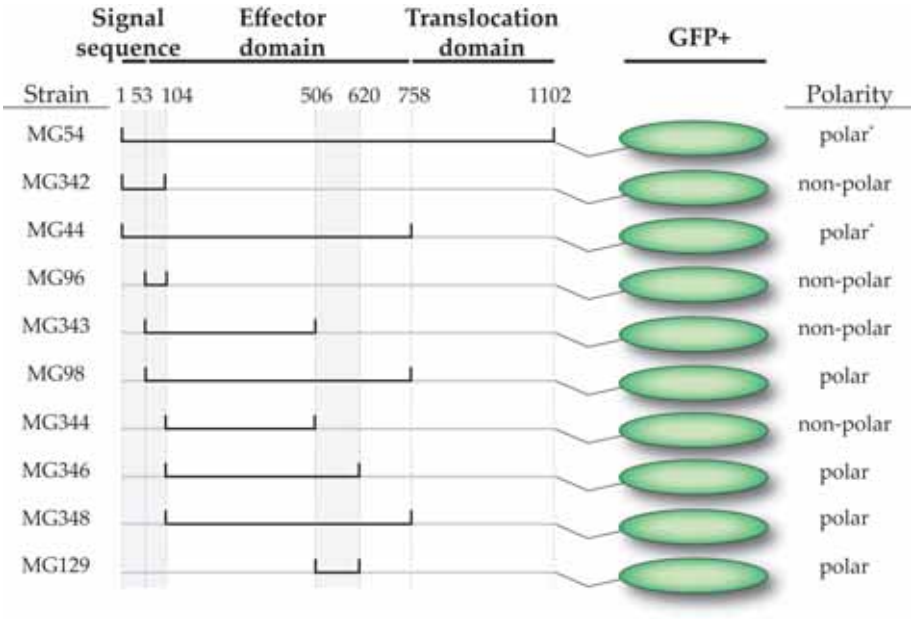

Figure 3.3: **Polarity of constructed IcsA fusions to GFP+**. Gene fusions were created by cloning IcsA regions in-frame with *gfp+* in plasmid pRMA2611. Fusion proteins were expressed in *E. coli* TOP10F′ or DH5α. Bacteria were grown to mid-log phase and placed on LB agar pads for microscopic analysis of fluorescence from 200 cells of each strain, as described in Section 2.17.2. Fusions spanning $IcsA_{506-620}$ were each observed to exhibit polar localisation (**polar**). Bacteria expressing GFP+ fusions of $IcsA_{1-1102}$ and $IcsA_{1-758}$ (strains MG54 and MG44, respectively), exhibited approximately 20% polarity (**polar***). All other fusions denoted as "polar" exhibited polar targeting in more than 90% of bacteria.

GFP+ owing to export of this fusion. However, the $IcsA_{53-104}$-GFP+ fusion (strain MG96), that lacked the signal sequence, was also non-polar (**Figure 3.3**). Likewise, $IcsA_{53-505}$-GFP+ was non-polar. In agreement with Charles *et al.* (2001), fusions that spanned the described amino terminal distal polar targeting region ($IcsA_{506-620}$) were observed to be polarly localised (**Figure 3.3**). Indeed, any fusions lacking this region did not have any discreet spatial positioning, remaining diffuse in the cytoplasm and being non-polar (**Figure 3.3**). These data suggested $IcsA_{1-104}$ was not able to determine polar positioning, while $IcsA_{506-620}$ was both sufficient and necessary for polar localisation in the cytoplasm of *E. coli*.

3.3 Polar targeting mutants

That $IcsA_{1-104}$ may be insufficient for polar targeting is supported by the linker insertion mutagenesis of IcsA by May and Morona (2008). In that study, two mutants were identified that were non-polar on the surface of *S. flexneri*. Both mutants bore insertions within the polar targeting region $IcsA_{506-620}$ verified above, at amino acid 532 ($IcsA_{i532}$) and 563 ($IcsA_{i563}$). In these mutants, $IcsA_{1-104}$ was unable to confer polar targeting independently of the mutagenised $IcsA_{506-620}$ region, as proffered by Charles *et al.* (2001). Whether these insertion mutants inactived the cytoplasmic polar targeting of the $IcsA_{506-620}$ region was directly assessed by constructing GFP+ fusions.

Mutants that abolish polarity had not previously been reported and would be valuable in the biochemical analysis of the polar targeting region. To facilitate such studies, the $IcsA_{506-620}$ region from $IcsA_{WT}$, $IcsA_{i532}$, and $IcsA_{i563}$ were cloned as GFP+ fusions with dual affinity tags: an N-terminal *Strep*-tag II epitope (*Strep*; WSHPQFEK) and a C-terminal His_6 epitope. A tobacco etch virus (TEV) protease recognition site (ENLYFQG) was cloned between the *Strep*-$IcsA_{506-620}$ fragment and GFP+-His_6, to allow for removal of the GFP+ peptide by Ni-NTA affinity chromatography using His_6-tagged TEV protease. Fusion proteins were therefore designed as depicted in **Figure 3.4**.

Consequently, the $icsA_{506-620}$ region of wild-type $icsA_{WT}$, $icsA_{i532}$, and $icsA_{i563}$ were PCR amplified using oligonucleotides "506_StrepII_*Nhe*I" and "620_TEV_*Xba*I" (Appendix F) that introduced the *Strep*-tag II and TEV sequences in-frame, as well as a flanking 5′ *Nhe*I site and a flanking 3′ *Xba*I recognition site. These amplicons were digested with *Nhe*I and *Xba*I and cloned in-frame with *gfp*+, into the *Nhe*I

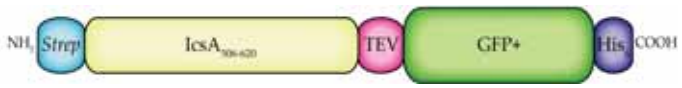

Figure 3.4: **Schematic of dual affinity tagged $IcsA_{506-620}$-GFP+ fusion proteins**. An N-terminal *Strep*-tag II sequence (WSHPQFEK) permits for affinity chromatography purification using *Strep*-tactin. A C-terminal His_6 tag allows for Ni-based affinity chromatography purification. The GFP+ peptide allows for *in vivo* visualisation of the complete fusion. A tobacco etch virus protease processing site (TEV) was incorporated to allow for removal of GFP+-His_6 from Strep-$IcsA_{506-620}$ using commercially available His_6-tagged TEV protease and Ni-based affinity purification.

site of pRMA2611, giving pMG404 (wild-type), pMG406 (i532), and pMG425 (i563). The fidelity of the constructed fusions was confirmed by sequencing. To incorporate the His_6 epitope, a variant plasmid of pQE60 was generated, introducing *Spe*I and *Sac*I recognition sequences. Briefly, complementary oligonucleotides "New_QE60_Spe-Sac_F" and "New_QE60_Spe-Sac_R" (Appendix D) were annealed together, as described in Section 2.9.1 (**Figure 3.5**). This process generated dsDNA that incorporated the recognition sites and possessed complementary *Bam*HI overhang. The dsDNA was then ligated into *Bam*HI linearised pQE60, giving pMG100 (**Figure 3.5**; strain MG100, Appendix A). The *Bam*HI site was retained during cloning.

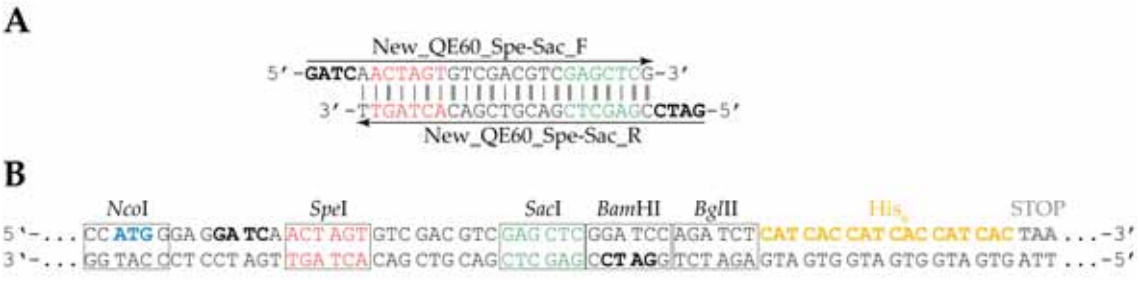

Figure 3.5: **Annealing and cloning of oligonucleotides that introduced *Spe*I and *Sac*I sites into the pQE60 derivative, pMG100**. (**A**) Complementary oligonucleotides "New_QE60_Spe-Sac_F" and "New_QE60_Spe-Sac_R" were annealed together as described in Section 2.9.1, creating terminal *Bam*HI overhangs and assembling *Spe*I (**red**) and *Sac*I (**green**) restriction sites. (**B**). The annealed oligonucleotide product was then ligated into *Bam*HI digested pQE60, introducing unique *Spe*I and *Sac*I sites and preserving the *Bam*HI recognition sequence, and producing plasmid pMG100. The plasmid permits *Nhe*I-*Sac*I fragments containing *gfp*+ fusions to be subcloned from pRMA2611 derivatives into the *Spe*I and *Sac*I sites of pMG100, such that the introduced gene is in-frame with the start codon (**blue**) and the His_6 epitope (**yellow**) of pMG100. Such subcloning invariably introduced an N-terminal peptide extension (MGGSS), and replaces YK from the GFP+ C-terminus for SSRS, prior to incorporation of His_6.

The *Strep*-$IcsA_{506-620}$-TEV-GFP+ fusions were then excised by restriction digest with *Nhe*I and *Sac*I, and then ligated, in-frame with His_6, into *Spe*I and *Sac*I linearised pMG100, giving pMG421 (wild-type), pMG422 (i532), and pMG426 (i563). Expression of these fusion proteins was regulated by P_{lac} and inducible with IPTG. To improve gene repression under IPTG-depleted conditions, the plasmids were transformed into *E. coli* BL21(DE3) that expressed $lacI^q$ from

plasmid pREP4, giving strain MG423 (wild-type), MG424 (i532), and MG426 (i563).

The constructed fusions were assessed for protein production by immunoblotting, as described in Section 2.12.4. Expression of the mutant fusions was equivalent to the wild-type fusion, as determined by detection with anti-GFP antibodies (**Figure 3.6**). Likewise, wild-type equivalent expression was observed when constructs were detected by probing with anti-*Strep*-tag II and anti-His_6 antibodies (**Figure 3.6**). Detection with each of these antibodies confirmed the success of the tagging strategy. No degradation products were observed, suggesting the fusions were stable in the cytoplasm.

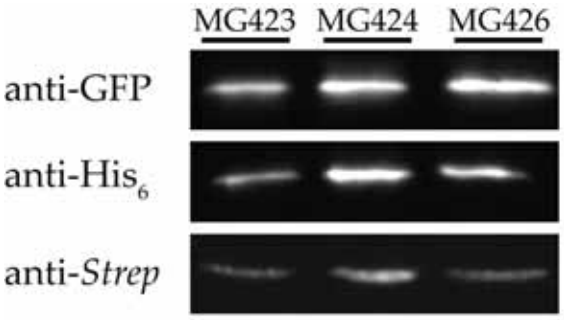

Figure 3.6: **Detection of epitope tagged IcsA$_{506-620}$-GFP+ fusions**. Strains MG423, MG424 and MG426 were grown to mid-log phase and induced with 0.2 mM IPTG for 1 h. Whole-cell lysates were prepared, and the equivalent of 5×10^7 bacteria was separated by SDS-PAGE, transferred to nitrocellulose sheets, and probed with the indicated antibodies, as described in Section 2.12.4. Expression of each of the constructs was confirmed with the specified of the antibodies (anti-*Strep* denotes antibodies against *Strep*-tag II epitope). The i532 and i563 mutants (expressed by strains **MG424** and**MG426**, respectively) had no detectable expression defects when compared to the wild-type construct (expressed by strain **MG423**).

3.3.1 *Protein concentration-dependent defective polar targeting*

The subcellular distribution of the constructed proteins was then assessed by epifluorescence microscopy. Strains MG423, MG424 and MG426 were grown to mid-log phase, induced with 0.2 mM IPTG for one hour, and then mounted onto 1% LB agar pads and 200 randomly chosen bacteria were visualised for each strain (as described in Section 2.17.2). Foci of fluorescence in MG423 (wild-type)

were polarly targeted in >90% of cells; while MG424 (i532) and MG426 (i563) displayed diffuse fluorescence in >95% of cells and were considered non-polar (**Figure 3.7**). However, in 2-3% of cells from strain MG424 and MG243 displayed foci of fluorescence that displayed rapid motion. These foci seemed to migrate

Figure 3.7: **Subcellular localisation of epitope tagged IcsA$_{506-620}$-GFP+ fusions**. Strains MG423 (IcsA$_{506-620(WT)}$), MG424 (IcsA$_{506-620(i532)}$) and MG426 (IcsA$_{506-620(i563)}$) were grown to mid-log phase and expression of fusion proteins was induced with 0.2 mM IPTG. Bacteria were washed in medium, mounted onto 1% agarose pads and visualised by microscopy, as described in Section 2.17.2. Polar foci of fluorescence were seen in MG423, expressing the wild-type IcA$_{506-620}$ region. MG424 and MG426, expressing this region from IcsA$_{i532}$ and IcsA$_{i563}$, did not form foci and were non-polar, with diffuse fluorescence in the cytoplasm. Bacterial cell shapes are outlined from corresponding phase contrast images. Scale bar represents 3 μm.

freely throughout the cell, in contrast to foci of the wild-type construct that were seen to be immobile at the pole. Live imaging was used to capture a time-lapse of representative motion of one such fluorescent focus of the IcsA$_{506-620(i532)}$ fusion over a 60 second time-series (**Figure 3.8**). The motion of this focus was further analysed by determining its displacement and its velocity. Assuming straight-line motion from frame-to-frame, the focus displayed rapid and highly variable velocity, averaging 0.4 μ/s (**Figure 3.9**). The focus travelled along the entire long axis of the bacterium, totalling approximately 24 μm over the 60 second time-course (**Figure 3.9**). This equated to more than 6 cell lengths. These data demonstrated directly that IcsA$_{i532}$ and IcsA$_{i563}$ of May and Morona (2008) were deficient in their ability to guide targeting to the pole within the cytoplasm.

Whether the the rapid motion of fluorescent foci from GFP+ fusions to mutated IcsA$_{506-620}$ polar targeting domains was concentration-dependent was investigated. Strains MG423, MG424 and MG426 were induced to greater expression of the fusion with 1 mM IPTG for one hour. Following induction, bacteria were mounted on 1% LB agar pads and visualised, as described in Section 2.17.2. Under these conditions, for all the constructs, more than 95% of cells exhibited

fluorescent foci that were immobile at the pole (**Figure 3.10**). Consequently, the loss of polarity that was evident for $IcsA_{506-620(i532)}$ and $IcsA_{506-620(i563)}$ GFP+ fusions was dependent on the cellular concentration of the fusion protein.

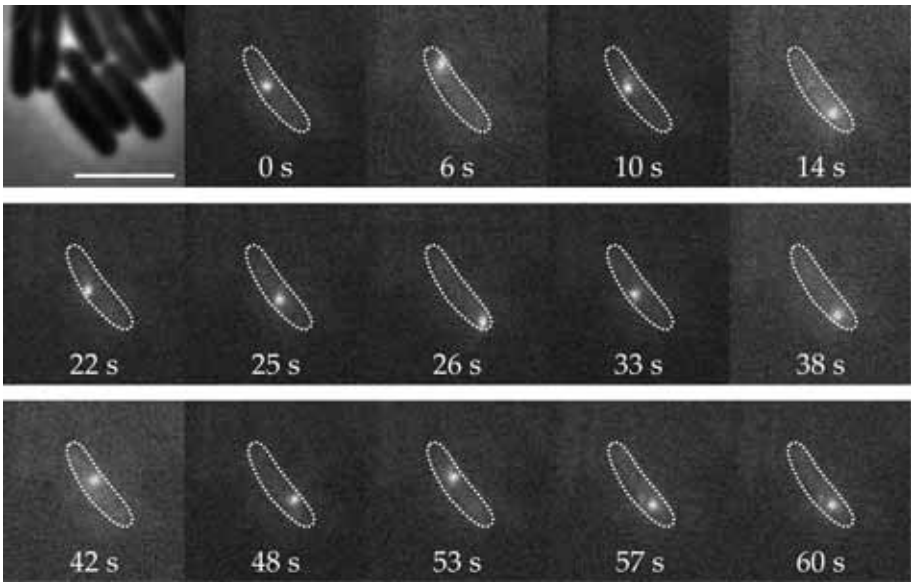

Figure 3.8: **Time-series of rapid motion displayed by a focus of a GFP+ fusion to the $IcsA_{506-620}$ region from $IcsA_{i532}$.** Strain MG424 was grown to mid-log phase and expression of the $IcsA_{506-i532-620}$-GFP+ was induced with 0.2 mM IPTG. Bacteria were washed in medium, mounted onto 1% LB agar pads and visualised by microscopy, as described in Section 2.17.2. Foci were identified and recorded at 1 frame per second over a period of 60 seconds. The representative motion of one such focus is shown above, with a phase contrast image of the bacterium. To avoid photobleaching, short exposure times (150 ms) were used. Consequently, the diffuse fluorescence of neighbouring cells is not distinguishable. Scale bar represents 3 μm.

Purification of these constructs using *Strep*-tactin and Ni-NTA affinity chromatography remains ongoing, as part of an effort to better understand both the biochemical characteristics of the fusion proteins and the polar targeting mechanism.

3.4 Refining the polar targeting region

Since the mutations within $IcsA_{i532}$ and $IcsA_{i563}$ directly interfered with cytoplasmic polar targeting, it was of interest to see if the sites of these mutations could delineate a more refined polar targeting subregion within $IcsA_{506-620}$. In-

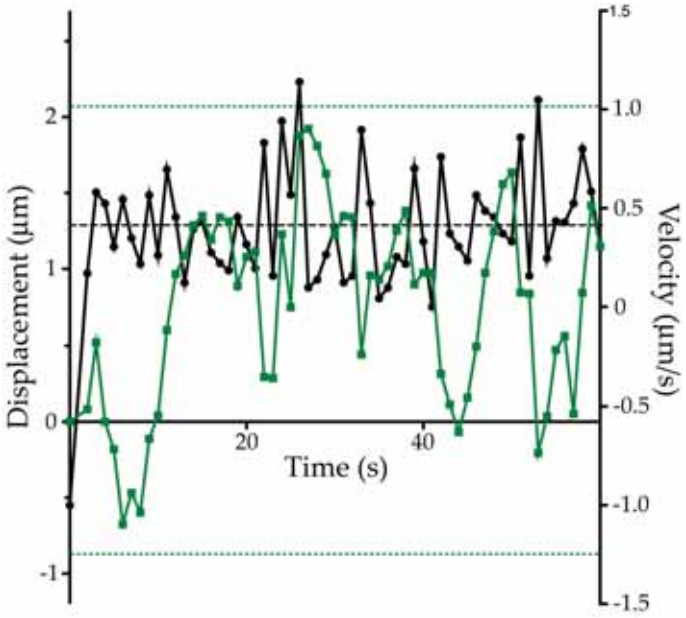

Figure 3.9: **Tracking analysis of a mobile focus in Figure 3.8**. Images from time-series acquired in **Figure 3.8** were analysed by MetaMorph (v6.7) point tracking function. Frames were taken every 1 second over a 60 second time-course. Velocity (**black, right Y axis**) is presented assuming straight line displacement from frame-to-frame. Average velocity is presented as the **black dotted line**. Displacement (**green, left Y axis**) is measured from original position of the focus at *t*=0. Displacement to the extremities of the cell (the poles) are marked with two **green dotted lines**. Scale bar represents 3 µm.

terestingly, the Robetta-predicted structure of IcsA generated by May (2007), suggested the presence of an α-helical loop region between the mutational insertion sites at E_{532} and T_{563} (**Figure 3.11**). This predicted structure could have been disrupted in the May and Morona (2008) mutants, leading to the non-polar phenotype observed in this work (**Figure 3.7**). Construction of a range of GFP+ fusions was informed by both the predicted structure and the sites of insertion mutations. Firstly, fusions that spanned and extended (in either the amino- or carboxy-terminal direction) the predicted α-helical region were constructed in *E. coli* DH5α ($IcsA_{506–562}$, $IcsA_{538–620}$, and $IcsA_{538–562}$; **Figure 3.11**). Additionally, a fusion was made spanning a larger region extending from the E_{532} to V_{570} that incorporated the predicated helix, but also two predicted β-strands ($IcsA_{532–570}$; **Figure 3.11**). Fusions extending in both amino- and carboxy-terminal directions were also made for this region ($IcsA_{506–570}$ and $IcsA_{532–620}$; **Figure 3.11**). GFP+ fusions were constructed as described previously in Section 3.2: *icsA* regions

Figure 3.10: **Representative images of fluorescent foci localisation at higher level of expression**. Strains MG423 ($IcsA_{506-620(WT)}$), MG424 ($IcsA_{506-620(i532)}$), and MG426 ($IcsA_{506-620(i563)}$) were grown to mid-log phase and expression of GFP+ fusions was induced with 1 mM IPTG for one hour. Bacteria were washed in medium, mounted onto 1% LB agar pads and visualised by microscopy, as described in Section 2.17.2. More than 95% of bacteria exhibited immobile polar foci of fluorescence. Bacterial cell shapes are outlined from corresponding phase contrast images. Scale bar represents 3 μm.

were amplified from pIcsA with oligonucleotides that introduced *Nhe*I and *Xba*I restriction sites to flank the amplicon at the 5′ and 3′ end, respectively. Digestion of the PCR products with *Nhe*I and *Xba*I allowed for in-frame cloning at nt 5 of *gfp*+ in pRMA2611. Oligonucleotides used to create each construct are detailed in Appendix C. Recombinant plasmids were transformed into *E. coli* DH5α, and the fidelity of clones was checked by sequencing (Appendix E). The subcellular distribution of fluorescence in the corresponding strains was determined by fluorescence microscopy of 200 cells from two experiments that selected randomly from phase contrast microscopy images.

Fluorescence from GFP+ fusions to $IcsA_{506-562}$ and $IcsA_{538-562}$ (expressed by strains MG351 and MG356, respectively) did not show any foci and was non-polar (**Figure 3.12**). However, expression of $IcsA_{538-620}$-GFP+ was observed to result in immobile polar foci of fluorescence in more than 70% of cells from strain MG353 (**Figure 3.11**). Likewise, polar localisation was observed with GFP+ fusions to $IcsA_{506-570}$ and $IcsA_{532-620}$ in approximately 70% of cells (expressed by strains MG357 and MG358, respectively). A reduced incidence of immobile polar foci was observed for strain MG360, expressing $IcsA_{532-570}$-GFP+, where approximately 40% of cells were observed with polar fluorescence.

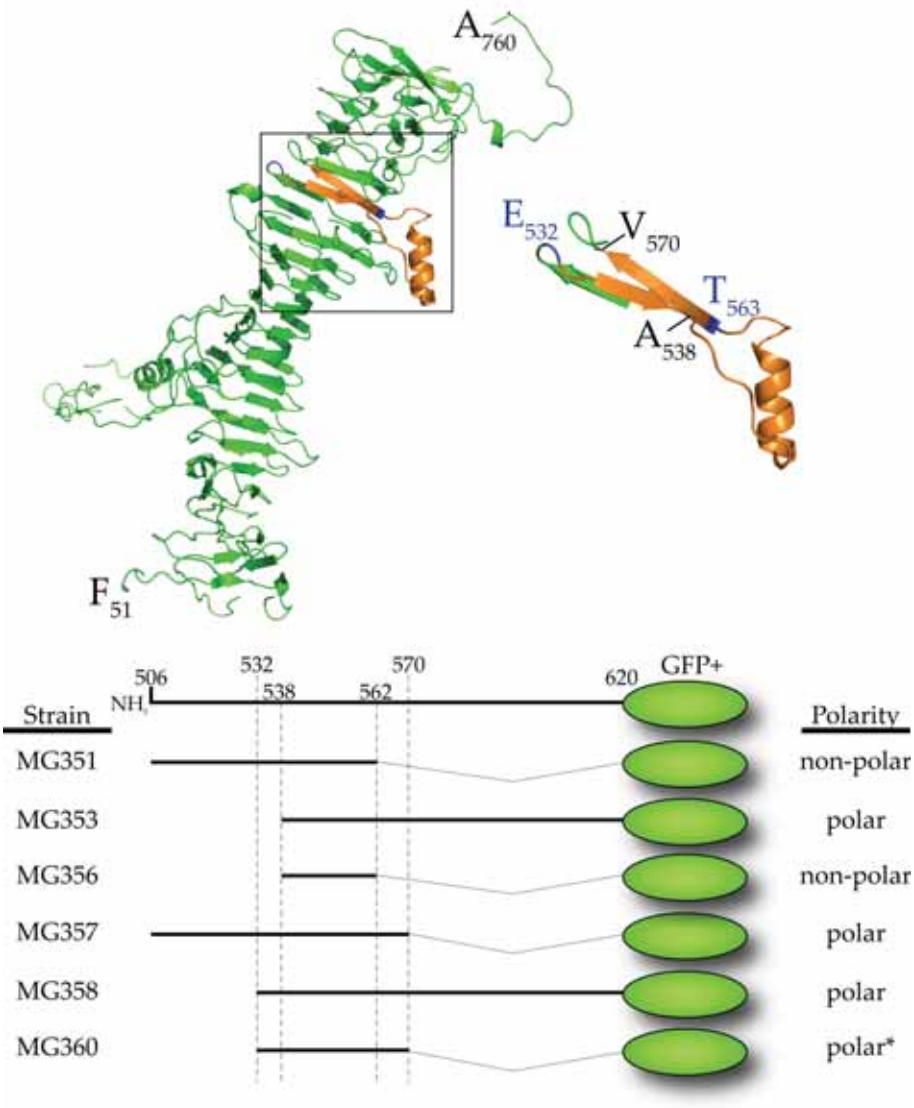

Figure 3.11: **Construction of GFP+ fusions to IcsA$_{506-620}$ subregions**. (**top, main**) The Robetta prediction of IcsA$_{51-760}$ structure generated by May (2007). (**top, inset**) the IcsA$_{533-570}$ region (**orange**) expanded, showing the sites of insertion for non-polar mutants i532 and i563 (**blue**). (bottom) Polar localisation of constructed GFP+ fusions. Strains were grown to mid-log phase, washed in medium, mounted on 1% agarose pads and imaged, as described in Section 2.17.2. Strains expressing polar foci of fluorescence in at least 70% of cells were defined as **polar**, with the exception of MG360 that expressed polar fluorescence in approximately 40% of cells (**polar***). **Non-polar** strains did not exhibit fluorescence foci.

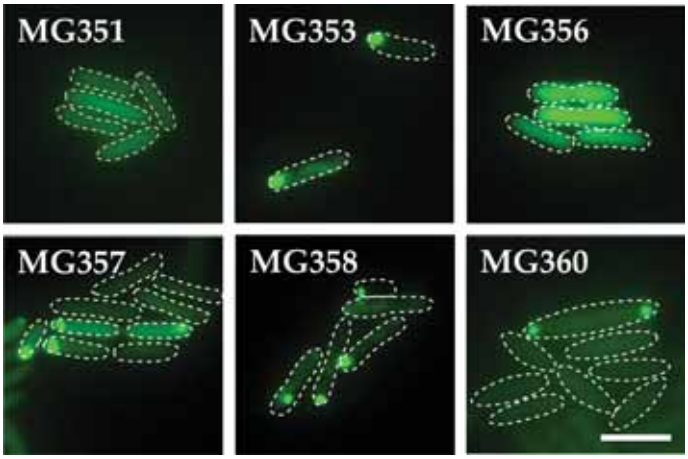

Figure 3.12: **Fluorescence localisation of GFP+ fusions to IcsA$_{506-620}$ subregions**. Indicated strains, expressing GFP+ fusions were grown to mid-log phase, washed in medium, mounted on 1% agar pads and visualised by fluorescence microscopy, as described in Section 2.17.2. Strains MG353, MG357 and MG358 expressed polar localisation of GFP+ fusions. Strains MG351 and MG356 were seen to have diffuse cytoplasmic fluorescence. Images are representative of fluorescence distribution across independent experiments. Bacterial cell shapes from corresponding phase contrast images are outlined. Scale bar represents 3 μm.

3.5 Summary

The polar targeting regions of IcsA described by Charles *et al.* (2001) were assessed in the presented experimental conditions. Any GFP+ fusion spanning the region IcsA$_{506-620}$ was found to be directed to the pole, in agreement with that study. However, in contrast with the findings of Charles *et al.* (2001), IcsA$_{1-104}$ was not sufficient for polar targeting in these conditions.

Strep-tag II and His$_6$ dual affinity-tagged GFP+ fusions of the IcsA$_{506-620}$ region from IcsA$_{WT}$, IcsA$_{i532}$, and IcsA$_{i563}$ were generated. The mutant fusions were found to be predominantly non-polar when expressed at a low-level, but displayed highly dynamic and mobile foci of fluorescence. Higher protein expression resulted in efficient polar targeting of the mutant-derived GFP+ fusions. The wild-type IcsA506-620 fusion was seen to form immobile fluorescent foci at the pole. The insertion mutants and a model of IcsA structure, guided creation of GFP+ fusions of fragments within the IcsA$_{506-620}$ region. IcsA$_{532-570}$ was found to be minimally sufficient for polar targeting, albeit at lower efficiency.

4

Polar targeting and the replicating chromosome

IcsA polarity has long been thought to be linked to the bacteria cell cycle. Goldberg *et al.* (1994) presented evidence suggesting that unipolar localisation was reinforced during cell division, with the "old" pole expressing high levels of IcsA and the "new" pole—formed on septation—being essentially devoid of the protein. Additionally, these same authors observed that 85% of intracellular bacteria expressing detectable IcsA were in the process of dividing. As reviewed in Section 1.7.4, *oriC* loci are the initiation sites of chromosomal replication in *E. coli*. The study of Lau *et al.* (2003) brought to light the dynamic motion of replicated *oriC* in live cells. *oriC* loci were found to be replicated at the mid-cell and, soon after, move towards opposing poles that following cytokinesis become "old" poles. The discovery of *C. crescentus* protein MipZ, published during these studies, demonstrated movement of that protein with the chromosomal origin of replication towards the cell poles (Thanbichler and Shapiro, 2006b). A similar mechanism whereby protein polar targeting is determined by the movement of replicated *oriC* loci was hypothesised as a possible basis for IcsA unipolarity, and would have been consistent with the reported links between IcsA biogenesis and bacterial cell division.

The aim of this chapter was to determine if IcsA polar targeting is correlated with the position of *oriC* during chromosome replication.

4.1 Constructing a plasmid for visualising IcsA polarity and *oriC*-motion in live *E. coli*

To visualise both *oriC* and $IcsA_{506–620}$ in live *E. coli* cells, the plasmid pLAU53 described by Lau *et al.* (2003) was adapted. pLAU53 encodes two fluorescent repressor protein fusions: TetR-EYFP and LacI-ECFP. These were used by Lau *et al.* (2003) to determine the subcellular position of chromosomal loci that were proximally tagged with arrays of repeating *lacO* or *tetO* operator sequences,

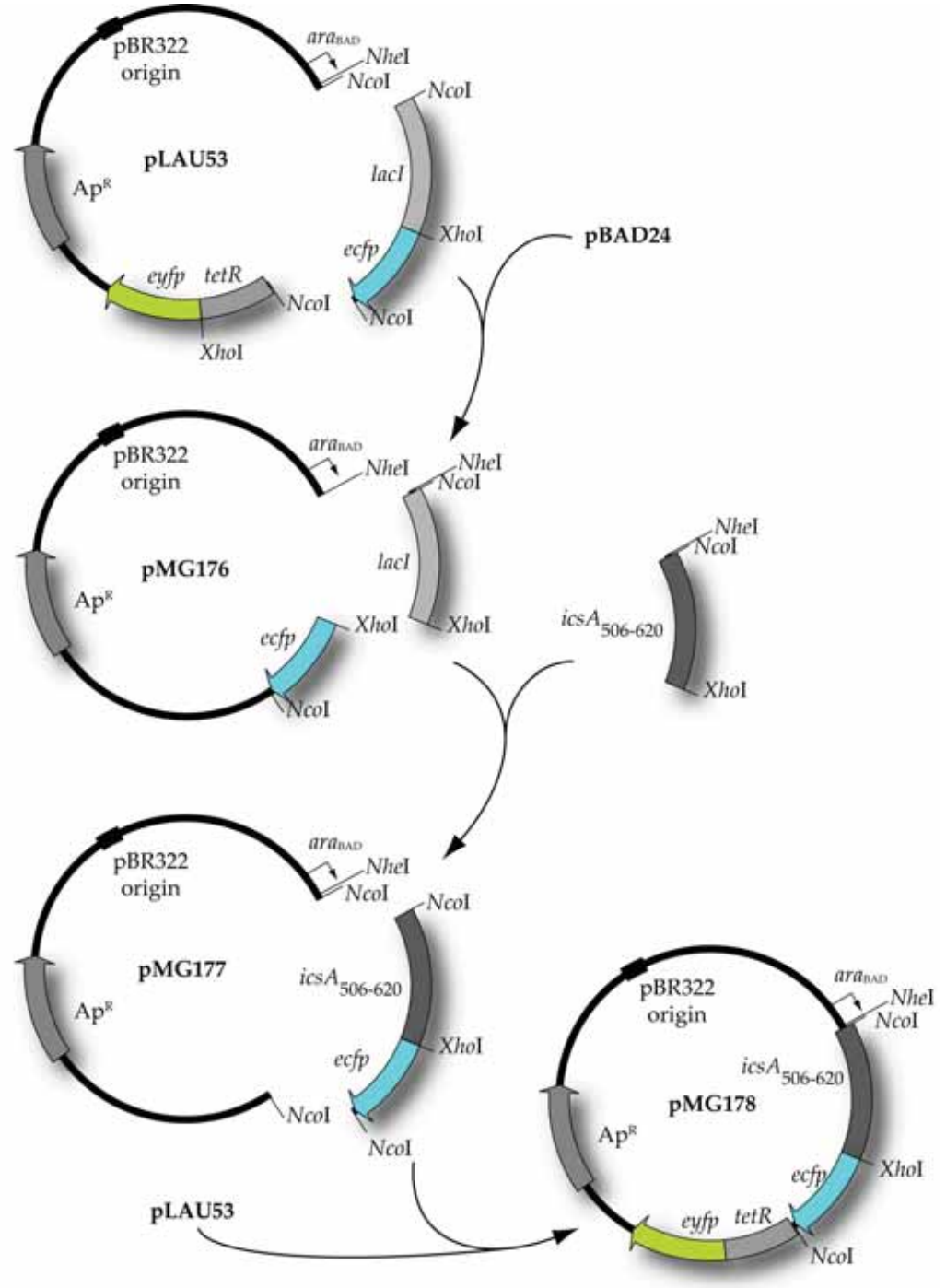

Figure 4.1: **Construction of pMG178 to visualise IcsA$_{506-620}$ and *oriC* in live *E. coli*.** *lacI-ecfp* was excised by *Nco*I digestion of pLAU53, and the fragment was cloned into the *Nco*I site of pBAD24, giving pMG176. *icsA*$_{506-620}$ was PCR amplified to include 5′ *Nhe*I and *Nco*I sites and a 3′ *Xho*I site. The *lacI* gene was then excised from pMG176 following *Nhe*I-*Xho*I digestions and replaced with similarly digested *icsA*$_{506-620}$ amplicon. Successful cloning constructed pMG177, expressing an in-frame gene fusion of *icsA*$_{506-620}$ to *ecfp*. This gene fusion was then excised from pMG177 using *Nco*I and cloned into the corresponding site in pLAU53, effectively replacing *lacI-ecfp* and generating pMG178.

respectively. When these recombinant fluorescent proteins were expressed in bacterial strains with the cognate operator sites, operator-repressor binding lead to discernible fluorescent foci that beaconed the position of a given genetic locus during the cell cycle.

In adapting the plasmid, *tetR-eyfp* was retained, since it was to be used to detect *tetO* arrays at *oriC* (Lau *et al.*, 2003). Consequently, the *Nco*I fragment encompassing *lacI-ecfp* was excised from pLAU53 and cloned into *Nco*I site of pBAD24, giving pMG176 (**Figure 4.1**). PCR was used to amplify $icsA_{506-620}$ from the plasmid pIcsA (Appendix B), using oligonucleotides "506_F_NheI-NcoI" and "620_R_XhoI" (Appendix F) that introduced flanking 5' *Nhe*I and *Nco*I sites, and a flanking 3' *Xho*I site. The amplicon was digested with *Nhe*I and *Xho*I, and cloned into the corresponding sites of pMG176 (**Figure 4.1**). This process replaced the *lacI* gene of pMG176 with $icsA_{506-620}$, and generated plasmid pMG177, that encoded a $IcsA_{506-620}$-ECFP gene fusion (**Figure 4.1**). The constructed fusion was then excised with *Nco*I and cloned into *Nco*I digested pLAU53, generating pMG178 (**Figure 4.1**). This plasmid encoded both $IcsA_{506-620}$-ECFP and a downstream TetR-EYFP fusion that, while co-transcribed, was in a different reading frame.

4.2 Examining polar targeting and *oriC*-motion

Plasmid pMG178 was transformed into the *E. coli* strain IL02 (Appendix A), as described in Section 2.10.1, generating strain MG182 (Appendix A). IL02 was generously donated by D. Sherratt (Oxford University), and carried an array of repeating *tetO* sequences near *oriC*. These operator sequences could be detected by TetR-EYFP encoded by pMG178. Since excessive operator-repressor binding could block DNA replication (Lau *et al.*, 2003), expression of TetR-EYFP (and consequently $IcsA_{506-620}$-ECFP) was regulated from an arabinose-inducible ara_{BAD} promoter. TetR-EYFP binding to *tetO* arrays was additionally regulated by growth in the presence of small amounts of the gratuitous inducer anhydrotetracycline (AhTc) that directly releases and prevents TetR binding of *tetO*, as described by Lau *et al.* (2003). Strain MG182 was grown overnight, subcultured 1:50 and grown to mid-log phase in LB broth supplemented with 0.2% glucose and 40 nM AhTc. Bacteria were then pelleted, washed in LB broth, and resuspended in equal volume of LB broth supplemented with 0.01% of the arabinose inducer, and 12

nM AhTc. Bacteria were induced in this way for 20 min, and then 0.2% glucose was added to cultures to suppress further gene expression. Bacteria were then immediately applied onto 1% LB or minimal medium agar pads, maintained at 37°C and a total of 300 cells from three experiments were examined by epifluoresence microscopy.

While foci of TetR-EYFP could be readily visualised, high autofluorescence hampered sensitive detection of $IcsA_{506-620}$-ECFP. Consequently, while 90% of bacteria contained discernible foci of EYFP fluorescence, only 61% contained clearly identifiable foci of ECFP fluorescence (**Figure 4.2**). Approximately 79% of cells contained at least two foci of TetR-EYFP fluorescence; an expected outcome of multifork replication that occurs in rapidly growing *E. coli* at 37°C (**Figure 4.2**). Of the 61% of cells containing $IcsA_{506-620}$-ECFP foci, >90% were found localised towards the polar region. Approximately 15% of cells were seen to have a single focus of $IcsA_{506-620}$-ECFP fluorescence that was at polar extremity; these cells also predominantly exhibited a single mid-cell TetR-EYFP focus (not shown).

When more two or more foci of $IcsA_{506-620}$-ECFP were evident (f=2, f>2), these foci were found to frequently co-localise with fluorescent TetR-EYFP foci (labelling *oriC*) in at least 78% of cells (for f=2; 91% co-localisation for f>2) (**Figure 4.2** and **Figure 4.3**). For cells exhibiting two foci (f=2) of $IcsA_{506-620}$-ECFP, co-localisation with TetR-EYFP occurred near the poles. When co-localisation was observed in the sub-population expressing more than two foci (f>2) of $IcsA_{506-620}$-ECFP, two foci of $IcsA_{506-620}$-ECFP and TetR-EYFP were predominantly found co-localised (not shown), and an additional focus of $IcsA_{506-620}$-ECFP was evident fixed at the polar extremity (**Figure 4.3**).

4.3 Verifying the specificity of IcsA and *oriC* co-localisation

The ECFP and EYFP fluorescent proteins are capable of Förster resonance energy transfer (FRET, also known as fluorescence resonance energy transfer). Hence, ECFP in its excited state is able to transfer energy to excite fluorescence emission of EYFP over short (<10 nm) distances. It was important to ensure that the observed co-localisation did not occur due to: (i) bleed-through fluorescence; (ii) FRET interactions; or (iii) translation from the same transcript. Therefore, control

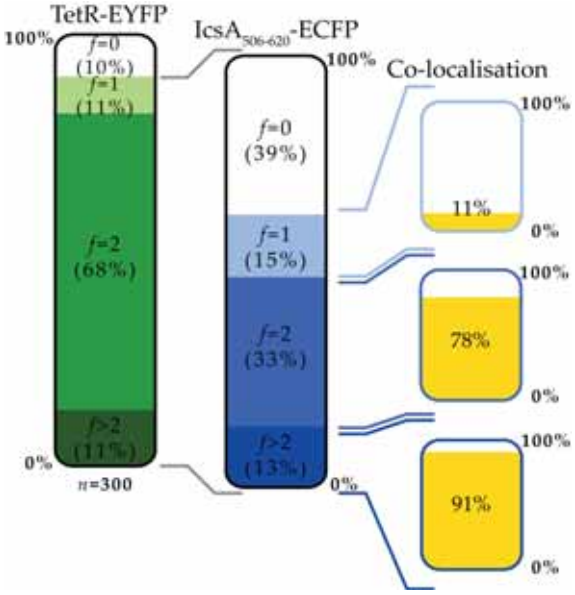

Figure 4.2: **Frequency of observed co-localisation of IcsA$_{506-620}$-ECFP and *oriC* labelled by TetR-EYFP**. Strain MG182 was grown and expression of fluorescent protein fusions induced as described in Section 4.2. A total of 300 bacteria from three independent experiments were identified from phase contrast images and the corresponding fluorescence images were analysed. Foci (*f*) of **TetR-EYFP** were evident in 90% of cells; these cells (n=269) were further analysed for expression of fluorescent foci of **IcsA$_{506-620}$-ECFP**. Bacteria that did not express TetR-EYFP foci (***f*=0**) were not further analysed. 61% of bacteria were seen to express at least a single focus of IcsA$_{506-620}$-ECFP fluorescence (***f*=1, *f*=2, *f*>2**). For these cells, the frequency of **co-localisation** was determined. Co-localisation was defined as exhibiting at least one set of co-incident foci of IcsA$_{506-620}$-ECFP and TetR-EYFP fluorescence. Detection of two or more IcsA$_{506-620}$-ECFP foci (***f*=2, *f*>2**) was seen to correlate with frequent co-localisation with TetR-EYFP labelled *oriC*.

strains were constructed such that foci of one fluorescent fusion were expected, while diffuse fluorescence was expected from the other fusion.

Strain MG184 was generated by transforming *E. coli* IL02 with pLAU53. This strain carried *oriC* proximal *tetO* arrays but no *lacO* sequences. Consequently, expression from pLAU53 of TetR-EYFP was expected to result in *tetO*-repressor foci; while diffuse fluorescence was expected from expressed LacI-ECFP. Indeed, when 200 randomly chosen cells were observed, fluorescence foci of TetR-EFYP were evident in more than 90% of bacteria, while LacI-ECFP foci were seen in fewer than 1% of bacteria (**Figure 4.4**).

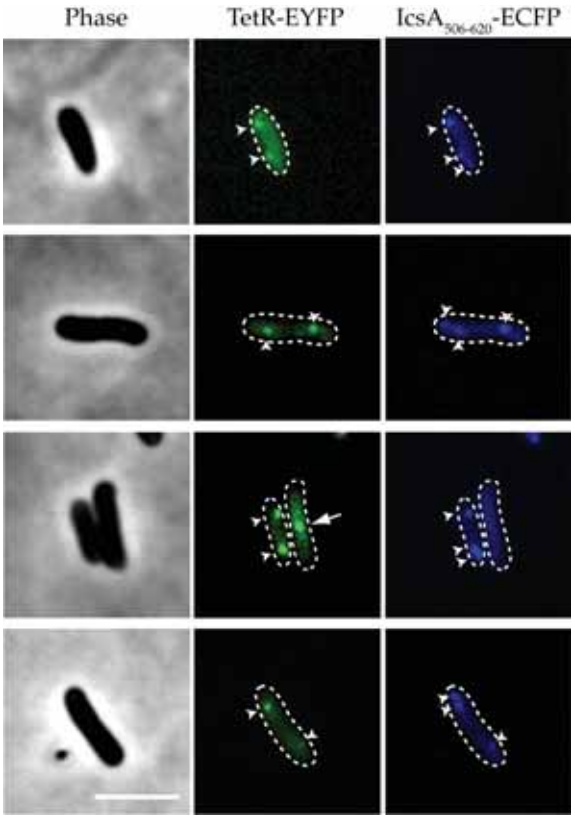

Figure 4.3: **Fluorescent foci of IcsA$_{506-620}$-ECFP and TetR-EYFP co-localise in live *E. coli*.** Strain MG182 was grown in LB broth supplemented with 0.2% glucose to mid-log phase, then washed once in LB broth, and finally resuspended in LB supplemented with 0.01% arabinose to induce expression of fluorescent protein fusions. Bacteria were grown in arabinose replete conditions for 20 min, then 0.2% glucose was added, and bacteria were mounted on 1% LB agar pads, as described in Section 2.17.2. Co-localisation of TetR-EYFP (labelling *oriC*) and IcsA$_{506-620}$-ECFP was observed in >90% of cells that displayed multiple ECFP foci (**arrowheads**). In approximately 70% of cells exhibiting co-localisation, an additional focus was seen fixed at the polar extremity. Cells that displayed a single focus of EYFP often lacked ECFP foci or contained foci fixed at the polar edge (**arrow**). Scale bar indicates 3 μm.

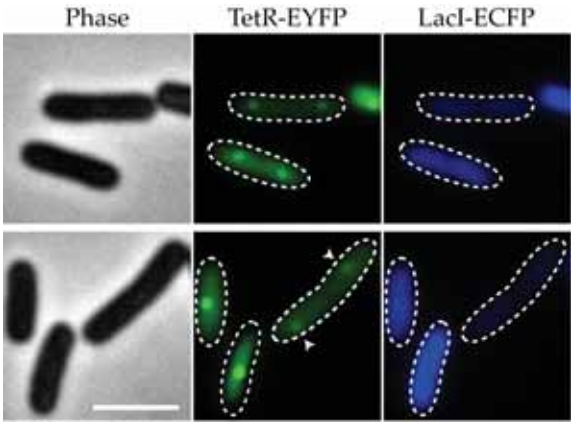

Figure 4.4: **No fluorescence co-localisation in strain MG184**. Strain MG184, carrying an array of repeating *tetO* and plasmid pLAU53 that expressed TetR-EYFP and LacI-ECFP, was grown and induced as described for MG182 in Section 4.2. While fluorescent TetR-EYFP foci were observed for 90% of cells, fewer than 1% of cells were seen to have LacI-ECFP fluorescent foci. **Arrowheads** highlight weakly fluorescent foci of TetR-EYFP. Scale bar indicates 3 μm.

Similarly, strain MG185 was generated by transforming *E. coli* IL03 with pMG178 . This strain carried a *lacO* array in the *ter* region of the chromosome, but lacked any *tetO* sites. Thus, expression from pMG178 of TetR-EYFP was expected to result in diffuse fluorescence without foci, while expression of $IcsA_{506–620}$-ECFP was expected to form foci near the poles. Indeed, from observation of 200 randomly chosen cells, $IcsA_{506–620}$-ECFP foci were seen near the cell poles in more than 60% of bacteria, while fewer than 1% of cells exhibited TetR-EYFP fluorescence (**Figure 4.5**). Again, high background fluorescence was likely to have contributed to the reduced detection of the $IcsA_{506–620}$ fluorescent fusion. $IcsA_{506–620}$-ECFP foci were also observed as multiple foci that were near the pole with or without additional foci at the polar extremity, mirroring the results obtained from strain MG182 (Section 4.2).

Taken together, these controls suggested that the observed co-localisation of $IcsA_{506–620}$-ECFP and TetR-EYFP in MG182 was specific to the inherent behaviour of the proteins in that *E. coli* strain.

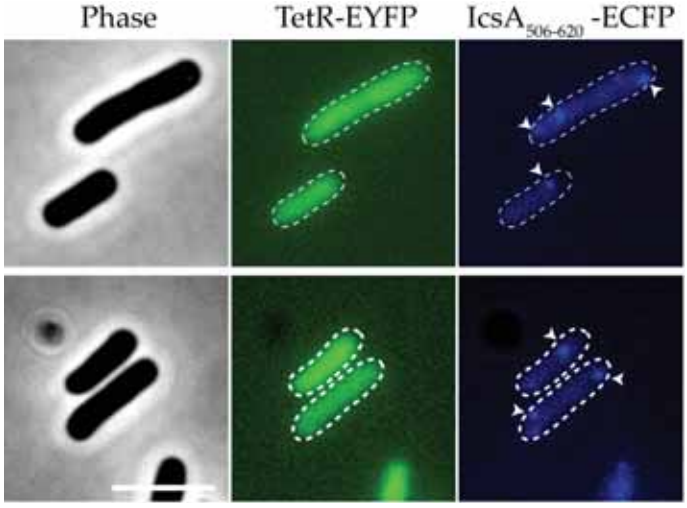

Figure 4.5: **No fluorescence co-localisation in strain MG185**. Strain MG185, carrying an array of repeating *lacI* and plasmid pMG178 that expressed TetR-EYFP and IcsA$_{506-620}$-ECFP, was grown and induced as described for MG182 in Section 4.2. While fluorescent IcsA$_{506-620}$-ECFP foci were observed in more than 60% of cells, fewer than 1% of cells were seen to have LacI-ECFP fluorescent foci. **Arrowheads** highlights weakly fluorescent foci of IcsA$_{506-620}$-ECFP. Scale bar indicates 3 μm.

4.3.1 *Filamented cells*

As reviewed in Section 1.8.2, Janakiraman and Goldberg (2004a) demonstrated that a IcsA$_{506-620}$-GFP fusion localises to nucleoid-free regions at regular intervals along the length of bacteria filamented by antibiotic treatment. To determine if the co-localisation of TetR-EYFP labelled *oriC* and IcsA$_{506-620}$-ECFP was maintained in filamented cells, bacteria were treated with the cell wall inhibitor cephalexin. Strain MG182 was grown, as described above (Section 4.2), with the modification that 30 μg/ml of cephalexin was added to growth media 1 hour after sub-culture. Expression of fluorescent protein fusions was induced following 2.5 hours of subculture by supplementing growth medium with 0.01% arabinose for 20-30 min. Following this induction, growth medium was supplemented with 0.2% glucose, and bacteria were mounted on 1% LB agar pads and immediately visualised by epifluorescence microscopy, as described in Section 2.17.2.

In filamented cells of MG182, IcsA$_{506-620}$-ECFP and TetR-EYFP fluorescent foci remained co-localised in approximately 90% of cells that displayed foci of both fluorescent protein fusions (**Figure 4.6**). Almost 80% of cells that exhibited

co-localisation, also contained foci that were at one or both poles, where *oriC* labelling was absent (**Figure 4.6**).

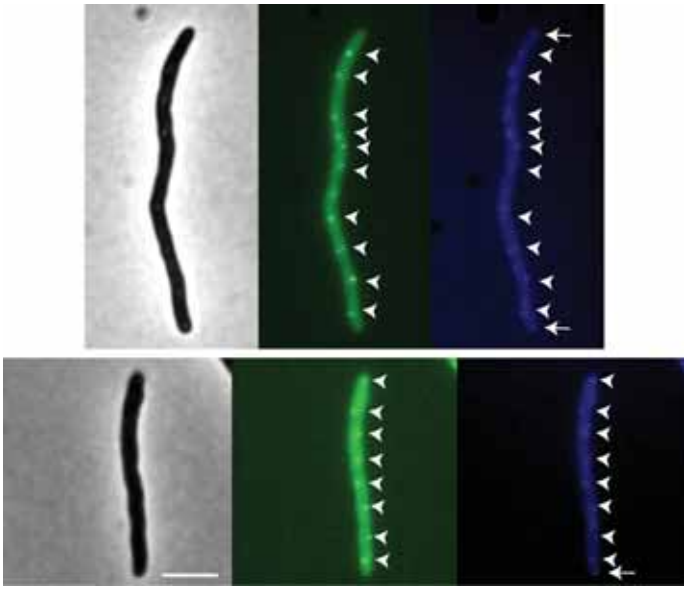

Figure 4.6: **IcsA$_{506-620}$-ECFP and *oriC* co-localisation is preserved in cephalexin-treated filamented cells**. Strain MG182 was grown and induced as described in Section 4.2, with the modification that 30 μg/ml cephalexin was added to growth medium 1 hour after subculture. Bacteria were grown in the presence of antibiotic for 1.5 hours, after which expression of fluorescent protein fusions was induced by addition of 0.01% arabinose to the growth medium for 20-30 minutes. Bacteria were then immediately mounted onto 1% LB agar pads and visualised. Co-localisation (**arrowheads**) of TetR-EYFP and IcsA$_{506-620}$-ECFP fluorescent foci was seen in 90% of cells that exhibited foci of both fusions. In approximately 80% of cells, an additional focus was also observed at the polar extremity that did not co-localise with TetR-EYFP (**arrows**). Scale bar represents 3 μm.

4.3.2 *MreB inhibition*

The prokaryotic actin homologue, MreB, defines cells shape by directing cell wall synthesis (Section 1.7.1). MreB forms filaments that can be seen spanning the long cell axis. These filaments can be depolymerised by the small molecule inhibitor A22 (*S*-[3,4-dichlorobenzyl]isothiourea). MreB filaments rapidly dissociate in the presence of A22, and within 2-3 generations gross alterations to cell morphology are evident (Gitai *et al.*, 2005). Previous work reported that in A22-treated spherical

cells, $IcsA_{506-620}$ polar targeting was seen to direct GFP fluorescence to discreet foci that likely corresponded to ectopic poles (Nilsen *et al.*, 2005; Pradel *et al.*, 2007). The localisation of $IcsA_{506-620}$-ECFP and TetR-EYFP labelled *oriC* was investigated in A22-treated cells to determine if the evident co-localisation was maintained, despite cell shape defects induced by the absence of MreB filaments.

Strain MG182 was grown as described above, with the alterations that 10 μg/ml of A22 was added to to mid-log phase cultures 2 hours after subculture. Bacteria were grown in the presence of A22 for between 1-2 hours, and then expression of fluorescent proteins were induced with 0.01% arabinose for 20 minutes. Bacteria (n=100) were visualised as described above on 1% LB agar pads. While >90 % of cells had defective morphologies, treatment with A22 significantly decreased the amount of bacterial cells and the inhibitor was likely to have been potently toxic. In cells that exhibited TetR-EYFP foci (approximately 60% of all cells), co-localisation with $IcsA_{506-620}$-ECFP was preserved in approximately 80% of cells, despite the defective cell shape (**Figure 4.7**).

4.4 Overexpressing the centromere-like *migS* sequence

The *E. coli migS* locus is a centromere-like DNA sequence proximal to *oriC* that had previously been reported to be important in the separation of *oriC* sequences after their replication. Loss of this region, or its overexpression on a high copy number plasmid, resulted in reduced migration of *oriC* away from the mid-cell, where chromosome replication is initiated (Yamaichi and Niki, 2004). Whether $IcsA_{506-620}$-ECFP co-localisation with TetR-EYFP labelled *oriC* would be preserved when *oriC* migration was disrupted by *migS* overexpression was investigated.

To overexpress the *migS* in *E. coli*, its 25 bp sequence was cloned into high copy number vector, pUC18, as described by Yamaichi and Niki (2004). This was achieved using epitope insertion by annealing oligonucleotides "pUC18_migS_F" and "pUC18_migS_R" (Appendix D), as described in Section 2.9.1). The annealed dsDNA formed *Bam*HI and *Sal*I compatible overhangs (**Figure 4.8**). This dsDNA was then cloned into *Bam*HI and *Sal*I linearised pUC18 vector, and a successful clone was denoted as pMG214.

Since pUC18 encoded an Ap^R marker, the plasmid pMG178 (also Ap^R) was modified to allow for selection of its carriage. The *$icsA_{506-620}$-ecfp* and *tetR-eyfp*

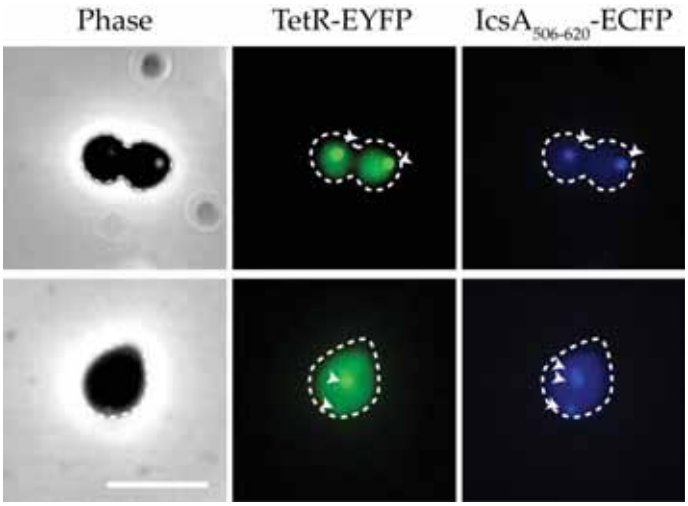

Figure 4.7: **IcsA$_{506-620}$-ECFP and *oriC* co-localise following MreB inhibition**. Strain MG182 was grown to mid-log phase as described in Section 4.2. After 1 hour of subculture, 10 μg/ml of A22 was added to the growth medium. Cells were grown in the presence of A22 for 1.5 hours, and then expression of fluorescent proteins fusions was induced by supplementing media with 0.01% arabinose for 30 minutes. Following induction, 0.2% glucose was added to media, and 100 bacteria were then immediately mounted onto 1% LB agar pads and visualised. Irregular, spherical cells were seen following A22 treatment. Despite defective shape, co-localisation of IcsA$_{506-620}$-ECFP with TetR-EYFP was retained in 80% of cells that exhibited foci of EYFP fluorescence. Approximately 40% of all cells displayed only diffuse fluorescence. Scale bar represents 3 μm.

containing *Bam*HI-*Hind*III fragment of pMG178 was subcloned into the same sites of pBAD30 (Appendix B), generating pMG236. Plasmids pMG214 and pMG236 were sequentially transformed into *E. coli* IL02, generating strain MG242, as described in Section 2.10.1. Strain MG242 was grown and induced as described for MG182 above (Section 4.2). Bacteria were mounted onto 1% LB agar pads and, at random, 200 cells from two experiments were chosen for inspection.

Unlike strain MG182, where approximately 80% of cells exhibited two foci of TetR-EYFP fluorescence, 47% of bacteria from MG242 showed only one discernible focus or two foci in very close proximity at the mid-cell (***f*=1; Figure 4.9**). This was in agreement with Yamaichi and Niki (2004). Bacteria that displayed foci of EYFP fluorescence were subsequently further analysed for their ECFP fluorescence. 46% of cells of analysed cells did not contain foci of IcsA$_{506-620}$-ECFP. When cells exhibited a single IcsA$_{506-620}$-ECFP focus (f=1), a TetR-EYFP focus was predom-

Figure 4.8: ***mig*S sequence construction by oligonucleotide annealing**. Complementary oligonucleotides were annealed together, as described in Section 2.9.1. The resultant dsDNA encoded the *migS* sequence (**green**) and generated *Bam*HI and *Sal*I compatible overhangs. This dsDNA was cloned into the corresponding sites of pUC18, and successful cloning gave pMG214.

inantly seen at mid-cell and only 7% co-localisation was evident (**Figure 4.10**). When co-localisation was observed in these cells, two foci of TetR-EYFP were evident near the poles. When two or more foci of $IcsA_{506-620}$-ECFP were present (f=2, f>2), co-localisation with TetR-EYFP was observed for approximately 30% of cells (**Figure 4.9 and Figure 4.10**).

4.5 Summary

The motion of replicated *oriC* loci towards the old poles, paralleled that which might have been expected for $IcsA_{506-620}$. Whether $IcsA_{506-620}$ polar delivery occurred concurrently with the motion of *oriC* was investigated. $IcsA_{506-620}$-ECFP was found to form foci at the polar extremity, but also to co-localise with the migrating TetR-EYFP labelled *oriC* near the poles. Interestingly, single *oriC* foci at the mid-cell—that were likely awaiting the initiation of chromosome replication—were not associated with detectable co-localisation. The observed $IcsA_{506-620}$-*oriC* co-localisation remained intact in cells treated with cephalexin to prevent septation and induce filamentous growth. Likewise, depletion of MreB filament and defective cell shape morphology did not disrupt the observed co-localisation. When the proposed centromere sequence, *migS*, was over-expressed inside cells, the distribution of *oriC* foci was altered and predominantly restricted to near the mid-cell. However, $IcsA_{506-620}$ continued to be delivered to the pole, and co-localisation between IcsA and *oriC* was reduced.

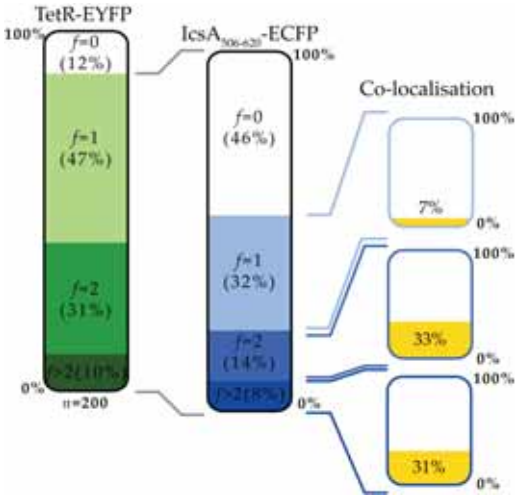

Figure 4.9: **Frequency of observed co-localisation of IcsA$_{506-620}$-ECFP and *oriC* labelled by TetR-EYFP in *E. coli* overexpressing *mig*S**. Strain MG242 was grown and expression of fluorescent protein fusions induced as described in Section 4.2. A total of 200 bacteria from two independent experiments were identified from phase contrast images and the corresponding fluorescence images were analysed. Foci (f) of **TetR-EYFP** were evident in 88% of cells; these cells (n=176) were further analysed for expression of fluorescent foci of **IcsA$_{506-620}$-ECFP**. Bacteria that did not express TetR-EYFP foci (f**=0**) were not further analysed. Cells denoted as expressing a single TetR-EYFP focus (f**=1**) also include cells that expressed two *oriC* foci in very close proximity to the mid-cell (that were not evident in MG182). 54% of bacteria were seen to express at least a single focus of IcsA$_{506-620}$-ECFP fluorescence (f**=1,** f**=2,** f**>2**). For these cells, the frequency of **co-localisation** was determined. Co-localisation was defined as exhibiting at least one set of co-incident foci of IcsA$_{506-620}$-ECFP and TetR-EYFP fluorescence. Where a single IcsA$_{506-620}$-ECFP focus was seen, co-localisation was seen in only 7% of cells. Detection of two or more IcsA$_{506-620}$-ECFP foci (f**=2,** f**>2**) was weakly correlated with TetR-EYFP labelled *oriC* co-localisation (approximately 30% of cells).

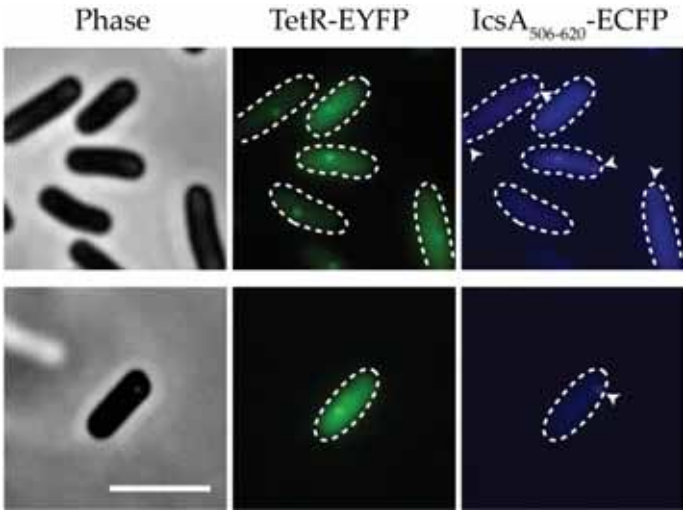

Figure 4.10: **Overexpression of *migS* reduced co-localisation of IcsA$_{506-620}$ and *oriC*.** Strain MG242 was grown and induced as described in Section 4.2, mounted onto 1% LB agar pads and visualised, as described in Section 2.17.2. A majority of cells exhibited single mid-cell foci, and IcsA$_{506-620}$-ECFP was predominately found at the poles of these cells, lacking co-localisation with TetR-EYFP labelled *oriC*.

5

Surface distribution of LPS modal lengths in *Shigella flexneri*

5.1 Introduction

The production of small anucleate minicells arising from the poles of mother cells is the hallmark of the *min* phenotype, produced on mutation of either *minC* or *minD* of the *minCDE* locus in *E. coli*, *S. flexneri* and other rod-shaped bacteria (Section 1.7.3) (de Boer *et al.*, 1989). Because minicells are enriched for polar cellular contents, they have been invaluable in identifying differences in sub-cellular constituency. Consequently, the composition of cell poles can now be differentiated from the rest of the cell by quantitative and qualitative differences in proteins, mRNA, rRNA, lipids, cell wall and even genetic loci, to the extent that the poles can be considered cytologically distinct (Levy, 1975; de Pedro *et al.*, 1997; Koppelman *et al.*, 2001; Lai *et al.*, 2004; Wang, 2005).

Numerous studies in *S. flexneri* and *E. coli* have attempted to address the apparent interplay between IcsA and LPS in the protein's localisation and function (reviewed in Section 1.6). Owing to the complex phenotypes associated with mutations in LPS biosynthesis, understanding this influence has been complicated. For example, rough mutations produce truncated LPS and result in both greater exposure of surface proteins, and (at least in one study) the increase of outer membrane fluidity (Section 1.6.2). Either of these phenotypes could independently account for the loss of surface IcsA unipolarity evident in rough mutants—improved detection of low concentration non-polar IcsA sub-populations, or IcsA migration away from the pole in a membrane with a reduced diffusion barrier.

A further hypothesis for the influence of LPS on protein surface polarity suggested that the distribution of LPS is itself non-uniform (Pugsley and Buddelmeijer, 2004). In particular, preferential localisation of shorter Oag chain length LPS molecules at the pole was proposed to enhance the perceived polar distribution of outer membrane proteins, especially those (such as IcsA) specifically targeted towards the pole. In this scenario, such proteins would encounter reduced LPS

masking at the pole, allowing greater accessibility to the external milieu and to environmental or host substrates, thereby concentrating protein function to the pole. However, the distribution of LPS molecule lengths at the bacterial surface has not previously been investigated.

The above hypothesis was particularly interesting when applied to *S. flexneri* 2457T (serotype 2a) which carries two Oag chain length determining proteins: Wzz_{SF} (providing short-type LPS) and Wzz_{pHS-2} (providing very long-type LPS) (reviewed in Section 1.6.1). Hence, these bacteria express two modal lengths of LPS molecules at their surface. The presence of both modal chain lengths seems to be required for optimised virulence and for IcsA function (Hong and Payne, 1997; Van Den Bosch *et al.*, 1997). Non-uniform distribution of either or both of these proteins might give rise to complex distributions of LPS. Notably, a recent study has demonstrated polar targeting of the biosynthesis and export of *E. coli* capsular polysaccharide (K antigen) when investigating the cellular distribution of proteins (KpsD and KpsE) involved in these processes (McNulty *et al.*, 2006). Whether there is any polar preference to the distribution of either Wzz_{SF} or Wzz_{pHS-2} had to-date remained unknown.

This chapter sought to identify any differences in the LPS composition of the polar and lateral surface of *S. flexneri* 2457T by assaying the membranes of minicell and whole-cell fractions, respectively, of a *min* mutant. Whether distribution of *S. flexneri* Wzz_{SF} and Wzz_{pHS-2} was non-uniform was also investigated.

5.2 Creation of a *S. flexneri* minicell mutant

A minicell producing mutant of *S. flexneri* was constructed by allelic exchange of chromosomal *minD* with a disrupted mutant allele. In a previous study, May (2007) had cloned the 2064 bp *S. flexneri minCDE* region (including 98 bp of upstream and 164 bp of downstream DNA) to give pKMRM96 (May, 2007). The 1493 bp Km^R cassette from pKD4 (Datsenko and Wanner, 2000) was then PCR amplified with oligonucleotides "P1_*Pac*I" and "P2_*Pac*I" (Appendix F) which introduced flanking *Pac*I sites and retained the FLP recognition target sites, permitting cassette excision when supplied with FLP recombinase in *trans* (Datsenko and Wanner, 2000; May, 2007). The Km^R cassette was then cloned into pKMRM96

at the native *Pac*I site within *minD*, disrupting the gene and giving pKMRM161 (May, 2007).

In the current work, oligonucleotides "minF" and "minR" (Appendix F) were used to PCR amplify the mutagenised *minD* allele. This amplicon was used to transform *S. flexneri* 2457T expressing the λ red recombinase on pKD46 (MG291; Appendix B) by electroporation (Section 2.10.4) (Datsenko and Wanner, 2000). Transformants were screened for a Km^R phenotype. Mutants were confirmed by diagnostic PCR using oligonucleotides "minF" and "minR" and displayed a single band of the expected amplicon of 3541 bp, whereas the wild-type allele generated the expected amplicon of 2064 kb (**Figure 5.1**).

Mutation was also proven phenotypically: phase-contrast microscopy was employed to confirm expression of the *min* phenotype. A putative mutant and its otherwise isogenic parent were grown to mid-log phase at 37°C in LB broth and placed on 1% LB agar pads and imaged (Section 2.17.2). Production of small spherical cells and filamentous cells was seen only in the mutant strain, and not in the wild-type (**Figure 5.2**).

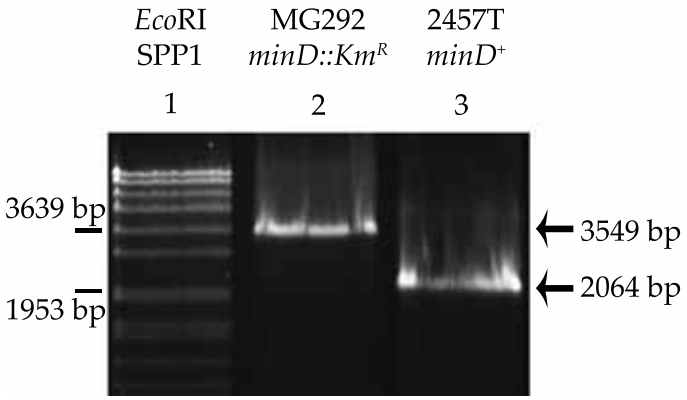

Figure 5.1: **Diagnostic PCR confirmation of *minD* mutation in *S. flexneri* 2457T**. Chromosomal DNA was obtained from *S. flexneri* 2457T and the putative *minD* mutant (MG292; Table G.2) and the *minCDE* locus was amplified with oligonucleotides "minF" and "minR". An expected wild-type amplicon of 2064 bp was detected for the parental strain, as expected (**Lane 3**). A larger, 3549 bp product corresponding to the expected size of a *minD*::Km^R disruption, was obtained from the putative mutant (**Lane 2**). Sizes were determined by comparison of band migration to *Eco*RI digested SPP1 DNA marker (**Lane 1**).

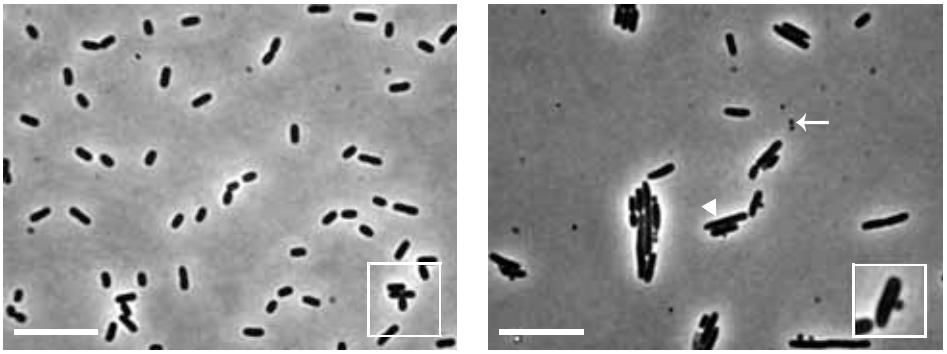

(a) (b)

Figure 5.2: **Phase contrast microscopy of the *min* phenotype displayed by *S. flexneri* *minD::Km*^{R}, MG292.** *S. flexneri* 2457T (**a**) and its *minD::Km*^{R} mutant, MG292 (**b**) were grown at 37°C to mid-log phase in LB, washed in medium, and placed on thin 1% agar LB pads prepared on glass microscope slides (as described in Section 2.17.2). Arrow indicates representative minicells; arrowhead identifies representative filamented whole-cell. Scale bar indicates 10 μm.

Phase contrast images of both wild-type and putative mutant were quantitated to determine cell length for a total of 1400 bacteria from two independent experiments (Section 2.17.4). Analysis demonstrated that while the wild-type parent predominantly exhibited cell size between 2-3 μm, the putative mutant produced a high proportion of small minicells (<1 μm) and very long cells (>6 μm) that were absent from the parental strain (**Figure 5.3**). These data confirmed a *minD* mutant of *S. flexneri* 2457T displaying a *min* phenotype had been isolated. The mutant was denoted as strain MG292 (Appendix A).

The small minicells of MG292 were expected to be enriched in constituents of the cell pole, while the large number of elongated whole-cells carried more components found on the lateral cell body. Hence, analysis of the protein and LPS content of the minicells and whole-cells of MG292 permitted comparison between the composition of these sub-cellular sites. That minicell production by MG292 was not evident at every division, was an expected outcome. Approximately 25% of cells were the wild-type equivalent 2-3 μm in length, having emerged from mid-cell division events. As reviewed in Section 1.7.3, in the absence of Min-mediated control of septum placement, the default cellular program of division selects either the mid-cell or the polar quarter-cell positions for septation. This likely arises from the physical and biochemical properties of FtsZ polymerisation and Z ring assembly (reviewed in Section 1.7.2).

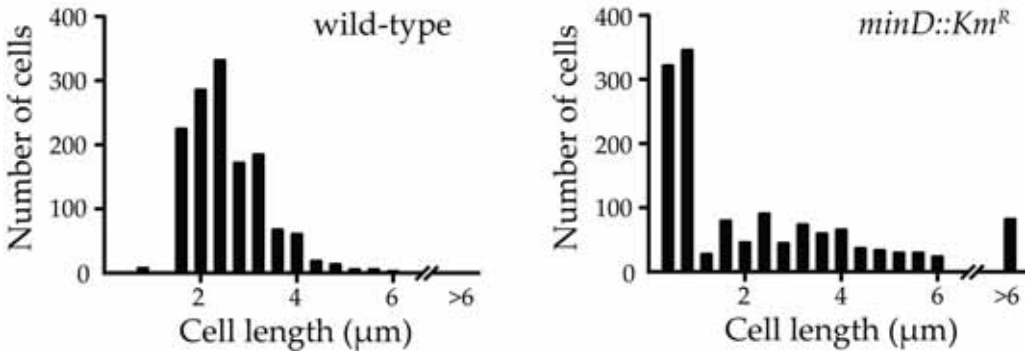

Figure 5.3: **Histograms of cell lengths of mid-log phase wild-type *S. flexneri* 2457T and *minD::Km*^{R} derivative, MG292.** Bacteria imaged by phase-contrast microscopy were quantitated using MetaMorph, as described in Section 2.17.4 with valid cells taken as phase dense areas >0.2 μm in length. From two independent experiments, 1400 bacteria were identified and cell length recorded.

5.3 Minicell purification and analysis

To assess the differences in constituency between the minicell and the whole-cell fraction of MG292, minicells were purified from whole-cells of M292 cultures using sucrose density gradient centrifugation, as described in Section 2.13.1. Cultures grown to both mid-log phase and to stationary phase were purified for subsequent analysis, since a recent study had reported growth stage-dependent alterations to LPS modal lengths in *S. flexneri* 2457T (Carter *et al.*, 2007). Purity of cellular preparations was confirmed by phase-contrast microscopy, with >99% of cells being minicell or whole-cell in their respective fractions (**Figure 5.4**).

5.3.1 *Distribution of Wzz proteins*

LPS export seems to occur throughout the outer membrane at discreet sites (which may correspond to the controversial Bayer's patches of cytoplasmic and outer membrane contact) (Mühlradt *et al.*, 1973). Differential subcellular distribution of either Wzz_{SF}, or Wzz_{pHS-2}, or both Oag chain length regulators could result in non-uniform distributions of LPS chain lengths at the cell surface, perhaps in regions overlying the corresponding Wzz proteins. Indeed, a previous study had identified a distinct sub-population of non-mobile *E. coli* LPS arranged along a helical band spanning the cell with polar reinforcement (Ghosh and Young,

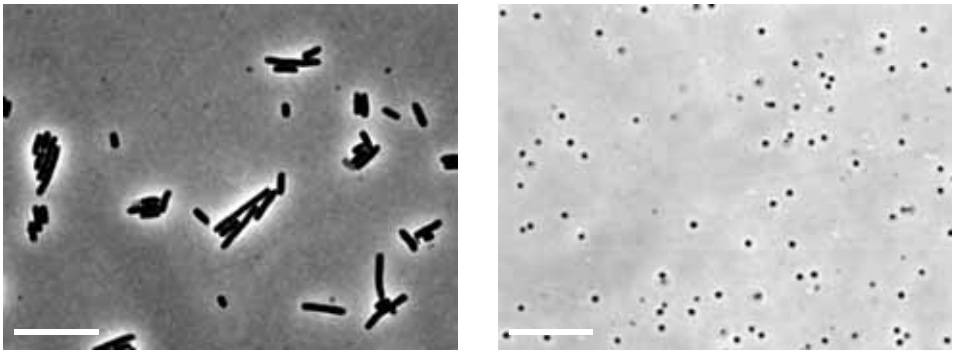

(a) (b)

Figure 5.4: **Representative phase-contrast microscopy of purified cell fractions of *S. flexneri* 2457T *minD*::Km^R derivative, MG292**. Density sucrose gradient centrifugation resolved whole-cells (**a**) and minicells (**b**) from cultures of MG292. Respective fractions were judged to be >99% pure for each cell type. Collected fractions were washed in LB broth, placed on 1% agar LB pads prepared on glass microscope slides. Slides were examined as described in Section 2.17.3. Scale bar indicates 10 μm.

2005). To determine if there is a polar bias for either of the *S. flexneri* Wzz proteins, total membranes from purified fractions of minicells and whole-cells were independently extracted as described in Section 2.13.1. Membrane preparations were standardised by total protein content, determined using the BCA assay (Section 2.13.1). SDS-PAGE was used to resolve 10 μg of membrane proteins, which were then transferred to nitrocellulose and analysed by independently western immunoblotting with antibodies specific for Wzz_{SF} and Wzz_{pHS-2} (Section 2.12.4). The amount of Wzz_{SF} was found not to differ between purified minicell and whole-cell membranes, indicating uniform distribution between lateral and polar cellular regions (**Figure 5.5**). Likewise, the amount of Wzz_{pHS-2} did not differ between the preparations, indicating uniform distribution (**Figure 5.5**). Since IcsA exhibits polar reinforcement of protein, immunoblotting with anti-IcsA was used to confirm that differences in protein localisation could be compared between minicell and whole-cell membrane protein fractions. Indeed, more IcsA was detected in purified minicell membrane preparations than in whole-cell preparations (**Figure 5.5**).

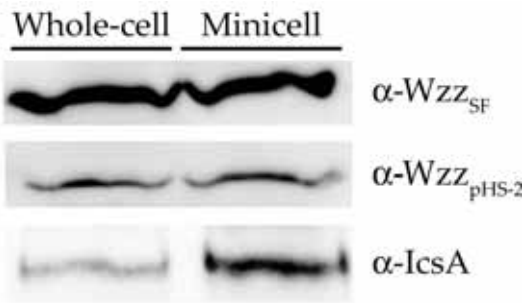

Figure 5.5: **Comparison of Wzz$_{SF}$ and Wzz$_{pHS-2}$ expression between minicell and whole-cell membranes of *S. flexneri minD::Km*^{R}, MG292**. Purified minicells and whole-cells were lysed by repeated passage through a French pressure cell, and total membranes isolated as described in Section 2.13.1. Samples were standardised by total protein content and 10 μg were resolved by SDS-PAGE, transferred to nitrocellulose and probed with polyclonal rabbit anti-Wzz$_{SF}$ or anti-Wzz$_{pHS-2}$ (as indicated), followed by a HRP-conjugated goat anti-rabbit. Immunoblots were visualised by enhanced chemiluminescence, as described in Section 2.12.4. The polarly targeted IcsA protein was used as a control for differential protein distribution, and was detected with anti-IcsA antibodies.

5.3.2 *Distribution of LPS*

The finding of inert populations of LPS at the pole by Ghosh and Young (2005), additionally raised the prospect of differential LPS chain length distribution through the biophysical properties of short, fluid LPS as compared to long, less fluid LPS molecules (Rottem and Leive, 1977; Yeh and Jacobs, 1992). To assess this, standardised membrane fractions isolated from purified minicells and whole-cells, grown to either mid-log phase or stationary phase, were Proteinase K-treated, and the remaining LPS was resolved on SDS-PAGE (Section 2.14.1, Section 2.14.2). LPS molecules were detected by silver staining, as described in Section 2.14.2. No difference in the abundance of LPS was seen between preparations from minicells or whole-cells of MG292, grown to either mid-log or stationary phases (**Figure 5.6**). Since the preparations were standardised by total protein content, the LPS:protein ratio was also equivalent between minicells and whole-cells. There was no evident difference in the distribution of modal lengths of LPS obtained from minicells and whole-cells in the same phase of growth (**Figure 5.6**). A slight lengthening of the modal length of S-type LPS was evident in preparations obtained from stationary phase, compared to LPS from mid-log phase. This was

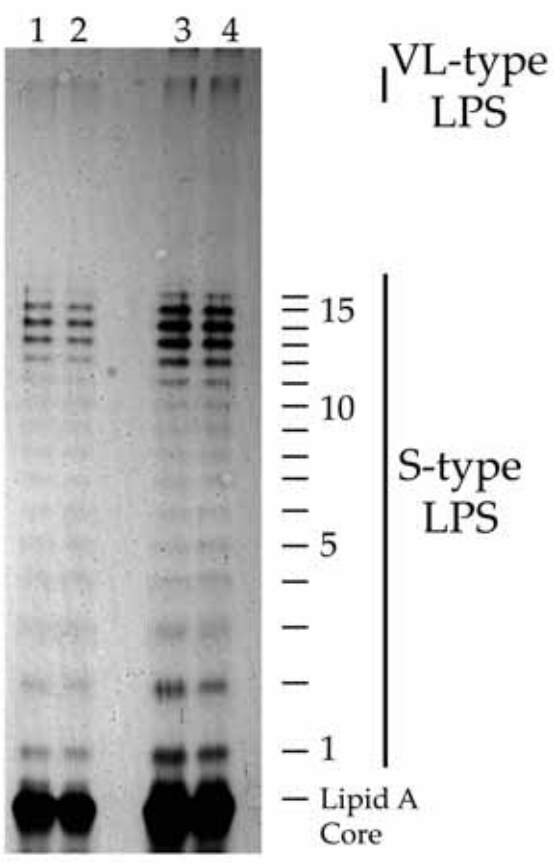

Figure 5.6: **Silver-stained SDS-PAGE analysis of LPS from minicells and whole-cells of *S. flexneri minD::Km*^{R}, MG292**. Membranes purified from minicells and whole-cells of MG292 grown to mid-log phase (**Lane 1** and **Lane 2**, respectively) and to stationary phase (**Lane 3** and **Lane 4**, respectively) were isolated and standardised by total protein content, as described in Section 2.13.1. Samples were Proteinase K-treated, resolved by SDS-PAGE, and visualised, as described in Section 2.14.2.

in agreement with the findings of Carter *et al.* (2007). Additionally, LPS prepared from stationary phase cultures seemed to have more VL-type LPS (**Figure 5.6**).

5.4 Summary

The surface distribution of *S. flexneri* LPS molecules had not previously been investigated. This chapter compared the cellular distribution of LPS and the two Wzz LPS Oag chain length regulators of *S. flexneri* 2457T by utilising a *minD::Km*$_{R}$ minicell producing mutant derivative, MG292. No differences were

seen between the abundance of either Wzz_{SF} or Wzz_{pHS-2} between the polar material-enriched minicells or the lateral material-enriched whole-cells purified from MG292. Likewise, no difference in the distribution of rough or smooth LPS molecules was observed and, aside from a slight increase in VL-type LPS from stationary phase bacteria, LPS seemed to be uniform between these cell populations. Consequently, the outer membrane is likely to be homogenous with regard to LPS molecule chain lengths, despite the observance of sub-populations of immobile LPS converging at the *E. coli* poles (Ghosh and Young, 2005). The findings of this chapter reject the notion that non-uniform LPS distribution could enhance polar surface distribution, or indeed promote polar distribution of proteins lacking polar targeting motifs (Pugsley and Buddelmeijer, 2004). Therefore, the establishment of IcsA polarity likely relies on the specific targeting mechanism directing unipolar localisation of nascent IcsA, and is not due to differential distribution of LPS modal lengths on the surface of *S. flexneri*.

6

IcsA behaviour in the outer membrane

While the process of IcsA export has been increasingly well documented, the behaviour of the exported protein within the outer-membrane has remained puzzling. Export across the outer membrane relies on BamA and is thought to be polarly focused. However, IcsA can also be detected at the lateral body of the cell cylinder in rough LPS expressing bacteria. How this non-polar IcsA subpopulation arises remains controversial and is proposed to occur either due to biophysical changes in the rough mutant outer-membrane that allows for protein diffusion away from the pole, or due to abolition of LPS masking in rough mutants that otherwise prevents detection of these proteins in wild-type bacteria (reviewed within Section 1.6.2 and Section 1.6.2).

The aim of chapter was to address these hypotheses by establishing a strategy for directly determining the behaviour of nascent IcsA in the outer-membrane of live bacteria.

6.1 Tagging IcsA by metabolic biotinylation

The biotin-streptavidin interaction is the strongest protein-ligand non-covalent interaction known in biology (K_d of between 10^{-13} and 10^{-15} M) and is highly specific (Choi-Rhee *et al.*, 2004). Biotinylation is also a rare protein modification. In *E. coli*, the BirA biotin protein ligase has only a single target: the cytoplasmic BCCP (biotin carboxyl carrier protein; encoded by *accB*), that is involved in the early stages of fatty acid biosynthesis (Chapman-Smith and Cronan, 1999). Despite such unique specificity, a recombinant 14 amino acid epitope (GLNDIFEAQKIEWH; referred to as "BIO" herein) is sufficient to direct BirA biotinylation of the lysine residue *in vivo* (Cull and Schatz, 2000). Biotinylation was chosen as a strategy for tagging exported IcsA due to: (i) the affinity and specificity afforded by the biotin-streptavidin interaction; (ii) the rapid detection offered by a range of fluorescent

streptavidin conjugate molecules; and (iii) the inherent absence of biotin from the *E. coli* (and *S. flexneri*) cell surface.

A previous linker-insertion mutagenesis study by May and Morona (2008) had identified sites within IcsA that were permissive for small insertions. One such insertion, at amino acid 87 ($IcsA_{i87}$), was chosen for cloning of the BIO epitope. The prototypical orientation of surface-exposed autotransporters orients the N-terminus furthest from the cell, potentially making the $IcsA_{i87}$ the most accessible insertion site of those generated by May and Morona (2008). In these mutants, *Not*I recognition sequences flank the insertional mutation. The *Not*I site within $icsA_{i87}$ was exploited for construction of a biotin-tagged IcsA construct.

The DNA sequence encoding the BIO tag was assembled by annealing together complimentary oligonucleotides (KM1_BIO_F and KM1_BIO_R; Appendix D), as described in Section 2.9.1, such that the dsDNA possessed *Not*I overhangs that facilitated in-frame cloning when ligated into *Not*I digested pKMRM1 plasmid that encoded $icsA_{i87}$ (**Figure 6.1**; Appendix B). Successful cloning gave plasmid pMG55, and the gene product was denoted as $icsA_{BIO}$. A negative control for biotinylation was similarly constructed within $IcsA_{i87}$. The control epitope was termed "BIOK10R" and replaced the biotin-accepting lysine of BIO with an arginine. Cloning of the epitope was performed as described above with complementary oligonucleotides BIO1_R(K)_F and BIO1_R(K)_R (Appendix D). The construct was denoted as $IcsA_{BIOK10R}$ and encoded by the plasmid pMG58. Gene expression in these plasmids was regulated by the native *icsA* promoter.

Because the major *E. coli* outer-membrane protease OmpT efficiently degrades exported IcsA, the constructed plasmids were expressed in *E. coli* UT5600, an *ompT* mutant (Section 1.4.4) (Nakata *et al.*, 1993). The protein expression of both $IcsA_{BIO}$ and $IcsA_{BIOK10R}$ (in strains MG57 and MG58, respectively) was confirmed by immunoblotting with anti-IcsA polyclonal antibodies (as described in Section 2.12.4). No significant difference in protein expression was seen between $IcsA_{i87}$, $IcsA_{BIO}$ or $IcsA_{BIOK10R}$ (**Figure 6.2**). Additionally, no significant degradation of the constructs was observed, suggesting the tagging strategy does not affect export of the proteins.

Biotinylation of $IcsA_{BIO}$ by BirA was expected to occur metabolically in the cytoplasm, prior to protein translocation. Whether the protein was successfully biotinylated was investigated by immunoblotting with direct detection of biotin by

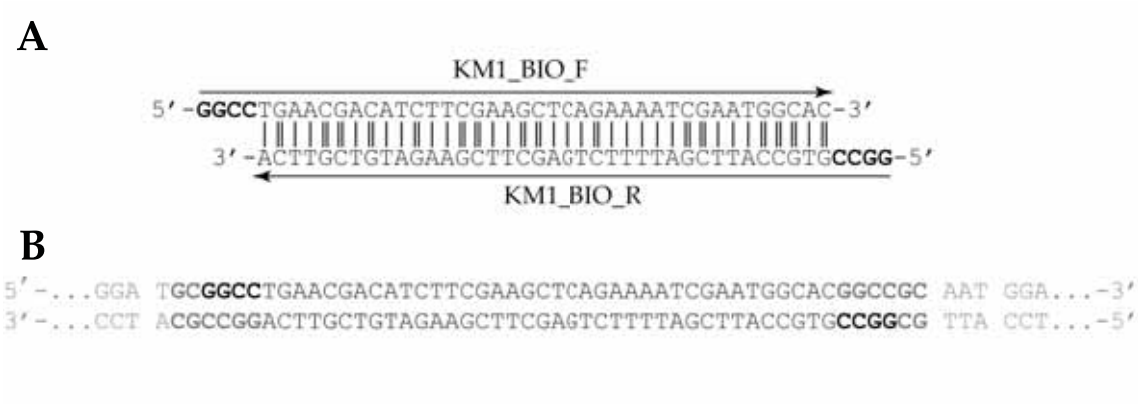

Figure 6.1: **BIO epitope construction and cloning into *icsA*$_{i87}$ of pKMRM1**. (**A**) Complementary oligonucleotides which were annealed together with the sequences encoding BIO (as described in Section 2.9.1), generating *Not*I overhangs (**bold**). (**B**) Annealed dsDNA (black) was ligated into *Not*I overhangs (**grey bold**) of digested *icsA*$_{i87}$ (**grey**) of pKMRM1, such that BIO was in-frame with *icsA*$_{i87}$, creating *icsA*$_{BIO}$ encoded by pMG55. The control epitope BIOK10R was constructed using the same strategy, giving pMG58.

streptavidin-HRP. While IcsA$_{BIO}$ was readily detected, IcsA$_{i87}$ was undetectable (**Figure 6.2**). Biotinylation of the control protein IcsA$_{BIOK10R}$ was also not detected (**Figure 6.2**). Clearly, IcsA$_{BIO}$ was being specifically biotinylated at the lysine of BIO; since the lysine to arginine substitution of BIOK10R abrogated biotinylation, the negative control protein was validated.

Figure 6.2: **Comparison of IcsA construct expression in *E. coli* UT5600**. Whole-cell lysates equivalent to 5×10^8 bacteria were prepared from *E. coli* UT5600 expressing IcsA$_{i87}$ (strain KMRM201), IcsA$_{BIO}$ (strain MG57) or IcsA$_{BIOK10R}$ (strain MG58). Lysates were subjected to immunoblotting (as described in Section 2.12.4). IcsA expression was detected with anti-IcsA polyclonal antibodies (**top**), and biotin was detected with streptavidin-HRP (**bottom**). Despite equivalent expression, only IcsA$_{BIO}$ was biotinylated.

6.2 Unipolarity is preserved in BIO-tagged IcsA

A key goal of this work was to monitor the behaviour of exported IcsA. Consequently, whether biotinylated $IcsA_{BIO}$ could be detected on the surface of bacteria was also investigated by indirect immunofluorescence (as described in Section 2.12.6). Moreover, despite the findings in Chapter 3 that dispute the involvement of $IcsA_{1-104}$ in polar targeting, and the apparent polar localisation reported for $IcsA_{i87}$, it was important to confirm that neither the introduction of BIO and its biotinylation would not result in loss of unipolar localisation.

To investigate localisation, $IcsA_{BIO}$ and $IcsA_{BIOK10R}$ were expressed in *S. flexneri icsA*::Tc^R (RMA2041; Appendix A) by transforming the strain with plasmids pMG55 and pMG58, yielding strains MG64 and MG162, respectively. Additionally, that $IcsA_{BIO}$ adopts a wild-type IcsA-equivalent circumferential distribution in rough LPS expressing bacteria was also investigated. Plasmids pMG55 and pMG58 were used to transform *S. flexneri icsA::*Tc^R *rmlD::*Km^R (RMA2043; Appendix A) that is unable to synthesise Oag due to a block in dTDP-rhamnose synthesis and is the rough LPS expressing derivative of RMA2041. Transformants were denoted as MG65 ($IcsA_{BIO}$) and MG163 ($IcsA_{BIOK10R}$).

The proteins could readily be readily detected at the bacterial cell surface of either smooth or rough bacteria through indirect immunoflourescence using anti-IcsA antibodies (Section 2.12.6), confirming export and retention in the outer-membrane (**Figure 6.3**). Moreover, the localisation of all the proteins was comparable to $IcsA_{WT}$ expressed from smooth or rough strains, as detected with anti-IcsA antibodies (**Figure 6.3**). Only $IcsA_{BIO}$ could be detected with streptavidin-Alexa488 and labelling was not observed for smooth or rough strains expressing either, $IcsA_{WT}$, $IcsA_{i87}$ or $IcsA_{BIOK10R}$, confirming that biotinylation was both specific and unique to $IcsA_{BIO}$ at the cell surface (**Figure 6.3**). Detection with streptavidin-Alexa488 was also polarly focused in smooth MG64 and circumferential with a polar cap in the rough MG65 strain. Consequently, construction of $IcsA_{BIO}$ did not seem to introduce defects in export or localisation compared to $IcsA_{WT}$ or $IcsA_{i87}$.

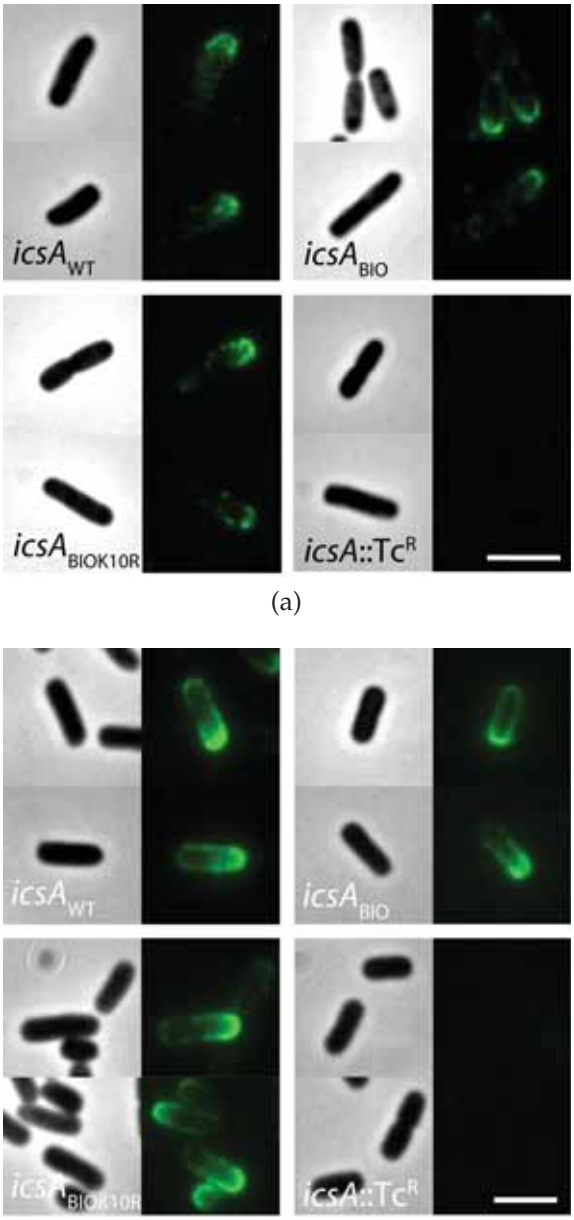

Figure 6.3: **Detection of IcsA constructs on the surface of smooth and rough *S. flexneri*.** Mid-log phase bacteria were formalin fixed, and visualised by immunofluorescence microscopy, performed as described in Section 2.12.6. Surface IcsA protein was detected by probing bacteria with rabbit anti-IcsA polyclonal antibodies, and then anti-rabbit-Alexa 488 fluorescent antibodies. (**a**) Smooth *S. flexneri icsA*::Tc^R expressing plasmid-borne $icsA_{WT}$, $icsA_{BIO}$ or $icsA_{BIOK10R}$ (strains RMA2090, MG64, and MG162, respectively) displayed characteristic unipolar distribution. Some staining of lateral regions was observed and was an expected consequence of the gene dosage effect of plasmid-borne *icsA*. (**b**) In rough *rmlD S. flexneri*, characteristic circumferential distribution, with polar focus was observed for each of the *icsA* complemented strains. The parental strain that lacked IcsA (*icsA*::Tc^R) was not stained, confirming the specificity of the antibodies. Scale bar represents 3 μm.

6.3 BIO-tagged IcsA remains functional

Plaque formation by *S. flexneri* on HeLa cell monolayers requires competence in actin-based motility and intercellular spread; both processes are IcsA-dependent (reviewed in Section 1.3). Consequently, plaque formation was used to verify that $IcsA_{BIO}$ remained functionally comparable to $IcsA_{WT}$. *S. flexneri* strains MG64 and MG162 (expressing $IcsA_{BIO}$ and $IcsA_{BIOK10R}$, respectively), an $IcsA_{WT}$-expressing isogenic control strain (RMA2090) and a strain expressing the parental $IcsA_{i87}$ (KMRM101), were tested for plaque formation, performed as described in Section 2.16.2. Plaques were imaged and then measured using a MetaMorph (Molecular Devices) workflow, described in Section 2.17.4.

As was expected, the IcsA-deficient strain RMA2041 was unable to form any plaques (Figure 6.4). There was no difference in the size of plaques formed by *S. flexneri icsA*::Tc^R complemented with either $IcsA_{WT}$ or $IcsA_{BIO}$ (Figure 6.4). Since $IcsA_{BIO}$ was capable of supporting wild-type equivalent plaque formation, the protein was likely to have retained wild-type equivalent function and conformation, despite the insertion of the BIO epitope.

6.4 Controlled expression of BIO-tagged IcsA

To specifically identify $IcsA_{BIO}$ soon after the protein is exported into the outer-membrane, the bacterial surface needed to be devoid of prior $IcsA_{BIO}$. Consequently, the expression of $icsA_{BIO}$ required tuneable control. To achieve this, $icsA_{BIO}$ was PCR amplified with oligonucleotides "IcsA.BIO-pBAD30_Eco" and "REPL.BIO-pBAD30_Sal" (Appendix F); the amplicon was digested with *Eco*RI and *Sal*I and ligated into the corresponding sites of pBAD30 (Appendix B). Ligated DNA was transformed into DH5α, and recombinant plasmids were identified, and denoted as pMG82.

In these plasmids, the expression of $icsA_{BIO}$ (or $icsA_{BIOK10R}$) was regulated from the promoter P_{ara}. Strains carrying the plasmid would repress $icsA_{BIO}$ when grown media supplemented with 0.2% glucose; and induce $icsA_{BIO}$ expression when grown in arabinose-replete conditions. The negative control $icsA_{BIOK10R}$ was likewise cloned into pBAD30, generating the strain MG83 (Table G.2). Plasmids

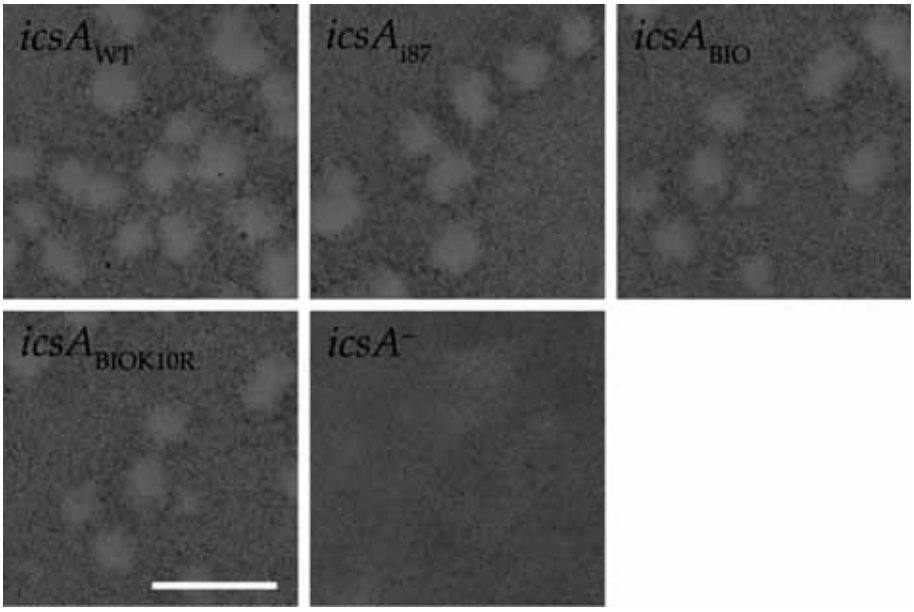

(a)

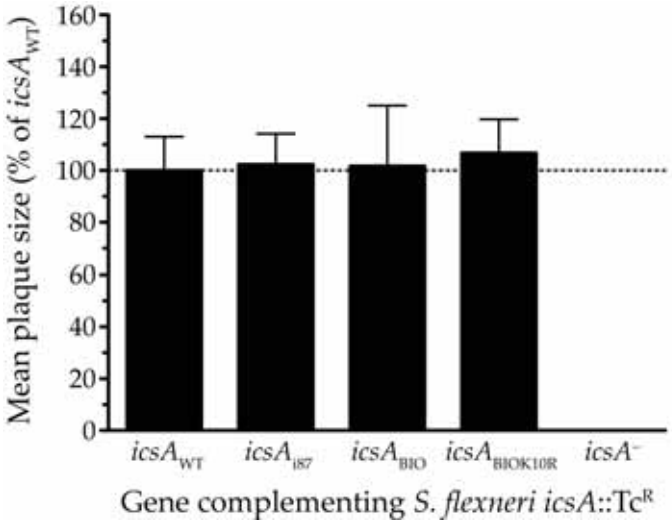

(b)

Figure 6.4: **Plaque formation on HeLa cell monolayers by *S. flexneri* expressing *icsA*$_{\mathrm{BIO}}$.** IcsA-dependent ABM and intercellular spreading was assessed by plaque formation on HeLa cell monolayers. *S. flexneri icsA*::Tc$^{\mathrm{R}}$ (RMA2090) was complemented with pBR322-derivative plasmids encoding either *icsA*$_{\mathrm{WT}}$, *icsA*$_{\mathrm{i87}}$ (strain KMRM101), *icsA*$_{\mathrm{BIO}}$ (strain MG64), or *icsA*$_{\mathrm{BIOK10R}}$ (strain MG162); the parent strain served as the negative control (*icsA*$^{-}$; RMA2041). *S. flexneri* were applied to monolayers, allowed to invade and spread laterally, and were visualised as described in Section 2.16.2. (**a**) Representative images of plaques formed by bacteria complemented with the indicated gene. Scale bar represents 3 mm. Images have been contrast enhanced. (**b**) Quantitation of mean plaque size, relative to those formed on complementation with *icsA*$_{\mathrm{WT}}$. No reduction from wild-type plaque size was evident for *icsA*$_{\mathrm{i87}}$, *icsA*$_{\mathrm{BIO}}$ or *icsA*$_{\mathrm{BIOK10R}}$. The parent strain did not form plaques (*icsA*$^{-}$). Data are mean $\pm$ standard deviation.

pMG82 and pMG83 were transformed into *E. coli* UT5600, generating strains MG84 and MG85, respectively.

Over-expression of IcsA on the *S. flexneri* surface leads to non-polar, circumferential detection of the protein (Section 1.4.4). In aiming to assess the sites of export and subsequent behaviour of newly exported $IcsA_{BIO}$, induction conditions needed to prevent over-expression, while allowing ready labelling of bacteria. To determine the appropriate induction conditions, immunoblotting was used to detect $IcsA_{BIO}$ following differing induction conditions. Strain MG57, carrying a plasmid that expressed $IcsA_{BIO}$ constitutively from the native promoter (P_{icsA}), served as a reference.

Bacteria were grown in LB broth supplemented with 0.2% glucose to mid-log phase. As expected, under these conditions no $IcsA_{BIO}$ could be detected from strain MG84 (**Figure 6.5**). Bacteria were then washed once with fresh broth and resuspended in LB broth supplemented with either 0.2% or 0.02% arabinose. Growth in the presence of arabinose induced $icsA_{BIO}$ expression over the time-course (**Figure 6.5**). When cultures were supplemented with 0.2% arabinose, resulted in strong expression of $IcsA_{BIO}$. Following 20 min of this induction, the amount of $IcsA_{BIO}$ was comparable to that produced from constitutive expression from P_{icsA} in MG64 (**Figure 6.5**). Induction with 0.02% arabinose resulted in readily detectable amounts of $IcsA_{BIO}$ that—after 20 min of growth in arabinose-replete conditions—was less than the amount of $IcsA_{BIO}$ expressed from P_{icsA} (**Figure 6.5**). Induction with 0.002% arabinose yielded barely detectable amounts of $IcsA_{BIO}$, even after 30 min of induction (not shown).

6.5 Creation of smooth UT5600 for expression of BIO-tagged IcsA

The nature of the LPS surrounding exported IcsA affects the distribution of the protein and possibly its function (Section 1.6.2). Therefore, it was important to consider both smooth and rough LPS phenotypes when assessing the surface behaviour of $IcsA_{BIO}$. Derivatives of *E. coli* K-12 (such as UT5600) are rough LPS mutants, owing to mutation of the *rfb* Oag biosynthesis locus (Stevenson *et al.*, 1994). To enable expression of complete LPS and to render UT5600 smooth, its mutant *rfbD1* allele was complemented. The cosmid pRMA154 (Appendix B), carrying the *rfb* locus of *S. flexneri*, was transferred to MG57 (expressing $IcsA_{BIO}$

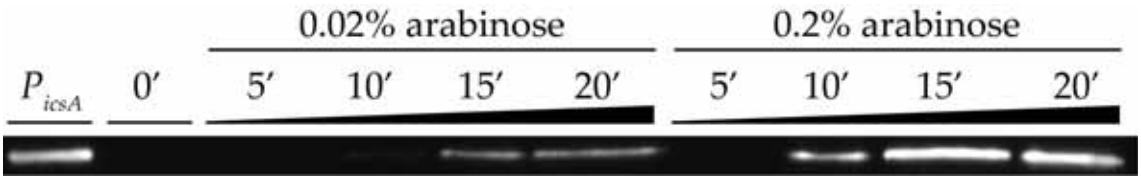

Figure 6.5: **Induction of P_{BAD} regulated $icsA_{BIO}$ with arabinose**. Overnight cultures of MG84 (carrying pBAD30::$icsA_{BIO}$) were grown in LB broth supplemented with 0.2% glucose, subcultured into fresh LB + 0.2% glucose broth and grown to mid-log phase. Cultures were then pelleted, washed once in fresh LB broth, and resuspended in LB broth supplemented with either 0.2% or 0.02% arabinose, as indicated. Whole-cell lysates were prepared from 5×10^8 cells of the induced cultures at 5′ intervals to 20′ post induction, as described in Section 2.12.1. Lysates taken at 0′ are pre-induction; P_{icsA} denotes lysate from strain MG64, expressing $icsA_{BIO}$ from the native *icsA* promoter.

.

from pMG55) by conjugation with *E. coli* strain RMA156, giving the exconjugate strain MG62. Conjugation with *E. coli* RMA160 transferred pJRD215 (the control cosmid for pRMA154) (Appendix B), and exconjugants were designated MG63. Corresponding *rfb* complemented (MG162) and control (MG163) strains were generated with strain MG58 expressing $IcsA_{BIOK10R}$.

LPS phenotypes were confirmed by separating LPS molecules by SDS-PAGE and visualising migration with silver staining, as described in Section 2.14.2. LPS samples were prepared from equivalent numbers of mid-log bacteria of MG62 and MG63 (Section 2.14.1). For comparison, LPS from smooth *S. flexneri icsA*::Tc^R *rmlD*$^+$ (RMA2041) its rough mutant *S. flexneri icsA*::Tc^R *rmlD*::Km^R (RMA2043) (each carrying IcA_{BIO} from pMG55) was also prepared and visualised in parallel.

Biosynthesis of complete smooth LPS was restored by carriage of pRMA154, while vector control exconjugants maintained rough LPS expression (**Figure 6.6**). The Oag modal chain length of the *E. coli* UT5600 strain MG62 LPS differed to that of the *S. flexneri* strain MG64, since the *ompT* mutation of UT5600 is a large deletion (Δ*ompT-fepC*) that spans *fepE*, the gene encoding the *E. coli* Oag chain length regulator that is homologous to *S. flexneri* Wzz. Consequently, restored Oag biosynthesis in UT5600 resulted in expression of smooth and unregulated Oag chains.

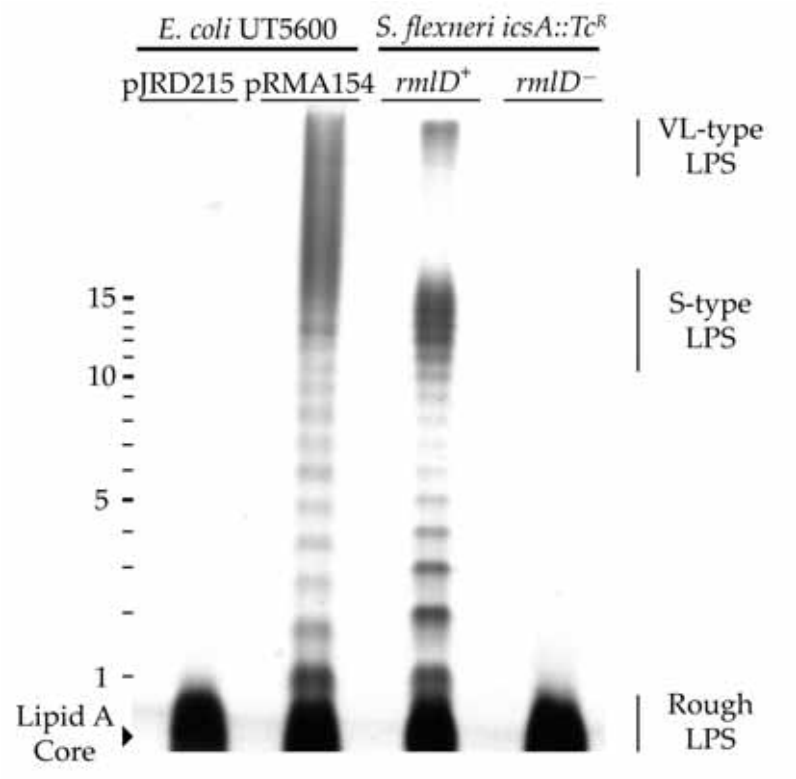

Figure 6.6: **Expression of smooth LPS by UT5600 by pRMA154**. LPS was isolated from 2×10^8 mid-log phase the indicated strains, as described in Section 2.14.1. Isolated LPS was resolved by SDS-PAGE and visualised by silver staining, as described in Section 2.14.2. *E. coli* UT5600 strain MG62 carrying pRMA154 (a pJRD215-derivative) expressed smooth LPS of longer modal length than *S. flexneri icsA*::Tc^R *rmlD*$^+$ (strain MG64). The vector control UT5600 carrying pJRD215 (strain MG63) expressed the inherent rough LPS phenotype of UT5600, that was comparable with the *S. flexneri icsA*::Tc^R *rmlD*$^-$ rough mutant (MG65).

6.6 Improving biotinylation of BIO-tagged IcsA

A key aim of this study was to specifically label nascent IcsA at the cell surface. A previous study determined that a biotin-tagged PhoA fusion protein was inefficiently biotinylated metabolically due to rapid export of the protein from the cytoplasm (Reed and Cronan, 1991). Therefore, to improve the efficiency of biotinylation, the cellular concentration of BirA was increased by providing *birA* expressed through basal-level transcription from P_{lac} on pBBR1MCS (Kovach *et al.*, 1994). Briefly, *birA* from plasmid pCY216 (Chapman-Smith *et al.*, 1994) was PCR amplified using oligonucleotides "BirA_F_XhoI" and "BirA_R_HindIII"

(Appendix F). The amplicon was then digested with *Xho*I and *Hind*III, and then ligated into the corresponding restriction sites of pBBR1MCS, as described in Section 2.6.2 and Section 2.9.4. A successful clone was identified in *E. coli* DH5α, verified by sequencing, and designated pMG226. Strain MG88 (UT5600 carrying inducible pBAD30::$icsA_{BIO}$ and pRMA154) was transformed with pMG226, and denoted as strain MG227. A vector control strain, carrying only pBBR1MCS, was also created and denoted as strain MG231.

To determine if biotinylation efficiency was improved by the increased BirA concentration, $icsA_{BIO}$ expression was induced with 0.02% arabinose in strains MG227 and the control strain MG231. Whole-cell lysates were prepared at 5 min intervals over a 20 min induction. immunoblotting with streptavidin-HRP was used to detect biotin. The presence of additional BirA improved the efficiency of $IcsA_{BIO}$ biotinylation, evident after 15 and 20 min of induced expression (**Figure 6.7**). $IcsA_{BIO}$ biotinylation was barely detectable 20 min post induction in the vector control strain (**Figure 6.7**). Increasing the cellular concentration of BirA in this system did not result in non-specific biotinylation (not shown). Additionally, growth in media supplemented with biotin did not improve biotinylation (not shown).

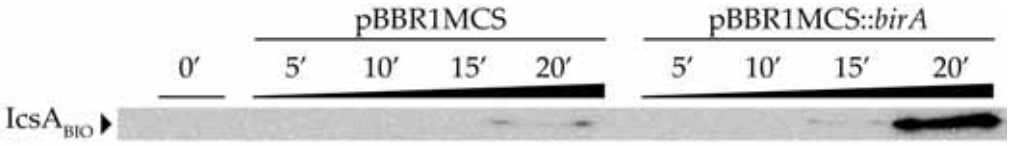

Figure 6.7: **Improved biotinylation of $IcsA_{BIO}$ on BirA overexpression**. Strains MG227 and MG231 were grown to mid-log phase in LB broth supplemented with 0.2% glucose, washed in LB broth, and resuspended into LB broth supplemented with 0.02% arabinose to induce expression of $icsA_{BIO}$. 5×10^8 bacteria from each strain were taken every 5 minutes during a 20 minute (20′) induction. Bacteria were pelleted and resuspended in loading buffer and resolved by SDS-PAGE, transferred to nitrocellulose membranes, as described in Section 2.12.2 and Section 2.12.4. Membranes were probed with streptavidin-HRP to detect biotin. Biotinylation of MG227 (carrying **pBBR1MCS::*birA***) was evident after 15′, and readily detectable after 20′ of induction. Biotinylation of MG231 (carrying **pBBR1MCS**) was only weakly evident after 20 min.

6.7 Detection of nascent BIO-tagged IcsA in the outer-membrane

Detection of nascent surface exposed $IcsA_{BIO}$ was required to enable tracking of the protein. In order to determine if biotinylated $IcsA_{BIO}$ could be detected on the bacterial surface with fluorescently labelled streptavidin, $IcsA_{BIO}$-expressing strains MG227 (smooth LPS) and MG229 (rough LPS), and the corresponding $IcsA_{BIOK10R}$-expressing control strains MG228 (smooth LPS) and MG230 (rough LPS), were grown to mid-log phase in LB supplemented with 0.2% glucose, pelleted, washed in LB broth, and resuspended in LB broth supplemented with 0.2% arabinose for 20 min. High level protein expression was induced to verify that labelling was specific for $IcsA_{BIO}$ and could not be detected for $IcsA_{BIOK10R}$, even at high protein levels. Induced bacteria (2×10^6) were pelleted, resuspended in 150 µl of PBS with 10 µg/ml of streptavidin-Alexa 488, and incubated at 37°C for five minutes. Bacteria were then pelleted and resuspended in 500 µl of LB broth pre-warmed to 37°C and supplemented with (i) 0.1 µg/ml biotin to prevent further detection of protein, and (ii) 0.2% glucose to repress further protein expression. Bacteria were then wet mounted with 1 µm latex beads (as described in Section 2.17.2), and immediately visualised in a microscopy chamber pre-warmed to 37°C. The total time, from culture to microscope stage, for such labelling reactions was eight minutes.

This labelling method was successful in detecting biotinylated surface $IcsA_{BIO}$ in >90% of cells from either smooth and rough LPS expressing strains (**Figure 6.8**). Labelling was specific and no $IcsA_{BIOK10R}$ expressing strains were observed to be fluorescently labelled. Despite the high level of protein induction, polar reinforcement was evident in approximately 20% of smooth LPS bacteria (**Figure 6.8**). Polar reinforcement was not detected for any rough LPS expressing labelled bacteria. It should be noted that unlike immunofluorescence, where a fluorescent secondary antibody amplifies the detection of the primary antibody (anti-IcsA), the direct detection of biotin by streptavidin-Alexa 488 was expected to result in lowered fluorescence. This lowered fluorescence is seen as noise in the captured images and likely contributed to the poor detection of polar reinforcement (**Figure 6.8**).

6.8 Rapid single molecule detection of nascent BIO-tagged IcsA

The ultimate aim of this chapter was to detect of the earliest molecules of $IcsA_{BIO}$ exported across outer-membrane. To enable tracking of individual $IcsA_{BIO}$ molecules as they appear at the cell surface, streptavidin conjugated to Quantum dots (Qdots) was used. Qdots provide bright fluorescence with minimal photobleaching, allowing for extremely short exposure times to excitational UV light that harms illuminated cells. Additionally, because Qdots are large (approximately 10 nm in diameter) and exhibit periodic blinking, they allow for identification of a single fluorophore. Since expression of $IcsA_{BIO}$ was being weakly induced in this system (to detect nascent protein), a single Qdot would beacon the position of a single biotinylated $IcsA_{BIO}$ protein.

To determine if single molecule labelling was achievable under conditions of weak $IcsA_{BIO}$ expression, strain MG227, MG228, MG229 and MG230 were grown as described in Section 6.7), with the modification that $IcsA_{BIO}$ was induced by supplementing growth media with 0.02% arabinose for 10 min. 2×10^6 bacteria was then taken from each culture, pelleted in a bench-top centrifuge at 13,000×g for 30 seconds, resuspended 40 µl of pre-warmed PBS supplemented with 10 µg/ml streptavidin-Qdot 605 and incubated for 1 minute at 37°C, then pelleted again for 30 seconds and resuspended in 200 mul of pre-warmed LB broth supplemented with 0.2% glucose and 0.1 µg/ml biotin. Bacteria were immediately wet mounted, as described in Section 2.17.2, and visualised by epifluorescence microscopy inside a heated chamber. The total labelling time (from culture to microscope) was approximately 4 minutes.

Strains expressing $IcsA_{BIO}$ could be readily detected using this procedure. Approximately 30% of cells were observed to be fluorescently labelled. Bacteria were labelled with large foci of fluorescence typical of streptavidin-Qdot fluorescence (**Figure 6.9**). Most cells exhibited between 2-3 foci of blinking Qdot fluorescence, suggesting that labelling could yet be achieved at earlier times during induction. No labelling was observed for strains expressing the $IcsA_{BIOK10R}$ control protein, confirming the specificity of the observed labelling (**Figure 6.9**).

6.9 Summary

In order to directly determine the properties of IcsA in the outer-membrane, metabolic biotinylation was adapted to allow for sensitive and specific detection of nascent IcsA. The BIO epitope was sufficient to direct biotinylation of $IcsA_{BIO}$, despite export of the protein from the cytoplasm. Biotinylation was significantly improved following overexpression of the BirA biotin protein ligase. Tagging of $IcsA_{i87}$ with BIO retained wild-type equivalent protein function and localisation. The $IcsA_{BIO}$ construct was placed under tight and inducible gene regulation to allow for detection of nascent surface IcsA. *E. coli* UT5600 was complemented to restore biosynthesis of complete LPS to allow for experiments in rough and smooth LPS backgrounds. Finally, an extremely rapid detection was developed that allowed for labelling of individual proteins in a 4 minute reaction.

Due to a lack of time, tracking could not be undertaken; but this system is a promising approach that can be used in future live imaging experiments.

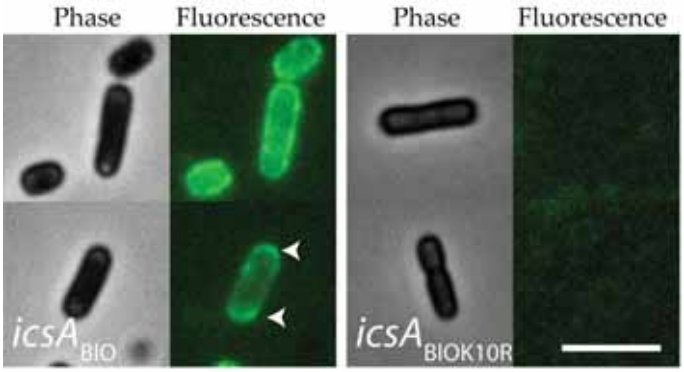

(a) Smooth LPS

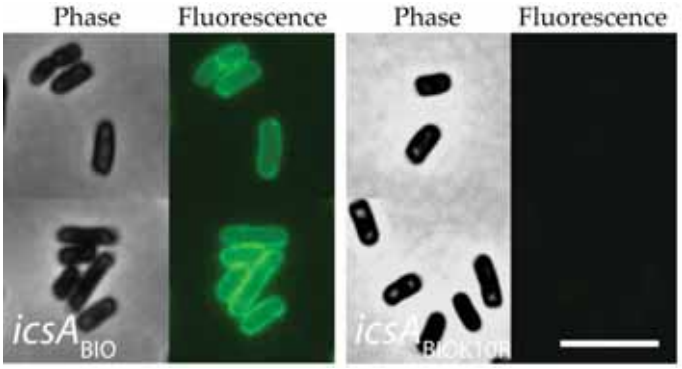

(b) Rough LPS

Figure 6.8: **Detection of $IcsA_{BIO}$ in smooth and rough LPS expressing *E. coli* by streptavidin-Alexa 488**. Strains expressing (**a**) smooth LPS MG227 ($icsA_{BIO}$) and MG228 ($icsA_{BIOK10R}$); and strains expressing rough LPS MG229 ($icsA_{BIO}$) and MG230 ($icsA_{BIOK10R}$) were grown to mid-log phase in LB broth supplemented with 0.2% glucose, pelleted, washed in LB broth, and resuspended in LB broth supplemented with 0.2% arabinose for 20 min. 2×10^6 bacteria were then pelleted, resuspended in 150 µl of PBS with 10 µg/ml of streptavidin-Alexa 488, and incubated at 37°C for five minutes. Bacteria were again then pelleted, the supernatant removed and resuspended in 500 µl of LB broth pre-warmed to 37°C, supplemented with 0.1 µg/ml biotin and 0.2% glucose. Cells were wet mounted with 1 µm latex beads, coverslips sealed with VALAP, and immediately visualised by microscopy performed at 37°C, as described in Section 2.17.2. Strains expressing $IcsA_{BIO}$ were readily detected with streptavidin-Alexa 488, while no labelling of $IcsA_{BIOK10R}$ was detected, confirming the specificity of detection. Despite high level induction, unipolarity was occasionally detected in smooth LPS expressing bacteria (**arrowheads**), and was not detected in rough LPS expressing bacteria. Scale bars represent 3 µm.

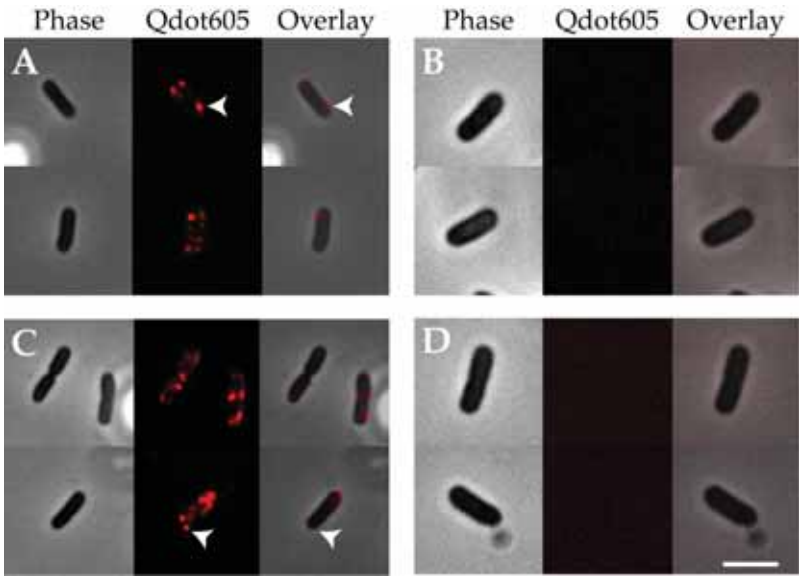

Figure 6.9: **Extremely rapid detection of single IcsA$_{BIO}$ at the surface of rough and smooth LPS *E. coli*.** Strains expressing smooth LPS (**A and B**) MG227 (**A**; *icsA*$_{BIO}$) and MG228 (**B**; *icsA*$_{BIOK10R}$); and strains expressing rough LPS (**C and D**) MG229 (**C**; *icsA*$_{BIO}$) and MG230 (**D**; *icsA*$_{BIOK10R}$) were grown to mid-log phase in LB broth supplemented with 0.2% glucose, pelleted, washed in LB broth, and resuspended in LB broth supplemented with 0.02% arabinose for 10 min. 2×10^6 bacteria were then pelleted, resuspended in 20 µl of pre-warmed PBS with 10 µg/ml of streptavidin-QDOT 605, and incubated at 37°C for 1 minute. Bacteria were again pelleted, the supernatant removed and resuspended in 200 µl of LB broth pre-warmed to 37°C, supplemented with 0.1 µg/ml biotin and 0.2% glucose. Cells were wet mounted with 1 µm latex beads, coverslips sealed with VALAP, and immediately visualised by microscopy performed at 37°C, as described in Section 2.17.2. IcsA$_{BIO}$ proteins were readily labelled using this protocol (**A and C**); while no labelling of IcsA$_{BIOK10R}$ was observed (**B and D**). Large round foci of fluorescence represent individual streptavidin-QDOT 605 conjugates that were likely to represent single IcsA$_{BIO}$ molecules. Scale bar represents 3 µm.

7

Functional oligomerisation of exported IcsA

While a subgroup of the autotransporter family forms homo-trimeric complexes, the oligomerisation of conventional autotransporters has been reported rarely, despite attempts to identify oligomerisation in others (Section 1.5.3). Nonetheless, Veiga *et al.* (2002) demonstrated a large multimeric structure formed by the translocation domains of *N. meningitidis* IgA1 protease in the outer-membrane. Whether outer-membrane oligomerisation is a broadly applicable autotransporter strategy and whether the oligomeric state was functionally relevant had to-date remained unknown.

Linker-insertion mutagenesis of the IcsA effector domain identified a number of mutants ($IcsA_i$) defective in ability to recruit N-WASP, form F-actin tails, and spread from cell-to-cell (May and Morona, 2008) . The majority of these defect phenotypes could be restored to wild-type by complementing *S. flexneri* with plasmid-borne $IcsA_{WT}$ (May, 2007). However, some mutants exerted negative dominance and $IcsA_{WT}$ complemented *S. flexneri* remained deficient in those processes. Additionally, chemical cross-linking of wild-type *S. flexneri* by May (2007) consistently demonstrated a high molecule weight (>460 kDa) cross-linked product that contained IcsA.

The observance of negative dominance and a high molecular weight IcsA-containing complex suggested that the functionally relevant state of IcsA might be multimeric. In this hypothesis, the incorporation of certain $IcsA_i$ mutants into mixed oligomers with $IcsA_{WT}$ would have a net result of creating a functionally deficient structures. While this genetic evidence strongly suggested oligomerisation of IcsA—and that the oligomer was functionally relevant—no direct evidence of oligomerisation had been obtained.

The aim of this chapter was to investigate the state of IcsA in the outer-membrane, and to determine the existence of IcsA oligomers.

7.1 Surface IcsA expression in negative dominant strains

The negative dominance of $IcsA_{i563}$ and $IcsA_{i677}$ over $IcsA_{WT}$ when the proteins are co-expressed could arise from reduced surface expression of $IcsA_{WT}$. May (2007) had previously shown that total IcsA expression had not been altered on co-expression of $IcsA_{WT}$ with either $IcsA_{i563}$ or $IcsA_{i677}$, and that the distribution of the co-expressed IcsA proteins had remained polarly focused. However, IcsA is only functional in above virulence processes when present at the cell surface. The oligomer model of autotransporter export proposes cooperative export of multiple proteins through an assembled large oligomeric pore (Section 1.5.3). Mutant $IcsA_i$ proteins could be deficient in such export; creation of hypothetical mixed $IcsA_i$-$IcsA_{WT}$ oligomers would thereby reduce the surface expression of $IcsA_{WT}$ and account for the observed virulence deficiencies.

To determine if co-expression of $IcsA_{i563}$ or $IcsA_{i677}$ with $IcsA_{WT}$ resulted in reduced surface presentation of functional $IcsA_{WT}$, a tagged protein was constructed to allow for differential labelling. Briefly, May (2007) introduced a FLAG epitope into the insertional mutation of $IcsA_{i87}$ and the protein was used to complement *S. flexneri icsA*::Tc^R, generating strain KMRM250. In this strain, $IcsA_{FLAG}$ retained wild-type equivalent expression, localisation and function (May, 2007). Consequently, $IcsA_{i563}$ and $IcsA_{i677}$ were each co-expressed with $IcsA_{FLAG}$ in *S. flexneri icsA*::Tc^R, generating strains KMRM276 and KMRM277, respectively (May, 2007).

In this work, the surface expression of $IcsA_{FLAG}$ in these strains was investigated by flow cytometry. Strains KMRM250, KMRM276, KMRM277 were grown to mid-log phase in LB broth, formalin fixed and surface proteins were probed with rabbit anti-FLAG antibodies, and then Alexa-488 conjugated anti-rabbit fluorescent antibodies (as described in Section 2.17.5). Strain RMA2090, *S. flexneri icsA*::Tc^R, complemented with $IcsA_{WT}$ was included as a control for labelling specificity. The extent of fluorescent labelling on each bacterium of the given strains was assessed by flow cytometry. There was no difference in the amount of anti-FLAG labelling when $IcsA_{FLAG}$ was expressed alone or when co-expressed with $IcsA_{i563}$ or $IcsA_{i677}$ (**Figure 7.1**). No anti-FLAG labelling was observed for the otherwise isogenic RMA2090, expressing $IcsA_{WT}$ (**Figure 7.1**). These results demonstrated that negative dominance is unlikely to arise as a consequence of

reduced surface expression of $IcsA_{WT}$ (or the wild-type equivalent $IcsA_{FLAG}$) when co-expressed with $IcsA_{i563}$ or $IcsA_{i677}$ in *S. flexneri*.

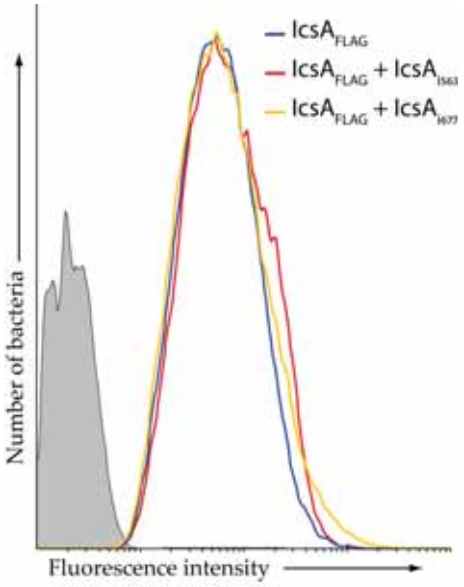

Figure 7.1: **Surface presentation of wild-type equivalent $IcsA_{FLAG}$ is not altered on co-expression with $IcsA_{i563}$ or $IcsA_{i677}$.** *S. flexneri icsA*::Tc^R complemented with either $IcsA_{FLAG}$ along (strain KMRM250), $IcsA_{FLAG}$ with $IcsA_{i563}$ (strain KMRM276), or $IcsA_{FLAG}$ with $IcsA_{i677}$ (strain KMRM277), were grown to mid-log phase in LB broth, formalin fixed, and labelled with rabbit anti-FLAG antibodies, and then anti-rabbit Alexa-488 fluorescent antibodies, as described in Section 2.17.5. Bacteria were diluted in PBS, and fluorescence was determined for 50,000 bacteria by flow cytometry using a BD FACSCanto. As expected, *S. flexneri icsA*::Tc^R complemented with $IcsA_{WT}$ was not fluorescently labelled and served as a negative control. The extent of fluorescent labelling of surface $IcsA_{FLAG}$ did not differ when $IcsA_{FLAG}$ was expressed alone, or with either of the $IcsA_i$ mutants. Distribution of fluorescence intensity greater than 0, taken as auto-fluorescence of mock labelled KMRM250.

7.2 Reciprocal co-purification confirmed IcsA oligomerisation

While negative dominance constitutes genetic evidence of protein-protein interaction, no direct evidence had been presented for IcsA oligomerisation. Reciprocal pull-down was used to determine if IcsA-IcsA interactions could be detected. $IcsA_{BIO}$ and $IcsA_{FLAG}$ were used to permit affinity purification that could pull-down the reciprocal epitope tagged IcsA. These proteins were expressed in *E. coli*

ompT strain UT5600 to facilitate expression and purification. From results presented in the current work, biotinylation of $IcsA_{BIO}$ was improved on overexpression of biotin protein ligase, BirA (Section 6.6). Consequently, the *birA* encoding plasmid pCY216 (a gift of S. Polyak, Chapman-Smith *et al.*, 1994) was additionally utilised in strain construction. Plasmids pMG55 ($icsA_{BIO}$), pKMRM252($icsA_{FLAG}$), and pCY216 were sequentially used to transform strain UT5600, as described in Section 2.10.1. The resultant strain was designated MG157 (Appendix A). Control strains, that individually replaced one of the affinity tagged IcsA constructs with the untagged parent protein $IcsA_{i87}$, were additionally generated and designated MG251 (expressing $icsA_{BIO}$, $icsA_{i87}$, and *birA*) and MG250 (expressing $icsA_{i87}$, $icsA_{FLAG}$, and *birA*).

Strain MG157, and the control strains MG250 and MG251, was grown for sixteen hours at 30°C in five litres of terrific broth (Section 2.3.1) and outer-membranes prepared as described by Veiga *et al.* (2002), and presented in detail in Section 2.12.5. Briefly, bacteria were pelleted, resuspended in TN buffer, lysed by repeated passage in a pressure cell, and centrifuged at 100,000×*g* to pellet the whole membrane fraction. The supernatant was discarded and this pellet was solubilised in TN buffer supplemented with 1.5% Triton X-100 on ice for 30 min, and again centrifuged at 100,000×*g*. The resulting supernatant was discarded and the membrane pellet was solubilised in TN buffer supplemented with 1% Zwittergent 3-14 for 30 min on ice, and centrifuged at 100,000×*g*. The pellet was discarded and the solubilised material—constituting purified outer-membrane fraction—was collected, and diluted to 0.1% Zwittergent 3-14 with TN buffer. This solubilised material was then used in affinity purification using FLAG M2 resin (Sigma) or streptavidin-Dynabeads (Invitrogen). The purification procedure is described in Section 2.12.5. As expected, purification using FLAG M2 resin readily purified $IcsA_{FLAG}$; while streptavidin-Dynabeads readily purified $IcsA_{BIO}$ (**Figure 7.2**).

Proteins from outer-membranes prepared from MG157 were affinity purified using FLAG M2 resin, then the protein-bound resin was heated to 100°C for 5 min, the resin pelleted, and the protein-containing supernatant was diluted in loading buffer and resolved by SDS-PAGE, as described in Section 2.12.5. Likewise, following streptavidin-Dynabead purification, samples were heated to 100°C for 10 min, and the beads pelleted by placing samples in a magnetic

tube rack for 5 min; the supernatant was collected, diluted in loading buffer and resolved by SDS-PAGE, as described in Section 2.12.5. Immunoblotting with either anti-FLAG antibodies or streptavidin-HRP was used to identify purified IcsA.

Following purification from FLAG M2 resin, $IcsA_{BIO}$ was found to co-purify along with $IcsA_{FLAG}$ (**Figure 7.2**). Using this affinity purification, $IcsA_{BIO}$ could not be purified from outer-membranes prepared from strain MG251 that expressed $IcsA_{i87}$ in place of $IcsA_{FLAG}$ **Figure 7.2**. Similarly, when outer-membrane preparations from MG157 were purified using streptavidin-Dynabeads, $IcsA_{FLAG}$ co-purified along with $IcsA_{BIO}$ (**Figure 7.2**). When outer-membranes from MG250, that expressed $IcsA_{i87}$ in place of $IcsA_{BIO}$, were subjected to this same purification procedure, $IcsA_{FLAG}$ could not be purified (**Figure 7.2**). The absence of purification in the control strains indicated that observed reciprocal co-purification was specific.

7.3 Defining the region mediating IcsA-IcsA interaction

The Veiga *et al.* (2002) study presented strong evidence that the translocation domain of *N. meningitidis* IgA1 protease formed an outer-membrane oligomer. Whether the IcsA translocation domain likewise mediated the apparent IcsA-IcsA interaction in the outer-membrane was investigated.

Suzuki *et al.* (1996) had functionally investigated a range of IcsA effector domain truncation mutants. Three of their constructed proteins were used in chemical cross-linking experiments, to determine whether regions of the effector domain were involved in IcsA-IcsA interactions. *S. flexneri* expressing either $IcsA_{1-1102}$ (strain RMA2205), $IcsA_{\Delta 508-730}$ (strain RMA2208), or $IcsA_{\Delta 103-507}$ (strain RMA2209) (encoded by pD10-1, pD10-*virG3*, and pD10-*virG4*, respectively) were grown to mid-log phase, washed in PBS, and cross-linked with dithiobis(succinimidylpropionate) (DSP), as described in Section 2.15.1. Bacteria were then lysed by repeated passage through a French pressure cell, centrifuged at 100,000×*g*, and pellets constituting whole membrane fractions were collected and resuspended in lysis buffer either with or without β-mercaptoethanol (described in Section 2.15.1). Samples were resolved by SDS-PAGE and immunoblotted with anti-IcsA, as described in Section 2.12.4. Prior to SDS-PAGE, cross-linked

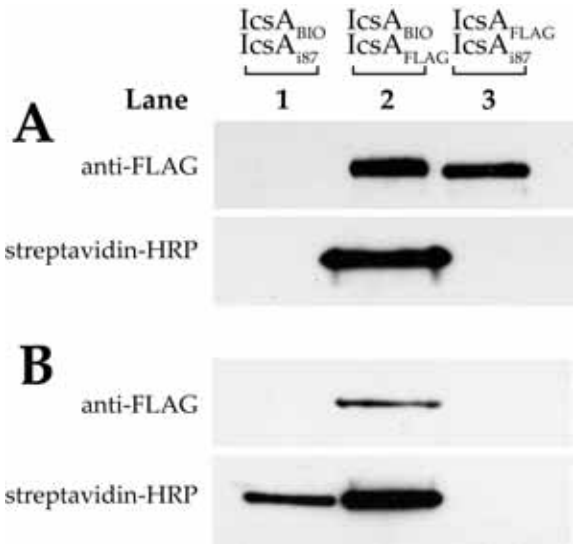

Figure 7.2: **Reciprocal co-purification of differentially tagged IcsA proteins from the outer-membrane**. *E. coli* UT5600 strains that overexpressed the biotin protein ligase BirA, were constructed to co-express $IcsA_{BIO}$ with $IcsA_{FLAG}$ (strain MG157), $IcsA_{FLAG}$ with $IcsA_{i87}$ (strain MG250), or $IcsA_{BIO}$ with $IcsA_{i87}$ (strain MG251). Bacteria were grown overnight at 30°C, lysed, and outer-membranes were isolated and solubilised with Zwittergent 3-14, as described in Section 2.12.5. Solubilised outer-membrane proteins were then subjected to affinity purification with either (**A**) FLAG M2 resin, or (**B**) streptavidin-Dynabeads. $IcsA_{BIO}$ was detected by immunoblotting with streptavidin-HRP, and $IcsA_{FLAG}$ was detected by immunoblotting with mouse anti-FLAG M2 antibodies, as indicated. $IcsA_{FLAG}$ was readily purified from all strains expressing this protein following FLAG resin affinity purification (**A; lanes 2, 3**); $IcsA_{BIO}$ was readily purified following streptavidin-Dynabead affinity purification from all strains expressing this protein (**B; lanes 1, 2**). $IcsA_{BIO}$ was found to co-purify with $IcsA_{FLAG}$ when the proteins were co-expressed and purified from FLAG M2 resin (**A; lane 2**). Likewise, $IcsA_{FLAG}$ was found to co-purify with $IcsA_{BIO}$ when the proteins were co-expressed (**B; lane 2**). Co-purification was specific, since $IcsA_{BIO}$ could not be purified from FLAG M2 resin (**A; lane 1**); and $IcsA_{FLAG}$ could not be purified from streptavidin-Dynabeads (**B; lane 3**), when either of these proteins was co-expressed with untagged $IcsA_{i87}$, that is the equivalent of $IcsA_{WT}$.

samples were heated to 60°C for 5 min in the absence of β-mercaptoethanol; for parallel samples, the cross-linker was cleaved by heating to 100°C for 10 min in the presence 10% β-mercaptoethanol (Section 2.15.1).

Cross-linking of strain RMA2005 expressing $IcsA_{1-1102}$ produced high molecular weight complexes (>460 kDa), reminiscent of those described by May (2007) (**Figure 7.3; lane2**). Cross-linking of bacteria expressing either $IcsA_{\Delta 508-730}$ or $IcsA_{\Delta 103-507}$ likewise produced high molecular weight products (>460 kDa (**Figure 7.3; lanes 4 and 6**). Cleavage of the cross-linker abolished the high molecular weight product and was also seen to result in some degradation of the IcsA proteins (**Figure 7.3; lanes 1, 3, and 5**). Since all of these IcsA proteins successfully cross-linked, the region of the IcsA that permits this cross-linking, and perhaps mediates IcsA-IcsA interactions, is likely to be within $IcsA_{54-103}$ or $IcsA_{730-1102}$.

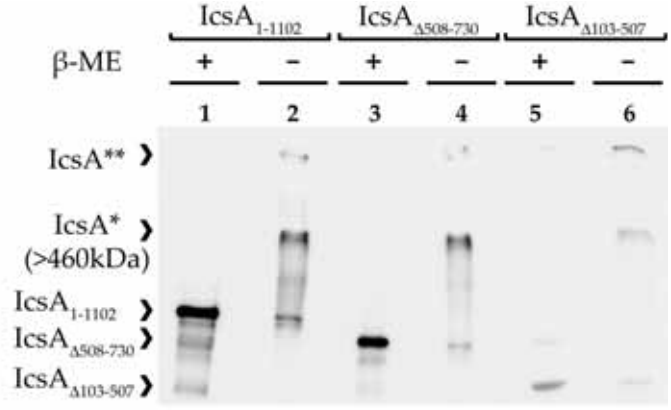

Figure 7.3: **Chemical cross-linking of IcsA effector domain deletion mutants**. *S. flexneri icsA*::Tc^R complemented to express either $IcsA_{1-1102}$ (strain RMA2205), $IcsA_{\Delta 508-730}$ (strain RMA2208), or $IcsA_{\Delta 103-507}$ (strain RMA2209) were grown to mid-log phase in LB broth, and cross-linked with DSP, as described in Section 2.15.1. Cell membranes were prepared, as described in Section 2.15.1 and cross-linked samples were heated to 60°C prior to SDS-PAGE (**β-ME -; lanes 2, 4, 6**); in parallel, cross-linking was cleaved by heating to 100°C in the presence of β-mercaptoethanol (**β-ME +; lanes 1, 3, 5**). Samples were resolved by SDS-PAGE (7.5% acrylamide) and analysed by immunoblotting with polyclonal anti-IcsA antibodies, as described in Section 2.12.4. Cross-linked samples presented high molecular weight complexes (**IcsA***) that were larger than 460 kDa, as observed by May (2007). Very large complexes were also detected (**IcsA****) that may represent large accumulations of cross-linked proteins. Cleavage of cross-linkers presented the expected size of the IcsA constructs, albeit with some observed degradation, leading to detection of smaller fragments.

7.4 Summary

The data presented in this chapter strongly suggest that IcsA-IcsA interactions indeed occur in the outer-membrane, and supported the hypothesis of IcsA oligomerisation. Negative dominance over $IcsA_{WT}$ described for a subset of $IcsA_i$ insertion mutants described by May and Morona (2008) provided genetic evidence for IcsA-IcsA interactions occurring in the outer-membrane that were relevant for net IcsA function in *S. flexneri* N-WASP recruitment, actin polymerisation and intercellular spreading. This work confirms that the observed phenotypes do not arise due to reduced surface presentation of $IcsA_{WT}$ when co-expressed with $IcsA_i$ mutants. Reciprocal co-purification provides biochemical evidence of direct IcsA-IcsA interactions. In light of the reported oligomerisation of the IgA1 protease translocation domain, chemical cross-linking supports the involvement of $IcsA_{730-1102}$ in mediating this interactions. However, it remains possible that $IcsA_{54-103}$ is capable of mediating oligomerisation. Efforts to directly determine if the translocation domain ($IcsA_{758-1102}$) is sufficient for oligomerisation detectable by reciprocal co-purification and cross-linking are ongoing.

Part III

DISCUSSION

8

Discussion

The IcsA (VirG) autotransporter is critical to the pathogenesis of *S. flexneri*. The invasive bacteria gain access to the cytoplasm of epithelial cells in the colon and initiate a motility that potentiates bacterial intercellular spread, a vital stage of the disease process. *Shigella* motility relies on the function of IcsA in recruiting and activating the host N-WASP actin regulatory protein as the preliminary step in triggering host F-actin polymerisation that generates the propulsive forces driving bacterial motility. The unique unipolar presentation of IcsA at the bacterial surface provides a focus for actin polymerisation and propulsive force generation.

How IcsA biogenesis is directed to one pole has long been a curiosity, despite an increasingly comprehensive understanding of prokaryotic biology. This work critically assessed two reported polar targeting domains of IcsA and was successful in confirming the involvement of one of them, while rebutting another. Mutations within this recognised targeting domain were found to be defective in addressing polar localisation in a protein concentration-dependent manner. Additionally the peptide sequence minimally sufficient for polarity was refined to a 38 amino acid region. Polar targeting was also seen to be co-incident with the motion of replicated origins of chromosome replication (*oriC*), and DNA replication is a likely cue for polar delivery and retention.

The IcsA-LPS interplay within the outer membrane is also influential to the function and localisation of surface presented IcsA. The composition of polar LPS, in comparison with the lateral cell body, was shown to be uniform with respect to LPS quantity and chain length distribution. How IcsA sub-populations localised away from the cell pole arise has yet to be directly resolved. A method enabling identification and tracking of single nascent IcsA proteins was developed and demonstrated. Finally, the existence of direct IcsA-IcsA interaction at the cell surface was confirmed, adding support to previous genetic evidence. These findings and chemical cross-linking support a model of IcsA oligomerisation that is likely mediated by the translocation domain.

8.1 The polar targeting of IcsA

Two regions, $IcsA_{1-104}$ and $IcsA_{506-620}$, identified by Charles *et al.* (2001) were reported to confer polar targeting of IcsA. These authors observed that the two peptides could independently deliver nascent IcsA to the pole prior to translocation from the cytosol. It was important to verify the involvement of these regions in polar targeting.

8.1.1 *The amino terminal proximal polar targeting region*

The work present in Section 3.2 refutes the capacity of the amino terminal proximal polar targeting region $IcsA_{1-104}$ to direct polarity, while verifying that $IcsA_{506-620}$ mediates cytoplasmic polar targeting (**Figure 3.1**). That $IcsA_{1-104}$ did not exhibit polarity in the presented system was an unexpected finding. Charles *et al.* (2001) had additionally observed that a GFP fusion to a subregion that lacked the signal peptide ($IcsA_{53-104}$) still facilitated polarity, albeit at lower frequency. The signal sequence in the $IcsA_{1-104}$-GFP+ construct might have impeded the ability to detect polar foci in this system, since export of the fusion would not yield fluorescence (Thomas *et al.*, 2001). However, a constructed $IcsA_{53-104}$-GFP+ fusion was similarly diffusely distributed throughout the cytoplasm and lacked discernible polarity. Moreover, not only were $IcsA_{1-104}$ and $IcsA_{53-104}$ unable to guide polar targeting themselves, a larger fusion, $IcsA_{53-505}$, was also non-polar (**Figure 3.3**). Clearly, in the system presented in this thesis, this amino terminal proximal polar targeting region was insufficient for polarity. While this finding is an unexpected departure from previous literature, it is nonetheless supported by results from May and Morona (2008). In that study, linker mutagenesis of IcsA yielded two mutants that each introduced five amino acid mutations within $IcsA_{506-620}$ (at positions 532 and 563). These mutations resulted in loss of unipolarity at the cell surface, despite these mutants retaining a wild-type $IcsA_{1-104}$ region. Clearly $IcsA_{1-104}$ could not compensate for mutation of $IcsA_{506-620}$. The data presented in this work, together with the non-polar phenotype exhibited by $IcsA_{i532}$ and $IcsA_{i563}$, suggests that $IcsA_{1-104}$ may not be able to independently confer polarity as had been reported, and likely does not impart polar targeting itself.

8.1.2 *The amino terminal distal polar targeting region and its mutants*

In the system described in this work, the region $IcsA_{506-620}$ was seen to direct polar targeting (**Figure 3.3**). Additionally, GFP+ fusions to broader regions of IcsA that span $IcsA_{506-620}$ were also observed as foci at the pole (**Figure 3.3**). These data firmly verified $IcsA_{506-620}$ in mediating polar targeting, as was first revealed by Charles *et al.* (2001). Having validated $IcsA_{506-620}$ in polar targeting, the $IcsA_{i532}$ and $IcsA_{i563}$ mutant proteins, that bear insertion mutations within this region and are non-polar at the cell surface, were investigated directly for their ability for polar deliver of fused GFP+. The mutant fusion proteins ($IcsA_{506-620(i532)}$-GFP+ and $IcsA_{506-620(i563)}$-GFP+) were seen to be defective in polar targeting in the cytoplasm (Section 3.3. At low expression levels, diffuse fluorescence throughout the cytosol was predominantly observed, in contrast to the polar foci evident in *E. coli* expressing $IcsA_{506-620(WT)}$-GFP+. However in 2-3% of cells, the mutant polar targeting regions formed foci that exhibited rapid and seemingly random motion throughout the cell (Section 3.3, **Figure 3.8**). Curiously, when expression of these mutant fusions was increased, stable and immobile polar foci (equivalent to those formed by $IcsA_{506-620(WT)}$-GFP+) were predominant (**Figure 3.7**). These data suggested that insertion mutations i532 and i563 directly resulted in defective polar targeting in a protein concentration-dependent manner, but did not entirely abrogate the polar phenotype.

8.1.3 *A model: aggregating towards the pole*

The rapid motion of the fluorescent foci exhibited by GFP+ fusions to $IcsA_{506-620}$ regions from mutant $IcsA_{i532}$ and $IcsA_{i563}$ is a novel finding. The production levels of the $IcsA_{506-620(i532)}$-GFP+ and $IcsA_{506-620(i563)}$-GFP+ mutant constructs was comparable with that of the wild-type $IcsA_{506-620(WT)}$-GFP+. Since these mutants were capable of polarity at higher protein concentration, it was thought the mobile foci could represent early events that lead to the establishment of polar foci. The correlation between protein expression and polarity evident in these mutants, suggested (though did not directly demonstrate) that polar targeting and/or polar retention occurs in these mutants when sufficient protein is assembled into a focus. That no rapidly mobile foci were observed for the $IcsA_{506-620(WT)}$-GFP+

in this system, was presumably because the higher efficiency polar targeting in this fusion required less protein to establish polarity.

In a study published recently, Rokney *et al.* (2009) described rapid motion for foci of wild-type $IcsA_{506–620}$-GFP protein. That study directly showed that as the production of the fusion was increased, the mobile foci were addressed to the pole and resided there as essentially immobile foci. The formation of these polar foci required DnaK and DnaJ chaperones and the proton motive force. The requirement of DnaK in this model rationalised the proteomic screen identifying DnaK involvement in polar targeting from the work of Janakiraman *et al.* (2009). Rokney *et al.* (2009) further demonstrated the majority of the GFP fusion was an insoluble aggregate and that cytoplasmic chaperones ClpB and DnaK could remove protein from the aggregate in an energy-dependent process, suggesting that protein aggregation mediated the polar deliver of the GFP fusion protein (Rokney *et al.*, 2009). The proposed model proffered that $IcsA_{506–620}$ mediates aggregation of full length IcsA in the cytoplasm, delivering the nascent protein to the pole. Chaperones then extract IcsA from the aggregate and render it translocation-competent, thereby spatially concentrating IcsA cytoplasmic secretion to the pole. Rapid export across the periplasm would then preserve the polarity determined in the cytoplasm.

The findings of the present work could fit this proposed model. Presumably, the $IcsA_{506–620}$ regions from $IcsA_{i532}$ and $IcsA_{i563}$ have a reduced capacity for aggregation and therefore require greater expression of the protein to reach a critical mass that permits formation of a sufficiently large aggregate that is stably retained at the pole. This model of protein concentration-dependent aggregation also offers an explanation of the non-polar surface distribution of $IcsA_{i532}$ and $IcsA_{i563}$ reported by May and Morona (2008): while the polar targeting domain of either of these mutants are capable of polar targeting at high protein levels, they are unable to achieve this at the physiological levels of IcsA in *S. flexneri*.

Bioinformatic prediction of aggregation prone sequence remains difficult. However, a speculative assessment of the $IcsA_{506–620}$ region by the AGGRESCAN algorithm (Conchillo-Solé *et al.*, 2007), identified five sub-regions ($IcsA_{533–538}$, $IcsA_{545–557}$, $IcsA_{565–579}$, $IcsA_{590–598}$ and $IcsA_{608–613}$) as potential "hot spots" for mediating protein aggregation. Interestingly two of these regions are adjacent to the polar targeting defective insertional mutations, i532 and i563. Whether the

polar targeting region from these mutants have reduced aggregation capacity—consistent with the insertional mutation disrupting these "hot spots"—is a pressing question for further investigation that could validate the Rokney *et al.* (2009) model of polar targeting. Since protein aggregation is a root cause of a broad range of pathological disease, such as Huntington's disease, Alzheimer's disease, systemic amyloidosis and various prion diseases, the polar targeting of IcsA could yet be a useful model in probing the formation of aggregates and their disaggregation.

8.1.4 *Refinement of the polar targeting domain*

GFP+ fluorescence requires folding, and the molecule can be used as a marker for folding of a fusion protein. In the case of full length IcsA, the protein is thought to be maintained in an export-competent unstructured conformation by chaperones in the cytoplasm. Since $IcsA_{506–620}$-GFP+ emits observable and polarly located fluorescence, it is possible that the $IcsA_{506–620}$ region could adopt an intermittent structure that guides polar targeting prior to translocation of IcsA. A structural motif could be an attractive explanation in generating polarity: despite the increasing number of polarly targeted proteins, none share regions of notable homology to $IcsA_{506–620}$. Affinity tagged fusions were generated in this work to facilitate biochemical investigations that seek to (i) determine whether this region forms a tertiary structure; (ii) and how this potential structure might differ in the polarity defective i532 and i563 mutants (Section 3.3). Unfortunately, purification of these tagged constructs has to-date remained elusive and requires further work.

The site of the polar targeting-deficient insertional mutants and their location on a predicted IcsA structure hinted that the region between the mutants may be important in determining protein polarity, and could have been disrupted by insertions. This work assessed GFP+ fusions that spanned across the polar targeting domain in N- and C-terminal directions around the regions $IcsA_{532–570}$ and $IcsA_{538–563}$. To the author's knowledge, no other investigation of sequences within this polar targeting region had previously been reported. Interestingly, $IcsA_{506–562}$ and $IcsA_{538–562}$ were found to be insufficient for polar targeting of a GFP+ fusion (Section 3.4). In contrast, $IcsA_{506–570}$ and $IcsA_{532–570}$ were both

polarly targeted, albeit at lower frequency for $IcsA_{532-570}$-GFP+ (Section 3.4). These data suggest that the eight amino acid sequence $IcsA_{562-570}$ might be critical to the development of polarity. This sequence is predicted to include an aggregation prone region ($IcsA_{565-579}$), perhaps lending further weight to aggregation model, though clearly this requires direct confirmation. Consequently, this work has defined the 38 amino acid region $IcsA_{538-563}$ as being minimally sufficient to impose polar protein targeting. The hope is that this narrowly defined region might permit more specific analysis—such as amino acid substitution—of the sequences that might be important to the process of polar targeting.

8.2 IcsA polarity and the replicating chromosome

Replication of the *E. coli* chromosome is initiated at the mid-cell by DnaA at the *oriC* locus. Soon after being replicated, sister *oriC* loci move towards the poles of the dividing bacterium (Section 1.7.4). Since upon cytokinesis these poles become the same "old" poles to which IcsA is delivered, it was of interest to determine if the motion of *oriC* was linked to the polar delivery of $IcsA_{506-620}$. Indeed, the link previously established between the biogenesis of unipolar IcsA and cellular division, had made such a model both attractive and consistent with the literature (Goldberg *et al.*, 1994). In Chapter 4 whether the delivery of $IcsA_{506-620}$ to the poles occurred together with *oriC* segregation was directly investigated.

An arabinose-inducible $IcsA_{506-620}$-ECFP fluorescent protein fusion was constructed. The polar delivery of $IcsA_{506-620}$-ECFP was seen to co-localise with segregating *oriC* loci that were labelled by TetR-EYFP detection of proximal *tetO* repeat arrays (Section 4.2). This co-localisation was shown to be specific and not an artefact of the fluorescent proteins used in the system (**Figure 4.4** and **Figure 4.5**). Moreover, alterations in cell shape, either by antibiotic filamentation or depolymerisation of MreB, preserved this co-localisation (sec:cephalexin and Section 4.3.2). That IcsA and *oriC* polar delivery was observed co-localised does not necessary implicate a common mechanism, and it may be that the initiation of DNA replication may trigger a cell cycle cue for polar delivery.

The ability to induce expression of $IcsA_{506-620}$-ECFP allowed for visualisation of foci that while near the poles, nevertheless were not at the polar extremity (e.g. **Figure 4.3**). Such foci were not seen for the GFP+ fusion of this same $IcsA_{506-620}$

region when it was expressed constitutively (Section 3.2). In accordance with the above aggregation model, constitutive expression could have lead to efficient formation of polar foci, while the weak induction conditions applied throughout experiments described in Chapter 4 may have allowed for detection of foci that had not yet been incorporated into an immobile polar aggregate. An extended live imaging time-course would likely provide further insight, but this was difficult to accomplish in the current system since expression of the fluorescent protein fusions was kept necessarily weak, and was therefore poorly detectable using the present facilities for multiple generations (where doubling time of bacteria on agar pads was approximately 90 minutes). However, investigation of an inducible $IcsA_{506-620}$-GFP+ may be more readily attainable and equally informative.

Observation of rapid motion of nascent $IcsA_{506-620}$-ECFP foci is suggested by the aggregation model, as for foci that are evident for GFP+ fusions to $IcsA_{506-620(i532)}$ and $IcsA_{506-620(i563)}$). That such motion was not detected for $IcsA_{506-620}$-ECFP foci being deliver to the pole coincident with *oriC*, might be due to the limited sensitivity of $IcsA_{506-620}$-ECFP detection in a majority of cells, owing to high autofluorescence background in the system used. Such constrained sensitivity is likely to have limited detection to only larger and more highly fluorescent foci. Data presented in this work (Section 3.3) and by Rokney *et al.* (2009) suggest the that incorporation of $IcsA_{506-620}$ fluorescent protein fusions into larger foci is likely to be required for slowing motion and stable retention of foci at the pole. The $IcsA_{506-620}$ and *oriC* co-localisation presented in this work, may additionally implicate cell cycle cues (initiated by chromosome replication) in stabilisation of these foci and in their polar delivery.

Overexpression of the *migS* sequence (a centromere-like sequence that mediates polar migration of *oriC*), reduced the frequency of observed co-localisation between $IcsA_{506-620}$-ECFP and TetR-EYFP labelled *oriC* (**Figure 4.9**). In these bacteria (strain MG242), the migration of *oriC* towards the poles seemed to be impeded, with a higher number of cells displaying mid-cell localised *oriC* fluorescence, compared to the control (strain MG182) (Section 4.4). Nonetheless, foci of $IcsA_{506-620}$-ECFP remained localised near the poles or at the polar extremities (Section 4.4). It is likely that on *migS* overexpression, the *oriC* segregating mechanism continues to operate and delivers unlabelled plasmid-borne *migS* centromere to the pole (Yamaichi and Niki, 2004). These data suggest that $IcsA_{506-620}$ and

oriC co-localisation can be specifically broken by interfering with the migration of *oriC* and support the specificity of the observed co-localisation in the wild-type parent situation.

An intriguing link between DNA replication and protein polar targeting has recently been uncovered. The activity of DnaA in initiating DNA replication at *oriC* is regulated by nucleotide exchange facilitated by the anionic phospholipid, cardiolipin (itself enriched at the poles) (Kaguni, 2006; Mileykovskaya and Dowhan, 2000). The polar localisation of the *E. coli* osmoregulatory protein ProP has been shown to require cardiolipin (Romantsov *et al.*, 2007). Moreover, biophysical modelling of the properties of cardiolipin suggests that—owing to the head:tail ratio of this lipid that favours curvature—the formation of sufficiently large cardiolipin domains in the inner-membrane, can spontaneously trigger their migration towards the poles where curvature is favoured. Moreover, this polar migration was modelled to be influenced by pinning to the cell wall, in agreement with observations by Pradel *et al.* (2007) that at least some cues that demarcate the poles and attract $IcsA_{506–620}$ are derived outside the cytoplasm. It might be tempting to speculate that following the initiation of replication by DnaA, *oriC* motion might be cardiolipin-dependent and the spontaneous redistribution of cardiolipin domains to the pole may deliver *oriC*. A comparable mechanism could apply to proteins or protein aggregates. However, while the polar targeting of ProP was seen to be cardiolipin dependent, a more recent and broader evaluation of polarly targeted proteins by the same group suggests that polarity can be established in both a cardiolipin-dependent and a cardiolipin-independent manner (Romantsov *et al.*, 2010). Preliminary work undertaken during these studies using conditional *pgsA* mutation that results in reduced cardiolipin content in the inner-membrane, suggests that $IcsA_{506–620}$ polarity might be established in a mechanism that is independent of cardiolipin (not shown).

That polar delivery of a protein component of the *E. coli* chemosensory machinery occurs with migrating *oriC* has recently been shown (Thiem *et al.*, 2007). Very recent work could rationalise the link between polar targeting and *oriC* migration observed in the work presented in this thesis. Winkler *et al.* (2010) demonstrated that formation of aggregates at the poles relies on nucleoid occlusion that when disrupted, results in misplaced and non-polar aggregates. Consequently, the observed co-localisation of *oriC* and $IcsA_{506–620}$ result from the nucleoid occlu-

sion mechanisms at-play during chromosome replication. Whether $IcsA_{506-620}$ polar targeting, or polar aggregation, is mechanistically linked directly to the replication of the chromosome, or whether polarity and replication are trigger by a common cell cycle cues is an exciting question for future exploration.

8.3 IcsA within the outer membrane

The properties of the outer membrane remain poorly defined and only recently have successful efforts been made to visualise the organisation of LPS and protein at the cell surface. This work assessed the subcellular distribution of LPS chain lengths and developed a rapid and sensitive method for tracking the motion and behaviour of nascent proteins in the outer membrane

8.3.1 *The LPS modal length distribution*

The LPS context is critical for IcsA function, and relies on the modal length of Oag rather than on its chemical composition (Sandlin *et al.*, 1996). Ghosh and Young (2005) observed helical bands and polar caps of immobile LPS at the *E. coli* surface. IcsA diffusion had previously been suggested to occur away from the pole. However, increasing Oag chain length had also been suggested to correlate with reduced outer membrane diffusion. The polar caps of immobile LPS and IcsA diffusion seemed to offer conflicting accounts of the properties of the polar outer membrane. The distribution of LPS Oag chain lengths had not previously been investigated. This work assessed the LPS populations of the poles and the lateral cell surface (Chapter 5). Representative polar and lateral LPS was obtained from minicell and whole-cell fractions of a *S. flexneri min* mutant.

Analysis of the distribution of Wzz_{SF} and Wzz_{pHS-2} polysaccharide co-polymerases that confer Oag length to *S. flexneri* conclusively showed that these proteins, unlike IcsA, do not exhibit polar targeting (**Figure 5.5**). When the population of LPS residing at the poles was compared to the whole-cell derived lateral LPS, chain length distributions were also found not to differ. These data suggested that LPS chain lengths were uniformly distributed over the cell surface. However, the existence of localised patches of predominantly short, long, or very-long LPS remains possible and may not have been detectable in these experiments.

8.3.2 *A strategy for tracking nascent IcsA*

Helically patterned diffusion within the outer membrane had been suggested, but perhaps inconclusively demonstrated, for the *E. coli* LamB protein (Robbins *et al.*, 2001b). However, a similar helical diffusion pattern was seen for some surface proteins when all surface proteins were non-specifically labelled (Robbins *et al.*, 2001b; Ghosh and Young, 2005). IcsA diffusion had been suggest by image analysis of chemically fixed cells, but had not directly been scrutinised in living bacteria. In this work, a system for sensitive and rapid detection of nascent IcsA was developed to address the properties of IcsA in the outer membrane.

Metabolic biotinylation was exploited for specificity in labelling and affinity in detection with streptavidin conjugates. A small 14 amino acid epitope (BIO) was sufficient to direct protein biotinylation and an amino acid substitution epitope (BIOK10R) served as a specificity control. In the case of IcsA, when BIO was inserted into a permissive site, the protein retained wild-type equivalent function, expression and localisation. However, it should be noted that while complementation of *S. flexneri* Δ*icsA*::Tc^R with $IcsA_{BIO}$ restores wild-type equivalent plaque formation, these data cannot directly discriminate whether biotinyl-$IcsA_{BIO}$ (compared to unbiotinylated $IcsA_{BIO}$) remains functional. The covalent attachment of the biotin moiety would be predicted to have little effect on protein structure, and the site of BIO insertion (amino acid position 87) is outside the recognised N-WASP binding domain (**Figure 1.3**). Moreover, other exogenously biotinylated proteins retain function (Reed and Cronan, 1991).

$IcsA_{BIO}$ remained export competent. Since biotinylation occurs in the cytoplasm and $IcsA_{BIO}$ could be biotinylated, this work support post-translational export of the protein. The data presented in Section 6.6 suggested that metabolic biotinylation could be improved by overexpressing the BirA biotin protein ligase. While detection of biotinylated $IcsA_{BIO}$ by immunoblotting or epifluorescence at early time points (15-20 minutes) following weak induction of protein expression suggests that biotinylation was occurring efficiently, the absolute efficiency of biotinylation in this system remains to be determined.

Previous studies present conflicting explanations for the presence of non-polar sub-populations of IcsA, proposing either diffusion or direct export to the lateral cell body (Section 1.6.2). To assess possible IcsA diffusion, the ability to rapidly

detect $IcsA_{BIO}$ following its appearance at the cell surface was considered essential in this system. Biotinylated $IcsA_{BIO}$ could readily and specifically be detect with streptavidin-Alexa 488 when production of the protein was strongly induced. Following weak induction of $IcsA_{BIO}$ expression, biotinyl-$IcsA_{BIO}$ could readily be labelled with stretpavidin-Qdot 605 (**Figure 6.9**).

Streptavidin is a tetrameric complex capable of binding multiple biotinyl-$IcsA_{BIO}$ proteins. The occurrence of single molecule labelling was not directly demonstrated in presented experiments. Despite this, conditions of weak induction would mean few $IcsA_{BIO}$ molecules were present at the surface when labelling was occurring, and it is likely detection by stretpavidin-Qdot 605 was of single biotinyl-$IcsA_{BIO}$ molecules. That single streptavidin-Qdot 605 molecules were being observed was verified by observation of Qdot fluorescence "blinking", an inherent physical property of Qdots. The use of streptavidin-Qdots to fluorescently detect nascent $IcsA_{BIO}$ permits visualisation of bright and discreet foci of fluorescence that will facilitate tracking. Preliminary tracking data suggest biotinyl-$IcsA_{BIO}$ remains immobile in the outer membrane, using this system (not shown)

Metabolic biotinylation requires only the insertion of a small well tolerated epitope and could constitute a broadly applicable strategy to investigate the outer membrane behaviour of a range of surface proteins. Assessed together, such experiments of individual proteins could be compiled into a more complete appreciation of the dynamics within the outer membrane.

8.3.3 *IcsA oligomerisation*

The observation of negative dominance of some $IcsA_i$ mutants over $IcsA_{WT}$ when co-expressed, suggested the existence of a functional interaction between IcsA molecules at the bacterial surface. However, this phenotype could be explained by interference of $IcsA_i$ mutants in the export of $IcsA_{WT}$. Indeed, one model of outer membrane export of autotransporters suggests oligomerisation of translocation domains into a large pore and co-operative export of effector domains through this pore (Section 1.5.3; Veiga *et al.*, 2002). Additionally, intramolecular autochaperone regions assist in the efficient outer membrane translocation of at least some autotransporters (Section 1.4.8). Remarkably, defective autochaper-

one regions can be complemented *in trans* by wild-type autochaperone regions, further suggesting some level of cooperative export (Ohnishi *et al.*, 1994; Dutta *et al.*, 2003; Oliver *et al.*, 2003b). One of the negative dominant mutations, i677, resides in the region $IcsA_{634-735}$ that is likely to be an IcsA autochaperone region (Section 1.4.8). The data presented in this thesis indicate that the reported negative dominance of IcsAi mutants is not simply a consequence of reduced export and surface expression of $IcsA_{WT}$. By quantitative surface labelling of a FLAG epitope labelled IcsA-derivative ($IcsA_{FLAG}$), that is functionally equivalent to $IcsA_{WT}$, no changes in the level of protein expression at the cell surface were evident, either when $IcsA_{FLAG}$ was expressed alone or co-expressed with $IcsA_i$ negative dominant mutants (**Figure 7.1**). Consequently the amount of fully functional IcsA at bacterial surface remained constant in strains with evident negative dominant phenotypes.

Negative dominance was a genetic indication of IcsA-IcsA interactions and the existence of a multimeric complex in the outer membrane that is functionally relevant. This complex could become defective upon incorporation of negative dominant $IcsA_i$ mutants into a mixed complex with $IcsA_{WT}$. In bacteria co-expressing fully functional $IcsA_{BIO}$ and $IcsA_{FLAG}$, specific reciprocal co-purification was discovered, and this work directly identified IcsA-IcsA interaction in a hetero-oligomer within the outer membrane (Section 7.2).

Oligomerisation has only rarely been reported for conventional autotransporters: *N. meningitidis* IgA1 protease translocation domains form a large pore; *H. pylori* VacA toxin effector domains form an astral array when released from the cell surface (El-Bez *et al.*, 2005). Other studies have specifically excluded oligomerisation for *E. coli* AIDA and *N. meningitidis* NalP autotransporters (Oomen *et al.*, 2004; Müller *et al.*, 2005; Skillman *et al.*, 2005). Chemical cross-linking of effector domain deletion constructs still resulted in observation of HMW complexes, suggesting that $IcsA_{103-730}$ may not be required for oligomerisation (Section 7.3). Consequently, it seems likely that the translocation domain mediates oligomerisation, but the involvement of $IcsA_{53-103}$ cannot be excluded by these data. While further work will be required to define the size and nature of the IcsA oligomer, the finding that oligomerisation in the outer membrane is functionally relevant is an exciting development that will assist in understanding the IcsA-N-WASP interaction that is vital to *Shigella* pathogenesis. IcsA oligomerisation is consistent with

a broader pattern of strategies that achieve multivalency for bacterial proteins that engage host proteins of the WASP family: self-association for Enterohaemorrhagic *E. coli* intimin-tir; spatial clustering for *L. monocytogenes* ActA; and internal repeats for Enterohaemorrhagic *E. coli* $EspF_U$/Tccp (Touzé *et al.*, 2004; Footer *et al.*, 2008; Sallee *et al.*, 2008).

8.4 Concluding remarks

Investigation of polar targeting of the *S. flexneri* IcsA autotransporter has verified the essentiality of the $IcsA_{506-620}$ region for polar delivery of the protein in the cytoplasm. For the first time, insertional mutations have been identified that interfere with polar targeting. Rapid motion of foci formed by GFP+ fusions to these mutated polar targeting domains ($IcsA_{506-620(i532)}$ and $IcsA_{506-620(i563)}$) likely hints at the preliminary stage of targeting and retention at the pole. Using *in silico* modelling and the location of these mutations, the polar targeting domain has been refined to $IcsA_{532-570}$. The data of this thesis support a model of aggregation for polar delivery.

Polar targeting was seen to be coincident with DNA replication and the separation of *oriC* loci into daughter cell compartments. The co-localisation of $IcsA_{506-620}$-ECFP with *oriC* was robust and retained in filamented and shape-defective bacteria. Interruption of *oriC* segregation resulted in reduced co-localisation, suggesting that cell cycle cues that trigger DNA replication and *oriC* migration may additionally trigger polar delivery of proteins. While this trigger may be common, the mechanisms involved in the polar motion of oriC and the polar targeting of proteins are likely to be distinct. Together, the findings of this thesis support a model of aggregate-mediated polar delivery of IcsA that occurs soon after chromosomal replication is initiated.

Direct IcsA-IcsA interaction in the outer membrane has been demonstrated, and data supporting the presence of large IcsA-containing complexes at the cell surface has been presented in support of previous genetic evidence. Data is presented indicating the translocation domain mediates the formation of this complex. The oligomerisation of IcsA is the first demonstration of a functional autotransporter oligomer in the outer membrane. The LPS context is critical to both IcsA localisation and function. Polar *S. flexneri* LPS was shown to be

quantitatively and qualitatively equivalent to LPS found at the lateral cell body. Moreover, a method for sensitively and rapidly detecting nascent exported IcsA has been validated and will allow for direct scrutiny of the properties of IcsA in the outer membrane and the LPS-IcsA interplay.

For more than twenty years, IcsA has been a key model in understanding the motility of intracellular bacteria. Now, the protein holds promise as a tool to unravel the fundamental processes that contribute to the subcellular organisation within the cytosol and the outer membrane of prokaryotes.

Part IV

APPENDICES

A

Appendix A

Table A.1: Bacterial strains described in this work

STRAIN	RELEVANT CHARACTERISTICS
Bacterial hosts from lab stocks	
E. coli K-12	
UT5600	F$^-$ *ara-14 leuB6 secA6 lacY1 proC14 tsx-67* Δ(*ompT-fepC*)266 *entA403 trpE38 rfbD1 rpsL109 xyl-5 mtl-1 thi-1*
DH5α	F$^-$ *endA1 glnV44 thi-1 recA1 relA1 gyrA96 deoR nupG* ϕ80d*lacZ*ΔM15 Δ(*lacZYA-argF*)U169, *hsdR17*(r_K^- m_K^+), λ$^-$
BL21(DE3)	F$^-$ *ompT gal dcm lon hsdSB*(r_B^- m_B^-) λ(DE3 [*lacI lacUV5*-T7 gene 1 *ind1 sam7 nin5*])
TOP10F′	F′[*lacI*^{q} Tn*10*(*tetR*)] *mcrA* Δ(*mrr-hsdRMS-mcrBC*) ϕ80*lacZ*ΔM15 Δ*lacX74 deoR nupG recA1 araD139* Δ(*ara-leu*)7697 *galU galK rpsL*(Str^R) *endA1* λ$^-$
AB1157	*thr-1 araC14 leuB6*(Am) Δ(*gpt-proA*)62 *lacY1 tsx-33 qsr′-0 glnV44*(AS) *galK2*(Oc) *hisG4*(Oc) *rfbC1 mgl-51 rpoS396*(Am) *rpsL31*(Str^R) *kdgK51 xylA5 mtl-1 argE3*(Oc) *thi-1*
IL02	AB1157 *oriC*Ω(*tetO*$_{240}$::Gm^R::*tetO*$_{240}$)
IL03	AB1157 *oriC*Ω(*lacI*$_{240}$::Km^R::*lacI*$_{240}$)
S. flexneri	
2457T	wild-type *S. flexneri* serotype 2a
RMA2041	2457T Δ*icsA*::Tc^R
RMA2043	2457T Δ*icsA*::Tc^R Δ*rmlD*::Km^R
RMA2090	2457T Δ*icsA*::Tc^R [pIcsA; Ap^R]

Bacterial strains described in this work (*continued...*)

STRAIN	RELEVANT CHARACTERISTICS
Chapter 3	
this study	
MG44	DH5α [pRMA2611::$icsA_{1-758}$; Km^R]
MG54	BL21(DE3) [pRMA2611::$icsA_{1-1102}$; Km^R]
MG96	DH5α [pRMA2611::$icsA_{54-104}$; Km^R]
MG98	DH5α [pRMA2611::$icsA_{54-758}$; KmR]
MG100	DH5α [pQE60::*Spe*I-*Sac*I; Ap^R]
MG129	DH5α [pRMA2611::$icsA_{506-620}$; Km^R]
MG342	DH5α [pRMA2611::$icsA_{1-105}$; Km^R]
MG343	DH5α [pRMA2611::$icsA_{54-505}$; Km^R]
MG344	DH5α [pRMA2611::$icsA_{105-505}$; KmR]
MG346	DH5α [pRMA2611::$icsA_{105-620}$; KmR]
MG348	DH5α [pRMA2611::$icsA_{105-758}$; KmR]
MG351	DH5α [pRMA2611::$icsA_{506-562}$; Km^R]
MG353	DH5α [pRMA2611::$icsA_{538-620}$; Km^R]
MG356	DH5α [pRMA2611::$icsA_{538-562}$; Km^R]
MG357	DH5α [pRMA2611::$icsA_{506-570}$; Km^R]
MG358	DH5α [pRMA2611::$icsA_{532-620}$; Km^R]
MG360	DH5α [pRMA2611::$icsA_{532-570}$; Km^R]
MG423	BL21(DE3) [pRMA2611::*Strep-*$icsA_{506-620}$-TEV; Km^R]
MG424	BL21(DE3) [pRMA2611::*Strep-*$icsA_{506-i532-620}$-TEV; Km^R]
MG426	BL21(DE3) [pRMA2611::*Strep-*$icsA_{506-i570-620}$-TEV; Km^R]
Chapter 4	
this study	
MG182	IL02 [pBAD24::$icsA_{506-620}$-*ecfp*, *tetR-eyfp*; Ap^R]
MG183	IL02 [pBAD24::$icsA_{506-620}$-*ecfp*, *tetR-eyfp*; Ap^R]
MG185	IL03 [pBAD24::$icsA_{506-620}$-*ecfp*, *tetR-eyfp*; Ap^R]
MG218	IL02 Δ*migS* [pBAD24::$icsA_{506-620}$-*ecfp*, *tetR-eyfp*; Ap^R]
MG242	IL02 [pBAD33::$icsA_{506-620}$-*ecfp*, *tetR-eyfp*; Cm^R] [pUC18::*migS*; Ap^R]

Bacterial strains described in this work (*continued...*)

STRAIN	RELEVANT CHARACTERISTICS
Chapter 5	
this study	
MG292	2457T *minD*::Km^R
Chapter 6	
donated	
KMRM201	UT5600 [pKMRM1; Ap^R] (May, 2007)
this study	
MG57	UT5600 [pKMRM1::BIO; Ap^R]
MG58	UT5600 [pKMRM1::BIO; Ap^R]
MG64	RMA2041 [pKMRM1::BIO; Ap^R]
MG65	RMA2043 [pKMRM1::BIO; Ap^R]
MG82	DH5α [pBAD30::*icsA*$_{BIO}$; Ap^R]
MG83	DH5α [pBAD30::*icsA*$_{BIOK10R}$; Ap^R]
MG84	UT5600 [pMG82; Ap^R]
MG85	UT5600 [pMG83; Ap^R]
MG86	UT5600 [pMG82; Ap^R] [pCY216; Cm^R]
MG87	UT5600 [pMG83; Ap^R] [pCY216; Cm^R]
MG88	UT5600 [pMG82; Ap^R] [pRMA156; Km^R]
MG89	UT5600 [pMG83; Ap^R] [pRMA156; Km^R]
MG90	UT5600 [pMG82; Ap^R] [pRMA160; Km^R]
MG91	UT5600 [pMG83; Ap^R] [pRMA160; Km^R]
MG92	UT5600 [pMG82; Ap^R] [pCY216; Cm^R] [pRMA156; Km^R]
MG162	RMA2041 [pKMRM1::BIOK10R; Ap^R]
MG163	RMA2043 [pKMRM1::BIOK10R; Ap^R]

Bacterial strains described in this work (*continued...*)

STRAIN	RELEVANT CHARACTERISTICS
MG227	MG88 [pBBR1MCS::*birA*; Cm^R]
MG228	MG89 [pBBR1MCS::*birA*; Cm^R]
MG229	MG90 [pBBR1MCS::*birA*; Cm^R]
MG230	MG91 [pBBR1MCS::*birA*; Cm^R]
MG231	MG88 [pBBR1MCS; Cm^R]
MG232	MG89 [pBBR1MCS; Cm^R]
MG233	MG90 [pBBR1MCS; Cm^R]
MG234	MG91 [pBBR1MCS; Cm^R]
Chapter 7	
donated	
KMRM250	DH5α [pKMRM1::FLAG; Ap^R] (May, 2007)
KMRM276	RMA2041 [pKMRM11; Ap^R] [pKMRM270; Km^R] (May, 2007)
KMRM277	RMA2041 [pKMRM34; Ap^R] [pKMRM270; Km^R] (May, 2007)
RMA2205	RMA2041 [pD10-1; Tp^R] (Suzuki *et al.*, 1996)
RMA2208	RMA2041 [pD10-*virG3*; Tp^R] (Suzuki *et al.*, 1996)
RMA2209	RMA2041 [pD10-*virG4*; Tp^R] (Suzuki *et al.*, 1996)
this study	
MG157	UT5600 [pMG55; Ap^R] [pKMRM270; Km^R] [pCY216; Cm^R]
MG250	UT5600 [pKMRM1; Ap^R] [pKMRM270; Km^R] [pCY216; Cm^R]
MG251	UT5600 [pMG55; Ap^R] [pKMRM252; Km^R] [pCY216; Cm^R]

B

Appendix B

Table B.1: Plasmids described in this work

PLASMID	DESCRIPTION
Cloning vectors	
pBAD24	in Guzman *et al.* (1995); P_{BAD} expression, pBR322 ori; Ap^R
pBAD30	in Guzman *et al.* (1995); P_{BAD} expression, pACYC184 ori; Ap^R
pBAD33	in Guzman *et al.* (1995); P_{BAD} expression, pACYC184 ori; Ap^R
pBBR1MCS	in Kovach *et al.* (1994); P_{lac}, broadhostori, LacZα; Km^R
pBBR1MCS2	in Kovach *et al.* (1995); P_{lac}, broadhostori, LacZα; Km^R
pGEM-T Easy	Promega; LacZα; Ap^R
pKMRM1	in May and Morona (2008); pBR322::$icsA_{i87}$; Ap^R
pRMA2611	(lab stock, unpublished); pBBR1MCS::*gfp*+; Km^R
pQE60	Promega; Ap^R
pUC18	NEB; LacZα; Ap^R
Other plasmids	
pIcsA	in Morona and Van Den Bosch (2003b); pBR322::$icsA_{WT}$, ColE1; Ap^R
pJRD215	broad host range cosmid, *mob*; Km^R, Sm^R
pKD4	in Datsenko and Wanner (2000); FLP Km^R template; Km^R
pKD46	in Datsenko and Wanner (2000); λ red recombinase; Ap^R
pCP20	in Datsenko and Wanner (2000); FLP recombinase; Ap^R
pKMRM250	in May (2007); $IcsA_{i87::FLAG}$; Ap^R
pRMA154	in Macpherson *et al.* (1991) pJRD215::*rfb*; Km^R
pRMA2496	(unpublished, L. Purins) FLP Tc^R template; Tc^R

C

Appendix C

Table C.1: Oligonucleotides amplifying *icsA* regions for GFP+ fusions in Chapter 3

STRAIN AND FUSION CONSTRUCT	FORAWARD	REVERSE
MG54 ($IcsA_{1-1102}$-GFP+)	IcsA_1_Nhe	IcsA_1102_Nhe
MG342 ($IcsA_{1-104}$-GFP+)	IcsA_1_Nhe	IcsA_104_Nhe
MG44 ($IcsA_{1-758}$-GFP+)	IcsA_1_Nhe	IcsA_758_Nhe
MG96 ($IcsA_{53-104}$-GFP+)	IcsA_53_Nhe	IcsA_104_Nhe
MG343 ($IcsA_{53-505}$-GFP+)	IcsA_53_Nhe	IcsA_505_Nhe
MG98 ($IcsA_{53-758}$-GFP+)	IcsA_53_Nhe	IcsA_758_Nhe
MG344 ($IcsA_{105-505}$-GFP+)	IcsA_105_Nhe	IcsA_505_Xba
MG346 ($IcsA_{105-620}$-GFP+)	IcsA_105_Nhe	IcsA_620_Xba
MG348 ($IcsA_{105-758}$-GFP+)	IcsA_105_Nhe	IcsA_758_Xba
MG129 ($IcsA_{506-620}$-GFP+)	IcsA_506_Nhe	IcsA_620_Xba
MG351 ($IcsA_{506-562}$-GFP+)	IcsA_506_Nhe	P2loop_R
MG353 ($IcsA_{538-620}$-GFP+)	P2loop_F	IcsA_620_Xba
MG355 ($IcsA_{538-562}$-GFP+)	P2loop_F	P2loop_R
MG357 ($IcsA_{506-570}$-GFP+)	IcsA_506_Nhe	P2_revised_R
MG358 ($IcsA_{532-620}$-GFP+)	P2_revised_F	IcsA_620_Xba
MG360 ($IcsA_{532-570}$-GFP+)	P2_revised_F	P2_revised_R

D

Appendix D

Table D.1: Oligonucleotides designed for assembling sequences by annealing

OLIGONUCLEOTIDES	SEQUENCE(5′→3′)
*Bam*HI of pQE60	(*Spe*I & *Sac*I sites)
New_QE60_Spe-Sac_F	gatcaactagtgtcgacgtcgagctcg
New_QE60_Spe-Sac_R	gatccgagctcgacgtcgacactagtt
*Not*I of pKMRM1	(cloning BIO epitope)
KM1_BIO_F	ggcctgaacgacatcttcgaagctcagaaaatcgaatggcac
KM1_BIO_R	ggccgtgccattcgattttctgagcttcgaagatgtcgttca
*Not*I of pKMRM1	(cloning BIOK10R epitope)
BIO1_R(K)_F	ggcctgaacgacatcttcgaagctcagcgaatcgaatggcac
BIO1_R(K)_R	ggccgtgccattcgattcgctgagcttcgaagatgtcgttca
*Not*I of pKMRM33	(cloning BIO epitope)
KM33_BIO_F	ggccaggcctgaacgacatcttcgaagctcagaaaatcgaatggcac
KM33_BIO_R	ggccgtgccattcgattttctgagcttcgaagatgtcgttcaggcca
*Bam*HI-*Sal*I of pUC18	(cloning *migS*)
pUC18_migS_F	tcgacttaacttccatttttgcgggtactcagcaaaattcttcgccatatcctc-gagcggcgg
pUC18_migS_R	gatcccgccgctcgaggatatggcgaagaattttgctgagtacccgca-aaaatggaagttaag

Oligonucleotides designed for assembling sequences by annealing (*cont...*)

OLIGONUCLEOTIDES	SEQUENCE(5′→3′)
*Nhe*I of pRMA1611-derivatives	(TEV site)
AO_TEV_NheI_F	ctagcgaaaacctgtattttcagggct
AO_TEV_NheI_R	ctagagccctgaaaatacaggttttcg
*Nhe*I of pRMA1611-derivatives	(flexible linker)
AO_link_NheI_F	ctagcggctctgcgggctctgcggcgggctctggcgaattta
AO_link_NheI_R	ctagtaaattcgccagagcccgccgcagagcccgcagagccg
*Nhe*I of pRMA1611-derivatives	(*Strep*-tag II)
AO_strep_tag_NheI_F	ctagctggagccacccgcagttcgaaaaga
AO_strep_tag_NheI_R	ctagtcttttcgaactgcgggtggctccag
*Sph*I of pMG175 & pMG181	(flexible linker)
AO_SphI_link_F	ggctctgcgggctctgcggcgggctctggcgaatttgccatg
AO_SphI_link_R	cgtttaagcggtctcgggcggcgtctcgggcgtctcgggtac
*Nhe*I of pBAD33	(start codon and *Nhe*I site)
MCS3_NheI_F	ctagaggaggaattcaccatggtacgctagc
MCS3_NheI_R	ctaggctagcgtaccatggtgaattcctcct

E

Appendix E

Table E.1: Oligonucleotides used for sequencing and diagnostic PCR

OLIGONUCLEOTIDE	SEQUENCE (5′→ 3′)
Vectors	
pQE60	
pQE60_R	ccattgggatatatcaacggtggtatatcc
pQE60_F	ggcgtatcacgaggcccttc
pRMA2611	
gfp+_F	gcgcgtgcagcccttattg
gfp+_R	gtcatgccgtttcatatgatcc
pBAD Myc His A	
BADMycHisA_R	cagaccgcttctgcgttctg
BADMycHisA_F	ctgtaacaaagcgggaccaaagc
pGEM-T Easy	
M13_F	cgccagggttttcccagtcacgac
M13_R	tcacacaggaaacagctatgac
pBAD24 & pBAD30	
pBAD30_F	caaaagtgtctataatcacggcag
pABD30_R	ggcatggggtcaggtgg

Oligonucleotides used for sequencing of clones and diagnostic PCR (*cont.*)

OLIGONUCLEOTIDE	SEQUENCE (5′→ 3′)
Genes	
icsA (NCBI GeneID: 1238021)	
icsA_218R	ggagaaagtccatcaacaggtg
icsA_400F	ggtggtgactctattaccggatctg
icsA_400R	cagatccggtaatagagtcaccacc
icsA_800F	ggctacggtggtaatgctatcacagg
icsA_1200F	ggtgagaacagttctttaaatttagctgg
icsA_1600F	ggaactctcattttggcgg
icsA_1640R	aatgcctgcattgatgttgg
icsA_2000F	atgcgtctggtattacctatgttgc
icsA_2400F	ccttctctctatgaccgacacgg
icsA_2800F	ggttaactggtgagaaatattccagc
icsA_3300R	gaaggtatatttcacacccaaaatacc
birA (NCBI GeneID: 948469)	
birA_1000R	ccttttctgcactacgcagg
birA_500R	ccatttaacacgaactttatctgcac
narW (NCBI GeneID: 946032)	
narW_-36_F	catcaccgaagtgcgcg
ltrA (GenBank: U50902.4)	
ltrA_781_R	gatagatgttggccaaaagagg
dnaA (GeneID: 948217)	
dnaA_500R	ccgccataaaggaacaacg
dnaA_1000R	ccttccagctcacgtacgttag
dnaA_1400R	acgatgacaatgttctgattaaatttg

F

Appendix F

Table F.1: Cloning oligonucleotides presented in this work

OLIGONUCLEOTIDE	SEQUENCE (5′→ 3′)
Chapter 3	
IcsA_1_Nhe	cacttactgataatatagtgcatggctagcattcac
IcsA_53_Nhe	gctgctagcctttcgggtactcaagaacttcatttttc
IcsA_104_Nhe	cgtagcttgctagcagatgcatgagagg
IcsA_105_Nhe	gcatctagagctagcctacggattaac
IcsA_505_Nhe	ccagaatagtactaacagtaaggctagcgttttctttc
IcsA_505_Xba	ccagaatagtactaacagtaagtctagagttttctttc
IcsA_506_Nhe	cgctgaagctagcgttagtactattctggc
IcsA_620_Xba	gaattctagaaccgtttttctccagag
IcsA_758_Nhe	ctagctcggctagcactcatttgagtag
IcsA_758_Xba	ctagctcgtctagaactcatttgagtag
IcsA_1102_Nhe	gcatttttattagctagcggtatatttc
P2loop_F	ctctcgctagcgcggaaaaaaatacctactctgg
P2loop_R	gcggttctagacatagcttcaactgtccccat
P2_revised_F	caaaagctagcgagggaactctcattttggc
P2_revised_R	gcacctctagaaacaataacaccagcggtacg
506_StrepII_NheI	gctagctggagccacccgcagttcgaaaaggttagtactattctggcag
620_TEV_XbaI	tctagagccctgaaaatacaggttttcaccgtttttctccagagtcatgttacc
Chapter 4	
506_F_NheI-NcoI	gaaagctagcaacccatggttagtactattctggcagat
620_R_XhoI	gagaatctcgagaccgtttttctccagagtc

Cloning oligonucleotides presented in this work (*cont...*)

OLIGONUCLEOTIDE	SEQUENCE (5′→ 3′)
Chapter 5	
minF	gacttgcctcaatataatcc
minR	tctgtgcgtgggaacagc
P1_PacI	ccttaattaagtgtaggctggagctgcttc
P2_PacI	ccttaattaacatatgaatatcctccttag
Chapter 6	
IcsA.BIO-pBAD30_Eco	cacttactgataatagaattcatgaatcaaattcac
REPL.BIO-pBAD30_Sal	cacgccctgtcgacttattatcagaagg
BirA_F_XhoI	atgctcgagatgaaggataacaccgtgc
BirA_R_HindIII	atgatgaagctttcatccttttctgcactacgcag

G

Appendix G

G.1 List of donated and laboratory stock bacterial strains

Table G.1: *E. coli* and *S. flexneri* donated to this work

strain	description
MG61	S. Polyak (University of Adelaide) (Chapman-Smith *et al.*, 1994)
MG168	S. Polyak (University of Adelaide) (Choi-Rhee *et al.*, 2004)
MG103	D. Sherratt (Oxford University) (Lau *et al.*, 2003))
MG104	D. Sherratt (Oxford University) (Lau *et al.*, 2003))
MG105	D. Sherratt (Oxford University) (Lau *et al.*, 2003))
MG106	D. Sherratt (Oxford University) (Lau *et al.*, 2003))
MG107	D. Sherratt (Oxford University) (Lau *et al.*, 2003))
MG108	D. Sherratt (Oxford University) (Lau *et al.*, 2003))
MG109	D. Sherratt (Oxford University) (Lau *et al.*, 2003))
MG110	D. Sherratt (Oxford University) (Lau *et al.*, 2003))
MG111	D. Sherratt (Oxford University) (Lau *et al.*, 2003))
MG112	T. Pugsley (Institut Pasteur) (Buddelmeijer *et al.*, 2009)
MG113	T. Pugsley (Institut Pastuer) (Buddelmeijer *et al.*, 2009)
MG142	K. May (laboratory stocks) (*unpublished*)
MG143	K. May (laboratory stocks) (May, 2007)
MG144	K. May (laboratory stocks) (May, 2007)
MG145	K. May (laboratory stocks) (May, 2007)
MG146	K. May (laboratory stocks) (May, 2007)
MG147	K. May (laboratory stocks) (May, 2007)
MG164	W. Dowhan (University of Texas) (Heacock and Dowhan, 1989)
MG165	W. Dowhan (University of Texas) (Xia and Dowhan, 1995)
MG166	E. Crooke (Georgetown University) (Zheng *et al.*, 2001)

G.2 List of Bacterial strains generated during this work

Table G.2: *E. coli* and *S. flexneri* generated during this work

STRAIN	DESCRIPTION
MG1	DH5α [pUT18::*icsB*; Ap^R]
MG2	DH5α [pUT18::*icsB*; Ap^R]
MG3	DH5α [pUT18::*icsB*; Ap^R]
MG4	DH5α [pUT18::*icsB*; Ap^R]
MG5	Top10F′ [pKT25::$icsA_{506-620}$; Km^R]
MG6	Top10F′ [pKT25::$icsA_{506-620}$; Km^R]
MG7	Top10F′ [pKNT25::$icsA_{506-620}$; Km^R]
MG8	Top10F′ [pKNT25::$icsA_{506-620}$; Km^R]
MG9	Top10F′ [pKT25::$icsA_{53-758}$; Km^R]
MG10	Top10F′ [pKT25::$icsA_{53-758}$; Km^R]
MG12	Top10F′ [pKNT25::$icsA_{53-758}$; Km^R]
MG13	Top10F′ [pUT18C::*icsB*; Ap^R]
MG14	Top10F′ [pUT18C::*icsB*; Ap^R]
MG15	Top10F′ [pKNT25::*ltrA*; Km^R]
MG16	Top10F′ [pKNT25::*icsB*; Km^R]
MG17	DH5α [pRMA2611::$icsA_{1-104}$; Km^R]
MG18	DH5α [pRMA2611::$icsA_{1-104}$; Km^R]
MG19	BTH101 [pKT25::$icsA_{506-620}$; Km^R]
MG20	BTH101 [pKT25::$icsA_{506-620}$; Km^R]
MG21	BTH101 [pKNT25::$icsA_{506-620}$; Km^R]
MG22	BTH101 [pKNT25::$icsA_{506-620}$; Km^R]
MG23	DHM1 [pKT25::$icsA_{506-620}$; Km^R]
MG24	DHM1 [pKT25::$icsA_{506-620}$; Km^R]

E. coli and *S. flexneri* generated in this work (*cont.*)

STRAIN	DESCRIPTION
MG25	DHM1 [pKNT25::$icsA_{506-620}$; Km^R]
MG26	DHM1 [pKNT25::$icsA_{506-620}$; Km^R]
MG27	BTH101 [pUT18::*icsB*; Ap^R]
MG28	BTH101 [pUT18C::*icsB*; Ap^R]
MG29	DHM1 [pUT18::*icsB*; Ap^R]
MG30	DHM1 [pUT18C::*icsB*; Ap^R]
MG31	BTH101 [pKT25::$icsA_{506-620}$; Km^R]
MG32	BTH101 [pKNT25::$icsA_{506-620}$; Km^R]
MG33	BTH101 [pKNT25::*ltrA*; Km^R]
MG34	BTH101 [pKT25::*zip*; Km^R]
MG35	BTH101 [pUT18C::*zip*; Ap^R]
MG36	*blank*
MG37	*blank*
MG38	*blank*
MG40	DHM1 [pUT18C::*zip*; Ap^R]
MG41	Top10F′ [pBADMycHisA::*icsA*; Ap^R]
MG42	Top10F′ [pBADMycHisA::*icsA*; Ap^R]
MG43	Top10F′ [pRMA2611::$icsA_{1-1102}$; Km^R]
MG44	Top10F′ [pRMA2611::$icsA_{1-758}$; Km^R]
MG45	Top10F′ [pRMA2611::$icsA_{1-104}$; Km^R]
MG46	Top10F′ [pRMA2611::$icsA_{1-104}$; Km^R]
MG47	Top10F′ [pRMA2611::$icsA_{105-505}$; Km^R]
MG48	Top10F′ [pRMA2611::$icsA_{506-620}$; Km^R]
MG49	Top10F′ [pRMA2611::$icsA_{506-620}$; Km^R]
MG50	Top10F′ [pBADMycHisA::$icsA_{759-1102}$; Ap^R]
MG51	Top10F′ [pBAD Myc His A::$icsA_{759-1102}$; Ap^R]
MG52	BL21(DE3) [pBADMycHis A::*icsA*; Ap^R]
MG53	BL21(DE3) [pBADMycHis A::*icsA*; Ap^R]
MG54	BL21(DE3) [pRMA2611::$icsA_{1-1102}$; Km^R]
MG55	DH5α [pKMRM1::BIO; Ap^R]

E. coli and *S. flexneri* generated in this work (*cont.*)

STRAIN	DESCRIPTION
MG56	DH5α [pKMRM1::BIO; Ap^R]
MG57	UT5600 [pKMRM1::BIO; Ap^R]
MG58	UT5600 [pKMRM1::BIO; Ap^R]
MG59	Top10F′ [pQE60::$icsA_{506-620}$; Ap^R]
MG60	Top10F′ [pQE60::$icsA_{506-620}$; Ap^R]
MG61	DH5α [pCY216::*birA*; Cm^R]
MG62	UT5600 [pKMRM1::BIO; Ap^R] [pRMA156; Km^R]
MG63	UT5600 [pKMRM1::BIO; Ap^R] [pRMA160; Km^R]
MG64	RMA2041 [pKMRM1::BIO; Ap^R]
MG65	RMA2043 [pKMRM1::BIO; Ap^R]
MG66	BL21(DE3) [pREP4; Km^R] [pQE60::$icsA_{506-620}$; Ap^R]
MG67	M15 [pREP4; Km^R] [pQE60::$icsA_{506-620}$; Ap^R]
MG68	UT5600 [pCY216::*birA*; Cm^R]
MG69	DH5α [pKMRM1::BIOK10R; Ap^R]
MG70	DH5α [pBAD30::$icsA_{BIO}$; Ap^R; P_{icsA}]
MG71	DH5α [pBAD30::$icsA_{BIO}$; Ap^R; P_{icsA}]
MG72	DH5α [pBAD30::$icsA_{BIOK10R}$; Ap^R; P_{icsA}]
MG73	DH5α [pBAD30::$icsA_{BIOK10R}$; Ap^R; P_{icsA}]
MG74	UT5600 [pMG70; Ap^R]
MG75	UT5600 [pMG71; Ap^R]
MG76	UT5600 [pMG72; Ap^R]
MG77	UT5600 [pMG73; Ap^R]
MG78	UT5600 [pCY216::*birA*; Cm^R] [pRMA156; Km^R]
MG79	UT5600 [pCY216::*birA*; Cm^R] [pRMA160; Km^R]
MG80	DH5α [pGEM-T Easy::$icsA_{BIO}$; Ap^R]
MG81	DH5α [pGEM-T Easy::$icsA_{BIOK10R}$; Ap^R]
MG82	DH5α [pBAD30::$icsA_{BIO}$; Ap^R; P_{BAD}]
MG83	DH5α [pBAD30::$icsA_{BIOK10R}$; Ap^R; P_{BAD}]
MG84	UT5600 [pBAD30::$icsA_{BIO}$; Ap^R]
MG85	UT5600 [pBAD30::$icsA_{BIOK10R}$; Ap^R]
MG86	UT5600 [pMG84; Ap^R] [pCY216::*birA*; Cm^R]

E. coli and *S. flexneri* generated in this work (*cont.*)

STRAIN	DESCRIPTION
MG87	UT5600 [pMG85; Ap^R] [pCY216::*birA*; Cm^R]
MG88	UT5600 [pMG84; Ap^R] [pRMA156; Km^R]
MG89	UT5600 [pMG85; Ap^R] [pRMA156; Km^R]
MG90	UT5600 [pMG84; Ap^R] [pRMA160; Km^R]
MG91	UT5600 [pMG85; Ap^R] [pRMA160; Km^R]
MG92	UT5600 [pMG84; Ap^R] [pCY216::*birA*; Cm^R] [pRMA156; Km^R]
MG93	UT5600 [pMG85; Ap^R] [pCY216::*birA*; Cm^R] [pRMA156; Km^R]
MG94	UT5600 [pMG84; Ap^R] [pCY216::*birA*; Cm^R] [pRMA160; Km^R]
MG95	UT5600 [pMG85; Ap^R] [pCY216::*birA*; Cm^R][pRMA160; Km^R]
MG96	DH5α [pRMA2611::$icsA_{53-104}$ (NheI-NheI); Km^R]
MG97	DH5α [pRMA2611::$icsA_{53-505}$ (NheI-NheI); Km^R]
MG98	DH5α [pRMA2611::$icsA_{53-758}$ (NheI-NheI); KmR]
MG99	*blank*
MG100	DH5α [pQE60::*Spe*I-*Sac*I; Ap^R]
MG101	DH5α [pQE60::*Spe*I-*Sac*I; Ap^R]
MG102	AB1157 {$recA^+$ *ara*-14 *lacY*1}
MG103	IL02 {*tetO* array at *oriC*}; Gm^R
MG104	IL03 {*lacO* array at *ter*}; Km^R
MG105	IL05 {*tetO* at *oriC*; *lacO* at *ter*}; Gm^R Km^R
MG106	AB1157 [pLAU43 (*lacO* array); Km^R]
MG107	AB1157 [pLAU44 (*tetO* array); Gm^R]
MG108	DH5α [pLAU53; Ap^R]
MG109	IL05 [pLAU53; Ap^R]
MG110	DH5α [pRSET B::*mCherry*; Ap^R]
MG111	DH5α [pRSET B::*mRFP*; Ap^R]
MG112	BL21(DE3) [pRSET B::*mCherry*; Ap^R] [pLysS; Cm^R]
MG113	BL21(DE3) [pRSET B::*mRFP*; Ap^R] [pLysS; Cmp^R]
MG114	DH5α [pSCRhaB2::*mCherry*; Tp^R]
MG115	DH5α [pSCRhaB2::*mCherry*; Tp^R]
MG116	DH5α [pSCRhaB2::*mRFP*; Tp^R]
MG117	DH5α [pSCRhaB2::*mRFP*; Tp^R]

E. coli and *S. flexneri* generated in this work (*cont.*)

STRAIN	DESCRIPTION
MG118	DH5α [pGEM-T Easy::$icsA_{53-758}$ (*Eco*RI-*Sal*I); Ap^R]
MG119	DH5α [pGEM-T Easy::*ltrA* (*Bam*HI-*Kpn*I); Ap^R]
MG120	DH5α [pGEM-T Easy::*ltrA* (*Bam*HI-*Kpn*I); Ap^R]
MG121	DH5α [pUT18::$icsA_{53-758}$; Ap^R]
MG122	DH5α [pUT18C::$icsA_{53-758}$; Ap^R]
MG123	DH5α [pKT25::*ltrA*; Km^R]
MG124	DH5α [pKNT25::*ltrA*; Km^R]
MG125	*blank*
MG126	DH5α [pGEM-T Easy::$icsA_{506-620}$; Ap^R]
MG127	DH5α [pMG100::*gfp*+; Ap^R]
MG128	DH5α [pRMA2611::$icsA_{538-562}$; Km^R]
MG129	DH5α [pRMA2611::$icsA_{506-620}$; Km^R]
MG130	DH5α [pGEM-T Easy::*mCherry*; Ap^R]
MG131	DH5α [pGEM-T Easy::$icsA_{506-620}$; Ap^R]
MG132	DH5α [pSCRhaB2::*mCherry*; Tp^R]
MG133	DH5α [pSCRhaB2::$icsA_{506-620}$-*mCherry*; Tp^R]
MG134	DH5α [pMG100::$icsA_{539-562}$-*gfp*+; Ap^R]
MG135	DH5α [pMG100::$icsA_{506-620}$-*gfp*+; Ap^R]
MG136	DH5α [pGEM-T Easy::*ltrA*; Ap^R]
MG137	DH5α [pRMA2611::*ltrA*-*gfp*+; Km^R]
MG138	Top10F′ [pRMA2611::$icsA_{53-104}$; Km^R]
MG139	Top10F′ [pRMA2611::$icsA_{53-505}$; Km^R]
MG140	Top10F′ [pRMA2611::$icsA_{53-758}$; Km^R]
MG141	Top10F′ [pRMA2611::$icsA_{538-562}$; Km^R]
MG142	UT5600 [pKMRM33::His_6; Ap^R]
MG143	UT5600[pKMRM1::FLAG; Ap^R]
MG144	UT5600 [pBBR1-MCS2::(pKMRM33::his_6 *Eco*RI-*Sal*I); Km^R]
MG145	UT5600 [pBBR1-MCS2::(pKMRM1::FLAG *Eco*RI-*Sal*I); Km^R]
MG146	UT5600 [pKMRM1::FLAG; Ap^R] [pMG144; Km^R]
MG147	UT5600 [pMG142; Ap^R] [pMG145; Km^R]
MG148	DH5α [pGEM-T Easy::$icsA_{506-620}$; Ap^R]

E. coli and *S. flexneri* generated in this work (*cont.*)

STRAIN	DESCRIPTION
MG149	DH5α [pSCRhaB2::*icsA*$_{506-620}$-*mCherry*; Tp^R]
MG150	IL03 [pKD46; 30°C Ap^R]
MG151	IL05 [pKD46; 30°C Ap^R]
MG152	UT5600 [pMG55; Ap^R] [pMG142; Km^R]
MG153	UT5600 [pMG55; Ap^R] [pMG143; Km^R]
MG154	RMA2041 [pMG55; Ap^R] [pMG142; Km^R]
MG155	RMA2041 [pMG55; Ap^R] [pMG143; Km^R]
MG156	MG152 [pCY216::*birA*; Cm^R]
MG157	MG153 [pCY216::*birA*; Cm^R]
MG158	MG154 [pCY216::*birA*; Cm^R]
MG159	MG155 [pCY216::*birA*; Cm^R]
MG160	DH5α [pRMA2611::*icsA*$_{532-570}$; Km^R]
MG161	Top10F′ [pRMA2611::*icsA*$_{532-570}$; Km^R]
MG162	RMA2041 [pKMRM1::BIOK10R; Ap^R]
MG163	RMA2043 [pKMRM1::BIOK10A; Ap^R]
MG164	HDL1001 {*pgsA*::Km^R ϕ[*lacOP-pgsA*$^+$] *lacZ′ lacY*::Tn*9* *recA srl*::Tn*10*}
MG165	MDL12 {*pgsA*::Km^R ϕ[*lacOP-pgsA*$^+$] *lacZ′ lacY*::Tn*9*}
MG166	HDL1001 [pZL606 (*dnaA*$_{L366K}$; Ap^R]
MG167	*E. coli* K-12 MG1655
MG168	DH5α [pK*birA*$_{R118G}$; Ap^R]
MG169	DH5α [pGEM-T Easy::*ltrA* (*Nhe*I-*Xba*I); Ap^R]
MG170	UT5600 [pMG55; Ap^R] [pCY216::*birA*; Cm^R]
MG171	UT5600 [pMG55; Ap^R] [pCY216::*birA*; Cm^R] [pRMA156; Km^R]
MG172	UT5600 [pMG55; Ap^R] [pCY216::*birA*; Cm^R] [pRMA160; Km^R]
MG173	DH5α [pBAD24::*birA*$_{R118G}$; Ap^R]
MG174	DH5α [pBAD24::*icsA*$_{506-620}$-*birA*$_{R118G}$; Ap^R]
MG175	DH5α [pBAD24::*icsA*$_{506-620}$-*gfp*+-*birA*$_{R118G}$; Ap^R]
MG176	DH5α [pBAD24::*lacI-ecfp* (*Nco*I fragment pLAU53); Ap^R]
MG177	DH5α [pBAD24::*icsA*$_{506-620}$-*ecfp*; Ap^R]
MG178	DH5α [pLAU53::*icsA*$_{506-620}$-*ecfp*; Ap^R]
MG179	DH5α [pBAD24::*birA*$_{WT}$; Ap^R]

E. coli and *S. flexneri* generated in this work (*cont.*)

STRAIN	DESCRIPTION
MG180	DH5α [pBAD24::*icsA*$_{506-620}$-*birA*$_{WT}$; Ap^R]
MG181	DH5α [pBAD24::*icsA*$_{506-620}$-*gfp*+-*birA*$_{WT}$; Ap^R]
MG182	IL02 [pLAU53::*icsA*$_{506-620}$-*ecfp*... *tetR-eyfp*]
MG183	IL02 [pLAU53::*icsA*$_{506-620}$-*ecfp*... *tetR-eyfp*]
MG184	IL02 [pLAU53]
MG185	IL03 [pLAU53::*icsA*$_{506-620}$-*ecfp*... *tetR-eyfp*]
MG186	IL02 [pKD46; 30°C Ap^R]
MG187	DH5α [pBAD33::(pMG128 *Pst*I-*Sph*I)]
MG188	DH5α [pBAD33::(pMG129 *Pst*I-*Sph*I)]
MG189	DH5α [pBAD33::(pMG160 *Pst*I-*Sph*I)]
MG190	DH5α [pBAD33::(pRMA2611 *Pst*I-*Sph*I)]
MG191	DH5α [pSCRhaB2::*dnaA*$_{L366K}$; Tp^R]
MG192	DH5α [pSCRhaB2::*dnaA*$_{WT}$; Tp^R]
MG193	IL05 [pLAU53::*icsA*$_{506-620}$-*ecfp*... *tetR-eyfp*]
MG194	IL02 *migS::Tc*^{R}
MG195	IL02 *narW::Tc*^{R}
MG196	IL02 Δ*migS*
MG197	IL02 Δ*narW*
MG198	IL02 *narW*::(*migS*::Tc^R)
MG199	IL02 *narW::migS*
MG200	IL02 Δ*narW*::(*migS*-Tc^R) Δ*migS*
MG201	IL02 Δ*narW*::*migS* Δ*migS*
MG202	IL02 {ϕ[*lacOP-pgsA*+] *lacZ′ lacY*::Tn*9* (Cm^R)}
MG203	IL02 {ϕ[*lacOP-pgsA*+] *lacZ′ lacY*::Tn*9* (Cm^R)}
MG204	IL02 {ϕ[*lacOP-pgsA*+] *lacZ′ lacY*::Tn*9* (Cm^R)} *pgsA*::Km^R}
MG205	IL02 {ϕ[*lacOP-pgsA*+] *lacZ′ lacY*::Tn*9* (Cm^R)} *pgsA*::Km^R}
MG206	*blank*
MG207	*blank*
MG208	HDL1001 [pMG178; Ap^R]
MG209	IL02 DmigS [pMG178; Ap^R]
MG210	DH5α [pGEM-T Easy::*mCherry* (*Not*I)]

E. coli and *S. flexneri* generated in this work (*cont.*)

strain	description
MG211	*blank*
MG212	*blank*
MG213	IL02 *yiaF::Tc*^{R}
MG214	DH5α [pUC18::*migS*]
MG215	DH5α [pBAD33MG]
MG216	UT5600 [pCY216::*birA*] [pKMRM1::BIO] [pRMA156]
MG217	HDL1001
MG218	IL02 Δ*migS* [pMG178; Ap^R]
MG219	MG204 [pMG178; Ap^R]
MG220	IL02 Δ*yiaF* [pMG178; Ap^R]
MG221	IL02 Δ*yiaF*
MG222	DH5α [pBBR1MCS] (Kovach *et al.*, 1994)
MG223	MG204 [pKD46; 30°C Ap^R]
MG224	MG204 [pKD46; 30°C Ap^R]
MG225	DH5α [pBBR1MCS2] (Kovach *et al.*, 1995)
MG226	DH5α [pBBR1MCS::*birA*]
MG227	MG88 [pBBR1MCS::*birA*]
MG228	MG89 [pBBR1MCS::*birA*]
MG229	MG90 [pBBR1MCS::*birA*]
MG230	MG91 [pBBR1MCS::*birA*]
MG231	MG88 [pBBR1MCS]
MG232	MG89 [pBBR1MCS]
MG233	MG90 [pBBR1MCS]
MG234	MG91 [pBBR1MCS]
MG235	BL21(DE3) [pREP4; Km^R] [pMG100::*icsA*$_{506-620}$-*gfp*+; Ap^R]
MG236	DH5α [pBAD33::pMG178; Cm^R]
MG237	DH5α [pBBR1MCS2::*birA*]
MG238	UT5600 [pKMRM1::BIO]
MG239	UT5600 [pKMRM1::BIO] [pBBR1MCS2::*birA*]
MG240	*blank*
MG241	IL02 [pBAD33::pMG178; Cm^R]

E. coli and *S. flexneri* generated in this work (*cont.*)

STRAIN	DESCRIPTION
MG242	IL02 [pBAD33::pMG178; Cm^R] [pUC18::*migS*; Ap^R]
MG243	UT5600 [pRMA2611::$icsA_{506-620}$ +1 frameshift]
MG244	UT5600 [pRMA2611::$icsA_{506-620}$ STOP]
MG245	UT5600 [pBAD33::pMG98]
MG246	UT5600 [pBAD33::pMG98]
MG247	UT5600 [pMG128::*Strep*-tag II]
MG248	UT5600 [pMG128::*Strep*-tag II]
MG249	UT5600 [pBBR1MCS2::(pKMRM1::FLAG)] [pKMRM1]
MG250	UT5600 [pBBR1MCS2::(pKMRM1::FLAG)] [pKMRM1][pCY216::*birA*]
MG251	UT5600 [pKMRM1::BIO] [pCY216::*birA*] [pKMRM252]
MG252	UT5600 [pMG100::pMG243($icsA_{506-620}$ +1 frameshift)]
MG253	UT5600 [pMG100::pMG244($icsA_{506-620}$ STOP)]
MG254	UT5600 [pMG100::pMG244($icsA_{506-620}$ STOP)]
MG255	UT5600 [pMG100::pMG247($icsA_{506-620}$::*Strep*-tagII)]
MG256	BL21(DE3) [pREP4; Km^R] [pMG100::::*Strep*-tagII)-$icsA_{506-620}$; Ap^R]
MG257	MG182 [pSCRhaB2::$dnaA_{L366K}$; Tp^R]
MG258	MG182 [pSCRhaB2::$dnaA_{WT}$; Tp^R]
MG259	UT5600 [pMG177; Ap^R]
MG260	UT5600 [pMG177; Ap^R]
MG261	MG204 [pKD46; 30°C Ap^R]
MG262	UT5600 [pRMA2611::$icsA_{506(+1)---TGATAA620AGGA}$-*gfp*+; Km^R]
MG263	UT5600 [pRMA2611::$icsA_{506(+1)---TGATAA620AGGA}$-*gfp*+; Km^R]
MG264	UT5600 [pRMA2611::$icsA_{506(STOP)---TGATAA620AGGA}$-*gfp*+; Km^R]
MG265	UT5600 [pRMA2611::$icsA_{506---TGATAA620AGGA}$-*gfp*+; Km^R]
MG266	UT5600 [pRMA2611::$icsA_{556-620}$; Km^R]
MG267	UT5600 [pRMA2611::$icsA_{581-620}$; Km^R]
MG268	UT5600 [pRMA2611::$icsA_{581-620}$; Km^R]
MG269	UT5600 [pRMA2611::$icsA_{581-620}$; Km^R]
MG270	UT5600 [pBAD30::$icsA_{1-52}$; Ap^R]
MG271	UT5600 [pBAD30::$icsA_{1-52}$; Ap^R]
MG272	MG182 [pSCRhaB2; TpR]

E. coli and *S. flexneri* generated in this work (*cont.*)

STRAIN	DESCRIPTION
MG273	MG62 [pBBR1MCS]
MG274	UT5600 [pRMA2611]
MG275	UT5600 [pMG129]
MG276	UT5600 [pMG135]
MG277	IL02 *rnhA*::TcR
MG278	IL02 *rnhA*TcR
MG279	B21(DE3) [pREP4; Km^R] [pMG100::*gfp*+]
MG280	B21(DE3) [pREP4; Km^R] [pMG100::*gfp*+]
MG281	B21(DE3) [pREP4; Km^R] [pMG100::pMG129 (*Nhe*I-*Sac*I); Ap^R]
MG282	B21(DE3) [pREP4; Km^R] [pMG100::pMG129 (*Nhe*I-*Sac*I); Ap^R]
MG283	B21(DE3) [pREP4; Km^R] [pMG100::pMG244 (*Nhe*I-*Sac*I); Ap^R]
MG284	B21(DE3) [pREP4; Km^R] [pMG100::pMG244 (*Nhe*I-*Sac*I); Ap^R]
MG285	UT5600 [pMG270-(his_6-$icsA_{758-1102}$); Ap^R]
MG286	C600 RK2
MG287	C600 RK2
MG288	IL02 Δ*rnhA*
MG289	IL02 Δ*rnhA*
MG290	IL02 Δ*rnhA* [pKD46; 30°C Ap^R]
MG291	2457T [pKD46; 30°C Ap^R]
MG292	2457T *minD*::Km^R
MG293	2457T [pQE30; Ap^R]
MG294	2457T [pQE30::wzz_{SF}; Ap^R]
MG295	2457T [pQE30::wzz_{pHS-2}]
MG296	DH5α [pGEM-T Easy::$icsA_{758-1102}$; Ap^R]
MG297	UT5600 [pRMA2611::$icsA_{506-KMRM\_R}$; Km^R]
MG298	UT5600 [pRMA2611::$icsA_{506-P2\_R}$; Km^R]
MG299	UT5600 [pRMA2611::$icsA_{506-P2\_R}$; Km^R]
MG300	2457T *minD*::Km^R [pQE30; Ap^R]
MG301	2457T *minD*::Km^R [pQE30::wzz_{SF}; Ap^R]
MG302	2457T *minD*::Km^R [pQE30::wzz_{pHS2}; Ap^R]
MG303	E964 {*dnaA5 polA1 endA*} 30°C)

E. coli and *S. flexneri* generated in this work (*cont.*)

STRAIN	DESCRIPTION
MG304	*blank*
MG305	E2047 [pBAD24::λ red recombinase]
MG306	E2047 [pBAD24::λ red recombinase]
MG307	E2047 [pBAD24::*mCherry*]
MG308	MG288 [pBAD24::λ red recombinase]
MG309	MG288 [pBAD24::λ red recombinase]
MG310	MG288 [pBAD24::λ red recombinase]
MG311	MG288 [pBAD24::λ red recombinase]
MG312	IL02 Δ*rnhA dnaA5*
MG313	IL02 Δ*rnhA dnaA5*
MG314	MG288 [pMG178]
MG315	MG288 [pMG178]
MG316	E2047 [pBAD24::$icsA_{506-620}$-*mCherry*]
MG317	MG292 [pCP20]
MG318	RMA2394 F′{$lacI^q$ Tn*10*}
MG319	RMA2395 F′{$lacI^q$ Tn*10*}
MG320	RAM3327 [pQE30]
MG321	RAM3327 [pRMA3331]
MG322	MG318 [pQE30]
MG323	MG318 [pRMA2779]
MG324	MG319 [pQE30]
MG325	MG319 [pRMA2779]
MG326	IL02 [pRMA2611]
MG327	IL02 [pMG129]
MG328	MG308 [pMG191]
MG329	MG208 [pMG192]
MG330	DH5α [pGEM-T Easy::flanking *dnaA*; Ap^R]
MG331	HDL1001 [pMG176]
MG332	HDL1001 [pMG259]
MG333	MG204 [pMG176]
MG334	MG204 [pMG259]

E. coli and *S. flexneri* generated in this work (*cont.*)

STRAIN	DESCRIPTION
MG335	DH5α [pBAD24::*gfp*+ (for C- fusion); Ap^R])
MG336	DH5α [pRMA2611::TEV]
MG337	DH5α [pRMA2611::TEV]
MG338	DH5α [pBAD24::*gfp*+ (for C- fusion); Ap^R]
MG339	DH5α [pMG337::$icsA_{506-620}$]
MG340	DH5α [pMG337::$icsA_{506-620}$]
MG341	DH5α [pMG337::$icsA_{506-620}$]
MG342	DH5α [pRMA2611::$icsA_{1-505}$; Km^R]
MG343	DH5α [pRMA2611::$icsA_{53-505}$; Km^R]
MG344	DH5α [pRMA2611::$icsA_{105-505}$; Km^R]
MG345	DH5α [pRMA2611::$icsA_{105-505}$; Km^R]
MG346	DH5α [pRMA2611::$icsA_{105-620}$; Km^R]
MG347	DH5α [pRMA2611::$icsA_{105-620}$; Km^R]
MG348	DH5α [pRMA2611::$icsA_{105-758}$; Km^R]
MG349	DH5α [pGEM-T Easy::Km^R (from pKD4); Ap^R Km^R]
MG350	KMRM270
MG351	DH5α [pRMA2611::$icsA_{506-562}$; Km^R]
MG352	DH5α [pRMA2611::$icsA_{506-562}$; Km^R]
MG353	DH5α [pRMA2611::$icsA_{538-620}$; Km^R]
MG354	DH5α [pRMA2611::$icsA_{538-620}$; Km^R]
MG355	DH5α [pRMA2611::$icsA_{538-562}$; Km^R]
MG356	DH5α [pRMA2611::$icsA_{538-562}$; Km^R]
MG357	DH5α [pRMA2611::$icsA_{506-570}$; Km^R]
MG358	DH5α [pRMA2611::$icsA_{532-620}$; Km^R]
MG359	DH5α [pRMA2611::$icsA_{532-620}$; Km^R]
MG360	*see MG437*
MG361	DH5α [pBAD24::$icsA_{1-53}$-His_6-$icsA_{759-1102}$; Ap^R]
MG362	DH5α [pBAD24::$icsA_{1-53}$-His_6-$icsA_{759-1102}$; Ap^R]
MG363	DH5α [pBAD24::$icsA_{1-53}$-His_6-$icsA_{759-1102}$; Ap^R]
MG364	DH5α [pGEM-T Easy::(*dnaA*::Km^R); Ap^R]
MG365	DH5α [pGEM-T Easy::(*dnaA*::Km^R); Ap^R]

E. coli and *S. flexneri* generated in this work (*cont.*)

STRAIN	DESCRIPTION
MG366	DH5α [pMG339::Strep-tagII; Km^R]
MG367	DH5α [pMG339::Strep-tagII; Km^R]
MG368	DH5α [pMG440::Strep-tagII; Km^R]
MG369	DH5α [pMG440::Strep-tagII; Km^R]
MG370	RMA2205 [pD10-1; Tp^R]
MG371	RMA2208 [pD10-*virG3*; Tp^R]
MG372	RMA2209 [pD10-*virG4*; Tp^R]
MG373	KMRM116 [pKMRM270; Km^R]
MG374	KMRM123 [pKMRM270; Km^R]
MG375	KMRM132 [pKMRM270; Km^R]
MG376	KMRM135 [pKMRM270; Km^R]
MG377	MG373; Congo Red^+
MG378	MG374; Congo Red^+
MG379	MG375; Congo Red^+
MG380	MG376; Congo Red^+
MG381	UT5600 [pMG361; Ap^R]
MG382	DH5α [pMG173::$icsA_{506-562}$; Ap^R]
MG383	DH5α [pMG179::$icsA_{506-562}$; Ap^R]
MG384	BW23473 *pir*$^+$
MG385	BW23474 *pir*-116
MG386	DH5α [pINT, 30°C, λ Int; Ap^R]
MG387	BW5328 [pAH69, 30°C, HK022 Int; Ap^R]
MG388	BW5328 [pAH57, 30°C, λ Int Xis; Ap^R]
MG389	BW5328 [pAH95121, 30°C, P21 Int; Ap^R]
MG390	BW23473 [pAH70, *att*HK022; Km^R]
MG391	BW23473 [pAH81, *att*P21; Ap^R]
MG392	BW23473 [pAH95, *att*P21; Km^R]
MG393	BW23322 *pir*-116 [pCAH56, *att*λ]
MG394	*blank*
MG395	*blank*
MG396	UT5600 [pBAD30::His_6-$icsA_{759-1102}$; Ap^R]

E. coli and *S. flexneri* generated in this work (*cont.*)

STRAIN	DESCRIPTION
MG397	UT5600 [pBAD30::His_6-$icsA_{759-1102}$; Ap^R]
MG370	UT5600 [pD10-1; Tp^R]
MG371	UT5600 [pD10-*virG3*; Tp^R]
MG372	UT5600 [pD10-*virG4*; Tp^R]
MG401	*dnaA5* [pMG129; Km^R]
MG402	*dnaA5* [pMG129; Km^R]
MG403	DH5α [pRMA2611::*Strep-icsA*$_{506-620(WT)}$-TEV-*gfp*+; Km^R]
MG404	DH5α [pRMA2611::*Strep-icsA*$_{506-620(WT)}$-TEV-*gfp*+; Km^R]
MG405	DH5α [pRMA2611::*Strep-icsA*$_{506-620(i532)}$-TEV-*gfp*+; Km^R]
MG406	DH5α [pRMA2611::*Strep-icsA*$_{506-620(i532)}$-TEV-*gfp*+; Km^R]
MG407	DH5α [pRMA2611::*Strep-icsA*$_{506-620(i563)}$-TEV-*gfp*+; Km^R]
MG408	DH5α [pRMA2611::*Strep-icsA*$_{506-620(i563)}$-TEV-*gfp*+; Km^R]
MG409	UT5600 [pBAD24::*icsA*$_{759-1102}$ (*Eco*RI-*Pst*I from pMG361; Ap^R]
MG410	UT5600 [pBAD24::*icsA*$_{759-1102}$ (*Eco*RI-*Pst*I from pMG361; Ap^R]
MG411	DH5α [pRMA2611::*icsA*$_{506-562}$; Km^R]
MG412	DH5α [pRMA2611::*icsA*$_{506-562}$; Km^R]
MG413	DH5α [pRMA2611::*icsA*$_{532-562}$; Km^R]
MG414	DH5α [pRMA2611::*icsA*$_{532-562}$; Km^R]
MG415	*dnaA5* [pMG129; Km^R] [pSCRhaB2; Tp^R]
MG416	*dnaA5* [pMG129; Km^R] [pSCRhaB2::*dnaA*$_{L366K}$; Tp^R]
MG417	*dnaA5* [pMG129; Km^R] [pSCRhaB2::*dnaA*$_{WT}$; Tp^R]
MG418	DH5α [pBAD24::His_6-$icsA_{759-1102}$; Ap^R]
MG419	DH5α [pBAD24::His_6-$icsA_{759-1102}$; Ap^R]
MG420	UT5600 [pMG419; Ap^R]
MG421	BL21(DE3) [pMG100::pMG404 (*Nhe*I-*Sac*I); Ap^R]
MG422	BL21(DE3) [pMG100::pMG406 (*Nhe*I-*Sac*I); Ap^R]
MG423	BL21(DE3) [pMG100::pMG404 (*Nhe*I-*Sac*I); Ap^R] [pREP4; Km^R]
MG424	BL21(DE3) [pMG100::pMG406 (*Nhe*I-*Sac*I); Ap^R] [pREP4; Km^R]
MG425	DH5α [pRMA2611::*icsA*$_{506-620(i536)}$; Km^R]
MG426	BL21(DE3) [pMG100::pMG425 (*Nhe*I-*Sac*I); Ap^R] [pREP4; Km^R]
MG427	IL02 [pINT, 30°C, λ Int; Ap^R]

E. coli and *S. flexneri* generated in this work (*cont.*)

STRAIN	DESCRIPTION
MG428	IL02 *dnaA5* Tc^R by P1*vir* transduction
MG429	IL02 *dnaA5* Tc^R by P1*vir* transduction
MG430	DH5α [pAH81::(pMG178 *Pst*I-*Cla*I); Ap^R]
MG431	IL02ΩpMG430
MG432	IL02ΩpMG430
MG433	IL02ΩpMG430
MG434	DH5α [pMG173::$icsA_{506-620(i532)}$; Ap^R]
MG435	DH5α [pMG179::$icsA_{506-620(i532)}$; Ap^R]
MG436	*blank*
MG437	DH5α [pRMA2611::$icsA_{532-570}$; Km^R]
MG438	DH5α [pRMA2611::$icsA_{532-570}$; Km^R]
MG439	*blank*

Achtman M, Manning PA, Edelbluth C, Herrlich P. Export without proteolytic processing of inner and outer membrane proteins encoded by F sex factor tra cistrons in *Escherichia coli* minicells. *Proc Natl Acad Sci USA* 1979; 76: 4837–41. (Cited on page 56.)

Addinall SG, Lutkenhaus J. FtsZ-spirals and -arcs determine the shape of the invaginating septa in some mutants of *Escherichia coli*. *Mol Microbiol* 1996; 22: 231–7. (Cited on page 29.)

Adler B, Sasakawa C, Tobe T, Makino S, Komatsu K, Yoshikawa M. A dual transcriptional activation system for the 230 kb plasmid genes coding for virulence-associated antigens of *Shigella flexneri*. *Mol Microbiol* 1989; 3: 627–35. (Cited on page 17.)

Adler HI, Fisher WD, Cohen A, Hardigree AA. MINIATURE *Escherichia coli* CELLS DEFICIENT IN DNA. *Proc Natl Acad Sci USA* 1967; 57: 321–326. (Cited on page 30.)

Al-Hasani K, Henderson IR, Sakellaris H, Rajakumar K, Grant T, Nataro JP, *et al*. The *sigA* gene which is borne on the *she* pathogenicity island of *Shigella flexneri* 2a encodes an exported cytopathic protease involved in intestinal fluid accumulation. *Infect Immun* 2000; 68: 2457–63. (Cited on page 4.)

Allaoui A, Mounier J, Prévost MC, Sansonetti PJ, Parsot C. *icsB*: a *Shigella flexneri* virulence gene necessary for the lysis of protrusions during intercellular spread. *Mol Microbiol* 1992; 6: 1605–16. (Cited on page 10.)

Ally S, Sauer NJ, Loureiro JJ, Snapper SB, Gertler FB, Goldberg MB. *Shigella* interactions with the actin cytoskeleton in the absence of Ena/VASP family proteins. *Cell Microbiol* 2004; 6: 355–66. (Cited on page 9.)

Barnard TJ, Dautin N, Lukacik P, Bernstein HD, Buchanan SK. Autotransporter structure reveals intra-barrel cleavage followed by conformational changes. *Nat Struct Mol Biol* 2007; 14: 1214–1220. (Cited on pages 17, 19, and 21.)

Bârzu S, Benjelloun-Touimi Z, Phalipon A, Sansonetti P, Parsot C. Functional analysis of the *Shigella flexneri* IpaC invasin by insertional mutagenesis. *Infect Immun* 1997; 65: 1599–605. (Cited on page 5.)

Bernardini ML, Mounier J, d'Hauteville H, Coquis-Rondon M, Sansonetti PJ. Identification of *icsA*, a plasmid locus of *Shigella flexneri* that governs bacterial intra- and intercellular spread through interaction with F-actin. *Proc Natl Acad Sci USA* 1989; 86: 3867–71. (Cited on pages 6 and 8.)

Bernhardt TG, de Boer P. SlmA, a nucleoid-associated, FtsZ binding protein required for blocking septal ring assembly over Chromosomes in *E. coli*. *Mol Cell* 2005; 18: 555–64. (Cited on page 32.)

Berthiaume F, Rutherford N, Mourez M. Mutations affecting the biogenesis of the AIDA-I autotransporter. *Res Microbiol* 2007; 158: 348–54. (Cited on page 16.)

Bi EF, Lutkenhaus J. FtsZ ring structure associated with division in *Escherichia coli*. *Nature* 1991; 354: 161–4. (Cited on page 29.)

Bigot S, Saleh OA, Lesterlin C, Pages C, Karoui ME, Dennis C, *et al.* KOPS: DNA motifs that control *E. coli* chromosome segregation by orienting the FtsK translocase. *EMBO J* 2005; 24: 3770–3780. (Cited on page 35.)

Bigot S, Sivanathan V, Possoz C, Barre FX, Cornet F. FtsK, a literate chromosome segregation machine. *Mol Microbiol* 2007; 64: 1434–41. (Cited on page 35.)

Bochner BR, Huang HC, Schieven GL, Ames BN. Positive selection for loss of tetracycline resistance. *J Bacteriol* 1980; 143: 926–33. (Cited on page 43.)

Boeneman K, Fossum S, Yang Y, Fingland N, Skarstad K, Crooke E. *Escherichia coli* DnaA forms helical structures along the longitudinal cell axis distinct from MreB filaments. *Mol Microbiol* 2009; . (Cited on page 35.)

Bradley P, Cowen L, Menke M, King J, Berger B. BETAWRAP: successful prediction of parallel β -helices from primary sequence reveals an association with

many microbial pathogens. *Proc Natl Acad Sci USA* 2001; 98: 14819–24. (Cited on page 12.)

Brandon LD, Goehring N, Janakiraman A, Yan AW, Wu T, Beckwith J, *et al.* IcsA, a polarly localized autotransporter with an atypical signal peptide, uses the Sec apparatus for secretion, although the Sec apparatus is circumferentially distributed. *Mol Microbiol* 2003; 50: 45–60. (Cited on pages 11, 18, 36, and 67.)

Brandon LD, Goldberg MB. Periplasmic transit and disulfide bond formation of the autotransported *Shigella* protein IcsA. *J Bacteriol* 2001; 183: 951–8. (Cited on pages 18 and 20.)

Buddelmeijer N, Krehenbrink M, Pecorari F, Pugsley AP. Type II secretion system secretin PulD localizes in clusters in the Escherichia coli outer membrane. *J Bacteriol* 2009; 191: 161–8. (Cited on page 161.)

Carter JA, Blondel CJ, Zaldívar M, Alvarez SA, Marolda CL, Valvano MA, *et al.* O-antigen modal chain length in *Shigella flexneri* 2a is growth-regulated through RfaH-mediated transcriptional control of the *wzy* gene. *Microbiology (Reading, Engl)* 2007; 153: 3499–507. (Cited on pages 99 and 102.)

Chapman-Smith A, Cronan JE. *In vivo* enzymatic protein biotinylation. *Biomol Eng* 1999; 16: 119–25. (Cited on page 105.)

Chapman-Smith A, Turner DL, Cronan JE, Morris TW, Wallace JC. Expression, biotinylation and purification of a biotin-domain peptide from the biotin carboxy carrier protein of *Escherichia coli* acetyl-CoA carboxylase. *Biochem J* 1994; 302 (Pt 3): 881–7. (Cited on pages 124 and 161.)

Charles M, Pérez M, Kobil JH, Goldberg MB. Polar targeting of *Shigella* virulence factor IcsA in Enterobacteriacae and Vibrio. *Proc Natl Acad Sci USA* 2001; 98: 9871–6. (Cited on pages 16, 35, 36, 67, 69, 70, 71, 79, 132, and 133.)

Chen Y, Erickson HP. Rapid *in vitro* assembly dynamics and subunit turnover of FtsZ demonstrated by fluorescence resonance energy transfer. *The Journal of biological chemistry* 2005; 280: 22549–54. (Cited on page 29.)

Chen Y, Smith MR, Thirumalai K, Zychlinsky A. A bacterial invasin induces macrophage apoptosis by binding directly to ICE. *The EMBO Journal* 1996; 15: 3853–60. (Cited on page 5.)

Chevalier N, Moser M, Koch HG, Schimz KL, Willery E, Locht C, *et al.* Membrane targeting of a bacterial virulence factor harbouring an extended signal peptide. *J Mol Microbiol Biotechnol* 2004; 8: 7–18. (Cited on pages 11 and 12.)

Choi-Rhee E, Schulman H, Cronan JE. Promiscuous protein biotinylation by *Escherichia coli*biotin protein ligase. *Protein Sci* 2004; 13: 3043–3050. (Cited on pages 105 and 161.)

Coimbra RS, Grimont F, Grimont PA. Identification of *Shigella* serotypes by restriction of amplified O-antigen gene cluster. *Res Microbiol* 1999; 150: 543–53. (Cited on page 4.)

Conchillo-Solé O, de Groot NS, Avilés FX, Vendrell J, Daura X, Ventura S. AGGRESCAN: a server for the prediction and evaluation of "hot spots" of aggregation in polypeptides. *BMC Bioinformatics* 2007; 8: 65. (Cited on page 134.)

Cooper S, Helmstetter CE. Chromosome replication and the division cycle of *Escherichia coli* B/r. *J Mol Biol* 1968; 31: 519–40. (Cited on page 32.)

Cull MG, Schatz PJ. Biotinylation of proteins *in vivo* and *in vitro* using small peptide tags. *Meth Enzymol* 2000; 326: 430–40. (Cited on page 105.)

Dajkovic A, Mukherjee A, Lutkenhaus J. Investigation of regulation of FtsZ assembly by SulA and development of a model for FtsZ polymerization. *J Bacteriol* 2008; 190: 2513–26. (Cited on page 29.)

Danilova O, Reyes-Lamothe R, Pinskaya M, Sherratt D, Possoz C. MukB colocalizes with the *oriC* region and is required for organization of the two *Escherichia coli* chromosome arms into separate cell halves. *Mol Microbiol* 2007; 65: 1485–92. (Cited on page 35.)

Datsenko KA, Wanner B. One-step inactivation of chromosomal genes in *Escherichia coli* K-12 using PCR products. *Proc Natl Acad Sci USA* 2000; 97: 6640–5. (Cited on pages 50, 96, 97, and 151.)

de Boer P, Crossley RE, Rothfield LI. A division inhibitor and a topological specificity factor coded for by the minicell locus determine proper placement of the division septum in *E. coli*. *Cell* 1989; 56: 641–9. (Cited on page 95.)

de Boer P, Crossley RE, Rothfield LI. Roles of MinC and MinD in the site-specific septation block mediated by the MinCDE system of *Escherichia coli*. *J Bacteriol* 1992; 174: 63–70. (Cited on pages 28 and 30.)

de Pedro MA, Quintela JC, Höltje JV, Schwarz H. Murein segregation in *Escherichia coli*. *J Bacteriol* 1997; 179: 2823–34. (Cited on pages 38 and 95.)

Desvaux M, Cooper LM, Filenko NA, Scott-Tucker A, Turner SM, Cole JA, *et al.* The unusual extended signal peptide region of the type V secretion system is phylogenetically restricted. *FEMS Microbiology Letters* 2006; 264: 22–30. (Cited on page 11.)

d'Hauteville H, Lagelouse RD, Nato F, Sansonetti PJ. Lack of cleavage of IcsA in *Shigella flexneri* causes aberrant movement and allows demonstration of a cross-reactive eukaryotic protein. *Infect Immun* 1996; 64: 511–7. (Cited on pages 14 and 16.)

d'Hauteville H, Sansonetti PJ. Phosphorylation of IcsA by cAMP-dependent protein kinase and its effect on intracellular spread of *Shigella flexneri*. *Mol Microbiol* 1992; 6: 833–41. (Cited on pages 15 and 16.)

Divakaruni AV, Baida C, White CL, Gober JW. The cell shape proteins MreB and MreC control cell morphogenesis by positioning cell wall synthetic complexes. *Mol Microbiol* 2007; 66: 174–88. (Cited on page 27.)

Divakaruni AV, Loo RRO, Xie Y, Loo JA, Gober JW. The cell-shape protein MreC interacts with extracytoplasmic proteins including cell wall assembly complexes in *Caulobacter crescentus*. *Proc Natl Acad Sci USA* 2005; 102: 18602–7. (Cited on page 27.)

Dorman CJ, Porter ME. The *Shigella* virulence gene regulatory cascade: a paradigm of bacterial gene control mechanisms. *Mol Microbiol* 1998; 29: 677–84. (Cited on page 17.)

DuPont HL, Levine MM, Hornick RB, Formal SB. Inoculum size in shigellosis and implications for expected mode of transmission. *J Infect Dis* 1989; 159: 1126–8. (Cited on page 4.)

Dutta PR, Sui BQ, Nataro JP. Structure-function analysis of the enteroaggregative *Escherichia coli* plasmid-encoded toxin autotransporter using scanning linker mutagenesis. *The Journal of biological chemistry* 2003; 278: 39912–20. (Cited on pages 16 and 142.)

Dworkin J, Losick R. Does RNA polymerase help drive chromosome segregation in bacteria? *Proc Natl Acad Sci USA* 2002; 99: 14089–94. (Cited on page 33.)

Dye NA, Pincus Z, Theriot J, Shapiro L, Gitai Z. Two independent spiral structures control cell shape in Caulobacter. *Proc Natl Acad Sci USA* 2005; 102: 18608–13. (Cited on page 27.)

Edwards DH, Errington J. The *Bacillus subtilis* DivIVA protein targets to the division septum and controls the site specificity of cell division. *Mol Microbiol* 1997; 24: 905–15. (Cited on page 38.)

Edwards DH, Thomaides HB, Errington J. Promiscuous targeting of *Bacillus subtilis* cell division protein DivIVA to division sites in *Escherichia coli* and fission yeast. *The EMBO Journal* 2000; 19: 2719–27. (Cited on page 36.)

Egile C, d'Hauteville H, Parsot C, Sansonetti PJ. SopA, the outer membrane protease responsible for polar localization of IcsA in *Shigella flexneri*. *Mol Microbiol* 1997; 23: 1063–73. (Cited on pages 14 and 15.)

Egile C, Loisel TP, Laurent V, Li R, Pantaloni D, Sansonetti PJ, *et al.* Activation of the CDC42 effector N-WASP by the *Shigella flexneri* IcsA protein promotes actin nucleation by Arp2/3 complex and bacterial actin-based motility. *J Cell Biol* 1999; 146: 1319–32. (Cited on pages 8 and 9.)

El-Bez C, Adrian M, Dubochet J, Cover TL. High resolution structural analysis of *Helicobacter pylori* VacA toxin oligomers by cryo-negative staining electron microscopy. *J Struct Biol* 2005; 151: 215–28. (Cited on page 142.)

Emsley P, Charles IG, Fairweather NF, Isaacs NW. Structure of Bordetella pertussis virulence factor P.69 pertactin. *Nature* 1996; 381: 90–2. (Cited on pages 12 and 13.)

Enninga J, Mounier J, Sansonetti PJ, Nhieu GTV. Secretion of type III effectors into host cells in real time. *Nat Methods* 2005; 2: 959–65. (Cited on page 47.)

Erickson HP, Stoffler D. Protofilaments and rings, two conformations of the tubulin family conserved from bacterial FtsZ to alpha/β and gamma tubulin. *J Cell Biol* 1996; 135: 5–8. (Cited on page 29.)

Erickson HP, Taylor DW, Taylor KA, Bramhill D. Bacterial cell division protein FtsZ assembles into protofilament sheets and minirings, structural homologs of tubulin polymers. *Proc Natl Acad Sci USA* 1996; 93: 519–23. (Cited on page 29.)

Esue O, Cordero M, Wirtz D, Tseng Y. The assembly of MreB, a prokaryotic homolog of actin. *J Biol Chem* 2005; 280: 2628–35. (Cited on page 27.)

Esue O, Wirtz D, Tseng Y. GTPase activity, structure, and mechanical properties of filaments assembled from bacterial cytoskeleton protein MreB. *J Bacteriol* 2006; 188: 968–76. (Cited on page 27.)

Fasano A, Noriega FR, Liao FM, Wang W, Levine MM. Effect of *Shigella* enterotoxin 1 (ShET1) on rabbit intestine *in vitro* and *in vivo*. *Gut* 1997; 40: 505–11. (Cited on page 5.)

Fasano A, Noriega FR, Maneval DR, Chanasongcram S, Russell R, Guandalini S, *et al. Shigella* enterotoxin 1: an enterotoxin of *Shigella flexneri* 2a active in rabbit small intestine *in vivo* and *in vitro*. *J Clin Invest* 1995; 95: 2853–61. (Cited on page 5.)

Fernandez-Prada CM, Hoover DL, Tall BD, Venkatesan MM. Human monocyte-derived macrophages infected with virulent *Shigella flexneri in vitro* undergo a rapid cytolytic event similar to oncosis but not apoptosis. *Infect Immun* 1997; 65: 1486–96. (Cited on page 5.)

Footer MJ, Lyo JK, Theriot JA. Close packing of *Listeria monocytogenes* ActA, a natively unfolded protein, enhances F-actin assembly without dimerization. *The J Biol Chem* 2008; 283: 23852–62. (Cited on page 143.)

Frischknecht F, Cudmore S, Moreau V, Reckmann I, Röttger S, Way M. Tyrosine phosphorylation is required for actin-based motility of vaccinia but not Listeria or *Shigella*. *Curr Biol* 1999; 9: 89–92. (Cited on page 16.)

Fukuda I, Suzuki T, Munakata H, Hayashi N, Katayama E, Yoshikawa M, *et al.* Cleavage of *Shigella* surface protein VirG occurs at a specific site, but the secretion is not essential for intracellular spreading. *J Bacteriol* 1995; 177: 1719–26. (Cited on pages 14, 15, and 16.)

Fullá N, Prado V, Durán C, Lagos R, Levine MM. Surveillance for antimicrobial resistance profiles among *Shigella* species isolated from a semirural community in the northern administrative area of santiago, chile. *Am J Trop Med Hyg* 2005; 72: 851–4. (Cited on page 3.)

Gerdes K. RodZ, a new player in bacterial cell morphogenesis. *EMBO J* 2009; 28: 171–2. (Cited on page 27.)

Ghosh AS, Young KD. Helical disposition of proteins and lipopolysaccharide in the outer membrane of *Escherichia coli*. *J Bacteriol* 2005; 187: 1913–22. (Cited on pages 25, 99, 101, 103, 139, and 140.)

Giangrossi M, Prosseda G, Tran CN, Brandi A, Colonna B, Falconi M. A novel antisense RNA regulates at transcriptional level the virulence gene *icsA* of *Shigella flexneri*. *Nucleic Acids Research* 2010; . (Cited on page 17.)

Gibbs KA, Isaac DD, Xu J, Hendrix RW, Silhavy TJ, Theriot J. Complex spatial distribution and dynamics of an abundant *Escherichia coli* outer membrane protein, LamB. *Mol Microbiol* 2004; 53: 1771–83. (Cited on page 25.)

Girardin SE, Boneca IG, Carneiro LAM, Antignac A, Jéhanno M, Viala J, *et al.* Nod1 detects a unique muropeptide from gram-negative bacterial peptidoglycan. *Science* 2003; 300: 1584–7. (Cited on page 7.)

Gitai Z, Dye NA, Reisenauer A, Wachi M, Shapiro L. MreB actin-mediated segregation of a specific region of a bacterial chromosome. *Cell* 2005; 120: 329–41. (Cited on pages 27, 33, and 89.)

Goldberg MB. Actin-based motility of intracellular microbial pathogens. *Microbiol Mol Biol Rev* 2001; 65: 595–626, table of contents. (Cited on page 6.)

Goldberg MB, Bârzu O, Parsot C, Sansonetti PJ. Unipolar localization and ATPase activity of IcsA, a *Shigella flexneri* protein involved in intracellular movement. *J Bacteriol* 1993; 175: 2189–96. (Cited on pages 14, 35, and 67.)

Goldberg MB, Theriot J. *Shigella flexneri* surface protein IcsA is sufficient to direct actin-based motility. *Proc Natl Acad Sci USA* 1995; 92: 6572–6. (Cited on page 8.)

Goldberg MB, Theriot J, Sansonetti PJ. Regulation of surface presentation of IcsA, a *Shigella* protein essential to intracellular movement and spread, is growth phase dependent. *Infect Immun* 1994; 62: 5664–8. (Cited on pages 35, 81, and 136.)

Guzman LM, Belin D, Carson MJ, Beckwith J. Tight regulation, modulation, and high-level expression by vectors containing the arabinose PBAD promoter. *J Bacteriol* 1995; 177: 4121–30. (Cited on page 151.)

Hale CA, de Boer PA. Direct binding of FtsZ to ZipA, an essential component of the septal ring structure that mediates cell division in *E. coli*. *Cell* 1997; 88: 175–85. (Cited on page 29.)

Hale CA, de Boer PA. Recruitment of ZipA to the septal ring of *Escherichia coli* is dependent on FtsZ and independent of FtsA. *J Bacteriol* 1999; 181: 167–76. (Cited on page 29.)

Hale CA, Rhee AC, de Boer PA. ZipA-induced bundling of FtsZ polymers mediated by an interaction between C-terminal domains. *J Bacteriol* 2000; 182: 5153–66. (Cited on page 29.)

Hale TL. Genetic basis of virulence in *Shigella* species. *Microbiol Rev* 1991; 55: 206–24. (Cited on page 4.)

Harrington A, Darboe N, Kenjale R, Picking WL, Middaugh CR, Birket S, *et al.* Characterization of the interaction of single tryptophan containing mutants of IpaC from *Shigella flexneri* with phospholipid membranes. *Biochemistry* 2006; 45: 626–36. (Cited on page 5.)

Heacock PN, Dowhan W. Alteration of the phospholipid composition of *Escherichia coli* through genetic manipulation. *J Biol Chem* 1989; 264: 14972–7. (Cited on page 161.)

Henderson IR, Navarro-Garcia F, Desvaux M, Fernandez RC, Ala'Aldeen D. Type V protein secretion pathway: the autotransporter story. *Microbiol Mol Biol Rev* 2004; 68: 692–744. (Cited on pages 11, 12, 14, 17, 18, and 19.)

High N, Mounier J, Prévost MC, Sansonetti PJ. IpaB of *Shigella flexneri* causes entry into epithelial cells and escape from the phagocytic vacuole. *The EMBO Journal* 1992; 11: 1991–9. (Cited on page 5.)

Hitchcock PJ, Brown TM. Morphological heterogeneity among Salmonella lipopolysaccharide chemotypes in silver-stained polyacrylamide gels. *J Bacteriol* 1983; 154: 269–77. (Cited on page 58.)

Ho HY, Rohatgi R, Ma L, Kirschner MW. CR16 forms a complex with N-WASP in brain and is a novel member of a conserved proline-rich actin-binding protein family. *Proc Natl Acad Sci USA* 2001; 98: 11306–11. (Cited on page 9.)

Ho HYH, Rohatgi R, Lebensohn AM, Ma L, Li J, Gygi SP, *et al.* Toca-1 mediates Cdc42-dependent actin nucleation by activating the N-WASP-WIP complex. *Cell* 2004; 118: 203–16. (Cited on page 9.)

Hong M, Payne SM. Effect of mutations in *Shigella flexneri* chromosomal and plasmid-encoded lipopolysaccharide genes on invasion and serum resistance. *Mol Microbiol* 1997; 24: 779–91. (Cited on pages 22, 23, and 96.)

Hu Z, Gogol EP, Lutkenhaus J. Dynamic assembly of MinD on phospholipid vesicles regulated by ATP and MinE. *Proc Natl Acad Sci USA* 2002; 99: 6761–6. (Cited on page 30.)

Hu Z, Lutkenhaus J. Topological regulation of cell division in *E. coli*. spatiotemporal oscillation of MinD requires stimulation of its ATPase by MinE and phospholipid. *Mol Cell* 2001; 7: 1337–43. (Cited on page 30.)

Hu Z, Mukherjee A, Pichoff S, Lutkenhaus J. The MinC component of the division site selection system in *Escherichia coli* interacts with FtsZ to prevent polymerization. *Proc Natl Acad Sci USA* 1999; 96: 14819–24. (Cited on page 30.)

Huang Y, Lemieux MJ, Song J, Auer M, Wang DN. Structure and mechanism of the glycerol-3-phosphate transporter from *Escherichia coli*. *Science* 2003; 301: 616–20. (Cited on page 30.)

Huitema E, Pritchard S, Matteson D, Radhakrishnan SK, Viollier PH. Bacterial birth scar proteins mark future flagellum assembly site. *Cell* 2006; 124: 1025–37. (Cited on page 38.)

Ieva R, Bernstein HD. Interaction of an autotransporter passenger domain with BamA during its translocation across the bacterial outer membrane. *Proc Natl Acad Sci USA* 2009; 106: 19120–5. (Cited on page 21.)

Ieva R, Skillman KM, Bernstein HD. Incorporation of a polypeptide segment into the β-domain pore during the assembly of a bacterial autotransporter. *Mol Microbiol* 2008; 67: 188–201. (Cited on page 21.)

Iwai N, Nagai K, Wachi M. Novel S-benzylisothiourea compound that induces spherical cells in *Escherichia coli* probably by acting on a rod-shape-determining protein(s) other than penicillin-binding protein 2. *Biosci Biotechnol Biochem* 2002; 66: 2658–62. (Cited on page 27.)

Jain S, Goldberg MB. Requirement for YaeT in the Outer Membrane Assembly of Autotransporter Proteins. *J Bacteriol* 2007; 189: 5393. (Cited on page 19.)

Jain S, van Ulsen P, Benz I, Schmidt MA, Fernandez R, Tommassen J, *et al.* Polar localization of the autotransporter family of large bacterial virulence proteins. *J Bacteriol* 2006; 188: 4841–50. (Cited on page 35.)

Janakiraman A, Fixen K, Gray A, Niki H, Goldberg MB. Genome-scale proteomic screen identifies role for DnaK in chaperoning of polar autotransporters in *Shigella*. *J Bacteriol* 2009; . (Cited on pages 11, 18, 39, and 134.)

Janakiraman A, Goldberg MB. Evidence for polar positional information independent of cell division and nucleoid occlusion. *Proc Natl Acad Sci USA* 2004a; 101: 835–40. (Cited on pages 37 and 88.)

Janakiraman A, Goldberg MB. Recent advances on the development of bacterial poles. *Trends Microbiol* 2004b; 12: 518–25. (Cited on page 35.)

Jennison AV, Verma NK. *Shigella flexneri* infection: pathogenesis and vaccine development. *FEMS Microbiol Rev* 2004; 28: 43–58. (Cited on page 4.)

Jones LJ, Carballido-López R, Errington J. Control of cell shape in bacteria: helical, actin-like filaments in *Bacillus subtilis*. *Cell* 2001; 104: 913–22. (Cited on page 27.)

Jose J, Jähnig F, Meyer TF. Common structural features of IgA1 protease-like outer membrane protein autotransporters. *Mol Microbiol* 1995; 18: 378–80. (Cited on page 19.)

Jun S, Mulder B. Entropy-driven spatial organization of highly confined polymers: lessons for the bacterial chromosome. *Proc Natl Acad Sci USA* 2006; 103: 12388–93. (Cited on pages 33 and 35.)

Jung HC, Eckmann L, Yang SK, Panja A, Fierer J, Morzycka-Wroblewska E, *et al.* A distinct array of proinflammatory cytokines is expressed in human colon epithelial cells in response to bacterial invasion. *J Clin Invest* 1995; 95: 55–65. (Cited on page 7.)

Junker M, Schuster CC, McDonnell AV, Sorg KA, Finn MC, Berger B, *et al.* Pertactin β-helix folding mechanism suggests common themes for the secretion and folding of autotransporter proteins. *Proc Natl Acad Sci USA* 2006; 103: 4918–23. (Cited on page 12.)

Kadurugamuwa JL, Rohde M, Wehland J, Timmis KN. Intercellular spread of *Shigella flexneri* through a monolayer mediated by membranous protrusions and associated with reorganization of the cytoskeletal protein vinculin. *Infect Immun* 1991; 59: 3463–71. (Cited on page 6.)

Kaguni JM. DnaA: controlling the initiation of bacterial DNA replication and more. *Annu Rev Microbiol* 2006; 60: 351–75. (Cited on pages 32 and 138.)

Karczmarek A, Martínez-Arteaga R, Baselga RMA, Alexeeva S, Hansen FG, Vicente M, *et al.* DNA and origin region segregation are not affected by the transition from rod to sphere after inhibition of *Escherichia coli* MreB by A22. *Mol Microbiol* 2007; 65: 51–63. (Cited on pages 27 and 33.)

Khalid S, Sansom MSP. Molecular dynamics simulations of a bacterial autotransporter: NalP from Neisseria meningitidis. *Mol Membr Biol* 2006; 23: 499–508. (Cited on page 19.)

Kim AS, Kakalis LT, Abdul-Manan N, Liu GA, Rosen MK. Autoinhibition and activation mechanisms of the Wiskott-Aldrich syndrome protein. *Nature* 2000; 404: 151–8. (Cited on page 9.)

Kim DE, Chivian D, Baker D. Protein structure prediction and analysis using the Robetta server. *Nucleic Acids Res* 2004; 32: W526–31. (Cited on page 13.)

Kim SY, Gitai Z, Kinkhabwala A, Shapiro L, Moerner WE. Single molecules of the bacterial actin MreB undergo directed treadmilling motion in *Caulobacter crescentus*. *Proc Natl Acad Sci USA* 2006; 103: 10929–34. (Cited on page 27.)

Kocks C, Marchand JB, Gouin E, d'Hauteville H, Sansonetti PJ, Carlier MF, *et al.* The unrelated surface proteins ActA of Listeria monocytogenes and IcsA of *Shigella flexneri* are sufficient to confer actin-based motility on Listeria innocua and *Escherichia coli* respectively. *Mol Microbiol* 1995; 18: 413–23. (Cited on page 8.)

Koppelman CM, Blaauwen TD, Duursma MC, Heeren RM, Nanninga N. *Escherichia coli* minicell membranes are enriched in cardiolipin. *J Bacteriol* 2001; 183: 6144–7. (Cited on page 95.)

Kotloff KL, Noriega F, Losonsky GA, Sztein MB, Wasserman SS, Nataro JP, *et al.* Safety, immunogenicity, and transmissibility in humans of CVD 1203, a live oral *Shigella flexneri* 2a vaccine candidate attenuated by deletions in aroA and virG. *Infect Immun* 1996; 64: 4542–8. (Cited on page 7.)

Kotloff KL, Taylor DN, Sztein MB, Wasserman SS, Losonsky GA, Nataro JP, *et al.* Phase I evaluation of delta virG *Shigella* sonnei live, attenuated, oral vaccine strain WRSS1 in healthy adults. *Infect Immun* 2002; 70: 2016–21. (Cited on page 7.)

Kotloff KL, Winickoff JP, Ivanoff B, Clemens JD, Swerdlow DL, Sansonetti PJ, *et al.* Global burden of *Shigella* infections: implications for vaccine development and implementation of control strategies. *Bull World Health Organ* 1999; 77: 651–66. (Cited on page 4.)

Kovach ME, Elzer PH, Hill DS, Robertson GT, Farris MA, Roop RM, *et al.* Four new derivatives of the broad-host-range cloning vector pBBR1MCS, carrying different antibiotic-resistance cassettes. *Gene* 1995; 166: 175–6. (Cited on pages 42, 67, and 151.)

Kovach ME, Phillips RW, Elzer PH, Roop RM, Peterson KM. pBBR1MCS: a broad-host-range cloning vector. *BioTechniques* 1994; 16: 800–2. (Cited on pages 114 and 151.)

Kruse T, Blagoev B, Løbner-Olesen A, Wachi M, Sasaki K, Iwai N, *et al.* Actin homolog MreB and RNA polymerase interact and are both required for chromosome segregation in *Escherichia coli*. *Genes Dev* 2006; 20: 113–24. (Cited on pages 27 and 33.)

Kruse T, Bork-Jensen J, Gerdes K. The morphogenetic MreBCD proteins of *Escherichia coli* form an essential membrane-bound complex. *Mol Microbiol* 2005; 55: 78–89. (Cited on page 27.)

Kruse T, Møller-Jensen J, Løbner-Olesen A, Gerdes K. Dysfunctional MreB inhibits chromosome segregation in *Escherichia coli*. *EMBO J* 2003; 22: 5283–92. (Cited on page 27.)

Lai EM, Nair U, Phadke ND, Maddock JR. Proteomic screening and identification of differentially distributed membrane proteins in *Escherichia coli*. *Mol Microbiol* 2004; 52: 1029–44. (Cited on page 95.)

Lam H, Schofield WB, Jacobs-Wagner C. A landmark protein essential for establishing and perpetuating the polarity of a bacterial cell. *Cell* 2006; 124: 1011–23. (Cited on page 38.)

Lan G, Dajkovic A, Wirtz D, Sun SX. Polymerization and bundling kinetics of FtsZ filaments. *Biophysical Journal* 2008; 95: 4045–56. (Cited on page 30.)

Lan G, Daniels BR, Dobrowsky TM, Wirtz D, Sun SX. Condensation of FtsZ filaments can drive bacterial cell division. *Proc Natl Acad Sci USA* 2009; 106: 121–6. (Cited on page 29.)

Lan R, Reeves PR. *Escherichia coli* in disguise: molecular origins of *Shigella*. *Microbes Infect* 2002; 4: 1125–32. (Cited on pages 4 and 14.)

Lau IF, Filipe SR, Soballe B, Okstad OA, Barre FX, Sherratt D. Spatial and temporal organization of replicating *Escherichia coli* chromosomes. *Mol Microbiol* 2003; 49: 731–743. (Cited on pages 32, 33, 81, 83, and 161.)

Lett MC, Sasakawa C, Okada N, Sakai T, Makino S, Yamada M, *et al.* virG, a plasmid-coded virulence gene of *Shigella flexneri*: identification of the virG protein and determination of the complete coding sequence. *J Bacteriol* 1989; 171: 353–9. (Cited on pages 6, 7, 8, and 12.)

Levine MM, Kotloff KL, Barry EM, Pasetti MF, Sztein MB. Clinical trials of *Shigella* vaccines: two steps forward and one step back on a long, hard road. *Nat Rev Microbiol* 2007; 5: 540–53. (Cited on pages 3, 4, and 7.)

Levy SB. Very stable prokaryotic messenger RNA in chromosomeless *Escherichia coli* minicells. *Proc Natl Acad Sci USA* 1975; 72: 2900–4. (Cited on page 95.)

Liu Z, Mukherjee A, Lutkenhaus J. Recruitment of ZipA to the division site by interaction with FtsZ. *Mol Microbiol* 1999; 31: 1853–61. (Cited on page 29.)

Loisel TP, Boujemaa R, Pantaloni D, Carlier MF. Reconstitution of actin-based motility of Listeria and *Shigella* using pure proteins. *Nature* 1999; 401: 613–6. (Cited on page 8.)

Löwe J, Amos LA. Crystal structure of the bacterial cell-division protein FtsZ. *Nature* 1998; 391: 203–6. (Cited on page 28.)

Löwe J, Amos LA. Tubulin-like protofilaments in Ca2+-induced FtsZ sheets. *EMBO J* 1999; 18: 2364–71. (Cited on page 29.)

Lutkenhaus J. Assembly dynamics of the bacterial MinCDE system and spatial regulation of the Z ring. *Annu Rev Biochem* 2007; 76: 539–62. (Cited on pages 26, 28, 29, 30, 31, and 32.)

Macpherson DF, Morona R, Beger DW, Cheah KC, Manning PA. Genetic analysis of the rfb region of *Shigella flexneri* encoding the Y serotype O-antigen specificity. *Mol Microbiol* 1991; 5: 1491–9. (Cited on pages 58 and 151.)

Madabhushi R, Marians KJ. Actin homolog MreB affects chromosome segregation by regulating topoisomerase IV in *Escherichia coli*. *Mol Cell* 2009; 33: 171–80. (Cited on page 27.)

Makino S, Sasakawa C, Kamata K, Kurata T, Yoshikawa M. A genetic determinant required for continuous reinfection of adjacent cells on large plasmid in *S. flexneri* 2a. *Cell* 1986; 46: 551–5. (Cited on pages 7 and 8.)

Malinverni J, Silhavy TJ. An ABC transport system that maintains lipid asymmetry in the Gram-negative outer membrane — PNAS. *Proc Natl Acad Sci USA* 2009; . (Cited on page 24.)

Maloy SR, Nunn WD. Selection for loss of tetracycline resistance by *Escherichia coli*. *J Bacteriol* 1981; 145: 1110–1. (Cited on page 43.)

Maurelli AT, Fernández RE, Bloch CA, Rode CK, Fasano A. "Black holes" and bacterial pathogenicity: a large genomic deletion that enhances the virulence of *Shigella* spp. and enteroinvasive *Escherichia coli*. *Proc Natl Acad Sci USA* 1998; 95: 3943–8. (Cited on page 4.)

Maurer J, Jose J, Meyer TF. Characterization of the essential transport function of the AIDA-I autotransporter and evidence supporting structural predictions. *J Bacteriol* 1999; 181: 7014–20. (Cited on page 19.)

May K, Morona R. Mutagenesis of the *Shigella flexneri* autotransporter IcsA reveals novel functional regions involved in IcsA biogenesis and recruitment of host neural Wiscott-Aldrich syndrome protein. *J Bacteriol* 2008; 190: 4666–76. (Cited on pages 12, 13, 17, 71, 74, 76, 106, 121, 128, 132, 134, and 151.)

May KL. Molecular characterisation of *Shigella flexneri* IcsA and the role of lipopolysaccharide O-antigen in actin-based motility. *PhD dissertation, University of Adelaide, Australia* 2007; . (Cited on pages 13, 76, 96, 97, 121, 122, 127, 149, 150, 151, and 161.)

McNulty C, Thompson J, Barrett B, Lord L, Andersen C, Roberts IS. The cell surface expression of group 2 capsular polysaccharides in *Escherichia coli*: the role of KpsD, RhsA and a multi-protein complex at the pole of the cell. *Mol Microbiol* 2006; 59: 907–22. (Cited on page 96.)

Meredith TC, Aggarwal P, Mamat U, Lindner B, Woodard RW. Redefining the requisite lipopolysaccharide structure in *Escherichia coli*. *ACS Chem Biol* 2006; 1: 33–42. (Cited on page 22.)

Miki H, Takenawa T. Regulation of actin dynamics by WASP family proteins. *Journal of Biochemistry* 2003; 134: 309–13. (Cited on page 9.)

Mileykovskaya E, Dowhan W. Visualization of phospholipid domains in *Escherichia coli* by using the cardiolipin-specific fluorescent dye 10-N-nonyl acridine orange. *J Bacteriol* 2000; 182: 1172–5. (Cited on page 138.)

Mileykovskaya E, Fishov I, Fu X, Corbin BD, Margolin W, Dowhan W. Effects of phospholipid composition on MinD-membrane interactions *in vitro* and *in vivo*. *The Journal of biological chemistry* 2003; 278: 22193–8. (Cited on page 30.)

Monahan LG, Robinson A, Harry EJ. Lateral FtsZ association and the assembly of the cytokinetic Z ring in bacteria. *Mol Microbiol* 2009; 74: 1004–17. (Cited on page 29.)

Moreau V, Frischknecht F, Reckmann I, Vincentelli R, Rabut G, Stewart D, *et al.* A complex of N-WASP and WIP integrates signalling cascades that lead to actin polymerization. *Nat Cell Biol* 2000; 2: 441–8. (Cited on page 9.)

Morona R, Daniels C, Van Den Bosch L. Genetic modulation of *Shigella flexneri* 2a lipopolysaccharide O antigen modal chain length reveals that it has been optimized for virulence. *Microbiology (Reading, Engl)* 2003; 149: 925–39. (Cited on pages 24 and 25.)

Morona R, Purins L, Tocilj A, Matte A, Cygler M. Sequence-structure relationships in polysaccharide co-polymerase (PCP) proteins. *Trends Biochem Sci* 2009; 34: 78–84. (Cited on page 22.)

Morona R, Van Den Bosch L. Lipopolysaccharide O antigen chains mask IcsA (VirG) in *Shigella flexneri*. *FEMS Microbiology Letters* 2003a; 221: 173–80. (Cited on pages 24, 25, and 26.)

Morona R, Van Den Bosch L. Multicopy *icsA* is able to suppress the virulence defect caused by the wzz(SF) mutation in *Shigella flexneri*. *FEMS Microbiology Letters* 2003b; 221: 213–9. (Cited on pages 24 and 151.)

Morona R, Van Den Bosch L, Manning PA. Molecular, genetic, and topological characterization of O-antigen chain length regulation in *Shigella flexneri*. *J Bacteriol* 1995; 177: 1059–68. (Cited on page 22.)

Moss JE, Cardozo TJ, Zychlinsky A, Groisman EA. The selC-associated SHI-2 pathogenicity island of *Shigella flexneri*. *Mol Microbiol* 1999; 33: 74–83. (Cited on page 4.)

Mounier J, Vasselon T, Hellio R, Lesourd M, Sansonetti PJ. *Shigella flexneri* enters human colonic Caco-2 epithelial cells through the basolateral pole. *Infect Immun* 1992; 60: 237–48. (Cited on page 5.)

Mühlradt PF, Menzel J, Golecki JR, Speth V. Outer membrane of salmonella. Sites of export of newly synthesised lipopolysaccharide on the bacterial surface. *Eur J Biochem* 1973; 35: 471–81. (Cited on page 99.)

Mukherjee A, Lutkenhaus J. Guanine nucleotide-dependent assembly of FtsZ into filaments. *J Bacteriol* 1994; 176: 2754–8. (Cited on page 28.)

Müller D, Benz I, Tapadar D, Buddenborg C, Greune L, Schmidt MA. Arrangement of the translocator of the autotransporter adhesin involved in diffuse adherence on the bacterial surface. *Infect Immun* 2005; 73: 3851–9. (Cited on pages 21 and 142.)

Murayama SY, Sakai T, Makino S, Kurata T, Sasakawa C, Yoshikawa M. The use of mice in the Sereny test as a virulence assay of *Shigella*e and enteroinvasive *Escherichia coli*. *Infect Immun* 1986; 51: 696–8. (Cited on page 8.)

Nakata N, Tobe T, Fukuda I, Suzuki T, Komatsu K, Yoshikawa M, *et al.* The absence of a surface protease, OmpT, determines the intercellular spreading ability of *Shigella*: the relationship between the ompT and kcpA loci. *Mol Microbiol* 1993; 9: 459–68. (Cited on pages 14 and 106.)

Nataro JP, Seriwatana J, Fasano A, Maneval DR, Guers LD, Noriega F, *et al.* Identification and cloning of a novel plasmid-encoded enterotoxin of enteroinvasive *Escherichia coli* and *Shigella* strains. *Infect Immun* 1995; 63: 4721–8. (Cited on page 5.)

Nelson DE, Young KD. Penicillin binding protein 5 affects cell diameter, contour, and morphology of *Escherichia coli*. *J Bacteriol* 2000; 182: 1714–21. (Cited on page 38.)

Nelson DE, Young KD. Contributions of PBP 5 and DD-carboxypeptidase penicillin binding proteins to maintenance of cell shape in *Escherichia coli*. *J Bacteriol* 2001; 183: 3055–64. (Cited on page 38.)

Nikaido H. Molecular basis of bacterial outer membrane permeability revisited. *Microbiol Mol Biol Rev* 2003; 67: 593–656. (Cited on page 22.)

Nilsen T, Ghosh AS, Goldberg MB, Young KD. Branching sites and morphological abnormalities behave as ectopic poles in shape-defective *Escherichia coli*. *Mol Microbiol* 2004; 52: 1045–54. (Cited on pages 27, 36, and 38.)

Nilsen T, Yan AW, Gale G, Goldberg MB. Presence of multiple sites containing polar material in spherical *Escherichia coli* cells that lack MreB. *J Bacteriol* 2005; 187: 6187–96. (Cited on pages 27, 33, 39, and 90.)

Niyogi SK. Shigellosis. *J Microbiol* 2005; 43: 133–43. (Cited on page 4.)

Nonaka T, Kuwabara T, Mimuro H, Kuwae A, Imajoh-Ohmi S. *Shigella*-induced necrosis and apoptosis of U937 cells and J774 macrophages. *Microbiology (Reading, Engl)* 2003; 149: 2513–27. (Cited on page 5.)

Oaks EV, Wingfield ME, Formal SB. Plaque formation by virulent *Shigella flexneri*. *Infect Immun* 1985; 48: 124–9. (Cited on pages 8 and 60.)

Ogawa H, Nakamura A, Nakaya R. Cinemicrographic study of tissue cell cultures infected with *Shigella flexneri*. *Jpn J Med Sci Biol* 1968; 21: 259–73. (Cited on pages 8 and 67.)

Ogawa M, Suzuki T, Tatsuno I, Abe H, Sasakawa C. IcsB, secreted via the type III secretion system, is chaperoned by IpgA and required at the post-invasion stage of *Shigella* pathogenicity. *Mol Microbiol* 2003; 48: 913–31. (Cited on page 10.)

Ogawa M, Yoshimori T, Suzuki T, Sagara H, Mizushima N, Sasakawa C. Escape of intracellular *Shigella* from autophagy. *Science* 2005; 307: 727–31. (Cited on pages 10 and 15.)

Ohnishi Y, Nishiyama M, Horinouchi S, Beppu T. Involvement of the COOH-terminal pro-sequence of Serratia marcescens serine protease in the folding of the mature enzyme. *The Journal of biological chemistry* 1994; 269: 32800–6. (Cited on pages 16 and 142.)

Okada N, Sasakawa C, Tobe T, Talukder KA, Komatsu K, Yoshikawa M. Construction of a physical map of the chromosome of *Shigella flexneri* 2a and the direct assignment of nine virulence-associated loci identified by Tn5 insertions. *Mol Microbiol* 1991; 5: 2171–80. (Cited on page 23.)

Oliver DC, Huang G, Fernandez RC. Identification of secretion determinants of the *Bordetella pertussis* BrkA autotransporter. *J Bacteriol* 2003a; 185: 489–95. (Cited on page 18.)

Oliver DC, Huang G, Nodel E, Pleasance S, Fernandez RC. A conserved region within the Bordetella pertussis autotransporter BrkA is necessary for folding of its passenger domain. *Mol Microbiol* 2003b; 47: 1367–83. (Cited on pages 16, 17, 18, and 142.)

Oomen CJ, van Ulsen P, Gelder PV, Feijen M, Tommassen J, Gros P. Structure of the translocator domain of a bacterial autotransporter. *EMBO J* 2004; 23: 1257–1266. (Cited on pages 17, 19, 21, and 142.)

Osawa M, Anderson DE, Erickson HP. Reconstitution of contractile FtsZ rings in liposomes. *Science* 2008; 320: 792–4. (Cited on page 29.)

Osawa M, Anderson DE, Erickson HP. Curved FtsZ protofilaments generate bending forces on liposome membranes. *EMBO J* 2009; 28: 3476–84. (Cited on page 29.)

Otto BR, Sijbrandi R, Luirink J, Oudega B, Heddle JG, Mizutani K, *et al.* Crystal structure of hemoglobin protease, a heme binding autotransporter protein from pathogenic *Escherichia coli*. *The Journal of biological chemistry* 2005; 280: 17339–45. (Cited on pages 12 and 13.)

Pallen MJ, Chaudhuri RR, Henderson IR. Genomic analysis of secretion systems. *Curr Opin Microbiol* 2003; 6: 519–27. (Cited on page 11.)

Pedro MAD, Young KD, Höltje JV, Schwarz H. Branching of *Escherichia coli* cells arises from multiple sites of inert peptidoglycan. *J Bacteriol* 2003; 185: 1147–52. (Cited on page 38.)

Perdomo JJ, Gounon P, Sansonetti PJ. Polymorphonuclear leukocyte transmigration promotes invasion of colonic epithelial monolayer by *Shigella flexneri*. *J Clin Invest* 1994; 93: 633–43. (Cited on page 7.)

Peters PC, Migocki MD, Thoni C, Harry EJ. A new assembly pathway for the cytokinetic Z ring from a dynamic helical structure in vegetatively growing cells of *Bacillus subtilis*. *Mol Microbiol* 2007; 64: 487–99. (Cited on page 29.)

Peterson JH, Szabady RL, Bernstein HD. An unusual signal peptide extension inhibits the binding of bacterial presecretory proteins to the signal recognition particle, trigger factor, and the SecYEG complex. *J Biol Chem* 2006; 281: 9038–48. (Cited on page 12.)

Peterson JH, Woolhead CA, Bernstein HD. Basic amino acids in a distinct subset of signal peptides promote interaction with the signal recognition particle. *The Journal of biological chemistry* 2003; 278: 46155–62. (Cited on page 11.)

Philpott DJ, Yamaoka S, Israël A, Sansonetti PJ. Invasive *Shigella flexneri* activates NF-kappa B through a lipopolysaccharide-dependent innate intracellular response and leads to IL-8 expression in epithelial cells. *J Immunol* 2000; 165: 903–14. (Cited on page 7.)

Pichoff S, Lutkenhaus J. Unique and overlapping roles for ZipA and FtsA in septal ring assembly in *Escherichia coli*. *The EMBO Journal* 2002; 21: 685–93. (Cited on page 29.)

Pichoff S, Lutkenhaus J. Tethering the Z ring to the membrane through a conserved membrane targeting sequence in FtsA. *Mol Microbiol* 2005; 55: 1722–1734. (Cited on page 29.)

Pohlner J, Halter R, Beyreuther K, Meyer TF. Gene structure and extracellular secretion of Neisseria gonorrhoeae IgA protease. *Nature* 1987; 325: 458–62. (Cited on page 19.)

Pradel N, Santini CL, Bernadac A, Fukumori Y, Wu LF. Biogenesis of actin-like bacterial cytoskeletal filaments destined for positioning prokaryotic magnetic organelles. *Proc Natl Acad Sci USA* 2006; 103: 17485–17489. (Cited on page 38.)

Pradel N, Santini CL, Bernadac A, Shih YL, Goldberg MB, Wu LF. Polar positional information in *Escherichia coli* spherical cells. *Biochem Biophys Res Commun* 2007; 353: 493–500. (Cited on pages 38, 90, and 138.)

Prévost MC, Lesourd M, Arpin M, Vernel F, Mounier J, Hellio R, *et al.* Unipolar reorganization of F-actin layer at bacterial division and bundling of actin filaments by plastin correlate with movement of *Shigella flexneri* within HeLa cells. *Infect Immun* 1992; 60: 4088–99. (Cited on page 6.)

Pugsley AP, Buddelmeijer N. Traffic spotting: poles apart. *Mol Microbiol* 2004; 53: 1559–62. (Cited on pages 95 and 103.)

Purdy GE, Fisher CR, Payne SM. IcsA surface presentation in *Shigella flexneri* requires the periplasmic chaperones DegP, Skp, and SurA. *J Bacteriol* 2007; 189: 5566–73. (Cited on page 18.)

Purdy GE, Hong M, Payne SM. *Shigella flexneri* DegP facilitates IcsA surface expression and is required for efficient intercellular spread. *Infect Immun* 2002; 70: 6355–64. (Cited on page 18.)

Rajakumar K, Sasakawa C, Adler B. Use of a novel approach, termed island probing, identifies the *Shigella flexneri she* pathogenicity island which encodes a homolog of the immunoglobulin A protease-like family of proteins. *Infect Immun* 1997; 65: 4606–14. (Cited on page 4.)

Raskin DM, de Boer P. Rapid pole-to-pole oscillation of a protein required for directing division to the middle of *Escherichia coli*. *Proc Natl Acad Sci USA* 1999; 96: 4971–6. (Cited on page 30.)

Ratcliff SW, Luh J, Ganesan AT, Behrens B, Thompson R, Montenegro MA, *et al.* The genome of *Bacillus subtilis* phage SPP1: the arrangement of restriction endonuclease generated fragments. *Mol Gen Genet* 1979; 168: 165–72. (Cited on page 45.)

Rathman M, de Lanerolle P, Ohayon H, Gounon P, Sansonetti P. Myosin light chain kinase plays an essential role in *S. flexneri* dissemination. *J Cell Sci* 2000a; 113 Pt 19: 3375–86. (Cited on page 6.)

Rathman M, Jouirhi N, Allaoui A, Sansonetti P, Parsot C, Nhieu GTV. The development of a FACS-based strategy for the isolation of *Shigella flexneri* mutants that are deficient in intercellular spread. *Mol Microbiol* 2000b; 35: 974–90. (Cited on page 10.)

RayChaudhuri D, Park JT. *Escherichia coli* cell-division gene ftsZ encodes a novel GTP-binding protein. *Nature* 1992; 359: 251–4. (Cited on page 28.)

Reed KE, Cronan JE. *Escherichia coli* exports previously folded and biotinated protein domains. *J Biol Chem* 1991; 266: 11425–8. (Cited on pages 114 and 140.)

Reyes-Lamothe R, Wang X, Sherratt D. *Escherichia coli* and its chromosome. *Trends Microbiol* 2008; 16: 238–45. (Cited on pages 33 and 34.)

Robbins JR, Monack D, McCallum SJ, Vegas A, Pham E, Goldberg MB, *et al.* The making of a gradient: IcsA (VirG) polarity in *Shigella flexneri*. *Mol Microbiol* 2001a; 41: 861–72. (Cited on pages 16, 23, 24, and 25.)

Robbins JR, Monack D, McCallum SJ, Vegas A, Pham E, Goldberg MB, *et al.* The making of a gradient: IcsA (VirG) polarity in *Shigella flexneri*. *Mol Microbiol* 2001b; 41: 861–72. (Cited on page 140.)

Robert V, Volokhina EB, Senf F, Bos MP, Gelder PV, Tommassen J. Assembly factor Omp85 recognizes its outer membrane protein substrates by a species-specific C-terminal motif. *Plos Biol* 2006; 4: e377. (Cited on pages 17 and 21.)

Rokney A, Shagan M, Kessel M, Smith Y, Rosenshine I, Oppenheim AB. *E. coli* transports aggregated proteins to the poles by a specific and energy-dependent process. *J Mol Biol* 2009; 392: 589–601. (Cited on pages 134, 135, and 137.)

Romantsov T, Battle AR, Hendel JL, Martinac B, Wood JM. Protein localization in *Escherichia coli* cells: comparison of the cytoplasmic membrane proteins ProP, LacY, ProW, AqpZ, MscS, and MscL. *J Bacteriol* 2010; 192: 912–24. (Cited on page 138.)

Romantsov T, Helbig S, Culham DE, Gill C, Stalker L, Wood JM. Cardiolipin promotes polar localization of osmosensory transporter ProP in *Escherichia coli*. *Mol Microbiol* 2007; 64: 1455–1465. (Cited on page 138.)

Rottem S, Leive L. Effect of variations in lipopolysaccharide on the fluidity of the outer membrane of *Escherichia coli*. *J Biol Chem* 1977; 252: 2077–81. (Cited on pages 24 and 101.)

Ruiz N, Kahne D, Silhavy TJ. Transport of lipopolysaccharide across the cell envelope: the long road of discovery. *Nat Rev Microbiol* 2009; 7: 677–83. (Cited on page 22.)

Sakaguchi T, Köhler H, Gu X, McCormick BA, Reinecker HC. *Shigella flexneri* regulates tight junction-associated proteins in human intestinal epithelial cells. *Cell Microbiol* 2002; 4: 367–81. (Cited on page 7.)

Sallee NA, Rivera GM, Dueber JE, Vasilescu D, Mullins RD, Mayer BJ, *et al.* The pathogen protein $EspF_U$ hijacks actin polymerization using mimicry and multivalency. *Nature* 2008; 454: 1005–8. (Cited on page 143.)

Sandlin RC, Goldberg MB, Maurelli AT. Effect of O side-chain length and composition on the virulence of *Shigella flexneri* 2a. *Mol Microbiol* 1996; 22: 63–73. (Cited on pages 23 and 139.)

Sandlin RC, Lampel KA, Keasler SP, Goldberg MB, Stolzer AL, Maurelli AT. Avirulence of rough mutants of *Shigella flexneri*: requirement of O antigen for correct unipolar localization of IcsA in the bacterial outer membrane. *Infect Immun* 1995; 63: 229–37. (Cited on pages 16 and 23.)

Sansonetti P, Phalipon A. Shigellosis: from molecular pathogenesis of infection to protective immunity and vaccine development. *Res Immunol* 1996; 147: 595–602. (Cited on page 5.)

Sansonetti PJ, Mounier J, Prévost MC, Mège RM. Cadherin expression is required for the spread of *Shigella flexneri* between epithelial cells. *Cell* 1994; 76: 829–39. (Cited on page 7.)

Sansonetti PJ, Nhieu GTV, Egile C. Rupture of the intestinal epithelial barrier and mucosal invasion by *Shigella flexneri*. *Clin Infect Dis* 1999; 28: 466–75. (Cited on pages 5 and 7.)

Sansonetti PJ, Phalipon A. M cells as ports of entry for enteroinvasive pathogens: mechanisms of interaction, consequences for the disease process. *Semin Immunol* 1999; 11: 193–203. (Cited on page 5.)

Sansonetti PJ, Phalipon A, Arondel J, Thirumalai K, Banerjee S, Akira S, *et al.* Caspase-1 activation of IL-1β and IL-18 are essential for *Shigella flexneri*-induced inflammation. *Immunity* 2000; 12: 581–90. (Cited on page 7.)

Santapaola D, Chierico FD, Petrucca A, Uzzau S, Casalino M, Colonna B, *et al.* Apyrase, the product of the virulence plasmid-encoded phoN2 (apy) gene of *Shigella flexneri*, is necessary for proper unipolar IcsA localization and for efficient intercellular spread. *J Bacteriol* 2006; 188: 1620–7. (Cited on page 38.)

Scholz O, Thiel A, Hillen W, Niederweis M. Quantitative analysis of gene expression with an improved green fluorescent protein. p6. *Eur J Biochem* 2000; 267: 1565–70. (Cited on page 67.)

Schroeder GN, Hilbi H. Molecular pathogenesis of *Shigella* spp.: controlling host cell signaling, invasion, and death by type III secretion. *Clin Microbiol Rev* 2008; 21: 134–56. (Cited on page 5.)

Schuch R, Sandlin RC, Maurelli AT. A system for identifying post-invasion functions of invasion genes: requirements for the Mxi-Spa type III secretion pathway of *Shigella flexneri* in intercellular dissemination. *Mol Microbiol* 1999; 34: 675–89. (Cited on page 6.)

Scott ME, Dossani ZY, Sandkvist M. Directed polar secretion of protease from single cells of *Vibrio* cholerae via the type II secretion pathway. *Proc Natl Acad Sci USA* 2001; 98: 13978–83. (Cited on page 36.)

Shere KD, Sallustio S, Manessis A, D'Aversa TG, Goldberg MB. Disruption of IcsP, the major *Shigella* protease that cleaves IcsA, accelerates actin-based motility. *Mol Microbiol* 1997; 25: 451–62. (Cited on pages 14 and 15.)

Shiomi D, Yoshimoto M, Homma M, Kawagishi I. Helical distribution of the bacterial chemoreceptor via colocalization with the Sec protein translocation machinery. *Mol Microbiol* 2006; 60: 894–906. (Cited on page 67.)

Sijbrandi R, Urbanus ML, ten Hagen-Jongman CM, Bernstein HD, Oudega B, Otto BR, *et al.* Signal recognition particle (SRP)-mediated targeting and Sec-dependent translocation of an extracellular *Escherichia coli* protein. *The Journal of biological chemistry* 2003; 278: 4654–9. (Cited on page 11.)

Simmons DA. Genetic and biosynthetic aspects of *Shigella flexneri* O-specific lipopolysaccharides. *Biochem Soc Trans* 1993; 21: 58S. (Cited on page 4.)

Singer M, Sansonetti PJ. IL-8 is a key chemokine regulating neutrophil recruitment in a new mouse model of *Shigella*-induced colitis. *J Immunol* 2004; 173: 4197–206. (Cited on page 7.)

Skillman KM, Barnard TJ, Peterson JH, Ghirlando R, Bernstein HD. Efficient secretion of a folded protein domain by a monomeric bacterial autotransporter. *Mol Microbiol* 2005; 58: 945–958. (Cited on pages 19, 20, 21, and 142.)

Sklar JG, Wu T, Gronenberg LS, Malinverni JC, Kahne D, Silhavy TJ. Lipoprotein SmpA is a component of the YaeT complex that assembles outer membrane proteins in *Escherichia coli*. *Proc Natl Acad Sci USA* 2007a; 104: 6400–5. (Cited on page 19.)

Sklar JG, Wu T, Kahne D, Silhavy TJ. Defining the roles of the periplasmic chaperones SurA, Skp, and DegP in *Escherichia coli*. *Genes Dev* 2007b; 21: 2473–84. (Cited on page 18.)

Snapper SB, Takeshima F, Antón I, Liu CH, Thomas SM, Nguyen D, *et al.* N-WASP deficiency reveals distinct pathways for cell surface projections and microbial actin-based motility. *Nat Cell Biol* 2001; 3: 897–904. (Cited on page 9.)

Steeghs L, den Hartog R, den Boer A, Zomer B, Roholl P, van der Ley P. Meningitis bacterium is viable without endotoxin. *Nature* 1998; 392: 449–50. (Cited on page 22.)

Steinhauer J, Agha R, Pham T, Varga AW, Goldberg MB. The unipolar *Shigella* surface protein IcsA is targeted directly to the bacterial old pole: IcsP cleavage of IcsA occurs over the entire bacterial surface. *Mol Microbiol* 1999; 32: 367–77. (Cited on page 14.)

Stevens JM, Galyov EE, Stevens MP. Actin-dependent movement of bacterial pathogens. *Nat Rev Microbiol* 2006; 4: 91–101. (Cited on page 9.)

Stricker J, Maddox P, Salmon ED, Erickson HP. Rapid assembly dynamics of the *Escherichia coli* FtsZ-ring demonstrated by fluorescence recovery after photobleaching. *Proc Natl Acad Sci USA* 2002; 99: 3171–5. (Cited on page 29.)

Sun Q, Margolin W. FtsZ dynamics during the division cycle of live *Escherichia coli* cells. *J Bacteriol* 1998; 180: 2050–6. (Cited on page 31.)

Suzuki T, Lett MC, Sasakawa C. Extracellular transport of VirG protein in *Shigella*. *J Biol Chem* 1995; 270: 30874–80. (Cited on pages 11, 17, and 19.)

Suzuki T, Miki H, Takenawa T, Sasakawa C. Neural Wiskott-Aldrich syndrome protein is implicated in the actin-based motility of *Shigella flexneri*. *EMBO J* 1998; 17: 2767–76. (Cited on pages 9 and 13.)

Suzuki T, Mimuro H, Suetsugu S, Miki H, Takenawa T, Sasakawa C. Neural Wiskott-Aldrich syndrome protein (N-WASP) is the specific ligand for *Shigella* VirG among the WASP family and determines the host cell type allowing actin-based spreading. *Cell Microbiol* 2002; 4: 223–33. (Cited on pages 9 and 13.)

Suzuki T, Murai T, Fukuda I, Tobe T, Yoshikawa M, Sasakawa C. Identification and characterization of a chromosomal virulence gene, vacJ, required for intercellular spreading of *Shigella flexneri*. *Mol Microbiol* 1994; 11: 31–41. (Cited on page 24.)

Suzuki T, Saga S, Sasakawa C. Functional analysis of *Shigella* VirG domains essential for interaction with vinculin and actin-based motility. *J Biol Chem* 1996; 271: 21878–85. (Cited on pages 13, 125, and 150.)

Suzuki T, Sasakawa C. Molecular basis of the intracellular spreading of *Shigella*. *Infect Immun* 2001; 69: 5959–66. (Cited on page 13.)

Szabady RL, Peterson JH, Skillman KM, Bernstein HD. An unusual signal peptide facilitates late steps in the biogenesis of a bacterial autotransporter. *Proc Natl Acad Sci USA* 2005; 102: 221–6. (Cited on pages 12 and 19.)

Szeto TH, Rowland SL, Habrukowich CL, King GF. The MinD membrane targeting sequence is a transplantable lipid-binding helix. *J Biol Chem* 2003; 278: 40050–6. (Cited on page 30.)

Szeto TH, Rowland SL, Rothfield LI, King GF. Membrane localization of MinD is mediated by a C-terminal motif that is conserved across eubacteria, archaea, and chloroplasts. *Proc Natl Acad Sci USA* 2002; 99: 15693–8. (Cited on page 30.)

Teather RM, Collins JF, Donachie WD. Quantal behavior of a diffusible factor which initiates septum formation at potential division sites in *Escherichia coli*. *J Bacteriol* 1974; 118: 407–13. (Cited on page 30.)

Thanbichler M, Shapiro L. Chromosome organization and segregation in bacteria. *J Struct Biol* 2006a; 156: 292–303. (Cited on page 32.)

Thanbichler M, Shapiro L. MipZ, a spatial regulator coordinating chromosome segregation with cell division in Caulobacter. *Cell* 2006b; 126: 147–62. (Cited on page 81.)

Thanedar S, Margolin W. FtsZ exhibits rapid movement and oscillation waves in helix-like patterns in *Escherichia coli*. *Curr Biol* 2004; 14: 1167–73. (Cited on page 29.)

Thiem S, Kentner D, Sourjik V. Positioning of chemosensory clusters in *E. coli* and its relation to cell division. *EMBO J* 2007; 26: 1615–1623. (Cited on page 138.)

Thomas JD, Daniel RA, Errington J, Robinson C. Export of active green fluorescent protein to the periplasm by the twin-arginine translocase (Tat) pathway in *Escherichia coli*. *Mol Microbiol* 2001; 39: 47–53. (Cited on pages 36 and 132.)

Touzé T, Hayward RD, Eswaran J, Leong JM, Koronakis V. Self-association of EPEC intimin mediated by the β-barrel-containing anchor domain: a role in clustering of the Tir receptor. *Mol Microbiol* 2004; 51: 73–87. (Cited on page 143.)

Tsai CM, Frasch CE. A sensitive silver stain for detecting lipopolysaccharides in polyacrylamide gels. *Anal Biochem* 1982; 119: 115–9. (Cited on page 58.)

Van Den Bosch L, Manning PA, Morona R. Regulation of O-antigen chain length is required for *Shigella flexneri* virulence. *Mol Microbiol* 1997; 23: 765–75. (Cited on pages 23, 41, and 96.)

Van Den Bosch L, Morona R. The actin-based motility defect of a *Shigella flexneri* rmlD rough LPS mutant is not due to loss of IcsA polarity. *Microbial Pathogenesis* 2003; 35: 11–8. (Cited on page 23.)

van den Ent F, Amos LA, Löwe J. Prokaryotic origin of the actin cytoskeleton. *Nature* 2001; 413: 39–44. (Cited on page 26.)

van den Ent F, Leaver M, Bendezu F, Errington J, de Boer P, Löwe J. Dimeric structure of the cell shape protein MreC and its functional implications. *Mol Microbiol* 2006; 62: 1631–42. (Cited on page 27.)

Varma A, Huang KC, Young KD. The Min System as a General Cell Geometry Detection Mechanism: Branch Lengths in Y-Shaped *Escherichia coli* Cells Affect Min Oscillation Patterns and Division Dynamics. *J Bacteriol* 2008; 190: 2106–2117. (Cited on page 27.)

Varma A, Pedro MAD, Young KD. FtsZ directs a second mode of peptidoglycan synthesis in *Escherichia coli*. *J Bacteriol* 2007; 189: 5692–704. (Cited on page 27.)

Veiga E, Sugawara E, Nikaido H, de Lorenzo V, Fernández LA. Export of autotransported proteins proceeds through an oligomeric ring shaped by C-terminal domains. *EMBO J* 2002; 21: 2122–31. (Cited on pages 20, 54, 121, 124, 125, and 141.)

Velarde JJ, Nataro JP. Hydrophobic residues of the autotransporter EspP linker domain are important for outer membrane translocation of its passenger. *The Journal of biological chemistry* 2004; 279: 31495–504. (Cited on page 18.)

Viollier PH, Thanbichler M, McGrath PT, West L, Meewan M, McAdams HH, *et al.* Rapid and sequential movement of individual chromosomal loci to specific subcellular locations during bacterial DNA replication. *Proc Natl Acad Sci USA* 2004; 101: 9257–62. (Cited on page 33.)

Voulhoux R, Bos MP, Geurtsen J, Mols M, Tommassen J. Role of a highly conserved bacterial protein in outer membrane protein assembly. *Science* 2003; 299: 262–5. (Cited on page 19.)

Voulhoux R, Tommassen J. Omp85, an evolutionarily conserved bacterial protein involved in outer-membrane-protein assembly. *Res Microbiol* 2004; 155: 129–35. (Cited on page 19.)

Wachi M, Doi M, Tamaki S, Park W, Nakajima-Iijima S, Matsuhashi M. Mutant isolation and molecular cloning of mre genes, which determine cell shape, sensitivity to mecillinam, and amount of penicillin-binding proteins in *Escherichia coli*. *J Bacteriol* 1987; 169: 4935–40. (Cited on page 26.)

Wagner JK, Heindl JE, Gray AN, Jain S, Goldberg MB. Contribution of the periplasmic chaperone Skp to efficient presentation of the autotransporter IcsA on the surface of *Shigella flexneri*. *J Bacteriol* 2009; 191: 815–21. (Cited on pages 15 and 18.)

Wang X. Dancing around the divisome: asymmetric chromosome segregation in *Escherichia coli*. *Genes Dev* 2005; 19: 2367–2377. (Cited on page 95.)

Wang X, Liu X, Possoz C, Sherratt D. The two *Escherichia coli* chromosome arms locate to separate cell halves. *Genes Dev* 2006; 20: 1727–31. (Cited on page 33.)

Ward JE, Lutkenhaus J. Overproduction of FtsZ induces minicell formation in *E. coli*. *Cell* 1985; 42: 941–9. (Cited on page 30.)

Waterman SR, Small PL. Identification of sigma S-dependent genes associated with the stationary-phase acid-resistance phenotype of *Shigella flexneri*. *Mol Microbiol* 1996; 21: 925–40. (Cited on page 4.)

Webb CD, Graumann PL, Kahana JA, Teleman AA, Silver PA, Losick R. Use of time-lapse microscopy to visualize rapid movement of the replication origin region of the chromosome during the cell cycle in *Bacillus subtilis*. *Mol Microbiol* 1998; 28: 883–92. (Cited on pages 32 and 33.)

Wei J, Goldberg MB, Burland V, Venkatesan MM, Deng W, Fournier G, *et al.* Complete genome sequence and comparative genomics of *Shigella flexneri* serotype 2a strain 2457T. *Infect Immun* 2003; 71: 2775–86. (Cited on page 4.)

Wild J, Altman E, Yura T, Gross CA. DnaK and DnaJ heat shock proteins participate in protein export in *Escherichia coli*. *Genes Dev* 1992; 6: 1165–72. (Cited on page 18.)

Winkler J, Seybert A, König L, Pruggnaller S, Haselmann U, Sourjik V, *et al.* Quantitative and spatio-temporal features of protein aggregation in *Escherichia coli* and consequences on protein quality control and cellular ageing. *EMBO J* 2010; . (Cited on page 138.)

Woldringh CL, Mulder E, Huls PG, Vischer N. Toporegulation of bacterial division according to the nucleoid occlusion model. *Res Microbiol* 1991; 142: 309–20. (Cited on page 32.)

Woldringh CL, Nanninga N. Structural and physical aspects of bacterial chromosome segregation. *J Struct Biol* 2006; 156: 273–83. (Cited on page 33.)

Wu T, McCandlish AC, Gronenberg LS, Chng SS, Silhavy TJ, Kahne D. Identification of a protein complex that assembles lipopolysaccharide in the outer membrane of *Escherichia coli*. *Proc Natl Acad Sci USA* 2006; 103: 11754–9. (Cited on page 19.)

Xia W, Dowhan W. In vivo evidence for the involvement of anionic phospholipids in initiation of DNA replication in Escherichia coli. *Proc Natl Acad Sci USA* 1995; 92: 783–7. (Cited on page 161.)

Yamaichi Y, Niki H. migS, a cis-acting site that affects bipolar positioning of *oriC* on the *Escherichia coli* chromosome. *EMBO J* 2004; 23: 221–233. (Cited on pages 33, 90, 91, and 137.)

Yeh HY, Jacobs DM. Characterization of lipopolysaccharide fractions and their interactions with cells and model membranes. *J Bacteriol* 1992; 174: 336–41. (Cited on pages 24 and 101.)

Young KD. Bacterial shape. *Mol Microbiol* 2003; 49: 571–80. (Cited on page 38.)

Yu XC, Margolin W. FtsZ ring clusters in min and partition mutants: role of both the Min system and the nucleoid in regulating FtsZ ring localization. *Mol Microbiol* 1999; 32: 315–26. (Cited on page 31.)

Zhao J, Lambowitz AM. Inaugural Article: A bacterial group II intron-encoded reverse transcriptase localizes to cellular poles. *Proc Natl Acad Sci USA* 2005; 102: 16133–40. (Cited on page 36.)

Zhao J, Niu W, Yao J, Mohr S, Marcotte EM, Lambowitz AM. Group II intron protein localization and insertion sites are affected by polyphosphate. *Plos Biol* 2008; 6: e150. (Cited on page 36.)

Zheng W, Li Z, Skarstad K, Crooke E. Mutations in DnaA protein suppress the growth arrest of acidic phospholipid-deficient *Escherichia coli* cells. *EMBO J* 2001; 20: 1164–72. (Cited on page 161.)

Zhou H, Lutkenhaus J. Membrane binding by MinD involves insertion of hydrophobic residues within the C-terminal amphipathic helix into the bilayer. *J Bacteriol* 2003; 185: 4326–35. (Cited on page 30.)

Zurawski DV, Mumy KL, Faherty CS, McCormick BA, Maurelli AT. *Shigella flexneri* type III secretion system effectors OspB and OspF target the nucleus to downregulate the host inflammatory response via interactions with retinoblastoma protein. *Mol Microbiol* 2009; 71: 350–68. (Cited on page 7.)

Zychlinsky A, Fitting C, Cavaillon JM, Sansonetti PJ. Interleukin 1 is released by murine macrophages during apoptosis induced by *Shigella flexneri*. *J Clin Invest* 1994; 94: 1328–32. (Cited on page 7.)

Zychlinsky A, Prevost MC, Sansonetti PJ. *Shigella flexneri* induces apoptosis in infected macrophages. *Nature* 1992; 358: 167–9. (Cited on page 5.)

Zychlinsky A, Thirumalai K, Arondel J, Cantey JR, Aliprantis AO, Sansonetti PJ. *In vivo* apoptosis in *Shigella flexneri* infections. *Infect Immun* 1996; 64: 5357–65. (Cited on page 5.)

AMENDMENTS

Page 3, line 1: "gleamed" should read, "*gleaned*"

Page 25, paragraph 3, line 4: "detect the low concentration lateral IcsA" should read, "detect the low concentration *of* lateral IcsA"

Section 1.7: *refers to bacterial cell biology of Escherichia coli, unless specifically denoted in text*.

Page 32, line 1: "the latter observation lead to" should read, "the latter observation *led* to"

Page 36, line 10: "positioning informations" should read, "positioning *information*"

Page 36, paragraph 2, line 2: "it was demonstrated the polarly localised" should read, "it was demonstrated *that* the polarly localised"

Page 74, line 3: "MG243" should read "*MG426*"

Page 77, paragraph 1, line 8: "cells from two experiments that selected" should read, "cells from two experiments that *were* selected"

Page 84, paragraph 3, line 1: "when more two or more foci" should read, "when two or more foci"

Page 90, paragraph 2, line 2: "A22 was added to to mid-log phase cultures" should read, "A22 was added to mid-log phase cultures"

Page 105, paragraph 2, line 1: "The aim of chapter" should read, "The aim of *this* chapter"

Page 108, paragraph 3, line 1: "The proteins could readily be readily detected" should read, "The proteins could readily be detected"

Page 110, paragraph 4, line 3: "when grown media" should read, "when grown *in* media"

Page 117, paragraph 1, line 1: "was to detect of the earliest" should read, "was to detect the earliest"

Page 121, paragraph 2, line 8: "molecule weight", should read "*molecular* weight"

Page 136, paragraph 3, line 9: "does not necessary implicate" should read, "does not *necessarily* implicate"

Page 137, paragraph 2, line 3: "and IcsA$_{506–620(i563)}$)" should read, "and IcsA$_{506–620(i563)}$"

Page 137, paragraph 2, line 4: "foci being deliver to the pole" should read, "foci being *delivered* to the pole"

Page 137, paragraph 2, line 9: "suggest the that incorporation" should read, "suggest *that the* incorporation"

Page 140, paragraph 5, line 1: "has been suggest" should read, "had been suggested"